AFAPL-TR-78-51
Volume I

② LEVEL Ⅲ

A064435

HIGH POWER MAGNETOHYDRODYNAMIC SYSTEM

D. W. SWALLOM
O. K. SONJU
D. E. MEADER
H. BECKER

MAXWELL LABORATORIES, INC.
200 WEST CUMMINGS PARK
WOBURN, MASSACHUSETTS 01801

JULY 1978

D D C

RECEIVED
FEB 21 1979

B

TECHNICAL REPORT AFAPL-TR-78-51, Volume I
Final Report May 1976 — June 1978

79

NOTICE

When Government drawings, specifications, or other data are used for any purpose other than in connection with a definitely related Government procurement operation, the United States Government thereby incurs no responsibility nor any obligation whatsoever; and the fact that the government may have formulated, furnished, or in any way supplied the said drawings, specifications, or other data, is not to be regarded by implication or otherwise as in any manner licensing the holder or any other person or corporation, or conveying any rights or permission to manufacture, use, or sell any patented invention that may in any way be related thereto.

This report has been reviewed by the Information Office, (ASD/OIP) and is releasable to the National Technical Information Service (NTIS). At NTIS, it will be available to the general public, including foreign nations.

This technical report has been reviewed and is approved for publication.

Robert F. Cooper
Program Manager

FOR THE COMMANDER

Philip E. Stover
Chief, High Power Branch

Copies of this report should not be returned unless return is required by security considerations, contractural obligations, or notice on a specific document.

i

REPORT DOCUMENTATION PAGE		READ INSTRUCTIONS BEFORE COMPLETING FORM
1. REPORT NUMBER AFAPL-TR-78-51 — Vol-1	2. GOVT ACCESSION NO.	3. RECIPIENT'S CATALOG NUMBER
4. TITLE (and Subtitle) HIGH POWER MAGNETOHYDRODYNAMIC SYSTEM		5. TYPE OF REPORT & PERIOD COVERED Final Technical Report, 17 May 76 —15 June 78
		6. PERFORMING ORG. REPORT NUMBER
7. AUTHOR(s) D. W. Swallom, O. K. Sonju, D. E. Meader, H. Becker		8. CONTRACT OR GRANT NUMBER(s) F33615-76-C-2104
9. PERFORMING ORGANIZATION NAME AND ADDRESS Maxwell Laboratories, Inc. 200 West Cummings Park Woburn, Massachuetts 01801		10. PROGRAM ELEMENT, PROJECT, TASK AREA & WORK UNIT NUMBERS 31452636 3145 17 20
11. CONTROLLING OFFICE NAME AND ADDRESS Air Force Aero Propulsion Laboratory (POD) Air Force Systems Command Wright-Patterson Air Force Base, Ohio 45433		12. REPORT DATE July 1978
		13. NUMBER OF PAGES 364
14. MONITORING AGENCY NAME & ADDRESS(If different from Controlling Office)		15. SECURITY CLASS. (of this report) Unclassified
		15a. DECLASSIFICATION/DOWNGRADING SCHEDULE

16. DISTRIBUTION STATEMENT (of this Report)

Approved for public release; distribution unlimited.

D D C
RECEIVED
FEB 21 1979
B

17. DISTRIBUTION STATEMENT (of the abstract entered in Block 20, If different from Report)

18. SUPPLEMENTARY NOTES — Major Subcontractors:
- Rocketdyne Division of Rockwell International - Combustor Subsystem and Development Testing Subcontractor.
- Magnetic Corporation of America - MHD Magnet Design Subcontractor.

19. KEY WORDS (Continue on reverse side if necessary and identify by block number)

Portable Power Supplies	Compact MHD Generator
Semi-Portable	Burst Power Supplies
MHD Generators	High Performance MHD Generator
Fast Start Power Supplies	Flightweight MHD

20. ABSTRACT (Continue on reverse side if necessary and identify by block number)

The technical effort discussed in this report covers Phase B of the High Power Magnetohydrodynamic System program, which is a multi-phase program to develop liquid oxygen/liquid hydrocarbon magnetodydrodynamic generators using cesium seed for high performance, portable power supply applications.

DD FORM 1473 1 JAN 73   EDITION OF 1 NOV 68 IS OBSOLETE

BLOCK 19 (Continued)

Lightweight Megawatt Power Supplies

Cesium Seeding of MHD Gases

JP-4 Fueled MHD

Filament Wound, Epoxy Coated Fiberglass

Portable High Power MHD Generators

Lightweight MHD

LOX/JP-4 Combustor System

Emulsified Fuel

Direct Energy Conversion Systems

BLOCK 20 (Continued)

During this phase a lightweight, high performance hot gas flow train using liquid oxygen and JP-4 was designed and component modeling completed. The magnetohydrodynamic channel/diffuser performance parameters which were used as the design criteria were an output power of 30 MWe, a specific energy extraction of 1.0 MJ/kg, and a specific power density of 200 MWe/m^3. To achieve these performance requirements, the required characteristic velocity efficiency of the combustion system was greater than 99%. During this program a limited amount of development testing was completed using a heat sink combustor and a diagnostics channel. These tests measured the combustor characteristic velocity efficiency and the gas electrical conductivity, as well as pressures, vibrations, and temperatures. The results of the development test program, which verified the design assumptions used to achieve the performance requirements, were a characteristic velocity efficiency of nearly 99% and a gas electrical conductivity at the magnetohydrodynamic channel inlet of 15 mhos/m.

FOREWORD

This final report was submitted by Maxwell Laboratories, Inc. under Contract No. F33615-76-C-2104. The effort was sponsored by the Air Force Aero Propulsion Laboratory, Air Force Systems Command, Wright-Patterson Air Force Base, Ohio, under Project 3145, Task 314526 and Work Unit 31452636 with Robert F. Cooper/AFAPL/POD as the Program Manager. Dr. Daniel W. Swallom and Dr. Otto K. Sonju of Maxwell Laboratories, Inc. were responsible for the technical work. The work discussed in this report was performed by Maxwell Laboratories, Inc., and two major subcontractors; Rocketdyne, A Division of Rockwell International and Magnetic Corporation of America.

The authors of this report appreciate the assistance given to them by the many individuals who contributed to the work performed on this report as well as the guidance given to them by USAF Program Manager, Robert F. Cooper, of the Air Force Aero Propulsion Laboratory.

This report was written and edited by the named authors of Maxwell Laboratories, Inc. Other individuals who participated in this work and contributed to the report include:

G. T. Heskey	Maxwell Laboratories, Inc.
R. V. Burry	Rockwell International
A. W. Huebner	Rockwell International
G. M. Suzuki	Rockwell International
J. M. Watkins	Rockwell International
D. D. Clarke	Rockwell International
R. J. Thome	Magnetic Corporation of America

Because of its length, this report is published in two volumes. The first contains Sections I through VI, Figures 1 through 155, Tables 1 through 46, References, and the List of Abbreviations. Volume II contains Sections VII through X, Appendices A through H, Figures 156 through 233 and C.1 through G.2, and Tables 47 through 79 and A.1 through H.1. The lists of References and Abbreviations are repeated.

iii

TABLE OF CONTENTS

TABLE OF CONTENTS(Continued)

TABLE OF CONTENTS (Continued)

TABLE OF CONTENTS (Continued)

LIST OF ILLUSTRATIONS

LIST OF ILLUSTRATIONS (Continued)

LIST OF ILLUSTRATIONS (Continued)

LIST OF ILLUSTRATIONS (Continued)

LIST OF TABLES

LIST OF TABLES (Continued)

SECTION 1

INTRODUCTION

A.   OVERVIEW

This is the final report of Contract No. F33615-76-C-2104, "High Power
Magnetohydrodynamic (MHD) System," between the Air Force Aero Propulsion
Laboratory, (AFAPL), Air Force Systems Command, Wright-Patterson Air
Force Base, Ohio, and Maxwell Laboratories, Inc. The period of perform-
ance for this work was from May 1976 through June 1978.

Because of the requirement for special testing facilities and a variety of
different technologies required to complete the technical effort of this program,
the work was performed by a team including: Maxwell Laboratories, Inc.;
Rocketdyne, a Division of Rockwell International; and Magnetic Corporation of
America (MCA); with Maxwell Laboratories, Inc. having the prime responsibility
for the program. Maxwell Laboratories was also responsible for the design and
fabrication of the diagnostics channel, the design of the high power MHD channel/
diffuser, and the reduction and interpretation of the diagnostics channel test data.
Rocketdyne designed and fabricated the heat sink combustor assembly and the
gas generator support systems, designed the cooled wall combustion system, and
conducted and evaluated the results of the development test program. MCA was
responsible for the magnet design aspects of the program which included the
evaluation of conventional magnet design tradeoffs as well as similar activities
for the superconducting magnet.

B.   BACKGROUND

The overall goal of the High Power MHD Systems (HPMS) program was
to develop the technology for portable or semi-portable MHD power systems over
the power range of 10-300 megawatts electrical (MW$_e$) output power with operating
times ranging from one to ten minutes. The overall HPMS program was divided
into the following four major phases:

> Phase A - Design and Trade-Off Analysis
> Phase B - Combustor Development Testing, Detailed
>   Component Designs, and Component Modeling
> Phase C - Hot Gas Flow Train (HGFT) Performance Testing
>   and Component Development
> Phase D - Full Scale System Testing and Verification

1

Phase A consisted of parametric design studies and optimizations of various combustion MHD power supply systems for use as a prime power source in the range of 10-50 MW_e output power with operating periods of a few minutes. [1] Within a conservative range of extrapolation, the analysis indicated that for the power range of interest performance as high as 500-1000 MW_e/m^3 and 1.5-2.0 MJ/kg could be achieved. In these analyses both liquid and solid fuels were considered.

Based on the results of Phase A, an MHD power generation system utilizing JP-4 as the fuel and liquid oxygen (LO_2) as the oxidizer was chosen for development over competitive power systems, i.e., conventional and superconducting turbo alternator systems. Phase B, which is the present program, was then initiated to demonstrate the "reasonable" performance parameters that would validate the critical design data necessary for these short duration MHD power generation systems.

The next phase of the HPMS program, Phase C, will demonstrate the system performance in a conventional four Tesla tapered magnet system with a hydro-carbon/LO_2 combustion system. This performance test program will be conducted by AEDC in the HPMS test facility located at AEDC. This phase would also include some additional component development work and a preliminary design for the full scale system. Following the completion of Phase C, the final phase of the HPMS program, Phase D, would be initiated to complete the full scale system testing and performance verification. The Phase D power generation system will include all major MHD components, as well as the power conditioning, controls, protective devices, tankage, etc., necessary to demonstrate controlled, programmed, and predictable electrical power from a totally independent MHD power generation system.

C. OBJECTIVES

The objective of the overall HPMS program is to design, fabricate, and ground test an advanced liquid fueled MHD power generation system, including an advanced dc-dc power conditioning system and superconducting magnet, into a single passive load. For the combustor development testing, the detailed component designs, and the component modeling, specific performance goals were selected. These goals that were chosen were the simultaneous demonstration of three critical performance parameters, i.e., specific power density of 200 MW/m^3, specific enthalpy extraction of one megajoule per kilogram, and power output of 30 MW_e.

---

[1] O. K. Sonju and J. Teno, "Study of High Power, High Performance Portable MHD Generator Power Supply Systems," AFAPL-TR-76-87, AD#A040381, August 1976.

The objectives of Phase B were to design, fabricate, and test a JP-4/LO$_2$ gas generator and diagnostics channel and to design a cooled combustor and MHD channel/diffuser. This system consisted of a hot gas flow train of high performance combustor/nozzle and channel/diffuser. All major components fabricated or specifically modified or designed for use in this program, were made as lightweight as possible consistent with minimizing development risks. Existing hardware and design techniques were used whenever practical. The hot gas flow train was designed for testing in the HPMS facility at AEDC using the HPMS magnet and the associated AEDC data acquisition and control systems. All flow train hardware was designed to allow simultaneous demonstration of the three critical parameters: power density of 200 MW$_e$/m^3, enthalpy extraction of one megajoule per kilogram of total mass flow rate, and a power level of 30 MW$_e$. All flow train hardware was designed for five hours of operational life. The MHD power system was designed to provide full power within one second of the start command. Electrical and mechanical control systems were designed to be capable of demonstrating this response performance and of handling a controlled ± 20% variation in load.

D.   SCOPE

The present phase of the HPMS program had two major areas of emphasis: (1) the design and testing of major HGFT components; and (2) the modeling of major lightweight components. In the first area the heat sink combustor and the diagnostics channel have been designed, fabricated and tested. Figure 1 shows this hardware installed at the Santa Susana Field Laboratory (SSFL) for development testing. The cooled wall combustor and the high power MHD channel/diffuser designs have been completed and are awaiting integration of the development test program results prior to fabrication.

While the test program for the HGFT is required to be at full size or scale, the component development for the superconducting magnet (SCM) system and power conditioning components are not. Thus, in the second area of emphasis, modeling programs which were not part of the technical effort described in this report, are underway to provide appropriate sized modules for the SCM and the power conditioning systems. The test program for the initial HGFT performance optimization in Phase C will proceed with a conventional magnet system while the final system validation tests of Phase D will require the appropriate compact SCM system. Figure 2 shows a conceptual drawing of the Phase D hardware.

3

Figure 1. Development Test Hardware Installed at SSPL Brake Facility

6D931-3/22/78-S1*

DIFFUSER

DIFFUSER SUPPORT

COOLANT MANIFOLDS

CHANNEL ELECTRODES

MAGNET DEWAR

SUPPORT FRAME

GENERATOR CHANNEL

MAGNET COIL

THRUST BRACKETS

CRYOGENIC LEADS

COIL SUPPORT GIRDERS

NOZZLE THROAT

COMBUSTOR CHAMBER

FUEL INLET

FUEL PUMP

TURBINE EXHAUST

TURBINE

OXIDIZER PUMP

OXIDIZER INLET

OXIDIZER CONTROL VALVE

MHD GENERATOR SYSTEM, LIQUID FUEL COMBUSTOR
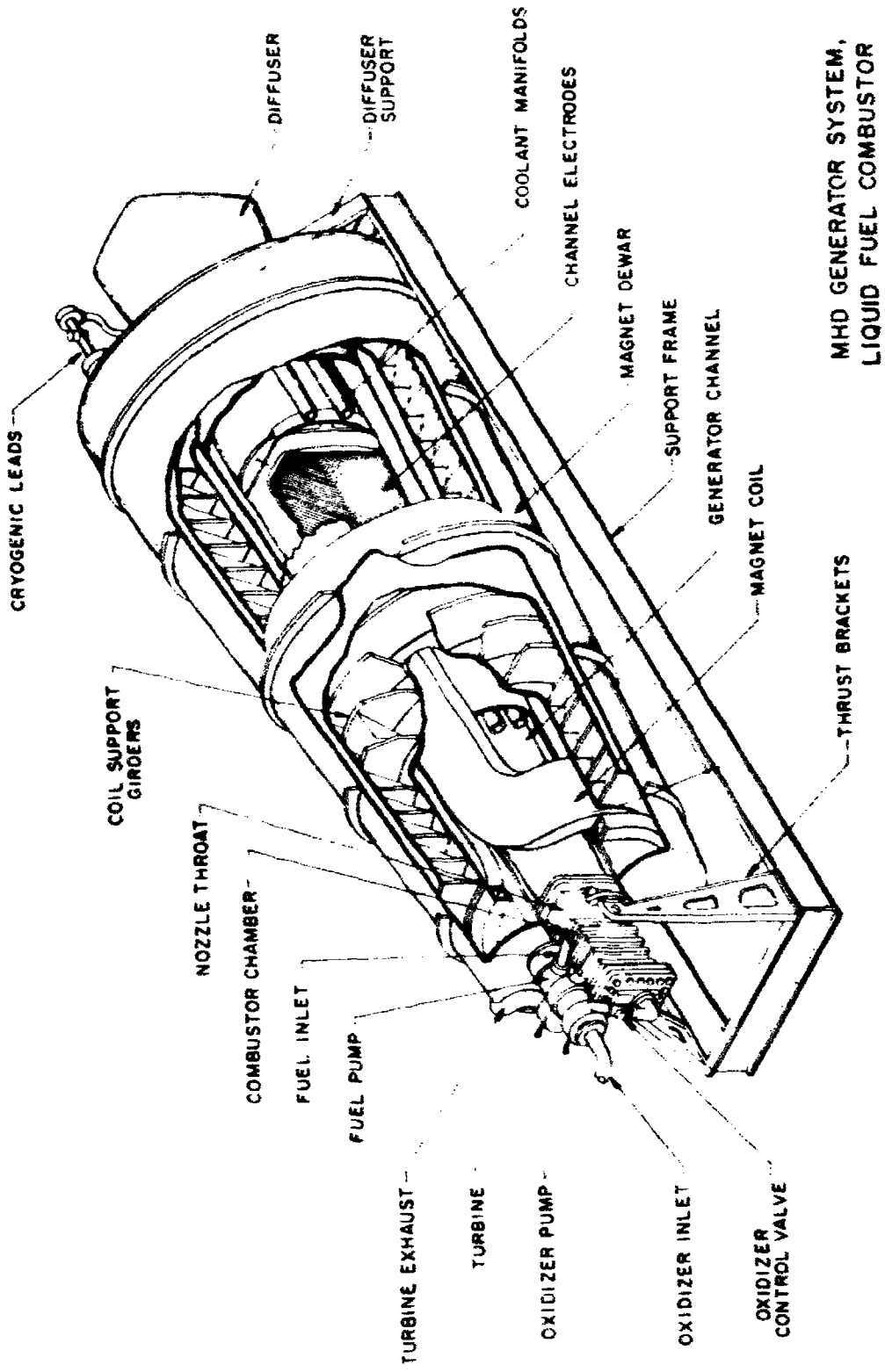
Figure 2. Phase D Prototype Hardware

SECTION II

SUMMARY AND CONCLUSIONS AND RECOMMENDATIONS

A. SUMMARY

The technical effort on this contract was directed toward completing a design for the hot gas flow train of a high power MHD system and a development test program to establish the system operating characteristics. Performance goals of 30 MW_e output power, 200 MW_e/m^3 specific power density, and one megajoule per kilogram specific enthalpy extraction were used for the hot gas flow train design. This section provides a brief system description and development test summary.

1. System Description

The gas generator system, shown in Figure 3, used a liquid reactant, rocket-type combustor with JP-4 as the fuel and liquid oxygen (LO_2) as the oxidizer. A water solution of Cs_2CO_3 seed was mixed with the fuel prior to injection into the combustor. The major components of the gas generator were the combustor/nozzle, injector, ignition system, and seed mixing system.

The diagnostics channel, which was built for the development test program, is shown in Figure 4. This channel was water cooled and was designed to be used with the heat sink combustor hardware. The major components of the diagnostics channel were the electrode frames, the filament wound fiberglass epoxy case, and the manifolds.

a. Combustor/Nozzle

The combustor was designed for nominal operating conditions of 30 kg/sec mass flow rate, 30 atm stagnation pressure, and a stagnation temperature of 3450 K. The combustor was to be capable of operating over a mass flow rate range of $\pm$ 20%. The primary considerations in the combustor design were high efficiency and uniform flow. To provide the high stagnation temperature, the characteristic velocity efficiency of the combustor/injector was required to approach 99%. This was significantly higher than has been demonstrated with previous LO_2/hydrocarbon combustors. To achieve this high efficiency, a combustor length from the injector face to the throat of 68.6 cm and a contraction ratio of two were selected. These provided the reactant stay-time necessary for the fuel droplet and seed particle vaporization while avoiding excess heat loss to the combustor wall.
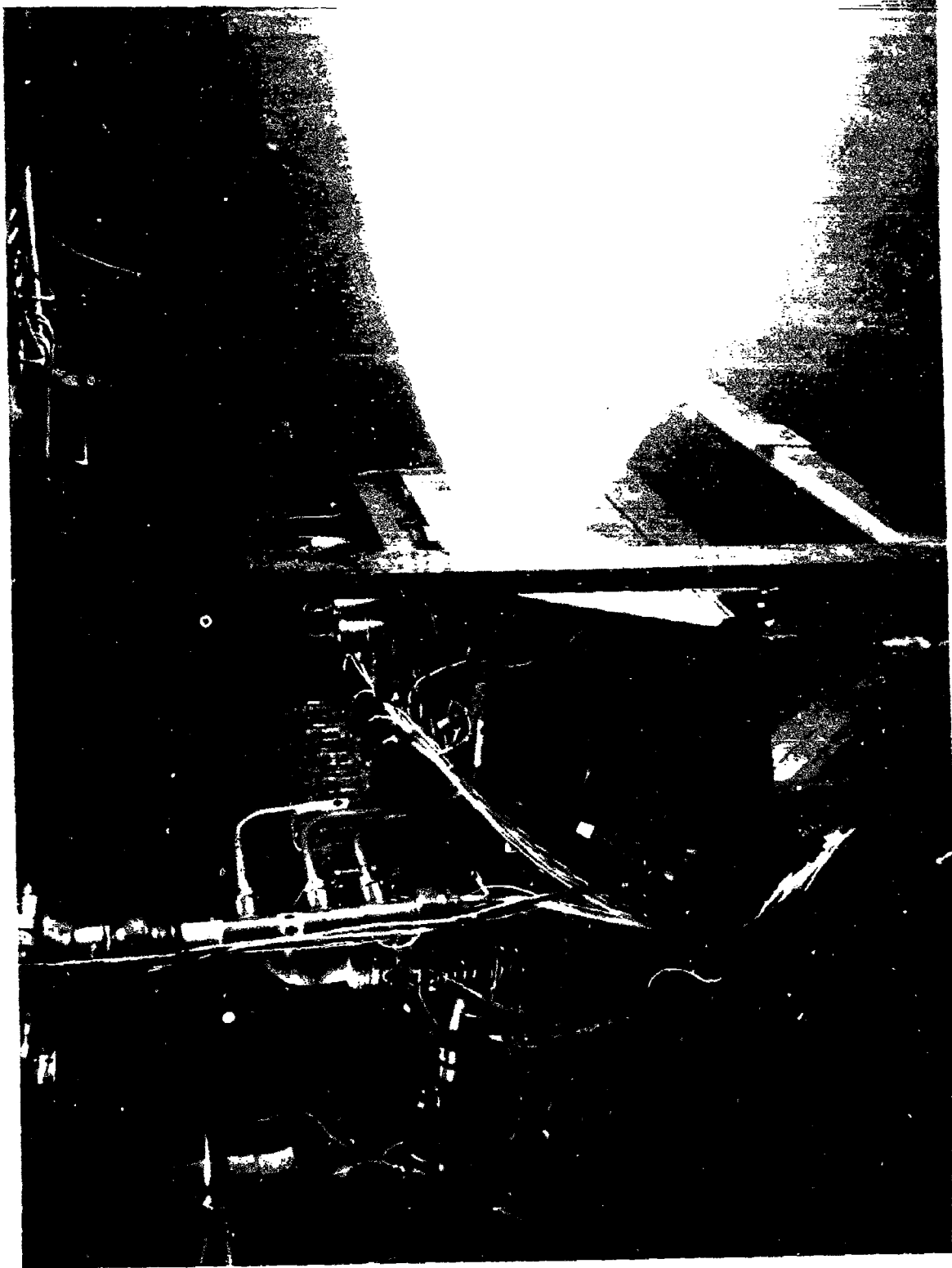
Fig. 5   Gas Generator System Test

7

DIAGNOSTICS CHANNEL SYSTEM

Diagnostics Channel

Water Manifold

Static Pressure Taps
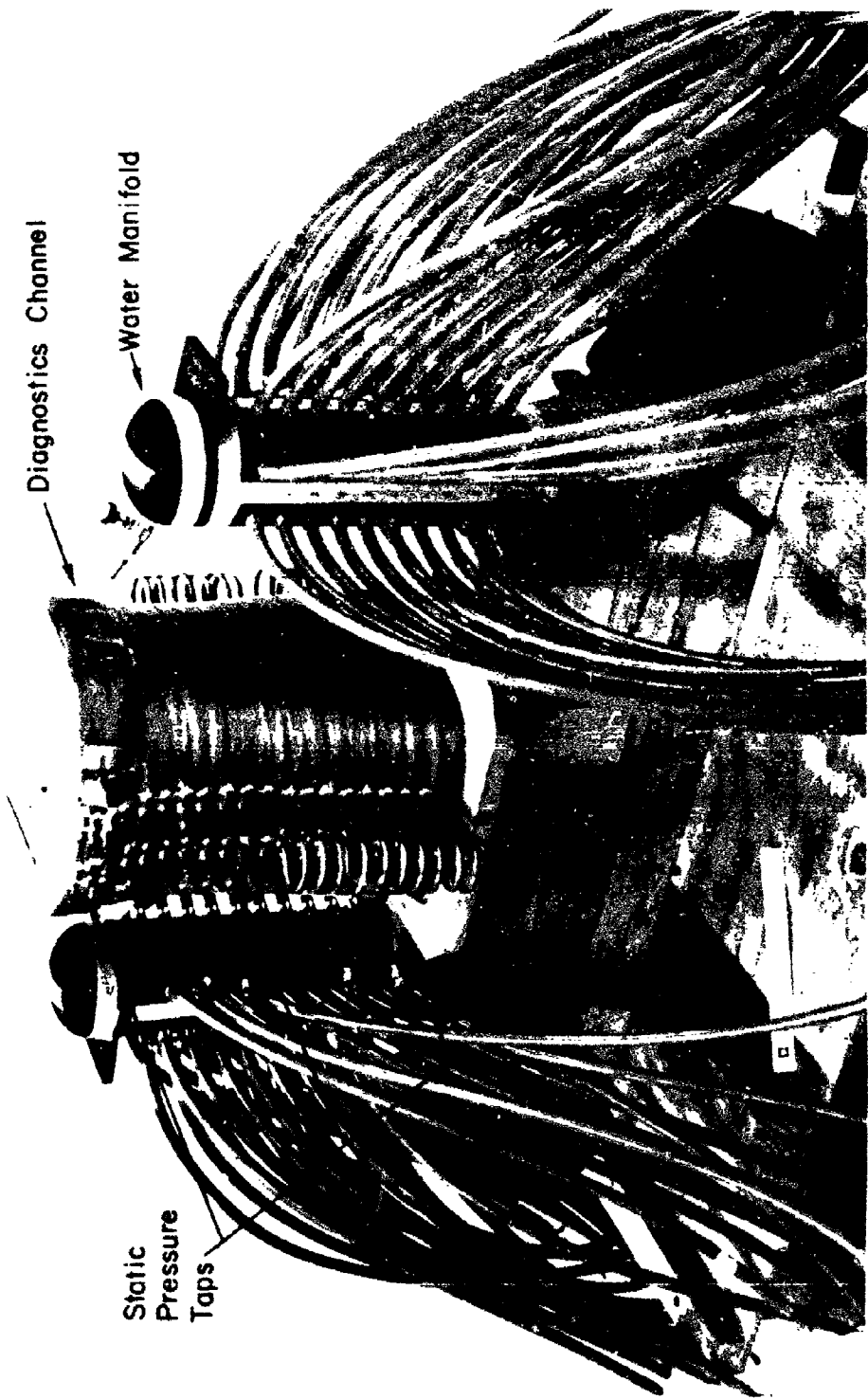
Figure 4. Diagnostics Channel.

A rectangular combustor cross section coupled with a two-dimensional expansion nozzle was selected. This design allowed matching the entrance of the rectangular high power MHD channel/diffuser while avoiding the flow cross section transition of a cylindrical combustor which would have created non-uniform flow.

The two-dimensional nozzle was designed to provide uniform flow at a Mach number of 2.07 at the exit plane. A two-dimensional, source flow nozzle contour was used to provide highly uniform flow at the exit. The peak-to-peak spatial variations in pressure in the gas core were calculated to be less than two percent of the mean value at the exit plane. The spatial variations in temperature and velocity were calculated to be less than 0.5% and 0.4%, respectively.

A lightweight, water-cooled combustor was designed. Water cooling was selected over fuel cooling for the initial design because of uncertainities in heat transfer rates and the long combustor length. The combustor used a thin inner liner of copper in which cooling grooves were machined. The coolant passages were closed by the electro-deposition of nickel to form the combustor shell. An outer structural shell of aluminum and the inlet and exit manifolds completed the design. The combustor was partially fabricated to the point of coolant groove machining. Electro-deposition process verification was also conducted. This demonstrated the fabrication technique, which was applicable to both the fuel and water-cooled combustors.

A heat sink combustor was fabricated for development testing. The internal geometry was identical to the cooled wall combustor. The combustor assembly consisted of four axial sections machined from oxygen free, high conductivity (OFHC) copper. The sections were bolted together to form the overall assembly. The joints were sealed with high temperature O-rings. The 7.6 cm thick copper walls acted as a heat sink allowing operating times of up to 3 sec. Water cooling was used at the throat to increase durability and at the nozzle exit to maintain the nozzle/diagnostics channel interface at less than 520 K.

b. Injector

The injector design was selected to provide high combustion efficiency with a uniform distribution of combustion products. Since combustion instability has been a frequent companion of high performance LO$_2$/hydrocarbon combustors, provisions were made to provide a method of damping instabilities.

A like-on-like injector element was selected based on successful use with LO$_2$/hydrocarbon rocket combustors. This element type combined the potential for high combustor efficiency with good stability characteristics relative to

9

element types such as a two-on-one element, in which fuel and oxidizer impinge prior to atomization. The element design was based on empirical relations developed for liquid injectors. Two injector designs were evaluated; 160 element (100 μm droplets) and 416 element (80 μm droplets) configurations. The 160 element injector was selected for fabrication. This design had good performance potential and was easier to fabricate than the higher element design.

The element size and injection velocity were selected to provide a mean fuel droplet diameter of $\approx 100 \mu$. The spray fans created by the individual elements were canted to provide a high degree of mixing. By producing this high degree of atomization, a combustion efficiency in excess of those demonstrated in previous rocket engines was targeted. When incorporated into the combustor cross section, this resulted in an element density of one element per 1.63 cm^2.

The elements were arranged in a rectangular pattern with the fuel elements on the outer periphery. A "quarter wave slot" was included around the injector face to provide acoustic damping. The area used for the quarter wave slot was six to eight percent of the injector surface area and was limited to avoid recirculation areas which could have diminished the uniformity. An allowance for additional acoustic cavity volume was provided through the use of an acoustic spacer in case additional damping was required.

The injector was fabricated with an OFHC copper face which was cooled by the reactants flowing through the injector. The injector flange, face plate and manifold were machined separately and brazed into an assembly. The injector fuel and oxidizer manifolds were external to the injector body.

During this program several events influenced the injector hardware: (1) the injector body was rebuilt following an internal failure because of a machining error; (2) the acoustic spacer was modified to provide added pressure oscillation damping; and (3) the acoustic spacer was modified for a water cooled design because of unexpected heating.

c. Ignition System

Dual augmented spark ignitors (ASI) were used to ignite the reactants in the combustor. The ASI's consisted of small gaseous oxygen/methane (GO_2/CH_4) combustors mounted on each side of the combustor approximately 2 cm from the injector. The GO_2/CH_4 mixture was ignited by a spark to produce a 1250 K gas stream at a flow rate approximately one-half percent of the nominal combustor flow rate. This hot gas stream was the ignition source for the main reactant.

10

The ASI's were started at the same time that LO$_2$ was introduced into the main combustor and continued until 90% of nominal combustion pressure was attained. The ignitor units were fabricated of OFHC copper. An exciter and spark plug unit of the type developed under the J-2 type rocket engine program were used.

d. Seed Mixing System

The Cs$_2$CO$_3$ seed was stored as a 71% by mass concentration in water. The Cs$_2$CO$_3$ solution was mixed in-line with the fuel using a two-stage mixer. and injected into the combustor through the fuel orifices. In this manner uniform Cs$_2$CO$_3$ concentration across the combustor was provided as well as the flexibility to change rapidly the concentration of the seed in the hot gas. The use of water led to a slight loss in temperature but this was offset by the increased convenience. The arrangement was calculated to produce a mean Cs$_2$CO$_3$ solution droplet size of 60-80 μ.

To promote the mixing of the JP-4 and the Cs$_2$CO$_3$ solution, a surfacant, SPAN-80, was premixed at a seven percent concentration with the JP-4. The SPAN-80, being a hydrocarbon, had a negligible effect on flame temperature and maintained the uniform distribution of the seed droplets in the fuel during the time (less than 0.2 sec) required for distribution to the injector.

e. High Power MHD Channel/Diffuser

The high power channel/diffuser was designed for nominal operating conditions of 30 kg/sec mass flow and combustor temperature and pressure stagnation conditions of 3450 K and 30 atm, respectively. The channel/diffuser was designed to operate over a range of variation in the mass flow rate of $\pm$ 20%. The primary considerations in the channel/diffuser design were electrical output power and lightweight construction. To achieve the lightweight construction, the use of metal was reduced to a minimum. This was accomplished by using, for structural support, a filament wound fiberglass epoxy shell.

The design of the high power MHD channel/diffuser incorporated water cooling to permit steady-state operation. Electrode frames, consisting of copper tubing, side rails and corner blocks, were formed and assembled around a contoured mandrel. This mandrel was designed to be used as the sizing guage and assembly station for the complete channel/diffuser assembly. The electrodes were completed using a zirconia to fill copper electrode cups containing Inconel screens. The interelectrode insulating ceramic was then emplaced between the electrode frames. Finally, the case assembly, consisting of an RTV layer and filament windings, was fabricated in place around the electrode frames assembly. Although the design of this channel was completed, only several sample electrode frames and full size sections of the fiberglass case were fabricated.

The high power MHD channel/diffuser design consisted of 159 electrode frames, and an exit and an entrance duct. The overall length of the channel/diffuser was 2.55m. The channel/diffuser design inlet cross section was 181mm by 197mm. The design exit cross section was 532mm by 672mm. Four different type of electrode frames were used in the channel design. These were upstream perpendicular frames, upstream transition frames, diagonal frames, and downstream transition frames. (See Figure 5). Details of each of these electrode frames are presented in more detail in Chapter IV.

Each of the perpendicular and diagonal electrode frames consisted of two half frame cooling loops, which were connected in parallel in the entrance region of the channel and in series in the exit region of the channel. No more than two half from cooling loops were connected in series. The transition electrode frames, because of their non-standard shape, required special cooling connections for each transition frame. A more detailed presentation of the cooling system design is provided in Chapter IV.

f. Diagnostics Channel

A diagnostics channel, consisting of forty electrode frames oriented perpendicular to the gas flow, was designed and constructed for use during the development test program. This channel was 453 mm long and had an inlet cross section identical to the high power MHD channel/diffuser and an exit cross section of 197 mm by 266 mm. The electrode pitch was 11.3 mm. This channel was very similar in design and construction to the channel/diffuser described in the previous section. The diagnostics channel was instrumented to provide temperature, pressure, vibration, and conductivity measurements during the development test program.

2. Development Testing

Fifty-five development tests were performed to check out the gas generator operation and verify the combustor performance. Thirty-one tests of the ASI system were conducted to evaluate the ignitor operation and verify the compatibility of the ASI with the combustor/injector components. Following these tests, twenty-four tests of the gas generator system were conducted. The initial series was conducted to verify combustor ignition and develop the start sequence. The next series of tests were completed to evaluate the combustor performance. These tests were conducted with LO_2 and JP-4/SPAN-80 without any Cs_2CO_3 solution present. Mixture ratios from 2.5 to 3.3 and combustor pressures from 25 to 36 atm were tested. In the course of these tests, the shutdown and purge sequence was modified to eliminate the presence of carbon formation during the cutoff transient. Following this test series, tests with Cs_2CO_3 seed solutions to five to ten percent of the total mass flow were conducted. These tests evaluated combustor performance and checked the start sequence with the Cs_2CO_3 solution. A single test to evaluate the dynamic stability of the combustor was conducted. This resulted in unstable combustion. Based on this test, a modified acoustic cavity was fabricated to provide increased damping. No self-excited instabilities occurred, and further

12
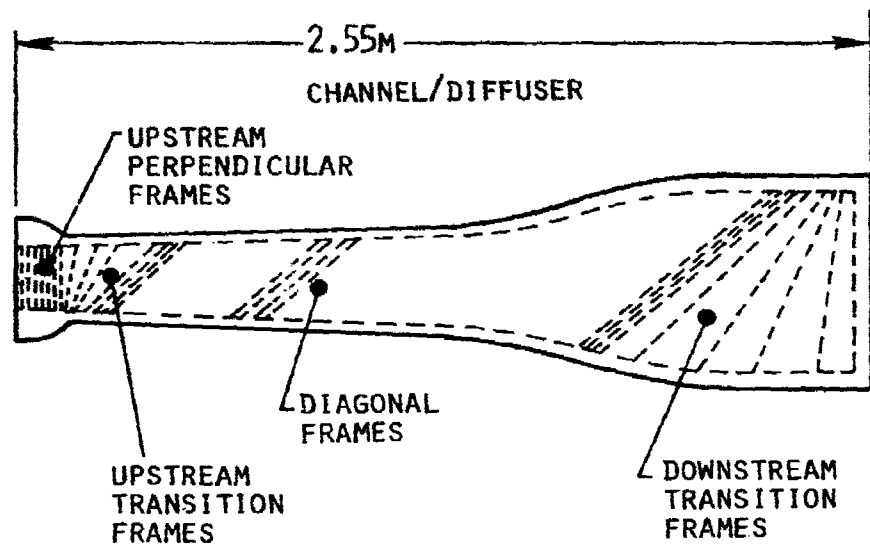
(A)
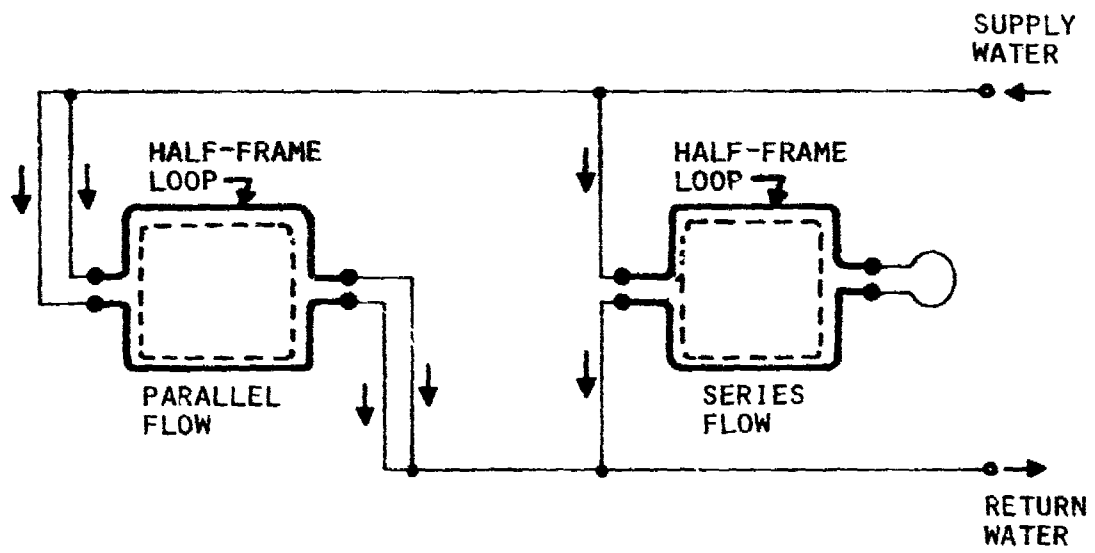
(B)

Figure 5 . Channel/diffuser electrode frames.

tests with triggered instabilities were not performed. Following this, the electrical conductivity of the gas for various mixture ratios and Cs_2CO_3 solution flow rates was evaluated using the diagnostics channel. The hardware installed on the Bravo I Test Stand at SSFL is shown in Figure 6.

a. Gas Generator Operation

The operation of the gas generator is illustrated by the combustor and ASI pressure traces shown as a function of time and sequence events in Figure 7. Following the priming of the lines down to the main control valves and setting the tank pressures, the signal for ignition start was given. From this point the entire operation was automatic. The ASI was ignited first as shown by the pressure rise in Figure 6. Next, the liquid oxygen valve was opened, and when the oxidizer manifolds were primed, the fuel valve was opened and gas generator combustion began. This is illustrated by the combustion pressure rise of Figure 7. When the combustor pressure reached 80% of the nominal pressure, the ASI's were cut off. Following approximately 2.5 sec of operation, the cutoff signal was given. Because of the valve sequencing and closure times, the chamber pressure decay occurred over a period of about one second.

Reliable ASI operation was verified in 31 ignition system tests. Combustor ignition occurred reliably in each of the 24 combustor starts. Since the Cs_2CO_3 solution was introduced after the combustor ignition had occurred, the solution had no impact on the gas generator start.

High pressure gaseous nitrogen purges were used during the start and cutoff processes. In the early tests the shutdown of the gas generator produced very fuel rich operation. This resulted in carbon formation on the combustor/ nozzle walls. Attempts to eliminate the carbon formation through minor sequence modification were unsuccessful. Consequently, the purge flow rate and pressure were increased resulting in a clean, carbon-free shutdown.

b. Combustor Performance

The combustor performance was measured by the characteristic velocity efficiency, η_c^*. Values of η_c^* for several tests are presented in Figure 8. Three effects were noted. First, the η_c^* value of $\approx 98.5\%$ was very high for LO_2/hydrocarbon combustors. Rocket engine combustors which have undergone extensive development using LO_2/RP-1 have had η_c^* values several percent lower than this value. This high efficiency was attributed to the injector orifices which were a factor of two smaller than in previous LO_2/hydrocarbon injectors. Second, the efficiency decreased as the mixture ratio was decreased. Since the injector was designed for a mixture ratio of 3.34,* this decreased efficiency at off-design mixture ratios was not unexpected. Third, combustion efficiency increased when the Cs_2CO_3

---

* All mixture ratios and seed percentages are identified on the basis of weight.
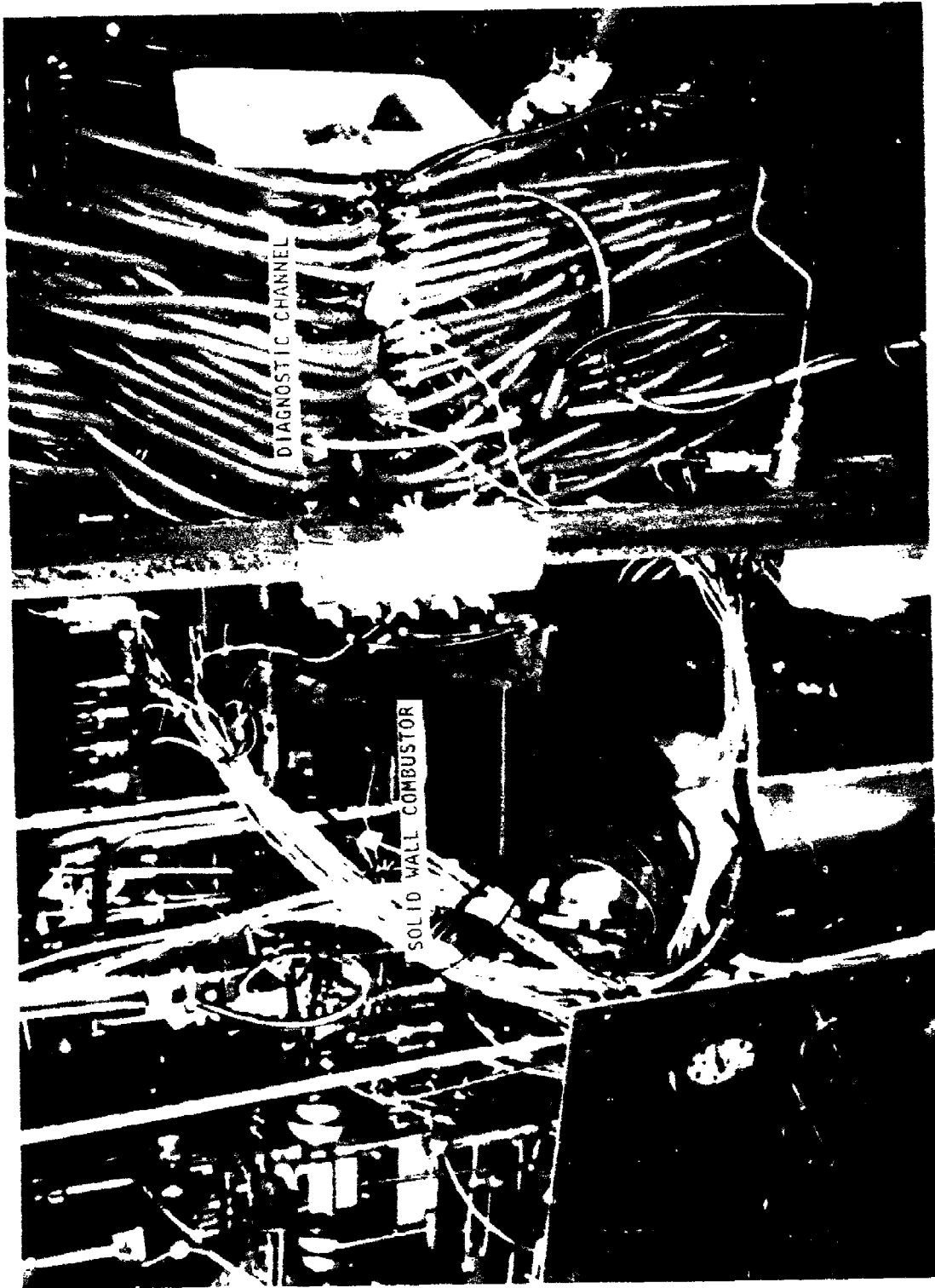
Figure 6. Development Test Hardware Installed at SSFL, Bravo 1 Facility.

15
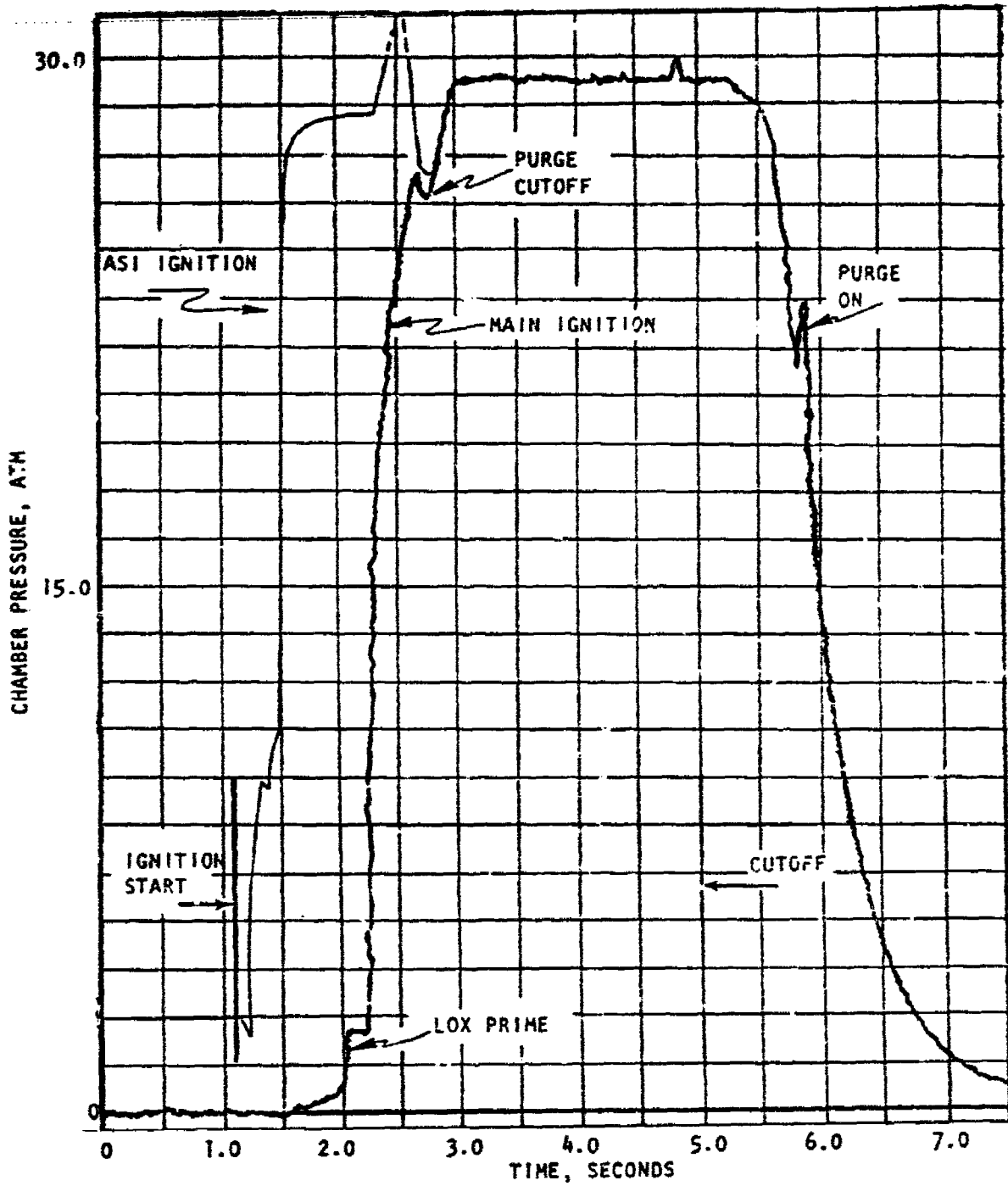
Figure 7. Gas Generator Pressure Time Trace.

16
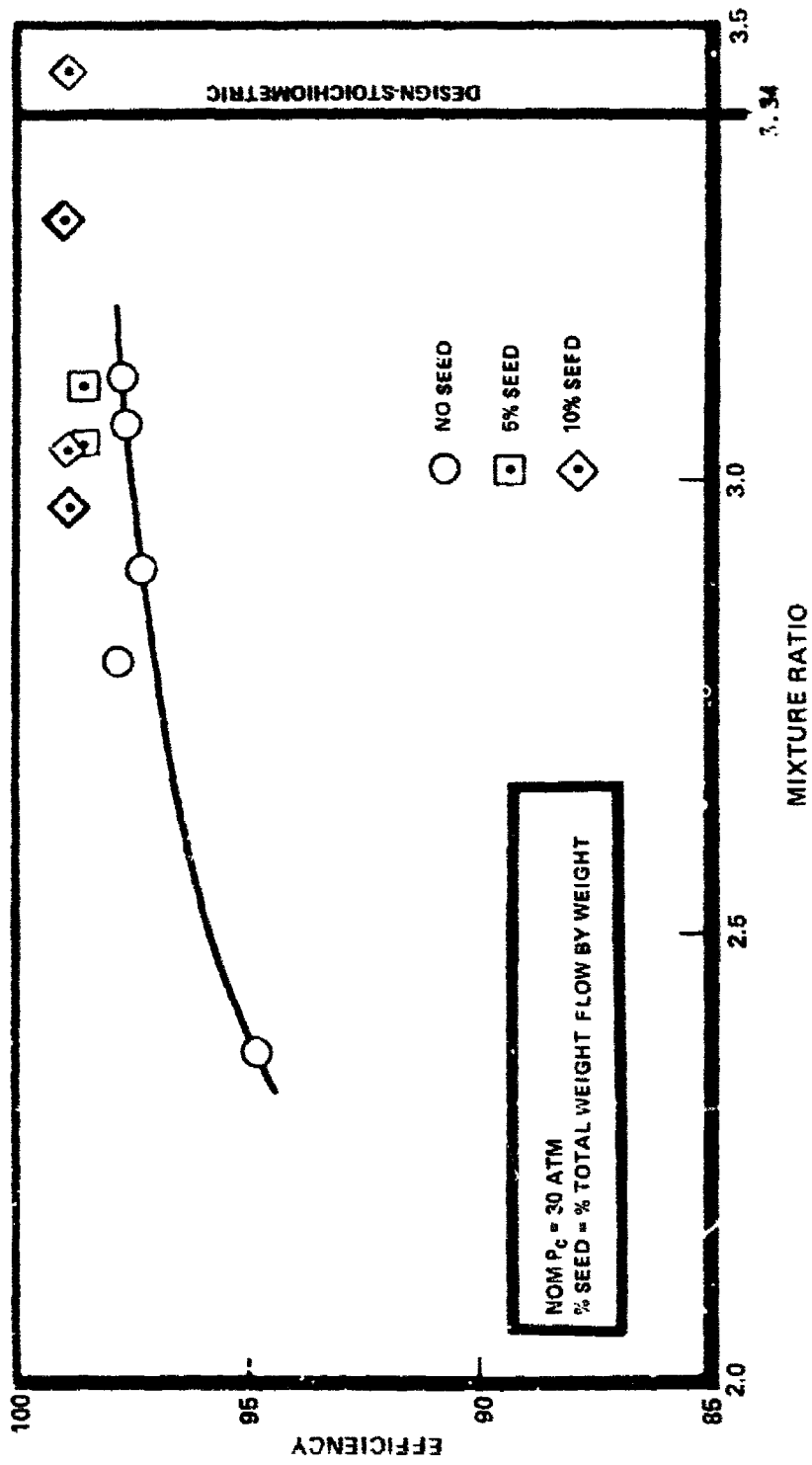
Figure 8. Characteristic Velocity Efficiency

solution was added. This increase of 0.8% occurred in a test with the Cs_2CO_3 solution amounting to 5% of the total mass flow or approximately 30% of the fuel mass flow.

A plot of the static wall pressure measurements in the combustor is presented as Figure 9. Prior to the contraction section, the major mechanism for pressure drop was heat addition resulting from combustion. The pressure profile, therefore, gave an indication of the completeness of the combustion. The pressure profile indicated that the major portion of the combustion occurred within 25-30 cm of the injector. This indicated that the pressure measurement at the 48 cm point, which was used in the characteristic velocity calculations, should have been a reliable indicator of the ηc^*, and that there was a potential for reducing combustor length.

c. Combustor/Nozzle Thermal Performance

The experimental gas side heat transfer coefficients were determined by temperature measurements from the eleven "heat flux" meters located along the combustor wall. These heat flux meters are made by machining copper plugs in the combustor wall. The machining operation forms an annular groove around the plug which acts as an isolation gap. A simple thermocouple records the backside plug temperature and analysis results in the thermal conditions at that specific location. Several hot gas side film coefficient profiles are presented in Figure 10. All film coefficients were lower than predicted. The maximum film coefficient values were 65-80% of the initial prediction. The film coefficient values varied with the amount of Cs_2CO_3 solution and mixture ratio. A third variable which influenced the film coefficient was the cleanliness of the combustor walls. Oxidation from the atmosphere and minor carbon deposition significantly reduced the heat flux. The test data substantiated the deposition of a minute carbon layer on the upstream combustor walls where experimental data was well below the analytical prediction. The extent of carbon deposition depended on the local gas mass flux. The higher the mass flux, the lower the carbon deposition and resistance. Redundant instrumentation in the convergent section showed the heat transfer coefficient for the contoured wall to be slightly higher than for the flat wall at the same axial location.

Because of the limited space, heat transfer measurements were not possible at the throat. By theoretically scaling the combustor/nozzle measurements, the throat film coefficient was estimated to be $0.44 - 0.59$ w/cm^2 K. These values were less than the values initially predicted.

d. Pressure Oscillations

The high frequency combustor pressure oscillations were measured at three locations in the combustor. In the initial testing pressure oscillations were observed in the 800 Hz and 4900 Hz regions. These corresponded approximately to predictions of the longitudinal resonant mode and the second transverse resonant mode of the combustor. The oscillations were within the general CPIA criteria for
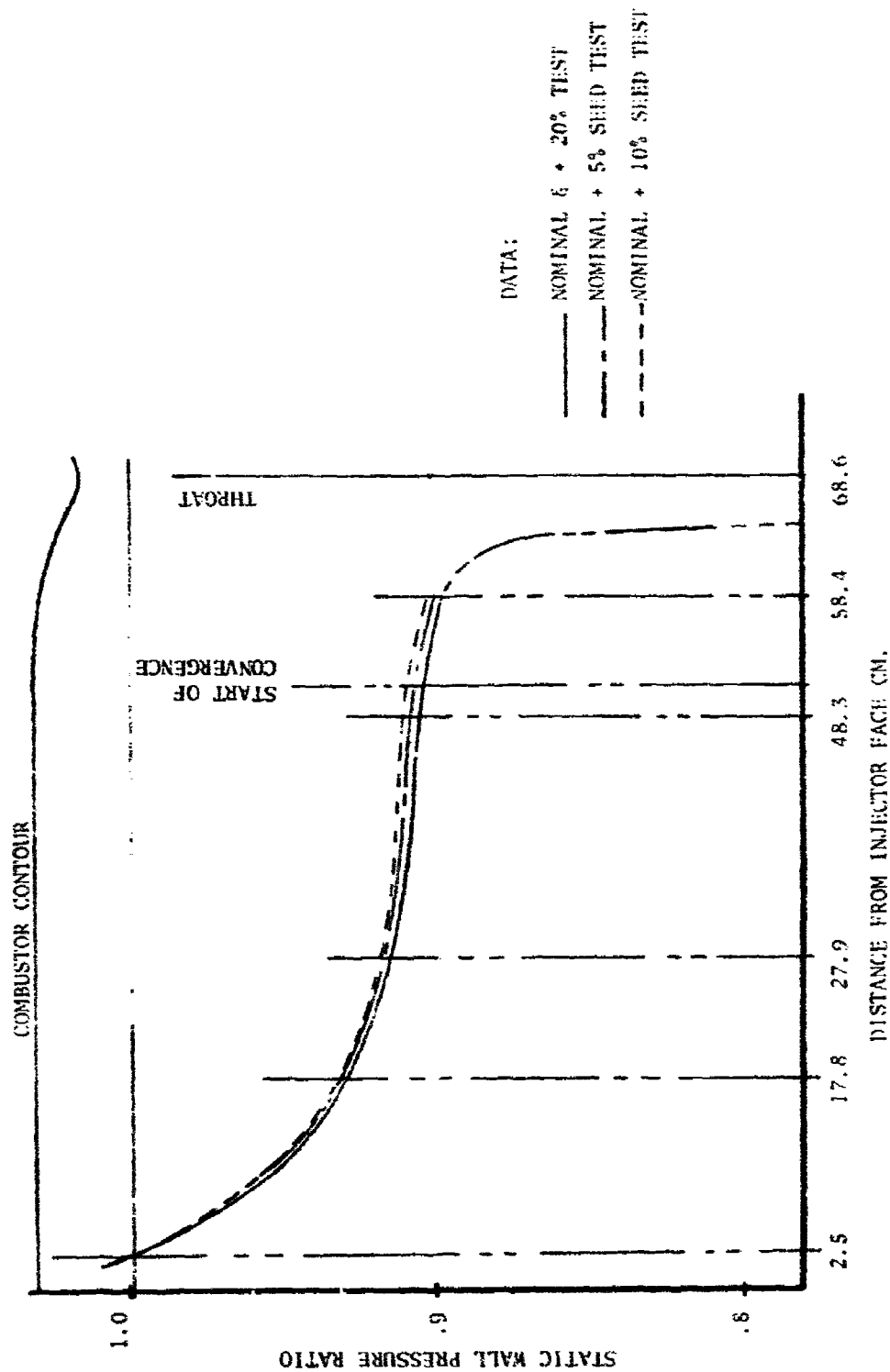
Figure 9. COMBUSTOR STATIC PRESSURE PROFILE

19
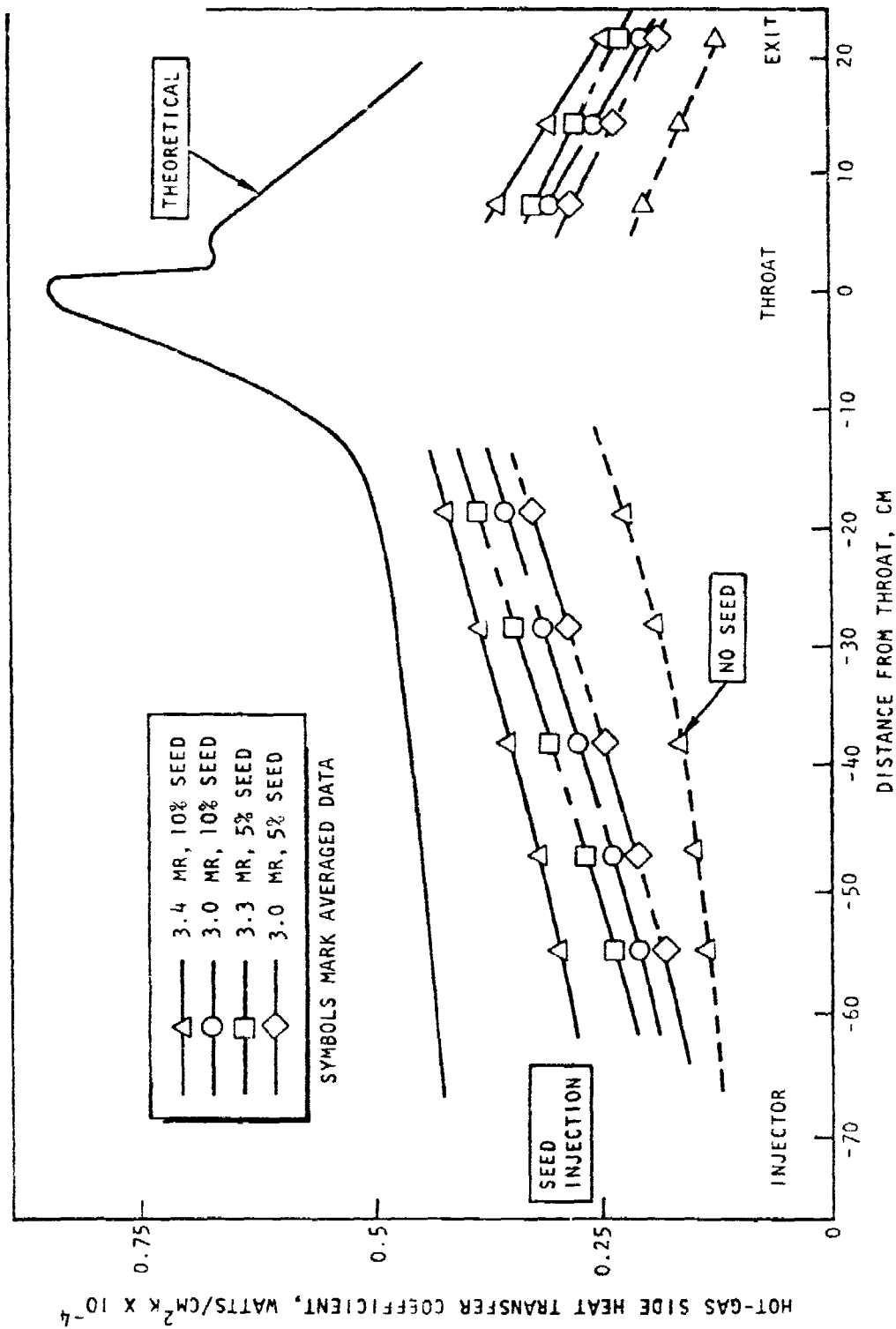
Figure 10. Measured Gas-Side Heat Transfer Coefficient vs. Distance from the Throat.

20

mode of the combustor. The oscillations were within the general CPIA criteria for stable combustion but somewhat higher than desired for MHD operation.[2]

The dynamic stability of the injector was assessed through the deliberate introduction of a sharp pressure pulse in the combustor. Unstable operation resulted with peak amplitude at 2800 Hz, a first transverse mode. Based on the results of this test, the acoustic slot was modified to increase damping. Although the dynamic stability was not verified, no indication of instability was observed and pressure oscillations were significantly reduced. This is illustrated in Figure 11 where the net peak to peak pressure oscillation was reduced by a factor of three with the introduction of the increased damping. The level of the pressure oscillation was less than 2.7% peak-to-peak. During normal operation no significant oscillation levels of the first transverse resonant modes were observed.

e. Conductivity Measurements

A test series to measure the electrical conductivity of the gas was also completed. The diagnostics channel along with an external power supply to provide electrical current to the channel was used for these measurements. The measured electrical conductivities for each of the four conductivity tests are shown in Figure 12. These results showed the effect of the lower mixture ratio on inlet electrical conductivity of the gas. A maximum inlet conductivity of 15 mhos/m occurred for a mixture ratio of 3.01 and a Cs_2CO_3 percentage of 5.15%.* The lowest inlet electrical conductivity of 14 mhos/m occurred for a mixture ratio of 3.40 and a Cs_2CO_3 percentage of 9.90%.* These results indicated higher electrical conductivity at a constant mixture ratio for a five percent Cs_2CO_3 flow rate than for a ten percent Cs_2CO_3 flow rate. Similarly, the electrical conductivity at a constant Cs_2CO_3 percentage was greater for the lower mixture ratio.

If the total combustor enthalpy losses were approximately 120 cal/g, the inlet electrical conductivity results agreed with the theory. For these test conditions the total combustor stagnation enthalpy was 2200-2250 cal/g. Except for test 007, the decrease in electrical conductivity with distance from the diagnostics channel/ nozzle interface closely approximated the theory. These results indicated that the electrical conductivity, although not optimized in only four tests, was above the lower limit of the design range of the high power MHD channel/diffuser.

---

* All $Cs_2 CO_3$ percentages are based on the $Cs_2 CO_3$ mass flow as a percentages of the total reactant mass flow.

---

[2] "Combustion Stability Specifications and Verification Procedures for Liquid Propellant Rocket Engines," CPIA Publication 247, October 1973.

21

PRESSURE- TIME TRACES

ORIGINAL ACOUSTIC SPACER
0% SEED
O/F = 3.1

MODIFIED ACOUSTIC SPACER
10% SEED
O/F = 3.0

PRE-RUN NOISE

PRE-RUN NOISE

COMBUSTION

COMBUSTION

4800 HZ

750 HZ

5.4 atm

5.4 atm

13.6 atm

13.6 atm

NET atm(PEAK-TO-PEAK) = 2.7

= 0.87
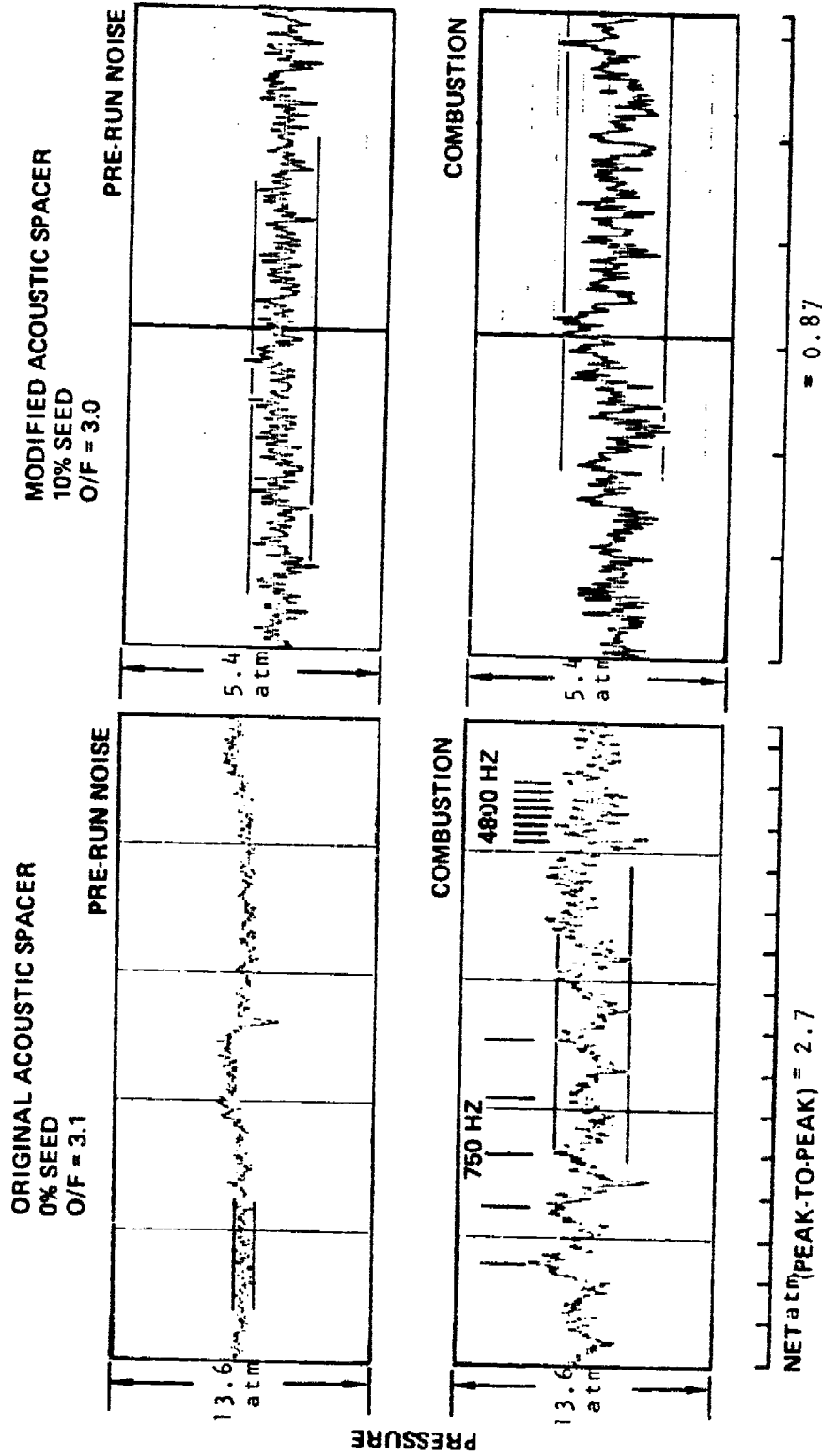
PRESSURE

TIME, MILLISECONDS

Figure 11. Combustor Pressure Oscillations.

22
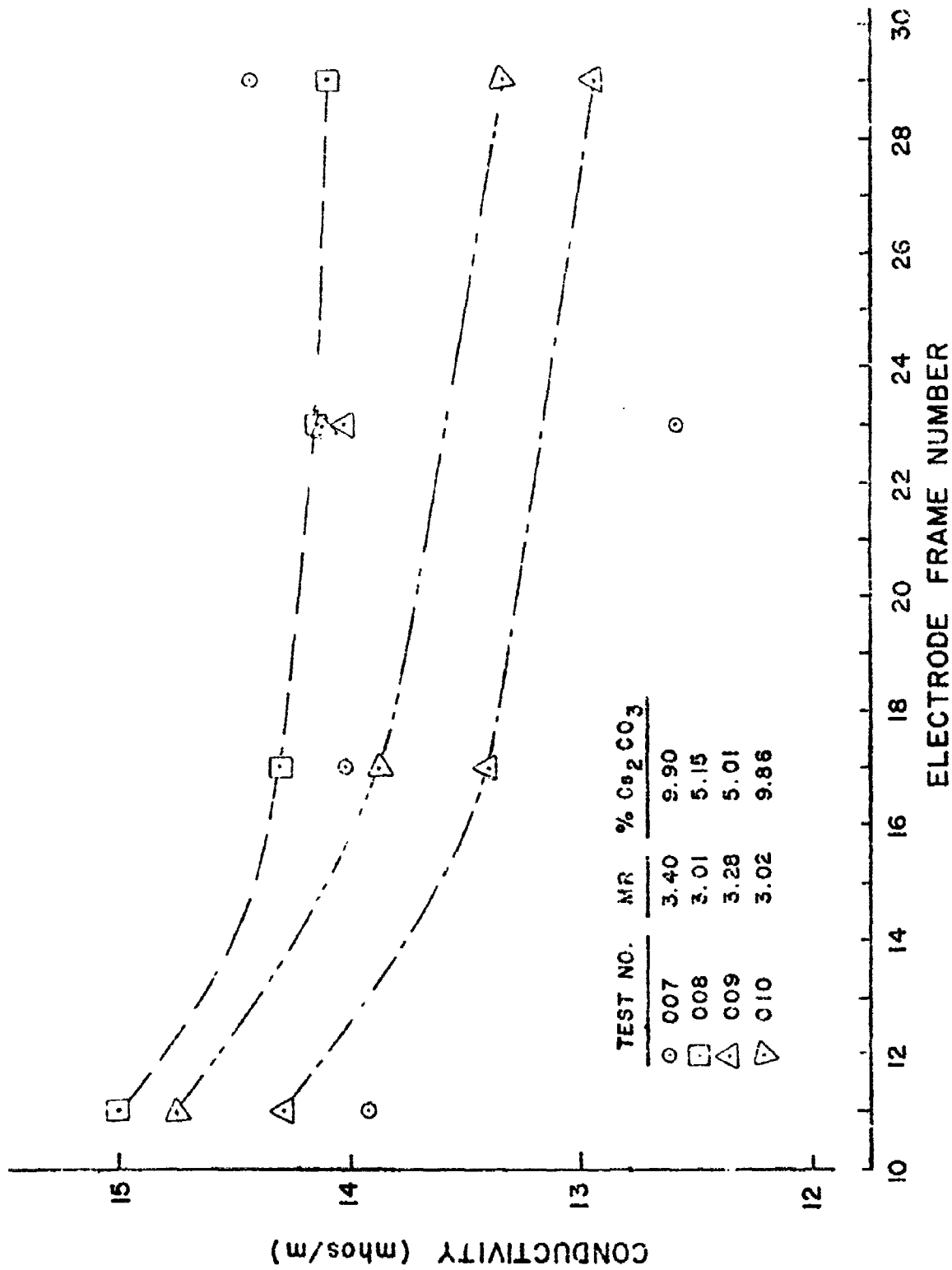
Figure 12. Gas Electrical Conductivity Measurements.

TEST NO.	MR	% Cs$_2$CO$_3$
⊙ 007	3.40	9.90
☐ 008	3.01	5.15
△ 009	3.28	5.01
▷ 010	3.02	9.86

Axis labels: CONDUCTIVITY (mhos/m) versus ELECTRODE FRAME NUMBER

f. Diagnostics Channel Thermal Performance

The diagnostics channel wall heat flux was determined for six axial locations by measuring the cooling water temperature rise. Figure 13 shows the experimental heat flux for test 008. Except for the entrance region of the diagnostics channel, the wall heat fluxes were relatively insensitive to variations in the mixture ratio or Cs_2CO_3 percentage. At the diagnostics channel entrance the heat flux increased for each test above the value for the previous test. No explanation for this anomaly was available.

Figure 13 also shows the comparison between the theoretical and the experimental heat flux for the conditions of test 008. Depending on the axial location, the experimental heat flux ranged from 60 to 72% of the theoretical value. The high theoretical heat fluxes were based on matching the boundary layer conditions at the diagnostics channel/nozzle interface. Consequently, any variations from the combustor/nozzle heat flux calculations were also present for similar calculations in the diagnostics channel.

g. Diagnostics Channel Vibration

High frequency measurements of the diagnostics channel were recorded during the development test program. These five accelerometer measurements showed that the diagnostics channel behavior was well within the design limits. The experimental vibration frequencies were above the theoretical pitch and yaw values; hence, the channel appears to have been isolated from these modes. The wall bending deflection frequency and the frame bending frequency were of the same order of magnitude as the 400 Hz frequency recorded during the experiments.

During steady state operation the acceleration levels of the most downstream accelerometer were the largest. These values reached a maximum amplitude of 13.5 g at the position most downstream from the diagnostics channel/diffuser interface. The diagnostics channel was designed for a 25 g load in each direction, single amplitude. Thus, the vibration load was only one-half the design value.

B. CONCLUSIONS AND RECOMMENDATIONS

Phase B of the HPMS program has been completed, and the interpretation of the experimental data obtained has been finished. Based on the hardware design, the hardware fabrication and installation, and the development test program, several significant conclusions and recommendations were made. These are discussed in detail in the following two subsections.
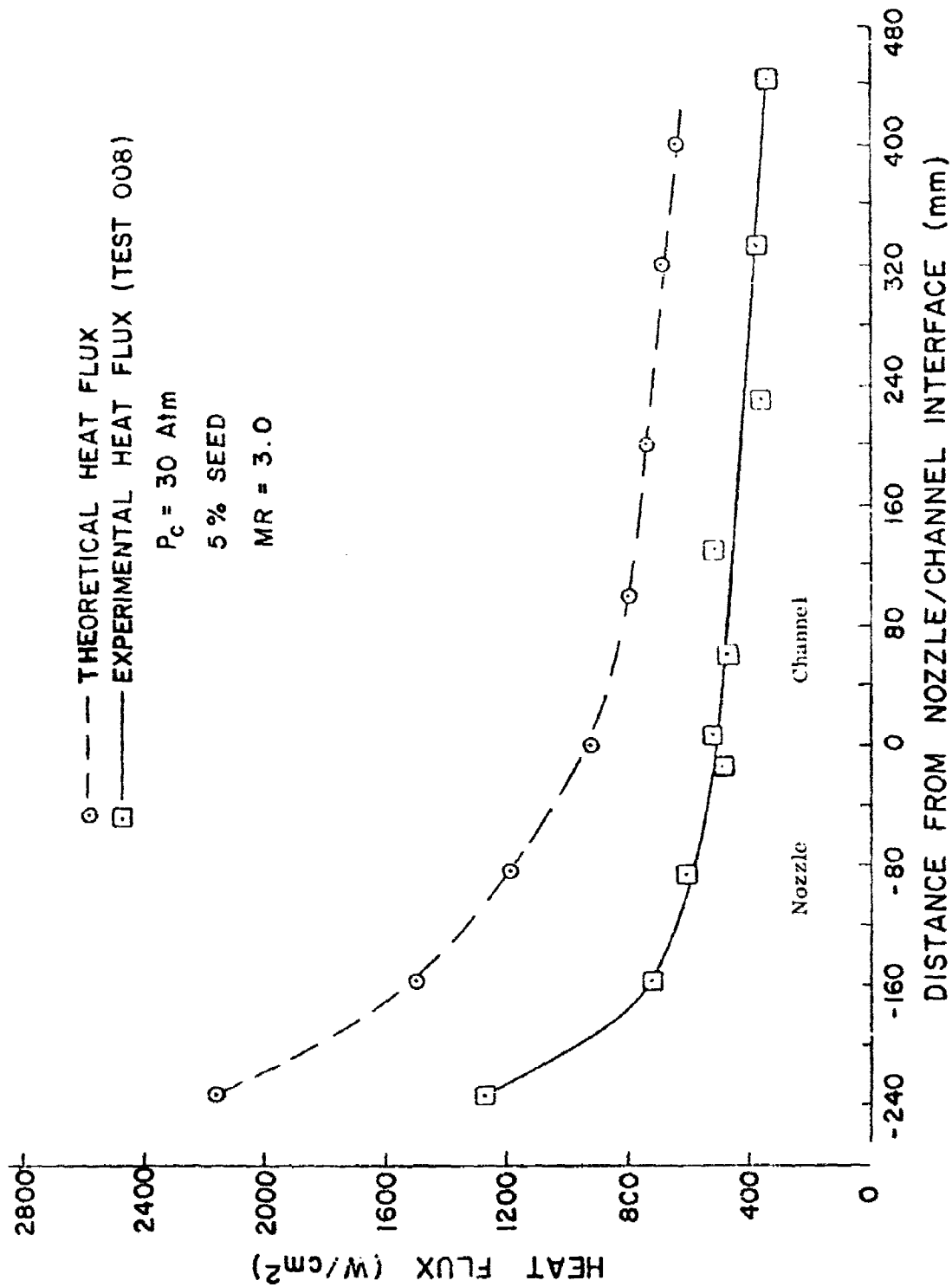
Figure 13. Axial Heat Flux Distribution.

THEORETICAL HEAT FLUX
EXPERIMENTAL HEAT FLUX (TEST 008)

P_c = 30 Atm
5 % SEED
MR = 3.0

Nozzle   Channel

DISTANCE FROM NOZZLE/CHANNEL INTERFACE (mm)

HEAT FLUX (W/cm²)

1. Conclusions

The results of the HPMS development program have provided additional information in the development of lightweight, high performance MHD generator development. Previous development programs have provided the basis for the technical activity of this program.[3,4] These technical efforts led to the design/development of this compact, transportable MHD generator systems capable of producing tens of megawatts of electrical output power. This power level resulted in an increase in the pertinent performance parameters such as enthalpy extraction ratio, volumetric efficiency, and specific power density. As demonstrated during this program, these increases in the performance levels can be obtained with the present design approach. These following specific conclusions resulted from the results of the development test program as well as the hardware design and fabrication portion of the effort.

A lightweight hot gas flow train consisting of a lightweight, cooled combustor/nozzle and a lightweight, high power MHD channel/diffuser was designed. The major fabrication processes for both of these components were demonstrated to be feasible. With the heat transfer data from the development test program to confirm the cooling system design, both of these components could be fabricated.

Combustor characteristic velocity efficiency values as high as 98.9% were achieved. This efficiency was three to four percent higher than has been achieved in previous LO_2/hydrocarbon combustors and was achieved with a relatively conventional rocket motor injector design. An injector with more, but smaller elements should offer improved efficiency. A review of the experimental combustion pressure profile indicated that combustion was complete and that a reduction in combustor length of 23-28 cm could be completed without any performance degradation.

Combustor heat flux levels were $\approx 60\%$ of the initially predicted values for a mixture ratio of three and a Cs_2CO_3 concentration of 5% of mass flow. Based on these lower values and a combustor length reduction, a regeneratively cooled combustor appeared feasible. However, the combustor heat flux level varied significantly with the seed concentration and combustor cleanliness. These effects must be better defined to confirm the heat flux level. The reactant injector performed reliably and had no apparent development problems such as

---

[3] O. K. Sonju, J. Teno, R. Kessler, L. Lontai, and D. E. Meader, "Status Report on the Design Study Analysis and the Design of a 10 MW Compact MHD Generator System," AFAPL-TR-74-47, Part II, June 1974.

[4] D. W. Swallom, O. K. Sonju, D. E. Meader, and G. T. Heskey, "MHD Lightweight Channel Development," AFAPL-TR-78-41, June 1978.

hot spots. The acoustic spacer around the injector showed evidence of hot gas recirculation heating. Although this was acceptable for this program, some revision of this area should be completed before long duration use.

The peak-to-peak combustor pressure oscillations during steady-state conditions were 2.7% of the nominal combustor pressure. This level of oscillations was low for a liquid/liquid reactanct injector and was acceptable for MHD operation. No inherent spontaneous instabilities were encountered in any of the twenty-four combustor tests. However, the combustor has not been demonstrated to be dynamically stable. The single dynamic stability test resulted in an instability and indicated that combustion was sensitive to disturbances. Although additional damping was provided and eight additional tests were conducted after the dynamic stability test without any incidents, additional testing is required to established dynamic stability. Previous experience has shown unstable combustion tends to increase the mixing process. This change is reflected in higher performance when mixing is poor but has also shown degradation of performance when mixing was good.

The Cs_2CO_3/H_2O solution and the SPAN-80/JP-4 mixing approach to seed solution injection operated successfully. Special attention was given to system cleanliness and solution preparation since the seed solution was corrosive and both mixtures were sensitive to impurities. In addition, since the introduction of water reduced the combustor stagnation temperature and hence, conductivity, alternate Cs_2CO_3 carriers should be evaluated.

The ASI system using GO_2 and CH_4 operated successfully during the start sequence in all twenty-four combustor tests. The system shutdown sequence produced consistent cut-off conditions with little or no carbon, fuel, or seed material present after shutdown. The minimum start time was 1350 msec, and the minimum shutdown time was 850 msec. The achievement of start and shutdown times close to one second appeared to be feasible. Some additional sequence development and hardware modification would be necessary.

The diagnostics channel tests produced gas electrical conductivities of 14-15 mhos/m for the various mixture ratios and Cs_2CO_3 percentages tested. Electrical conductivities in this range were above the lower limit of the electrical conductivity required for obtaining the design power level of 30 MW_e. These tests also demonstrated the compatibility of the nozzle/diagnostics channel interface. This same type of interface was used for the high power MHD system design.

2. Recommendations

Based on the results of this phase of the overall HPMS program, the following recommendations were made. Most of these recommendations resulted from the development test program and the interpretation of the test results.

Since only four gas electrical conductivity tests were completed, several additional tests should be conducted to optimize the conductivity. These tests should include a more comprehensive combination of the mixture ratio, Cs_2CO_3 percentage, and the combustor mass flow rate. Instrumentation should be reviewed based on the accumulated test data and modified if necessary to acquire additional measurements. In addition, fuel/Cs_2CO_3 carrier alternatives should be evaluated to reduce or eliminate the water, and hence, improve the electrical conductivity. Additional dynamic stability tests should be conducted, and the results of these tests should be used to assess whether a new injector design should be considered.

The effect of combustor cleanliness and Cs_2CO_3 concentration on the heat flux level should be evaluated. The test duration should be extended to improve the accuracy of the heat flux data. Sequence development tests should be conducted to reduce the transient operation and to demonstrate the potential for rapid on-off operation.

The performance of a reduced length combustor of ≈ 40 cm should be evaluated. If the performance is satisfactory, this behavior along with the reduced heat flux levels should make the use of a regeneratively cooled combustor feasible. This approach should be investigated because of the possibility for improved performance and smaller combustion system mass.

The cooled wall combustor/nozzle design as well as the high power MHD channel/diffuser design should be reviewed. All designs should be modified to account for the results of the development test program. After these data have been reviewed and analyzed, the complete cooled wall combustor/nozzle and MHD channel/diffuser should be fabricated and tested.

In addition to this gas generator and MHD channel/diffuser effort, parallel programs leading to the development of lightweight superconducting magnets, lightweight power conditioning systems, and advanced electrode/insulator systems should be implemented. Plasma diagnostics should be utilized more fully to provide more detailed data of the characteristics and the behavior of the MHD plasma. These programs should be implemented to fully develop the potential of lightweight, transportable, high power MHD generator power supply systems.

SECTION III

HIGH POWER MHD SYSTEM DESIGN AND INTEGRATION

A. SYSTEM OBJECTIVES AND PARAMETERS

This work is part of a continuing Air Force program to develop compact, portable high power MHD systems. The emphasis on high performance was largely initiated with the development of the 400 kW high performance channel in 1970.[5] This was followed by the Viking I and Viking II programs in 1973 and 1974, respectively.[3] Recently a lightweight, 200 kW MHD channel has been successfully tested using a novel design concept, which has also been utilized in the present work.[4]

The present work is a direct follow-on to a study entitled, "MHD High Power, Phase I Study," which is also referred to as Phase A of the overall HPMS program.[1] The major objective of this study conducted during Phase A was to make a detailed design study of various portable MHD generator systems for use as a prime power source in the range of output power from 10 to 50 MW_e operating for 60 to 120 sec total run time. Both single and multipulse operation were considered. A relatively wide range of operating parameters were specified as of interest, and in addition, eight specific point design conditions were studied for detailed consideration. The ranges of the operating parameters and the eight point design values which were analyzed are given in Table 1.

Both $JP-4/LO_2$ and solid fuel MHD generator systems were studied in the Phase A work. A conceptual drawing of a 25 MW_e $JP-4/LO_2$ type MHD generator system is shown in Figure 14. The length of the MHD system shown in Figure 14 was 2.85 m and the diameter was 1.14 m. In Table 2, a summary of the system and subsystem masses and volumes for point designs one through eight is given. The

---

[1] O. K. Sonju and J. Teno, "Study of High Power, High Performance Portable MHD Generator Power Supply Systems," AFAPL-TR-76-87, August 1976.

[3] O. K. Sonju, J. Teno, R. Kessler, L. Lontai, and D. E. Meader, "Status Report on the design Study Analysis and the Design of a 10 MW Compact MHD Generator System," AFAPL-TR-74-47, Part II, June 1974.

[4] D. W. Swallom, O. K. Sonju, D. E. Meader, and G. T. Heskey, "MHD Lightweight Channel Development," AFAPL-TR-78-41, June 1978.

[5] O. K. Sonju, J. Teno, J. W. Lothrop, and S. W. Petty, "Experimental Research on a 400 kW High Power Density MHD Generator, AFAPL-TR-71-5, May 1971.

TABLE 1. OPERATING PARAMETER RANGES AND POINT DESIGN VALUES

Parameter	Units	Range	Point Design Number							
			1	2	3	4	5	6	7	8
Power	MW$_e$	10-50	10	10	25	25	25	25	50	50
Voltage	KV	20-250	60	60	60	60	60	60	200	200
Duty Cycle										
On Time	Sec	1-120	21	21	4	120	21	21	25	12
Off Time	Sec	2-300	30	300	4	N/A	30	30	N/A	78
No. of Cycles/Mission	--	1-16	3	3	16	1	3	3	3	10
Total Run Time	Sec	30-120	63	63	64	120	63	63	75	120
Start-Up Time	Sec	1	1	1	1	N/A	1	1	1	1
Idle Time	Min	5-120	0	0	0	0	0	0	0	0

NOTE 1: The subsystem shall be designed for a 100 mission life (total life = 100 x no. of cycles above.)

NOTE 2: Electrical sources shall be designed to produce 50 kV, if possible. If the source cannot achieve 60 kV directly, design for minimum weight and volume regardless of voltage.

NOTE 3: The subsystem shall be designed for 1 sec start-up time, if possible. If one 1 sec start-up is not possible, design for minimum start-up time. If start-up time is greater than 3 sec, provide for 10 min idle.

30

DIFFUSER

DIFFUSER SUPPORT

COOLANT MANIFOLDS

CHANNEL ELECTRODES

MAGNET DEWAR

SUPPORT FRAME

GENERATOR CHANNEL

MAGNET COIL

THRUST BRACKETS

CRYOGENIC LEADS

COIL SUPPORT GIRDERS

NOZZLE THROAT

COMBUSTOR CHAMBER

FUEL INLET

FUEL PUMP

TURBINE EXHAUST

TURBINE

OXIDIZER PUMP

OXIDIZER INLET

OXIDIZER CONTROL VALVE

MHD GENERATOR SYSTEM, LIQUID FUEL COMBUSTOR

Figure 14. Phase D Prototype Hardware.

TABLE 2.   SUMMARY OF SYSTEM WEIGHTS AND VOLUMES
FOR THE EIGHT POINT DESIGNS USING LIQUID
FUEL (POWER DENSITY 200 MW_e/M^3)

Point Designs (Shielded)

	1 & 2	3	4	5 & 6	7	8
Burner, Nozzle & Reactants						
Mass (kg)	900	2100	3690	2080	4700	7250
Volume (m³)	0.77	2.0	3.5	1.9	4.5	6.0
Channel & Diffuser						
Mass (kg)	62	115	115	115	180	180
Volume (m³)	0.11	0.27	0.27	0.27	0.53	0.53
Magnet						
Mass (kg)	660 (1020)	1030 (1590)	1030 (1590)	1030 (1690)	1500 (2320)	1500 (2320)
Volume (m³)	0.84 (1.6)	1.4 (2.6)	1.4 (2.6)	1.4 (2.6)	2.0 (4.1)	2.0 (4.1)
DC-DC Converter						
Mass (kg)	250	510	510	510	1750	1750
Volume (m³)	0.58	1.15	1.15	1.15	4.3	4.3
Coolant System for Converter						
Mass (kg)	50	85	110	85	130	170
Volume (m³)	0.11	0.19	0.18	0.19	0.29	0.29
Overall System						
Mass (kg)	1920 (2280)	3840 (4400)	5460 (6020)	3820 (4380)	8260 (9080)	10850 (11670)
Volume (m³)	3.0 (3.8)	5.6 (6.8)	7.0 (8.3)	5.6 (8.3)	12.4 (14.5)	14.8 (16.9)
Coolant System for Overall System (kg)	430	540	750	540	720	900

32

magnet mass was the dominant dry mass in the system while the combustor and the reactants represented approximately one-half of the total system mass. In Figure 15 a comparison between a 25 MW_e solid fuel and a 25 MW_e liquid fuel MHD generator system is made. The figure shows that the solid fuel system had the minimum mass and volume. However, the Phase A study concluded that both liquid and solid fuel systems could meet the HPMS program goals.

The goals of the present work are discussed in the following paragraphs. The Air Force desires to develop a multi-megawatt short duration MHD power supply. The overall HPMS program consists of four phases. Phase A consisted of comparison studies as discussed previously. Phase B, the present effort, consisted of combustor development testing, detailed component designs, and component modeling. Phase C will consist of hot gas flow train performance testing and component development. Phase D is planned to provide the full scale system testing and verification.

Phase B has provided an experimental demonstration of the combustor performance.[6] This phase has also provided the preliminary design of the critical components. These activities have provided a baseline for proceeding to actual hot gas flow train fabrication in Phase C.

Phase C is planned to be an experimental demonstration of a 30 MW_e MHD generator. This phase will consist of two parts: critical component fabrication and tests, and the final design for Phase D. Little effort has been made to simultaneously demonstrate high power density, high enthalpy extraction, and high power levels with operational components. This phase will address these objectives.

Phase D is the final phase of the overall HPMS program. This phase will demonstrate a 30 MW_e MHD power system based on the design and performance results of Phase C. The power system will include all major MHD components as well as the power conditioning, controls, protection, tankage, etc., necessary to demonstrate controlled, programmed, and predictable power from a total independent MHD power system.

[6] O. K. Sonju, D. W. Swallom, D. E. Meader, H. Becker, R. V. Burry, A. W. Huebner, and R. F. Cooper, "Development of a Compact, Lightweight High Performance 30 MW MHD Generator System," 17th Symp. on Eng. Aspects of MHD, March 1978.

SOLID FUEL SYSTEM:

OUTPUT POWER: 25 MW

MASS: 2890 KG

LIQUID FUEL SYSTEM:

OUTPUT POWER: 25 MW

MASS: 3220 KG

NOTE: UNCOOLED AND UNSHIELDED PROFILES ARE SHOWN
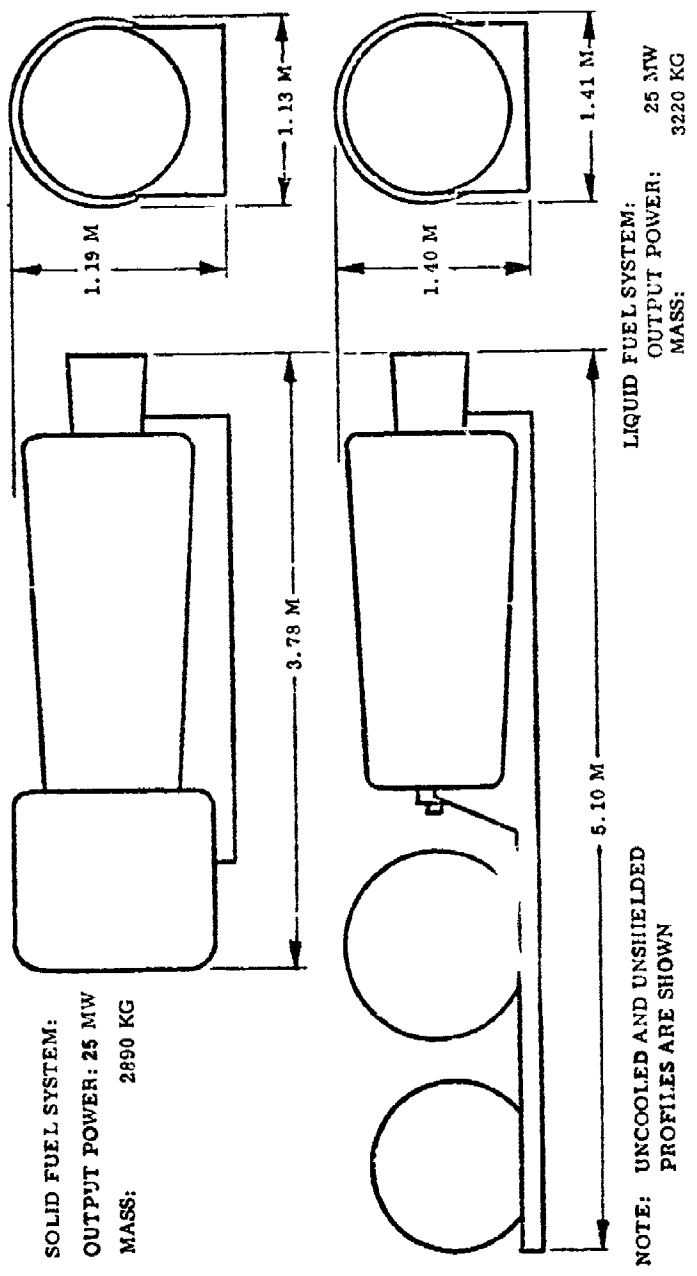
Figure 15. Solid Fuel and Liquid Fuel MHD Generator System Profiles – Point Design 5.

34

The gas generator combustor/nozzle objectives were to design, develop, and demonstrate a high performance $JP-4/LO_2$ combustor/nozzle system. This combustor assembly provided seed injection, and fast on–off capability. Provision was made for allowing a $\pm 20\%$ mass flow differential from the design optimum value of the MHD system to test off–design gasifier performance characteristics. To the maximum extent practical, existing and available combustor hardware and/or existing designs with minimum modification were used. In order to evaluate off–design flexibility, this assembly met performance specifications over a $\pm 20\%$ range of the total mass flow rate.

The MHD channel/diffuser objectives were to design a composite structure, cooled channel/diffuser assembly capable of producing 30 MW_e when coupled with the above combustor and the HPMS magnet assembly at AEDC. The MHD channel/diffuser assembly was designed to be operationally compatible with the HPMS test facility at AEDC. This channel was designed to have a power density of 200 MW_e/m^3 and design mass flow rate capability of at least 36 kg/sec. Using liquid hydrocarbon fuel and liquid oxygen, the channel was designed to be capable of demonstrating mechanical and electrical durability with five cumulative hours of life at design flow conditions as well as provide stable and reliable performance over a mass flow volt range of $\pm 20\%$ of the nominal condition.

The superconducting MHD magnet design objective was to provide a design and analysis of an advanced, shielded superconducting magnet system. The design upper limits for the critical magnet parameters were a useable magnetic field of 4.5 Tesla, superconductor current densities of 15,000 A/cm^2, and stress of 4080 atm. Emphasis in this design effort was given to fully potted coils, Nb–Ti twisted multi–filament combustor, composite structures, and a fully shielded system. The power conditioning system design objectives were to design a system capable of delivering 90% of the load power at 20 kV and 10% of the load power at 200 kV, simultaneously into two separate loads. The power conditioning equipment designs were to include the load and system power supply electrical fault protection, the multiple load CW designs, and the off–design requirements. Both of these efforts, which were originally part of Phase B, were later deferred until Phase C because of program delays and cost growths generated during the fabrication and test of the development hardware.

In the design of the MHD system, several design and operating parameters were considered. A summary of the parameters considered and an evaluation of their relative importance are shown in Table 3. In the Phase A and the present Phase B work, these parameters were considered in the selection of the operating conditions and the various subsystem designs.

A summary of some of the design considerations is given in the following paragraphs. In terms of the operating parameters of the MHD channel constraints, such as the electric field, the current density, the Hall parameter, the electrical conductivity, the loading parameter, and the magnetic field level, were placed on the design to insure proper operation of the high power MHD channel/diffuser. In addition, other parameters, such as the heat transfer rates, boundary layer shape factor, exit pressure level, diffuser recovery, length to diameter ratio of the channel, the electrode segmentation, and the voltage gradient between adjacent electrodes, were constrained to insure reasonable operation of the channel.

Also in designing the MHD channel/diffuser, the off-design performance was checked carefully. The sensitivity of the performance with respect to various input parameters such as conductivity was considered. Since four Tesla peak bore fields have been demonstrated in MHD saddle coils, a peak magnetic field strength of four Tesla was selected for the Phase B design. However, design values of five to seven Tesla were considered possible.

For the length to diameter ratio (L/D) of the channel, designs with L/D values of four or more were recommended. Two major considerations were involved here: (1) for smaller values, end effects became important and the generator performance was degraded; and (2) the overall system mass increased because the magnet became so short that the end regions dominated the mass. The Phase A study showed that as the power density increased, the channel length decreased holding other flow parameters constant. Therefore, to maintain the desired L/D, this led to lower values of D which, in turn, resulted in higher stagnation pressure. In addition, optimizing L/D for maximum energy extraction did not necessarily lead to the optimization of L/D for energy density or vice versa.

In addition, limits and constraints in terms of the electric fields, the Hall parameter, electrode current density, heat transfer rates in channel, and the combustor pressure were imposed. The following values were selected:

Electric Fields	–	≥ 5 kV/m
Hall Parameter	–	≤ 4
Electrode Current Density	–	≤ 10 A/cm^2
Heat Transfer Rate	–	≤ 1000 W/cm^2
Combustor Pressure	–	≤ 30 atm

TABLE 3. LISTING OF OVERALL PARAMETERS AND EVALUATION
OF THEIR IMPORTANCE TO
SINGLE LOAD MHD GENERATOR SYSTEMS

1. Power

Important, determines size of system.

2. Run Time

Important, determines requirement for expendables and necessary storage and hence, system mass.

3. Power Factor

MHD generator is a dc generator and as such does not have a power factor.

4. Voltage

Not important. The MHD generator can, in general, not output the required voltage directly. Therefore, power conditionary equipment such as a dc-dc converter is used. Accordingly, voltage is not an important external parameter for the MHD generator system and does not appear as a determinant factor in the mass or volume of the MHD system.

5. Number of Starts

For the case of MHD generators, the number of starts only affects life. Extended life requirements have extended effects on mass and volume. A trade-off exists between heavier mass and volume vs early reworking or replacement of affected parts.

6. Idle Time

Not important. MHD generator systems do not require idle time.

7. Efficiency or Energy Extraction

Important, has significant effect on system size and mass. For long operating times trade-off between fixed mass and efficiency possible.

8. Duty Cycle

Important when short run times are followed by down times sufficient to cool all components of the system; then, heat sink systems of very simple structure could be considered for application.

TABLE 3. LISTING OF OVERALL PARAMETERS AND EVALUATION
OF THEIR IMPORTANCE TO
SINGLE LOAD MHD GENERATOR SYSTEMS (Cont'd)

9. Start-Up Time

Not Important. Starting an MHD generator system is the equivalent of starting a rocket motor and can be accomplished in less than one second.

10. Regulation

Not Important. MHD generators are in effect constant current generators not constant voltage generator. Voltage control can be maintained by seed control at a given load.

11. Auxiliary Power Requirements

Not Important. Small amounts of auxiliary power will be required to maintain the magnetic field, to operate pumps, for controls and other similar functions.

12. Mission Time

Not too important if hours, but important if days.

13. Altitude

Important if operating at high altitude. With low ambient pressure the generator output can be increased significantly.

14. Ripple

Not Important.

15. Protection

Not Important.

16. Fast Transients

Not Important.

17. Shielding

Important if dc magnetic fields must be reduced to very low levels.

38

TABLE 3. LISTING OF IMPORTANT MHD DESIGN PARAMETERS AND
EVALUATION OF THEIR IMPORTANCE TO
SINGLE LOAD MHD GENERATOR SYSTEMS (Cont'd)

1. Magnetic Field

Required level very important. High fields result in
large masses.

2. Electric Field

A constraint on design. Maximum design level must be
specified.

3. Conductivity.

Very important. High conductivity results in lower masses.

4. Heat Transfer and Wall Temperature

Not too important, but result in design constraint at high levels.

5. Operating Pressure

Affects combustor system design.

6. Current Density

Design constraint. Maximum design level must be specified.

7. Channel Dimensions and Profile

Important. Affects magnet size requirements.

8. Channel Configuration

Chosen depending on operating requirements. Diagonal
configuration best in cases considered here.

B. CHANNEL/DIFFUSER AND MANIFOLDS

The main high power MHD channel design performance requirements were:

Power Density   - 200 MW_e/m^3
Power Output   - 30 MW_e
Energy Extraction - 1 MJ/kg

In addition, the channel will be operated in short bursts of up to 150 sec with an objective of a five hour accumulated test life. Designs satisfying these objectives and requirements appear feasible except for the life objective, which was much beyond the present experience for the type of operation required for this program.

The design concept used in this program for the MHD channel/diffuser is shown in Figure 16. The figure shows some of the novel features of the channel design. A composite case formed the outer structure and pressure vessel. The electrode construction consisted of water cooled copper frames with zirconia ceramic and Inconel screens for the electrode surfaces. The interframe insulating ceramic was alumina. The electrode frame assembly is constructed around an assembly mandrel, which is also used for the case fabrication. This design was developed specifically for the present type of applications. The design represents a compact lightweight construction which also has features that, when fully developed, should provide for high performance, reliable operation, and long life.

C. COMBUSTOR/NOZZLE AND ANCILLARY

The main high power MHD gas generator design performance requirements were:

Combustor Stagnation Pressure   - 24-36 atm
Nozzle Exit Conductivity   - 15-20 mhos/m
Start/Shutdown Time   - < 1 sec
Mode of Operation   - Steady-State or Multi-Pulse
Life Time   - 5 hr

In addition to these requirements, the combustor was required to demonstrate stable operation as well as spatial and temporal flow uniformity. These reductions in the flow non-uniformities were significant improvements over previous MHD nozzles.

The design concept used in this program for the gas generator is shown in Figure 14. This figure shows the combustor/nozzle expected to be developed for Phase D. Also shown in the figure are the fluid supply system and the support

GENERATOR CHANNEL

A ▸ A

A ▸ A

A-A

STABILIZED ZIRCONIA

CURRENT COLLECTORS, INCONEL WIRE

COPPER ELECTRODE FRAME

THIN WALL COPPER TUBE

COOLANT PASSAGE

INSULATING CERAMIC

SILICONE RUBBER HOT GAS SEAL

FIBERGLASS - EPOXY SHELL

TYPICAL
DIMENSIONS

0.8
cm

0.3 cm

2 cm

0.5 cm O.D.
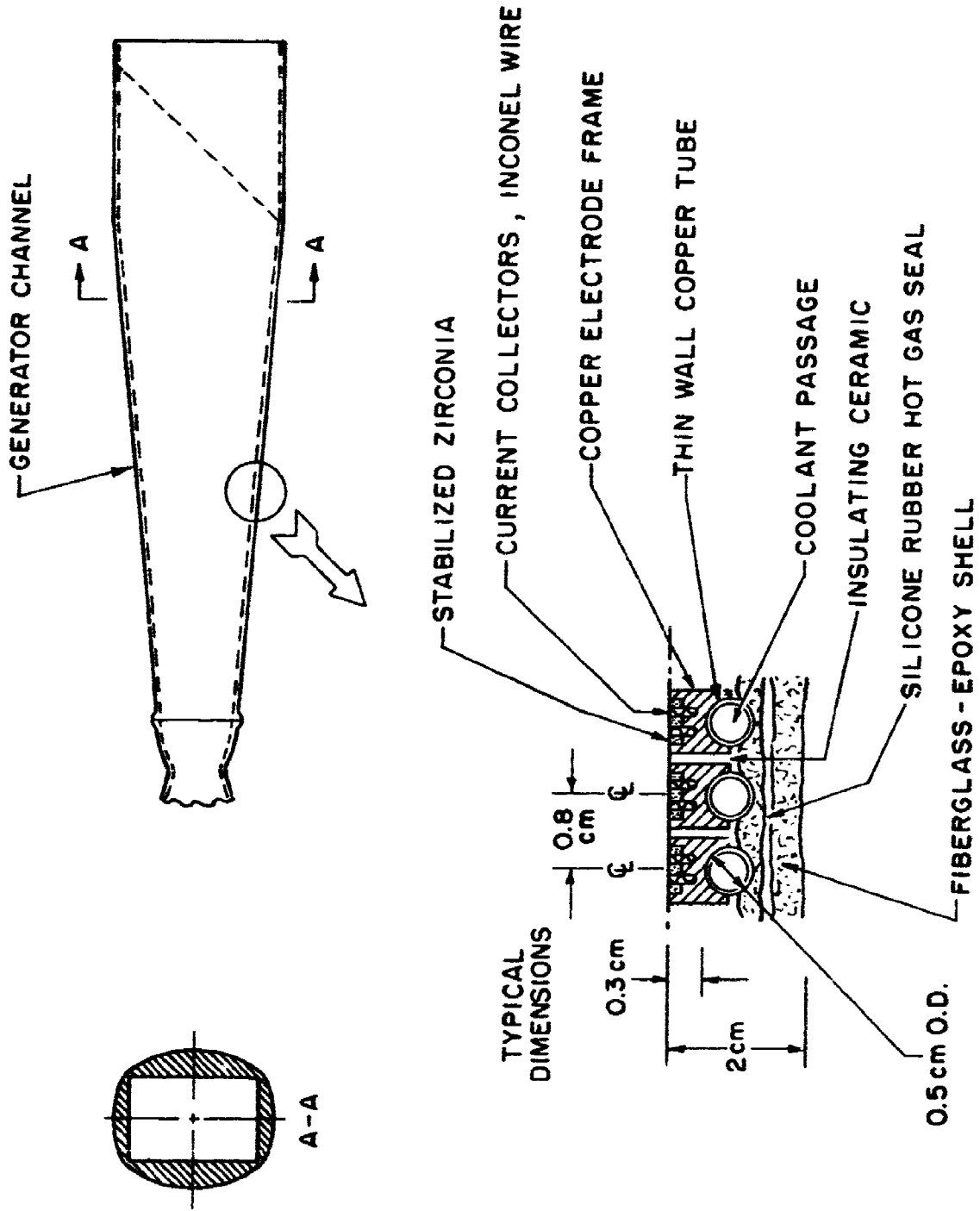
Figure 16. Composite Channel Wall Design Concept.

41

structure. This design, while utilizing many state-of-the-art concepts, was developed specifically for the present type of applications. The design represents a compact lightweight construction which, when fully developed, should provide for high performance, reliable operation, and long life.

D. SUPERCONDUCTING MAGNET

The preliminary superconducting magnet design criteria for the high power MHD system are shown in Table 4. The design peak magnetic field was four Tesla decreasing to three Tesla over a length of 1.3 m. The field homogeneity requirements within the channel volume were $\pm 5\%$. The magnet-dewar system requirements are also included in the table.

The stability criterion selected was metastable instead of cryostatically stable. The metastable approach has been applied primarily to small laboratory scale systems or systems where minimum mass was required. The advantages of the metastable system over the cryostatically stable system were small size and mass. However, the metastable system does lead to a higher overall current density. Furthermore, fabrication experience has been limited for complex geometries. Consequently, a need exists for the development of fabrication techniques to assure that the characteristics of the system are achieved. Therefore, before proceeding with the full scale HPMS magnet system, reduced scale magnet modeling programs should be conducted.

E. POWER CONDITIONING

The power conditioning design for the high power MHD system was required to deliver 90% of the load power at 20 kV and 10% of the load power at 200 kV. The power conditioning system must be a minimum mass, modest size design suitable for portable service. The design requirements for the inverter section of the power conditioning system fed by a dedicated MHD generator differed from those requirements for other similar applications. These differences are discussed in the following paragraphs.

The MHD system operated with an internal impedance approximately equal to the load impedance. As a result, the maximum possible output current from the generator was limited to twice the normal current. This self-limiting characteristic reduced the protection circuit requirements. Because of the nature of the MHD generator and the existance of only one load, the power conditioning system, short circuiting of the MHD generator in the case of a destructive fault was permissible.

TABLE 4. PRELIMINARY CRITERIA FOR MAGNET DESIGN

Warm Bore Dimensions

Diameter at Inlet	0.29 m
Diameter at Outlet	0.53 m

Active Field Requirements

At Channel Inlet	4.0 T
At Channel Outlet	3.0 T
Field Length	1.3 m
Field Homogeneity Within Channel	$\pm$ 5%

Magnet-Dewar System

Cryogen Required for Cooldown

LN_2	$300 < Q < 450$ liter
LHe	$200 < Q < 2000$ liter

Cooldown Time	$3 < t < 12$ hr
Cryogen for Operation	He I
Operating Temperature	$3.0 < T < 4.5$ K
Operating Pressure	$0.24 < p < 1.32$ atm
LHe Required for Operation	$5 < Q < 15$ liter/hr
Power Supply for Charging Sequence	$10 < P < 15$ kW
Charge Time	$3 < t < 8$ min
Shielding at 2.5 m from System Center	$10 < B < 50$ gauss
Target System Mass	1500 kg

Conductor and Windings

Stability Criteria	Metastable
Operating Current	2000 A
NbTi Filament Size	$20 < d_f < 200 \mu$
Copper/SC Ratio	$1.1 < csc < 3.0$

The MHD generator load line, or voltage current characteristics can be controlled by variations of the fuel, oxidizer, or seed on a time scale of less than 0.1 sec. Operation on a load line near the matched condition was desired for optimum energy transfer. Hence, the current drawn from the generator should be relatively constant.

Several approaches, including a transformerless dc-dc converter and a standing wave amplifier system, were evaluated as possible alternatives. The requirements listed in the preceding paragraph along with any particular or unique requirements of the load will have the major impact on the selection of the specific final power conditioning design.

SECTION IV

CHANNEL SUBSYSTEM DESIGN AND FABRICATION

A.   INTRODUCTION

1. High Power MHD System

The high power MHD system (HPMS) was a direct energy conversion
device which converted the thermal energy of the reactants into electrical energy.
The nominal goal for electrical output power was 30 MW.   The major components
of the system were the combustor/nozzle, fluid supply system, and support struc-
ture from Rocketdyne, the channel/diffuser from Maxwell Laboratories, and the
magnet and test facility from Arnold Engineering and Development Center (AEDC).
A development test program was conducted at Santa Susana Field Laboratory (SSFL)
and a performance test program is to be conducted at AEDC.   AEDC is to provide
the reactants, the control systems, the data acquisition system, and other neces-
sary support equipment for the performance testing.   This chapter discusses the
channel/diffuser design and fabrication processes.   The following chapter presents
a discussion of the combustor/nozzle including the injector and the augmented
spark ignitor.   Section VI provides the details of the design and fabrication of
the seed system, the fluid supply system, and the support structure.   Figure 17
shows a pictorial representation of the high power MHD system.

2. Hot Gas Flow Train

The purpose of the hot gas flow train, consisting of the combustor/nozzle
and channel/diffuser, was to demonstrate the performance goals of the light-
weight, high power MHD generator.   The high power MHD channel/diffuser was
designated to generate electrical power from the products of combustion of JP-4,
LO_2, Cs_2CO_3, SPAN-80, and H_2O.   The channel/diffuser is to be tested at AEDC
to verify the design performance goals.   To support the design approach for the
hot gas flow train, some components were constructed and tested for the develop-
ment test program.   These components are described in Section VII, and the
results of this test program are presented in Section VIII.

B.   GENERAL DESCRIPTION

1. Channel/Diffuser

The channel/diffuser received the ionized gas from the combustor/nozzle,
provided the flow duct from channel/nozzle interface to the diffuser exit, and

Magnet

RKDN Combustor

MLI Channel/Diffuser
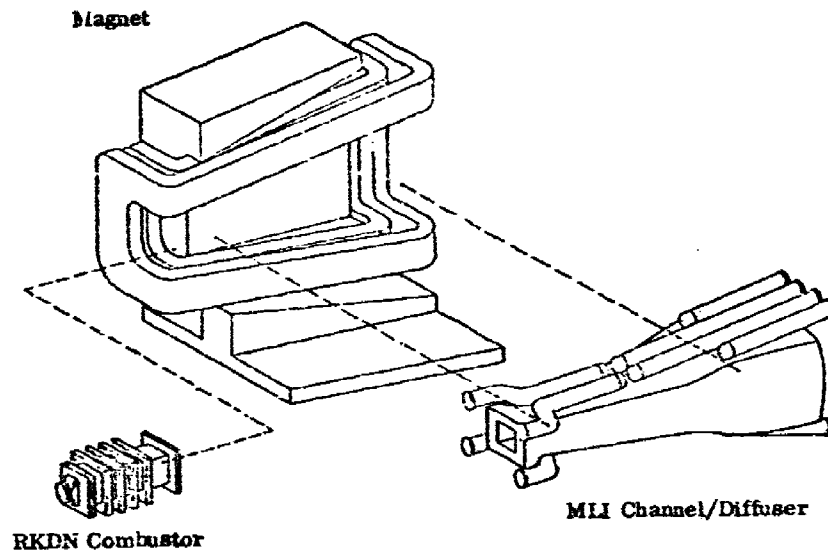
. Expanded View
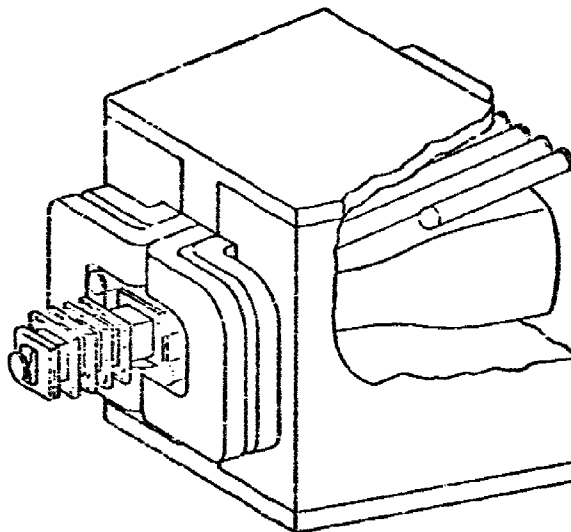
B. Assembled System

Figure 17.   General Arrangement of High Power MHD System.

extracted the electrical power. (See Figure 17.) The construction features of the high power channel/diffuser utilized a novel design concept that permitted the production of rugged, yet lightweight channels for MHD generators. This unique design approach is described in the following sections.

The high power MHD channel/diffuser consisted of water-cooled copper electrode frames which were oriented approximately 40 deg to the channel axis in the middle section of the channel. At the ends of the diagonal electrode frame section, transition electrode frames were used to change the electrode angle to match the perpendicular end flanges. The frames were supported in a fiberglass composite case which resisted the deformation action of the channel pressure and the static and vibratory forces imposed during operation. Figure 18 illustrates a section of the channel/diffuser system with the case spliced along the mid-plane of a diagnoal electrode frame.

The inlet end was attached to the nozzle exit by bolts and belleville washers. Three pins maintained alignment of the combustor and channel axis. The bolts preloaded an O-ring to generate a gas tight seal. The outlet end was supported in a manner which restrained the channel against movement because of dead weight and dynamic loads yet permitted axial growth induced by temperature changes.

a. Introduction

The primary subsystems of the channel/diffuser are listed in Table 5. The frame array served as the current collector, the initial insulator against the heat flux from the hot ionized gas, and the interframe electrical insulator. The case was the structural support for the frame array and the pressure vessel. There was partial sharing of functions between the two subsystems. For example, the frames supported part of the internal gas pressure. The frames also withstood vibration. However, the case was designed as though these functions were performed only by the case.

b. Frames

The most versatile component of the channel/diffuser was the frame. A sketch of a typical electrode frame is shown in Figure 19. The cross section shows the elements which provided the temperature controls that raised the surface temperature to 2000 K. These elements were required for the electrode frame to function effectively as a current collector while cooling the frame to enable it to survive the severe thermal environment. The assembly shows how coolant flowed through the frame and depicts the anchors which held each frame in place inside the composite case.

CORNER BLOCKS

COOLANT CONNECTIONS

SILICONE-RUBBER GAS BARRIER/EXPANSION INTERFACE

GLASS-EPOXY SHELL FILAMENT WOUND

FRAME ANCHORS

SIDE RAILS WITH SCREEN AND COOLING TUBE

CROSS RAILS WITH SCREEN AND COOLING TUBE
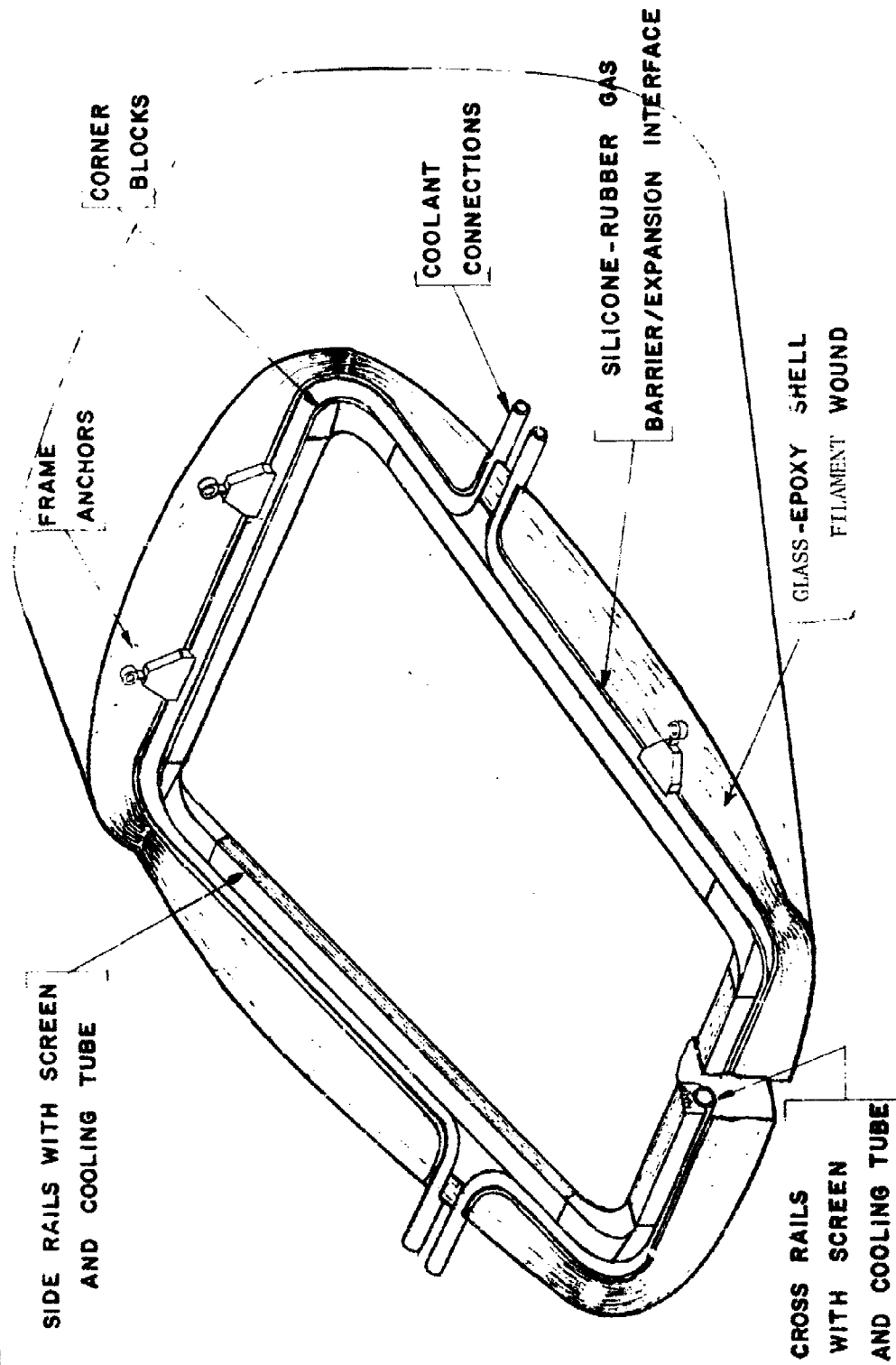
Figure 18. Sectioned Channel/Diffuser.

48

TABLE 5. CHANNEL/DIFFUSER SUBSYSTEMS

FRAME ARRAY SUBSYSTEM FUNCTIONS

1. Conversion of Hot Gas Power into Electrical Power

    MHD (ceramic, interframe and at gas face)

    Electrical (current collection and interframe insulation)

    Thermal (temperature and temperature gradients)

    Structural (static and dynamic responses)

    Hydraulic (flow rate, flow velocity and pressure drops)

2. Cooling Device

CASE SUBSYSTEM FUNCTIONS

1. Maintenance of Frame Array Alignment

2. Resistance to Internal Gas Pressure

3. Protection of Frames (metal and ceramic) from Vibration Damage

4. Seal Against Internal Gas Pressure

5. Provision for Interfaces (with RKDN Combustor, Viking Magnet, Exhaust Duct, and AEDC Facility)

GENERATING ELECTRODE FRAME

GAS FLOW

75.5 cm

FRAME ANCHORS

COOLANT CONNECTIONS

62.8 cm

51.9 cm

E

C

B

A

D

A, CURRENT COLLECTOR SCREEN
B, ELECTRODE CERAMIC
C, COPPER FRAME
D, COOLING TUBE
E, TOP RIGHT CORNER BLOCK
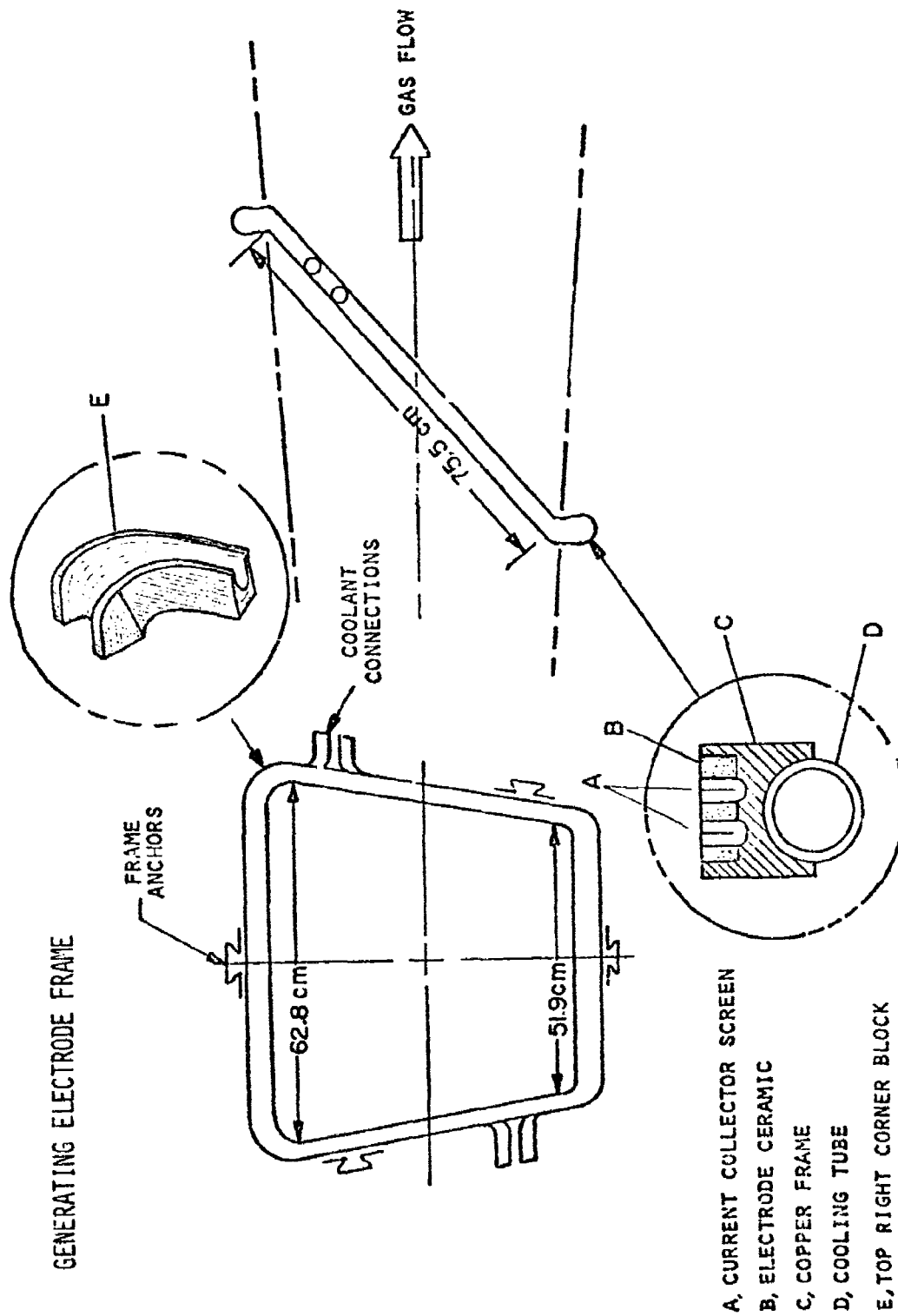
Figure 19. Generating Electrode Frame.

50

The electrode frames were oxygen free, high conductivity (OFHC) copper strips brazed into continuous trapezoidal rings with OFHC tubes brazed to the outsides of the rings to convey the cooling water. The anchors restrained the frames from motion normal to the gas face while permitting thermal growth along the sides parallel to the gas face. Small diameter holes for the static pressure instrumentation were drilled through some of the spacer blocks where the cooling tubes connected to the manifold hoses. The electrode frames were electrically insulated from each other by alumina which provided a partial gas seal.

The electrical current was collected at the hot gas surface. The electrode assembly consisted of a copper cup into which the electrode screen was brazed, and the ceramic material was cast. Calcia stabilized zirconia, operating at surface temperatures up to 2200 K, was used as the ceramic material, and Inconel 601, with a surface temperature close to its melting point of 1650 K was used. The copper surface temperature ranged from nearly 750 K at the channel entrance to less than 450 K at the channel exit.

In the transition regions the electrode frame crossbar width (along the channel distance in the direction parallel to the gas flow) varied from a single frame width at one side to as much as six frame widths at the opposite side because of the need to maintain control over segmentation and to minimize the transition distance between vertical and slant frame zones. The electrode frame pitch was the same in the vertical zones at the inlet and outlet and in the slanted frame zone in the middle of the channel. This required a reduction of the thickness of the diagonal crossbar as shown in Figure 19.

c. Case

The case, shown in Figure 20, was a fiberglass filled epoxy shell essentially rectangular in cross section. The main loading on the case was the pressure in the channel. For maximum efficiency in performing that role, the case consisted primarily of circumferentially wound roving. Layers of 0-90 and 45-45 glass cloth were included to provide axial and transverse stiffnesses and shear strengths. The fiberglass matte provided body on the flat sides to achieve buildup at the centers of the sides thereby acquiring curvature at those locations. This helped to avoid fiber buckling during curing. Each side was twice as thick at the center as it was at the corners.

The coolant tubes penetrated the case near the quarter points of the sides. This avoided stress concentrations at the corners where the internal bending moment from the channel pressure reached the greatest value. The penetrations were larger in diameter than the coolant tubes in order to provide an annulus for application of RTV as the gas seal. The RTV also provided a barrier between the

51

COMPOSITE CASE CONSTRUCTION

"A" = FIBERGLASS ROVING
"B" = FIBERGLASS FABRIC

A
B
A
B
A

SILICONE RUBBER

CHANNEL/DIFFUSER

COMPOSITE
CASE

SILICONE
RUBBER

ELECTRODE
FRAMES
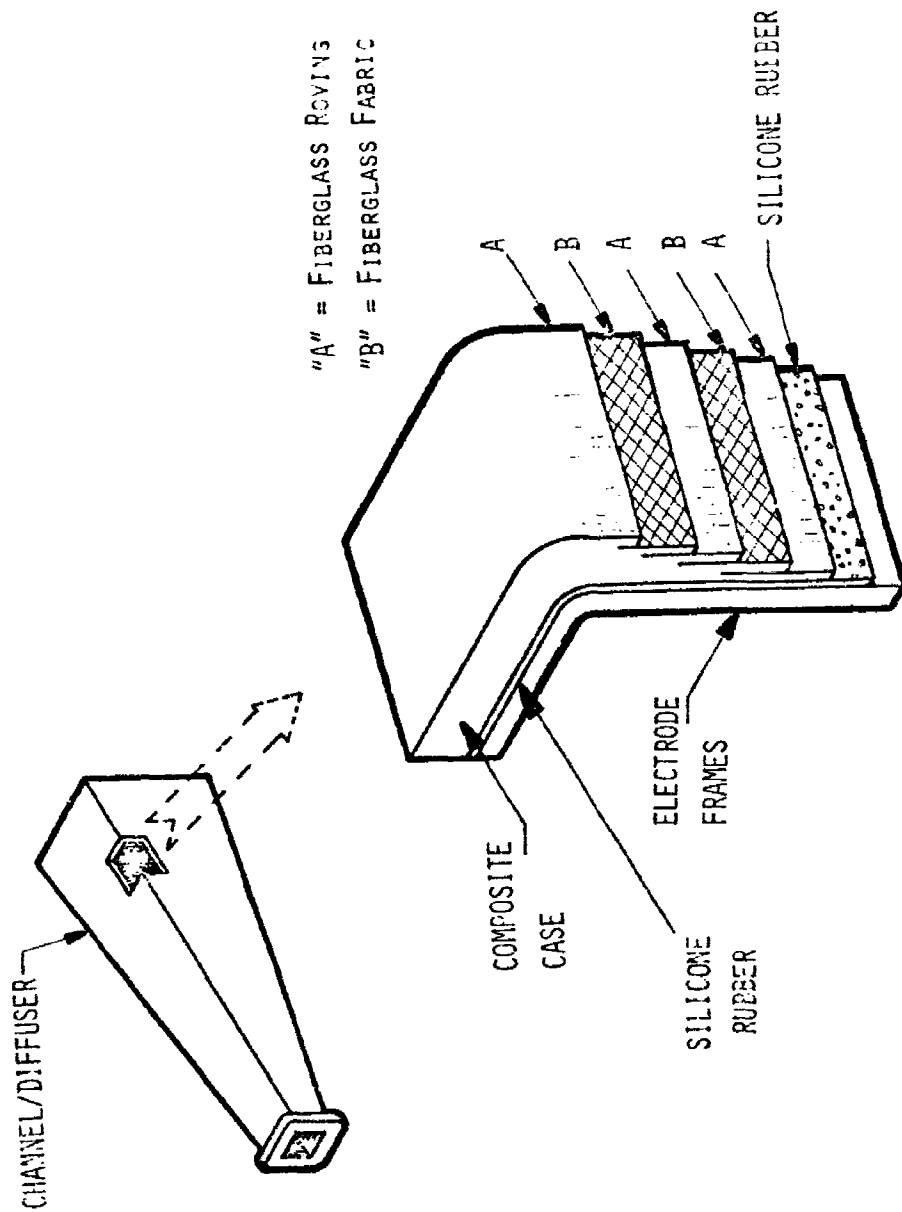
Figure 20.   Composite Case Construction.

52

outer surfaces of the frames and the inner surface of the case. In addition, the RTV acted as a structural cushion between the frames and the case to smooth load transfer between these components caused by the channel pressure and vibration. The RTV also acted as an energy dissipator for vibratory loads and functioned as the inner thermal barrier between the frames and the case. The case was the outer thermal barrier and contained the entrance interface structure for attachment to the combustor/nozzle and the trunnions near the exit to which the downstream structural supports were attached.

2. Channel Mandrel

The construction of the mandrel utilized a box beam design with four sections. The outer shape of the assembly was tailored to the gas passage contour of the channel/diffuser. The match to that contour was made with high accuracy to control the dimensions of the channel/diffuser. The channel/diffuser was designed to be fabricated by assembling the electrode frames on the mandrel. After the electrodes were correctly spaced on the mandrel, the interelectrode gaps were filled with castable alumina. The winding of the outer shell of epoxy coated continuous filaments provided the outer case of the channel/diffuser.

Two mandrels were designed for this program – one for use in the fabrication of the diagnostics channel and one for the high power MHD channel. The diagnostics channel mandrel design and fabrication is described in Section VII. The design of the high power MHD channel mandrel is discussed in this chapter. The mandrel design consisted of stiff, aluminum boxes with trunnions projecting at each end of the mandrel for rotation during fabrication and curing. The present design had four boxes, or sections. Each section could function as a work station allowing four assembly teams to work in parallel. Each of the sections would be joined together for the application of the final wrapping of the composite case and oven cure. Figure 21 shows a sketch of the multi-section mandrel.

3. Cooling Manifolds

The manifolds received water from and discharged to the facility coolant piping. They were typical hydraulic pipes closed at one end, flanged at the other and drilled and tapped for the nipples to which the interconnecting tubing would be attached. The interconnecting tubing would be flexible hose capable of withstanding the water pressure and temperature with a factor of safety greater than five. The flanges attached to mating flanges on the supply piping with compressed gaskets to avoid leakage upon installation. The manifolds were designed to be supported by the AEDC facility piping.
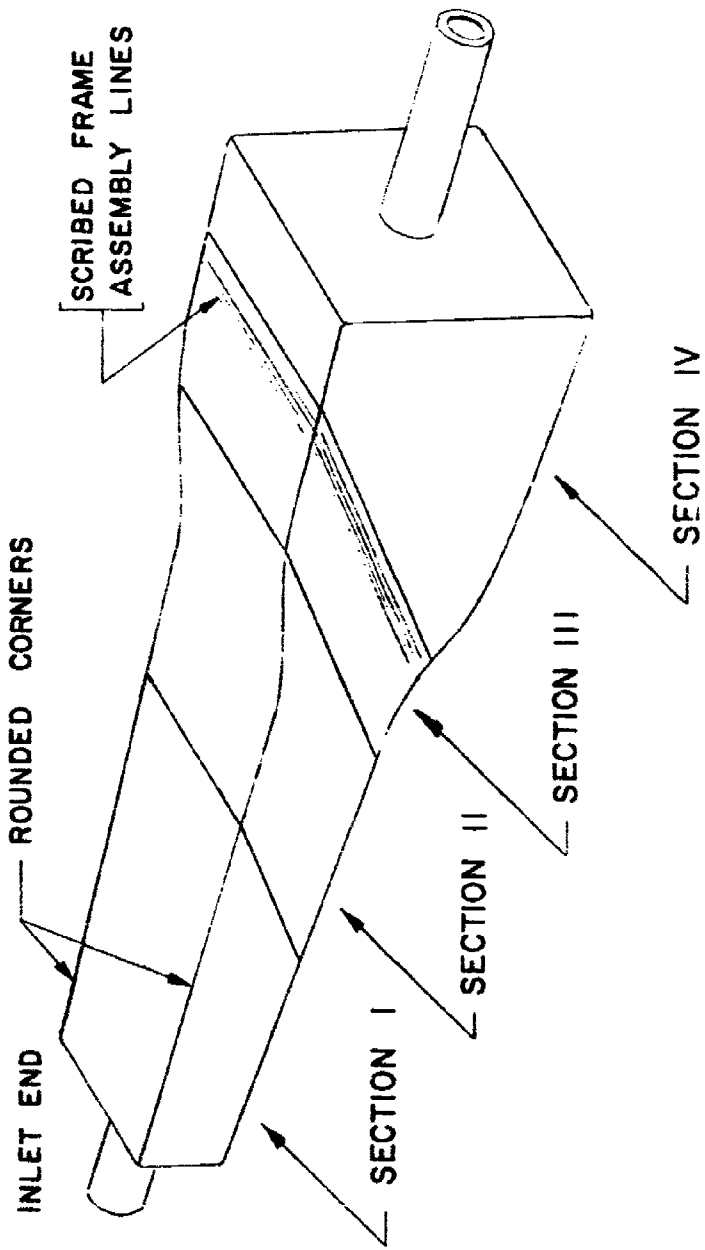
Figure 21. Multi-Section Mandrel.

54

4. Instrumentation

The channel/diffuser instrumentation is listed in Table 6. Figures 22 and 23 show schematically the locations and uses of the various types of instrumentation. The AEDC test program utilizing this information is discussed in more detail in Chapter IX. The test data from this instrumentation will be used to establish the electrical and gas dynamic performance of the high power MHD combustor/nozzle and channel/diffuser. The pressure taps, thermocouples, and electrical lugs will be installed in the channel/diffuser and checked out before delivery to AEDC. The pressure transducers and accelerometers will be calibrated and installed at AEDC. The voltage and current measuring instrumentation will be supplied by AEDC.

C. DESIGN CRITERIA

1. General

The high power MHD channel/diffuser was designed to be capable of generating the specified electrical power, power density, and energy extraction when coupled with the combustor/nozzle and installed in the magnet for testing at AEDC. The system design was required to demonstrate the ability to generate power at the specified levels and operating conditions and to provide data from which the overall electrical and mechanical performance can be evaluated. The channel/diffuser is to be reparable in order to maintain operability within the stipulated life as identified by the specifications. The channel/diffuser was designed to permit proper interfacing with the combustor/nozzle and support structure to fit into the HPMS magnet at AEDC and to match the appropriate interfaces with the required laboratory equipment at AEDC.

The channel/diffuser design was to provide for as many lightweight features as possible. The diagnostic instrumentation was selected by Maxwell Laboratories to monitor the performance during the testing. The data from subsequent channel/diffuser testing will permit an assessment of the MHD performance and mechanical integrity. Appropriate safety factors have been incorporated in the design to minimize danger to laboratory personnel and equipment during testing.

2. Magnetohydrodynamic

The high power MHD channel/diffuser was designed to be capable of delivering 30 MW of electrical power at a power density of 200 MW/m^3 and with an energy extraction greater than 1 MJ/kg. The base level channel test program encompassed 37 tests for a total time of 572 sec with a minimum test time of 3 sec and a maximum time of 150 sec. The total useful life was required to be greater than 5 hours. Table 7 lists the specific requirements for the MHD generator system.

TABLE 6. 30 MW CHANNEL/DIFFUSER TESTS

DIAGNOSTICS INSTRUMENTATION LIST

Measurement Type	Description	Range Of Interest	Units	Measurement Locations
Voltage	Channel Output Voltage	0 to 10	kV	2
Voltage	Hall Voltage Along Channel	0 to 10 in steps	kV	52
Current	Channel Output Current	1,000 to 15,000	A	1
Current	Channel Ends	0 to 1,500	A	40
Pressure	Channel Boundary Layer, Gas Static Pressure:			
	(a) Channel/Diffuser	0 to 6	atm	13
	(b) Diffuser	0 to 3	atm	7
Temperature	Channel/Diffuser Case	0 to 500	K	7
Temperature	Electrode Frames	0 to 500	K	13
Temperature	Cooling Water	0 to 500	K	13
Vibration	Channel/Diffuser Structure	5 to 10,000	Hz	5
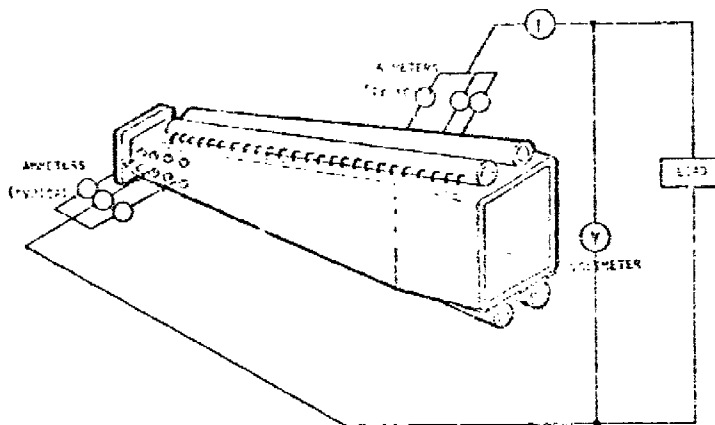
30 MW CHANNEL/DIFFUSER DIAGNOSTICS
OUTPUT VOLTAGE/CURRENT
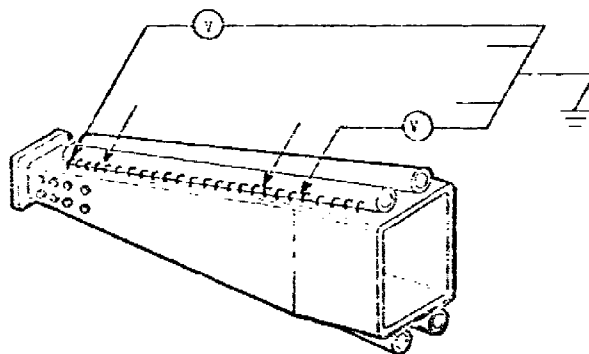
30 MW CHANNEL/DIFFUSER DIAGNOSTICS
HALL VOLTAGE
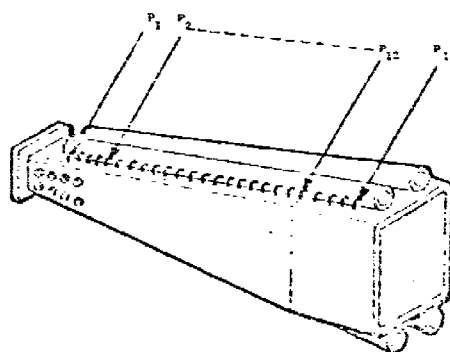
30 MW CHANNEL/DIFFUSER DIAGNOSTICS
PRESSURE (GAS, STATIC)

Figure 22. High Power MHD System Channel Diffuser Diagnostics.
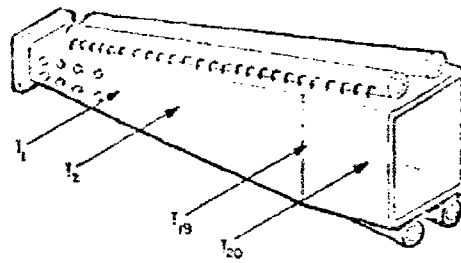
T_c = TEMP. CASE (7)
T_F = TEMP. FRAME (13)

30 MW CHANNEL/DIFFUSER DIAGNOSTICS
TEMPERATURE (WALL)

T_{IN} = WATER IN, TEMP.
T_O = WATER OUT, TEMP.
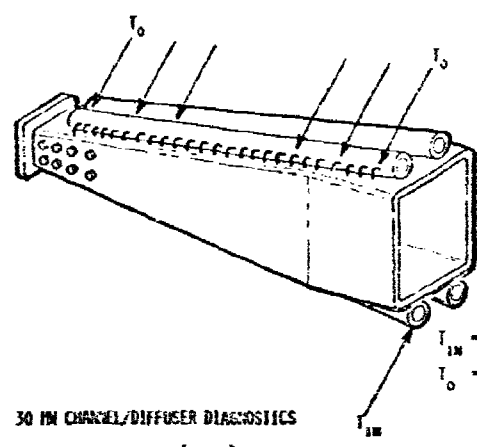
30 MW CHANNEL/DIFFUSER DIAGNOSTICS
TEMPERATURE (WATER)

DIRECTION OF
MOVEMENT

ACCELEROMETER
ORIENTATION OF BASE
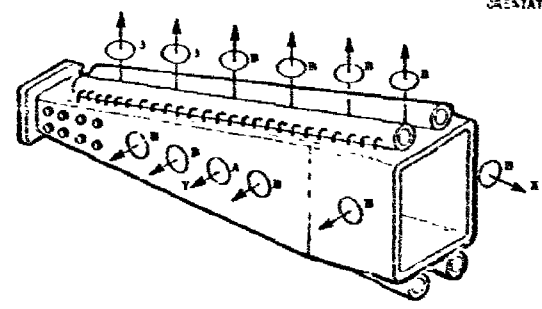
30 MW CHANNEL/DIFFUSER DIAGNOSTICS
VIBRATION

Figure 23.   High Power MHD System Channel/Diffuser Diagnostics.

58

TABLE 7.   MHD DESIGN CRITERIA

Power Output	30 MW_e
Energy Extraction	1 MJ/kg
Power Density in MHD Channel	200 MW_e/m^3
Reactants	Liquid Oxygen, JP Fuel, SPAN-80 and Cs_2CO_3
Total Reactant Flow Rate (Nominal)	30 kg/sec
Reactant Flow Rate Variation	$\pm$ 20%
Magnetic Field	$\leq$ 4.0 T
Single Run Capability	150 sec
Restart	Multi-Pulse Operation
Life	5 h

3. Thermal

The surface temperature of the ceramic in the electrode frame cups must be maintained at a sufficiently high temperature to obtain satisfactory electrical performance. The surface temperature of the copper frame must remain below the level where rapid degradation of useful life of an electrode would occur. The case inside temperature must be maintained below the useful operational limit to avoid degradation of the composite structural integrity, and the outside case wall temperature must be low enough to permit utilization of the sensors which record pressure and vibration.

4. Hydraulics

The water from the AEDC feed lines must be distributed into cooling water manifolds above the channel/diffuser, flow through the channel/diffuser electrode frames in a single pass, enter the cooling water exhaust manifolds, and return to the low pressure side of the pump. Frame interconnects to reduce the total water flow requirements may also be included. The cooling system design requirements must be within the flow and pressure limitations of the AEDC test facility cooling system.

5. Structural

The channel/diffuser was designed to be bolted to the combustor at the upstream face with three pins to maintain alignment. At the downstream end the channel/diffuser was designed to be supported against vertical and lateral movement. The structure loads include the channel pressure distribution, the channel mass, vibrations, and temperature fields. The total useful life of five hours has been assumed to consist of 1000 thermal cycles. The design structural integrity factor of safety was greater than ten based on life and greater than four based on the ultimate strength of the case. The breathing deflection has been limited to 0.75 mm.

The design criteria for the mandrel are shown in Table 3. A large variety of design possibilities could have been selected to meet the criteria. However, the need for stiffness was considered to be achieved best through the use of the arrangements shown in Figure 24 since bending rigidity was needed throughout 360 deg of rotation of the mandrel. Torsional rigidity was a minimal requirement since startup and shutdown times could be long, thereby minimizing torque loading.

TABLE 8. MANDREL STRUCTURAL DESIGN CRITERIA

Stiffness To Avoid:

> Cracking of the interframe ceramic during winding and curing, or
>
> Deformation of the frame array while winding and during curing.

Accessibilities During Fabrication For:

> Assembly of each frame from components,
>
> Removal of frames for application of zircoa,
>
> Replacement of frames after application of zircoa,
>
> Emplacement of interframe ceramic, and
>
> Application of fiberglass and epoxy.

Ease of fabrication, by teams, of frame array for high power MHD channel/diffuser.

Ease of introduction into oven for epoxy cure.

Accessibility for flow of hot air through mandrel during cure of epoxy.

Dimensional stability for avoidance of thermal stresses, or of gaps, during 375 K epoxy cure.

Ease of removability from finished channel.

Reusability.

TOP PLATE

SIDE PLATE (TYPICAL)

CORNER BRACKETS

SECTION TIE BOLTS

CROSS SECTION
(TYPICAL)

BOTTOM PLATE

I

II

III

IV
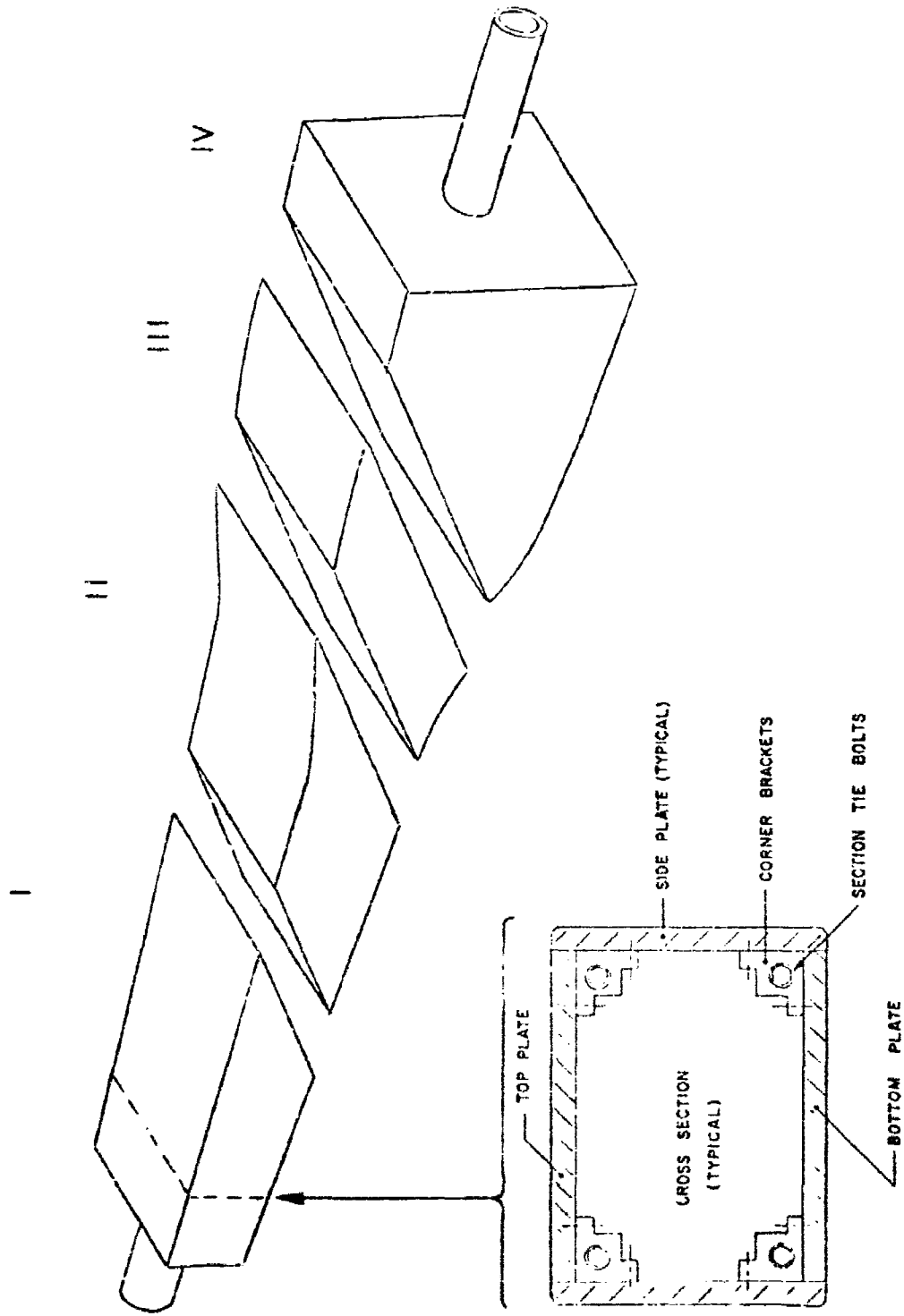
Figure 24. Mandrel Sections.

62

The requirement of dimensional stability influenced the choice of materials. For example, the use of wood would have involved some risk because of the long curing time and the presence of the fumes from the hot epoxy. These could have combined to change the wood dimensions in a manner which would have led to shifting of the electrodes, which could lead to cracking of the interframe ceramic.

D. DESIGN SPECIFICATIONS

1. General

The high power MHD channel/diffuser design specifications for the magneto-hydrodynamic, thermal, hydraulic, and structural requirements are defined in the following sections. Each subsection presents the specific requirements for each of the functional areas of the channel/diffuser system. As discussed in Section IV-C, the channel/diffuser was required to be designed to meet the performance requirements and for testing in the HPMS test facility at AEDC.

2. Magnetohydrodynamic

The magnetohydrodynamic design specifications are listed in Table 9. The specifications were used to complete the high power MHD channel/diffuser design. The channel/diffuser was designed for optimum operation at the nominal flow conditions shown in Table 9. Operation at off design flow rates of $\pm 20\%$ variation was also provided for in the overall design of the MHD channel/diffuser.

The channel design consisted of several groups of different types of electrode frames: (1) inlet perpendicular frames, (2) inlet transition frames, (3) diagonal frames, and (4) exit transition frames. The quantity and angle of each of these frames was selected to assure satisfactory performance of the channel/diffuser system.

3. Thermal

In order to obtain satisfactory electrical performance, the surface temperature of the electrode ceramic in the electrode frame cups was designed to reach 2000 K during steady state operation. To avoid any rapid degradation of the useful life of any of the electrode frames, the design copper frame temperature was maintained below 750 K. The design temperature of the inside of the case was kept below 420 K to prevent any degradation of the composite structural integrity, and the temperature of the outside of the case was designed to remain below 340 K to permit the utilization of pressure transducer and accelerometers to record the pertinent test data. The thermal design specifications along with the hydraulic and structural design requirements are given in Table 10.

63

TABLE 9. MHD DESIGN SPECIFICATIONS

Reactants

    Oxidizer   Liquid Oxygen

    Fuel   JP-4

    Emulsifier   SPAN-80

    Seed $Cs_2 CO_3/ H_2O$ Solution

Reactant Mass Flow Rate   24–36 kg/sec

Combustor Stagnation Pressure   24–36 atm

Seed Flow Rate   1–10% of Total Mass Flow

Nominal Flow Conditions

    Combustor Stagnation Pressure   30 atm

    Combustor Stagnation Temperature   3420 K

    Reactant Mass Flow Rate   30 kg/sec

    Seed Flow Rate   5% of Total Mass Flow

    Channel Inlet Pressure (Static)   3.0 atm

    Channel Expansion Ratio   10

    Cannel Inlet Mach. No.   2.06

    Channel Inlet Temperature (Static)   ~ 2800 K

    Peak Magnetic Field Strength   4.0 T

Nominal Electrical Condition

    Electrical Output Power   30 MW_e

    Energy Extraction   1 MJ/kg

    Power Density in MHD Channel   200 MW_e/m^3

    Electrical Load $\leq$1 Ω

    Axial Voltage Gradients $\leq$4000 V/m

    Electrode Current Density $\leq$10 A/cm^2

    Hall Parameter (Maximum)   4.0

Operating Conditions

    Steady-State   150 sec

    Transient   Up to 10 Pulses

TABLE 10. MECHANICAL DESIGN SPECIFICATIONS

THERMAL

Frame Temperature at the Gas Face	759 K
Frame Temperature at the RTV Face	366 K
Average Frame Temperature	563 K
Frame Temperature Gradient (Assumed Linear)	393 K
Case Inner Face Temperature (Assumed)	350 K
Case Outer Face Temperature (Assumed)	273 K

HYDRAULIC

Coolant Passage Pressure	27.2 atm
Frame Pressure Drop (Max)	24.0 atm
Assumed Coolant Temperature (Frame Inlet)	295 K
Assumed Coolant Temperature (Frame Outlet)	310 K
Coolant Velocity (Max)	24 m/sec
Frame Coolant Flow Rate (Max)	0.75 liters/sec
Total System Coolant Flow Rate	7200 liters/min

STRUCTURAL

Vibration Input

Amplitude (Maximum)	4 g in all directions
Frequency	5 to 200 Hz

Channel Mass		600 kg
Channel Pressure	Inlet	Exit
	4.5 atm (Internal)	0.15 atm (Internal)
	1.0 atm (External)	1.0 atm (External)
Design Δ P	3.5 atm (Internal)	0.85 atm (External)
Life		5 h
Cycles		1000

Factor of Safety

Life	10
Static Loads	4
Wall Deflection	2

Wall Deflection	0.76 mm
No Frame Buckling	--

Channel is to be bolted to the combustor/nozzle at the inlet with
pins to establish the collinearity of the combustor and channel axes
and with oversize bolt holes to avoid thermal stresses because of
differences in the radial movement of the combustor and channel at
the interface.

4. Hydraulic

The water cooling system design requirements for the high power MHD channel/diffuser must not exceed the capability of HPMS test facility at AEDC. These test facility limits were a maximum water flow rate of 315 liters/sec, a maximum system pressure drop of 27.2 atm, and a maximum system pressure of 28.2 atm. The channel/diffuser channel water manifolds were required to be located above and below the cooling and to fit within the available volume envelope between the channel and the HPMS magnet. To minimize any manifold pressure loss, the manifold water velocity was required to be less than 20% of the electrode frame to manifold connecting tube velocity. Interconnects between frames were used to reduce the total cooling water flow requirements.

5. Structural

In Table 10, a summary of the structural design specifications is provided. This table refers to the channel/diffuser structural design specifications only. Table 11 provides the structural design specifications for the mandrel design, which will be discussed in more detail in the next paragraph. The design specifications of Table 10 have been based on the design criteria discussed previously. The channel/diffuser design has accounted for the channel loading caused by the internal gas pressure, channel mass, vibrational inputs across the interfaces, and the magnetic field faces. These loads were used to determine the case thickness and electrode frame construction as well as the anchor spacing.

The mandrel design criteria were used to establish the design specifications shown in Table 11. Since the mandrel was designed to be used as the primary fabrication tool for the channel/diffuser, the design specifications were critical to producing a satisfactory mandrel. An important consideration in the establishment of the design specification was the number of mandrel sections to be incorporated. The details of this evaluation are discussed in Section IV-E.

E. DESIGN ANALYSIS

1. Introduction

Theoretical investigations were conducted on all aspects of the high power MHD channel/diffuser to establish the ability of the component to perform effectively in the hot gas flow train and to meet the life and performance design requirements with appropriate safety factors. Analyses of the magnetohydrodynamic, thermal, hydraulic, and structural requirements were conducted. The following sections present the results of those analyses.

TABLE 11. MANDREL STRUCTURAL DESIGN SPECIFICATIONS

Allowable Alternating Strain on Interframe Ceramic	0.001
Allowable Local Deflection of Frame Array Because of Roving Tension and Channel Mass	0.025 mm
Epoxy Curing Temperature	366 K
Maximum Allowable Freedom of Frames Because of Differential Expansion With Respect to Mandrel From Room Temperature to 366 K	0.025 mm
Maximum Allowable Coefficient of Friction Between Mandrel Strong-Back and Spacers	0.01
Rotation Rate to Prevent Epoxy Dripping During Winding	30-60 rpm
Total Number of Rotations (Assumed)	10^4

2. Magnetohydrodynamics

a. Introduction

The analysis of the high power MHD channel/diffuser performance was conducted by using an MHD generator computer program, discussed later in this section, designed for segmented generators. The program modeled the entire MHD generator hot gas flow train. The output from the program described the electrical and aerodynamic performance of the generator, the wall heat transfer rates, the electrical conductivity of the combustion products, the electrode voltage drop, and the aerodynamic effects relating to boundary layer separation and stall.

An MHD generator design analysis of this type was used to accurately design and select the geometric dimensions and the critical construction configurations of the generator gas flow train. Computer programs of this type have been used previously to design the High Performance APL Channel[5] and the Viking Channel.[3] Particular attention was given to the design of the generator channel since it was the most important subsystem in terms of achieving the desired electrical performance.

To design the channel and diffuser and to establish their appropriate geometrical dimensions required a detailed design analysis to insure optimum performance for the specified design operating conditions. In addition to the effects of the MHD interaction on the flow of the combustion products, such effects as the electrode voltage drop, electrode segmentation and construction, wall roughness and shear stress, and boundary layer separation and stall were considered to achieve a satisfactory channel design. Furthermore, to assure satisfactory performance of the channel, several constraints were imposed on the design including limits on the magnitudes of the electric fields, the Hall parameter, and the electric current density. The required operating time, the condition of the boundary layers, and for advanced high-interaction devices, such things as flow instabilities were also considered before selecting a channel design.

---

[3] O.K. Sonju, J. Teno, R. Kessler, L. Lontai, and D.E. Meader, "Status Report on the Design Study Analysis and the Design of a 10 MW Compact MHD Generator System," AFAPL-TR-74-47, Part II, June 1974.

[5] O.K. Sonju, J. Teno, J.W. Lothrop, and S.W. Petty, "Experimental Research on a 400 kW High Power Density MHD Generator," AFAPL-TR-71-5, May 1971.

b. Design Alternatives and Objectives

For the design of the MHD generator, certain facility and design constraints must be integrated into the channel/diffuser design. Some of these constraints result from MHD performance considerations while other constraints occur because of practical aspects of the fabrication processes. Some of the more important design alternatives are discussed in the following paragraphs.

Two channel cross sections, oval and rectangular, were evaluated to select the optimum shape. The oval cross section resulted in modified elliptical electrode shapes. Both geometries have been analyzed to optimize performance.[1] The analyses have shown that a more compact device can be produced by using the oval design. This result occurred because the oval design maximized the volumetric filling factor of the magnet warm bore and reduced the channel wall thickness since the wall stress levels were reduced. However, when the fabrication process was reviewed, the oval design was considerably more costly and time consuming than the rectangular design. Therefore, on this basis the rectangular cross section was used for the high power MHD channel/diffuser design.

Several development steps in the electrode development have resulted in a significant reduction in the electrode frame mass. The electrode frames in many existing MHD generators have been constructed by machining the trapezoidal central region out of solid copper plates. This approach produced a rather heavy, thick wall construction which was not competitive from an overall system design point of view. The details of various designs have been previously evaluated and will not be repeated here.[4] Figure 25 shows the evolution of the electrode frame design from the initial heavyweight design to the final lightweight configuration selected.

With the lightweight design shown in Figure 25, a significant reduction in the channel mass and volume was achieved by separating the pressure wall function from the electrode frame function. No interelectrode frame gas sealing was required for this design - a feature which was extremely important for reliable operation. In addition, the surfaces of the electrode frames did not have to be machined to either high precision dimensional flatness tolerances or critical surface finish requirements.

---

[1] O. K. Sonju and J. Teno, "Study of High Power, High Performance Portable MHD Generator Power Supply Systems," AFAPL-TR-76-87, August 1976.

[4] D. W. Swallom, O. K. Sonju, D. E. Meader, and G. T. Heskey, "MHD Lightweight Channel Development," AFAPL-TR-78-41, June 1978.

HOT GAS SURFACE

HEAVY COPPER
FRAMES

FRAME-TO-FRAME
BOLTS AND DOWELS

(a) Heavy Weight

HOT GAS SURFACE

MEDIUM WEIGHT
COPPER FRAMES

COMPRESSION TIE RODS

(b) Medium Weight

HOT GAS SURFACE

LIGHTWEIGHT
COPPER COOLING TUBES

GLASS EXPOXY SHELL
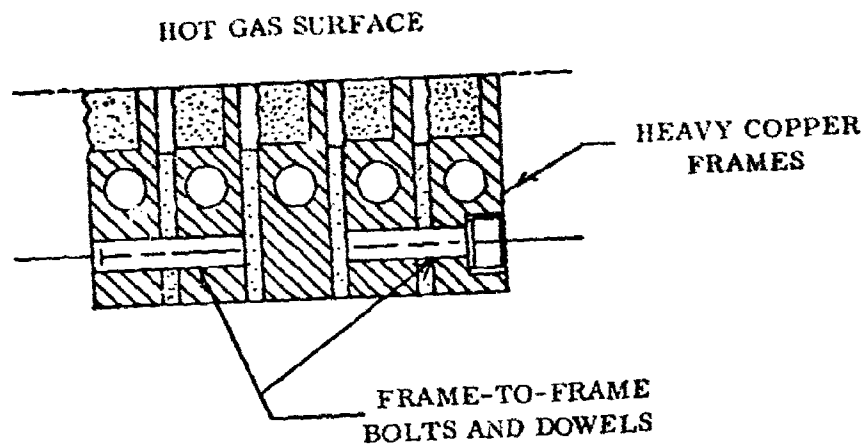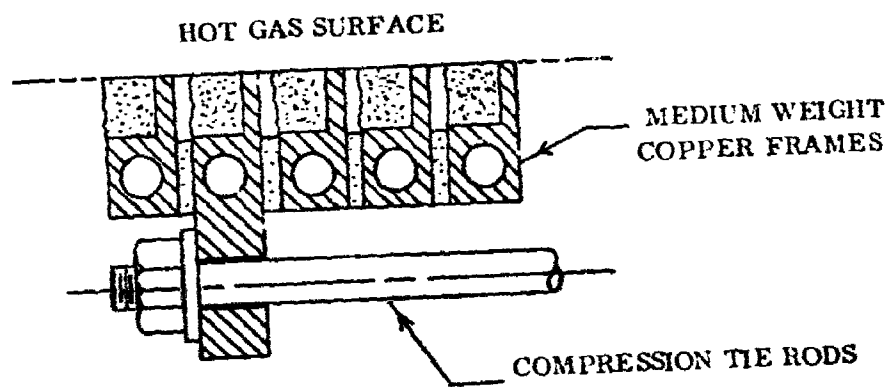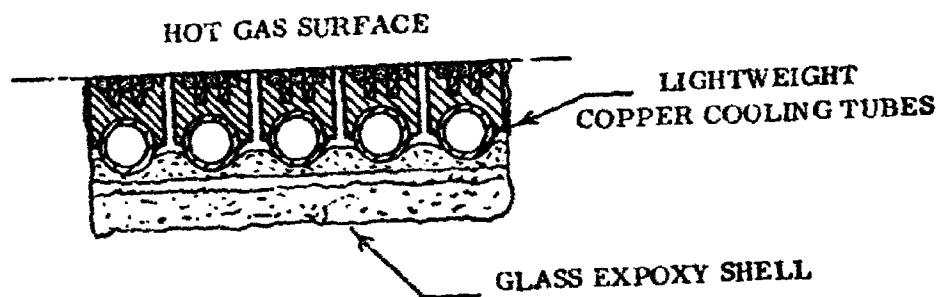
(c) Light Weight

Figure 25.   Electrode Frame Development.

70

In addition to the advantages obtained by reducing the channel mass and volume, other significant gains were achieved. Some of these advantages were: (1) potential for low cost fabrication; (2) increased reliability; (3) finer segmentation of the electrodes; (4) integral cooling passages without braze or weld joints or connections at elevated temperatures; (5) no gas sealing problems; (6) no critical tolerances inside the entire channel; (7) minimal thermal expansion problems since close tolerances of the mating surfaces of dissimilar materials were not required; (8) flexibility and simplicity of construction; and (9) mechanical simplicity. Since the overall channel design objective was a reduction of channel mass and volume along with increased reliability, decreased fabrication complexity and increased design flexibility, the general design approach selected was required to satisfy all of these objectives.

Another key feature in the reduction of the channel/diffuser mass was the use of a filament wound, fiberglass epoxy resin shell. This shell was fabricated in place around the outside of the electrode frames. The high strength-to-mass ratio of the shell was the result of the continuous glass filaments that were wound around the channel. These filaments formed the four walls without any seams or joints along the edges of the channel.

For the MHD channel/diffuser design analysis, the high power MHD system performance goals were used to evaluate the various design alternatives. In addition, constraints on the operating parameters of the MHD channel, such as limits on the electric field, the current density, the heat transfer rates, the Hall parameter, the electrical conductivity, the boundary layer shape factor, the loading parameter, the length to diameter ratio (L/D) of the channel, and the electrode segmentation and interelectrode voltage gradients, were imposed. Further restrictions resulted from the limitations imposed by the magnetic field, the available volume in the magnet for the channel, the test facility cooling capacity, and any other externally imposed constraints such as safety factors, etc. Thus, the total system configuration and performance was considered in the process of selecting the design point.

In addition, the off-design performance at mass flow variations of $\pm 20\%$ from the nominal were considered. The channel/diffuser configuration selected was designed based on a conservative value of the electrical conductivity. This approach provided an MHD channel design which would operate satisfactorily if the combustor did not perform as designed or if problems were encountered in obtaining satisfactory Cs_2CO_3 ionization or flow uniformity.

Since a maximum magnetic field strength of four Tesla was available, the field strength for the design analysis was fixed. Through previous experience limits and constraints were placed on some of the remaining design variables.[1] The electric fields and the electrode current densities were limited to a maximum of five kilovolts per meter and ten amperes per square centimeter, respectively. The Hall parameter was limited to a value less than or equal to four. The heat transfer rate was limited to 1000 W/cm^2.

In the selection of the L/D ratio of the channel, two major considerations were involved: (1) for small values of L/D, the end effects were important and generator performance was degraded; and (2) the overall system mass of the Phase D system would increase because the magnet would be so short that the end regions would dominate the magnet mass. However, as the power density increased, the channel length decreased if other flow parameters remained constant. This phenomena was particularly relevant in this effort in that several magnetic field profiles were considered before a final configuration was established. Each profile required a longer channel, and hence, a decrease in the power density occurred for successive iteration. For these conditions, a lower limit on L/D of four was selected. Since optimizing L/D for maximum energy extraction did not necessarily result in the optimization of L/D for energy density or vice versa some trade-offs were required to establish the most satisfactory design and operating conditions.

Using these design constraints the performance of the high power MHD generator system was analyzed. The combustor stagnation pressure was selected as 30 atm with a $\pm$ 20% variation. Inlet electrical conductivities of 14 to 18 mhos/m were analyzed, and the performance evaluated for each case. In the following two subsections, the analytical model is described and the results of the performance analysis are presented, respectively.

c. Analytical Model

In the present design analysis the flow was assumed to be developing rather than fully developed since for MHD channels of interest the length-to-diameter ratio was typically ten or less. Therefore, the flow was divided into an inviscid core region occupying most of the channel area and a boundary layer confined to the immediate vicinity of the channel walls. The boundary-layer displacement

thicknesses were calculated from the momentum integral equations, taking into consideration the shape factor, compressibility, and wall cooling effects. The wall roughness effects on the skin friction were also considered. The energy equation for the boundary layer was not considered. For channels built to date, the electrical dissipation in the boundary layer has been relatively small compared to the wall heat transfer rate. Consequently, the usual, non-MHD flow compressible flow relations between the velocity and enthalpy were sufficiently accurate so that satisfactory results were obtained without solving the energy boundary layer equation. The combustion products were assumed to be in chemical equilibrium at the local conditions at all points in the flow field.

The governing equations for the inviscid core flow region for the diagonally connected generator were the equations for continuity, momentum, and energy. [7] For the compressible boundary layer analysis the MHD momentum integral equation was used. The term in the one-dimensional momentum integral equation to account for the MHD effect,

$$(\rho u^2)^{-1} \quad [J_y(\text{core}) - J_y(\ell)]\, B d\ell,$$

vanishes for the electrode boundary layer since J_y on the average was constant through the boundary layer. However, for the insulator wall this term gave rise to the Hartman effect. [8]

In the momentum integral equation, a solution for the shape factor in terms of the other parameters was required. For compressible turbulent boundary layers, no really useful method for determining the shape factor directly was available. However, for incompressible flows several empirical correlations such as Garner's equation have been used. [9] No existing correlations accounted for the MHD effects. The incompressible shape factor was calculated as a function of the momentum thickness and the core properties in accordance with Garner's equation. As in boundary layer theory, the shape factor was used both as an approximate separation criterion and as a means of establishing the approximate velocity profiles.

---

[7] G.W.Sutton and A.Sherman, "Engineering Magnetohydrodynamics," McGraw Hill, 1967.

[8] O.K.Sonju, "Viscous Magnetohydrodynamic Flows," Stanford University Institute for Plasma Research, SUIPR Report No. 245, 1968.

[9] H.C.Garner, "The Development of Turbulent Boundary Layers," ARC of Britain R&M 2133, 1944.

To evaluate the shape factor, the density profile was also required. Crocco's relation for a compressible flow with zero pressure gradient and with a Prandtl number of one provided the enthalpy distribution.

$$\frac{h(\ell)}{h} = \frac{hw}{h} + (1 - \frac{hw}{h} - \frac{u^2}{2h})\frac{u(\ell)}{u} - \frac{u^2}{2h}(\frac{u(\ell)^2}{u})$$

where

h	= enthalpy
u	= velocity
hw	= wall enthalpy
h(ℓ)	= local enthalpy
u(ℓ)	= local velocity

With this enthalpy distribution and with the pressure constant through the boundary layer, the density profile was then determined from the chemical equilibrium calculations, and the usual integrations were performed to obtain the value of the shape factor. No detailed MHD boundary layer measurements existed for this type of flow and the accuracy of this technique has not been assessed in detail. However this technique has been used to accurately predict the performance of several generators and even boundary layer separation and stall have been accurately predicted.[3,5,10] In addition to the equations discussed previously, the equations for the axial and transverse current density, the axial and transverse electrical fields, and the loading parameter were required.

In the computer analysis the differential equations were integrated along the channel by a four point Runge-Kutta integration procedure. The values of the various parameters at the nozzle exit were used as the initial values to start the

---

[10] J. Teno, T.R. Brogan, S.W. Petty, J.W. Lothrop, and O.K. Sonju, "Research Studies and the Development of MHD Generators and Accelerators," AEDC-TR-70-14, January 1970.

integration. The channel area, the diagonal electrode connections, and the total load current were inputs. The thermodynamic and transport properties and the flow and the electrical performance parameters were calculated and tabulated as functions of the axial distance along the channel. Axial voltage and current characteristics were also available.

d.   Performance Analysis

The results of the computer analysis discussed in the previous section are presented in the figures of this section. The axial magnetic field profile of the HPMS magnet at AEDC is shown in Figure 26. The peak field was four Tesla. The internal cross sectional area of the MHD channel is shown in Figure 27. The channel area increased linerarly with distance until approximately 1.25 m from the nozzle/channel interface where the linear area increase continued, but at a much more rapid rate. Figure 28 illustrates the axial static pressure distribution for the generator under load operating at the nominal design conditions. The design heat fluxes to the generator walls are shown in Figure 29. The maximum design heat flux to the walls of ≈ 900 w/cm^2 occurred at the channel/nozzle interface and decreased to a value of ≈ 100 w/cm^2 at the channel exit.

Figures 30 and 31 show the boundary layer displacement thickness and the electrode voltage drop, respectively. Both parameters increased substantially as a function of axial distance from the channel/nozzle interface. The transverse current density is shown in Figure 32. These values are well below the upper limit of ten amperes per square centimeter. The axial voltage distribution is shown in Figure 33. The voltage profile was approximately linear with axial distance and increased to a value of nearly 5.5 kV at the channel exit. The conductivity as a function of axial position is shown in Figure 34. The inlet conductivity was 15 mhos/m and varied between 15 and 17 mhos/m throughout the channel length.

The total power output of the MHD channel as a function of axial distance is shown in Figure 35. The figure shows the design power level of approximately 32 MW$_e$ output power. Figure 36 shows the power density as a function of axial location in the channel. Because of the elongated axial magnetic field profile, the power density of 200 MW$_e$/m^3 is obtained only over a portion of the MHD channel. Figure 37 shows a summary of the performance of the generator at the nominal operating point and several other potential operating points. At the right side of the figure, a line has been drawn to indicate the upper limit of the electrode current density of 10 A/cm^2. Several lines representing various electric field limits are also shown as are curves for various values of the MHD channel inlet conductivity. Table 12 presents a summary of the results of the MHD calculations.

PREDICTION OF 30 MW DIAGONAL GENERATOR

CASE 1200.366Z=0366 AND I=6KA,SF=.8,PLOT
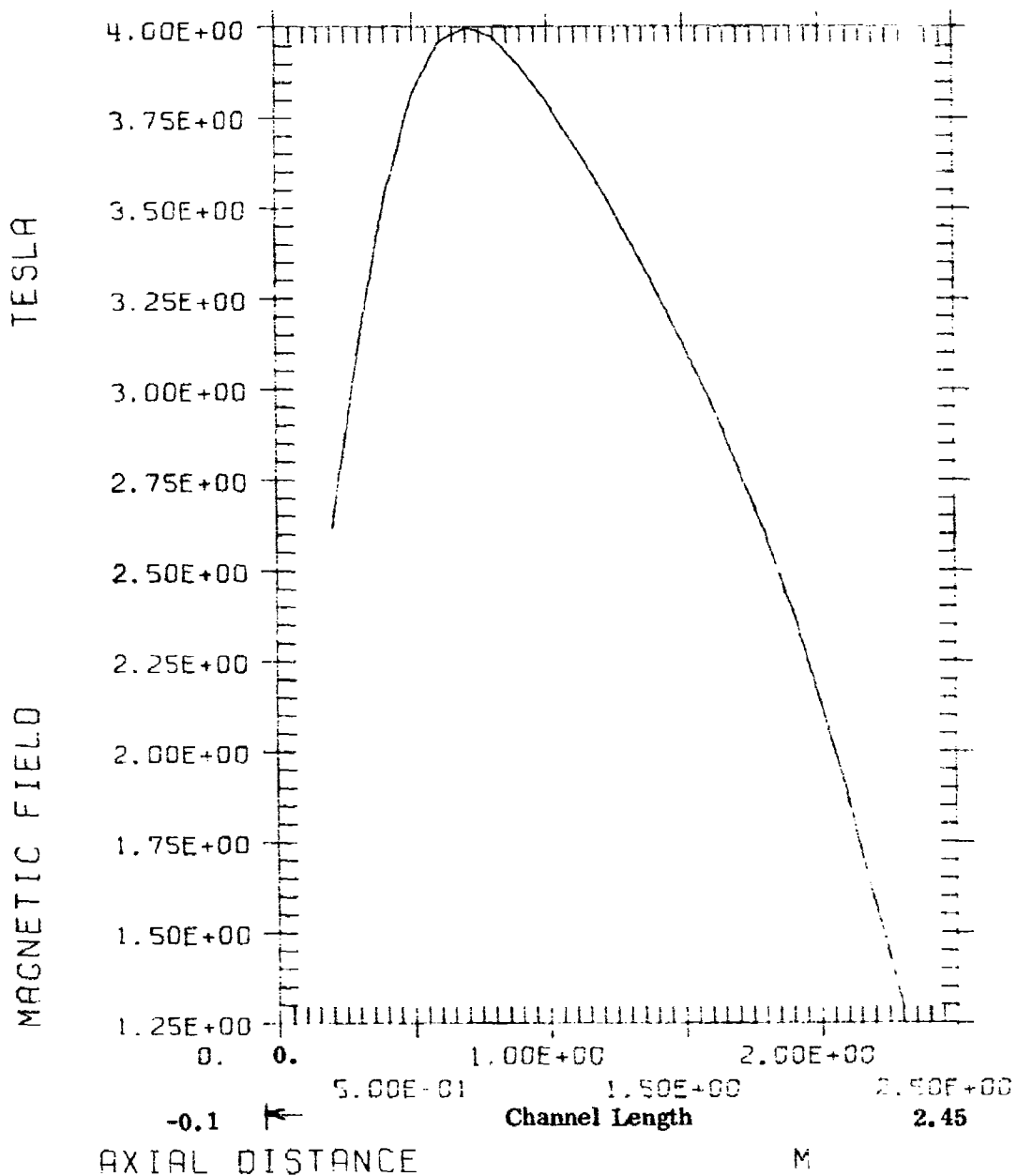
Figure 26. Axial Magnetic Field Profile.

PREDICTION OF 30 MW DIAGONAL GENERATOR

CASE 1200.366Z=0366 AND I=6KA,SF=.8,PLOT
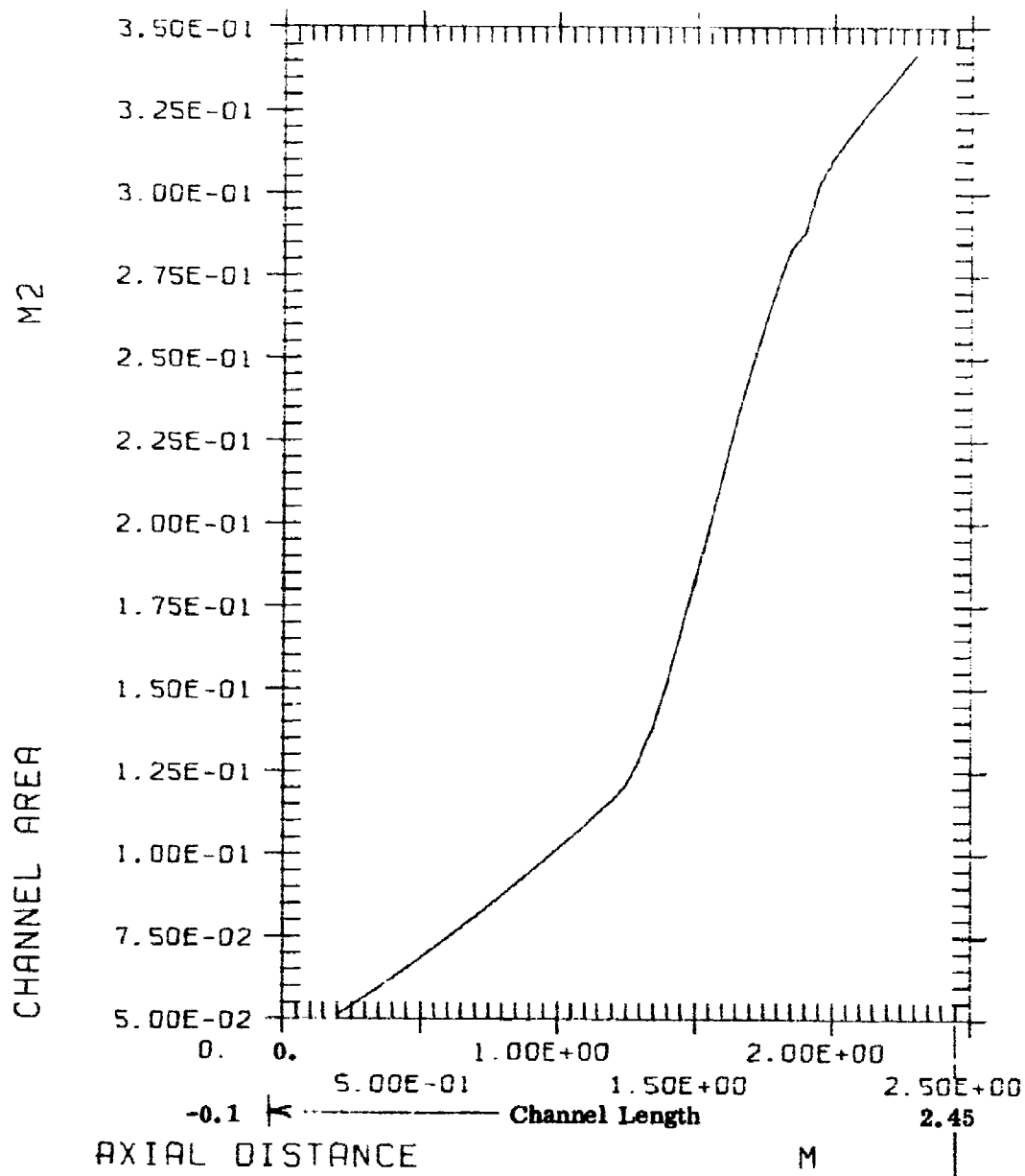
Figure 27.   Channel Area Profile.

PREDICTION OF 30 MW DIAGONAL GENERATOR

CASE 1200.366Z=0.366 AND I=6KA,SF=.8,PLOT
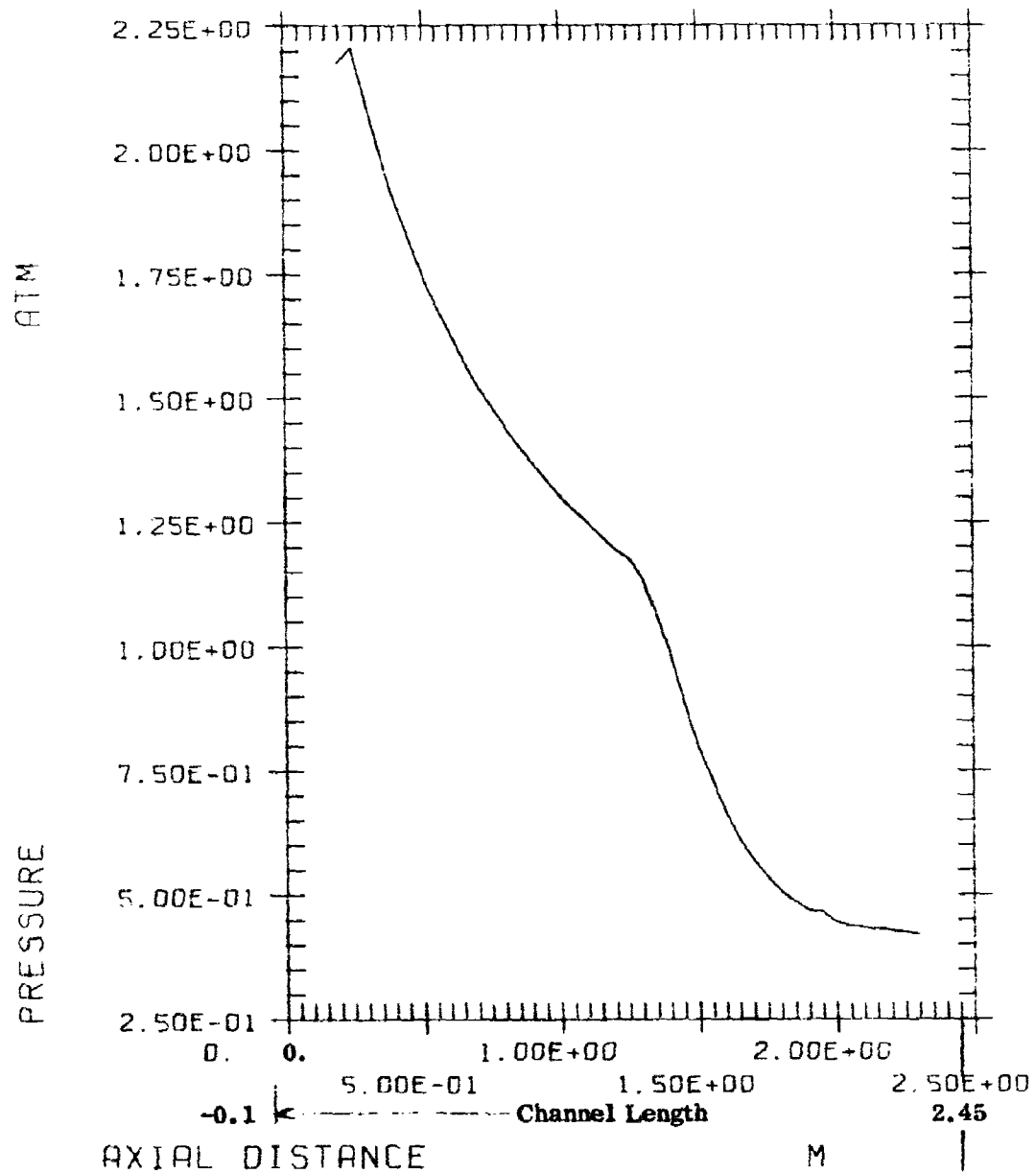
Figure 28.   Axial Static Pressure Distribution.

PREDICTION OF 30 MW DIAGONAL GENERATOR

CASE 1200.366Z=0366 AND I=6KA,SF=.8,PLOT
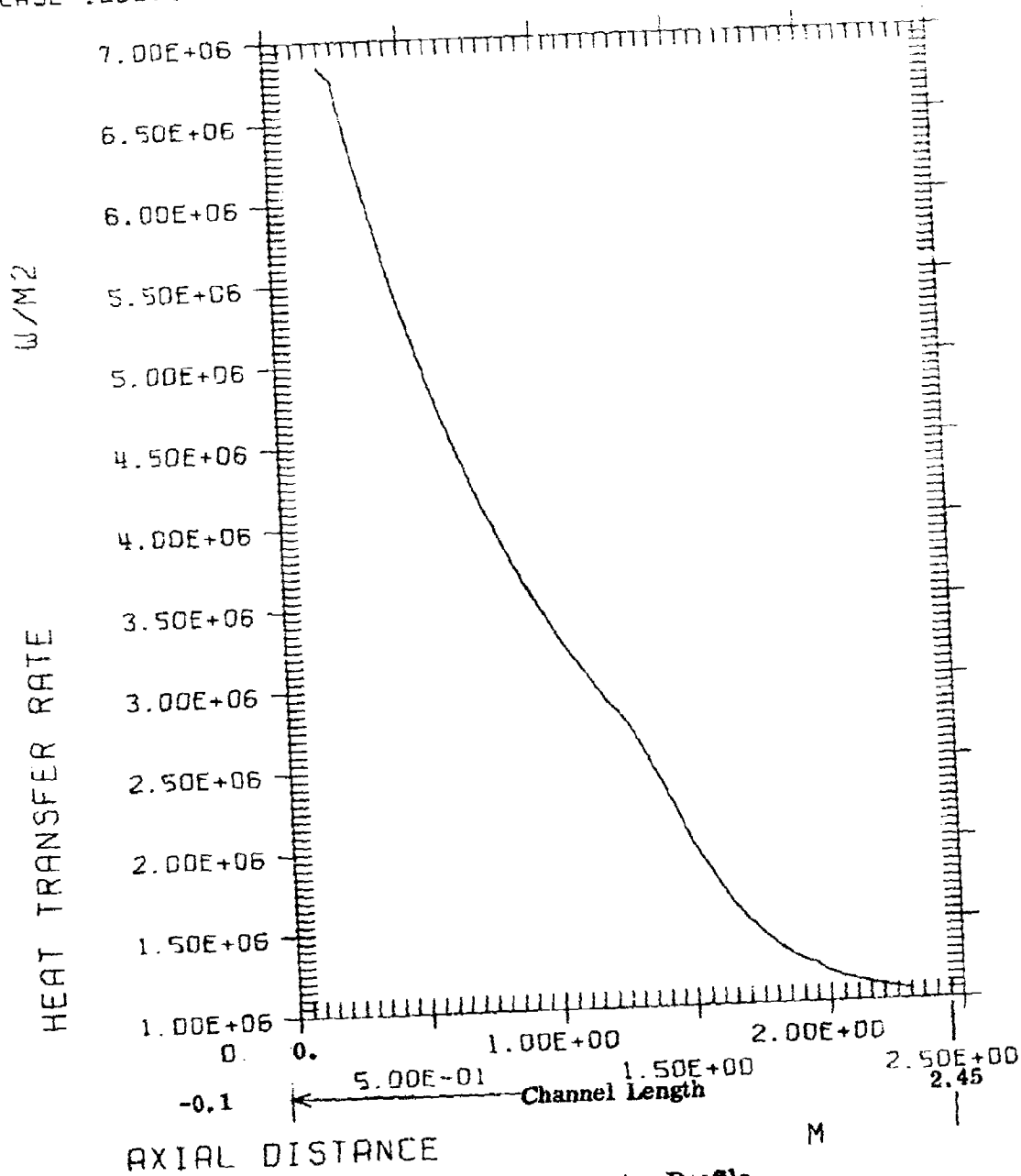
Figure 29.   Axial Heat Transfer Profile.
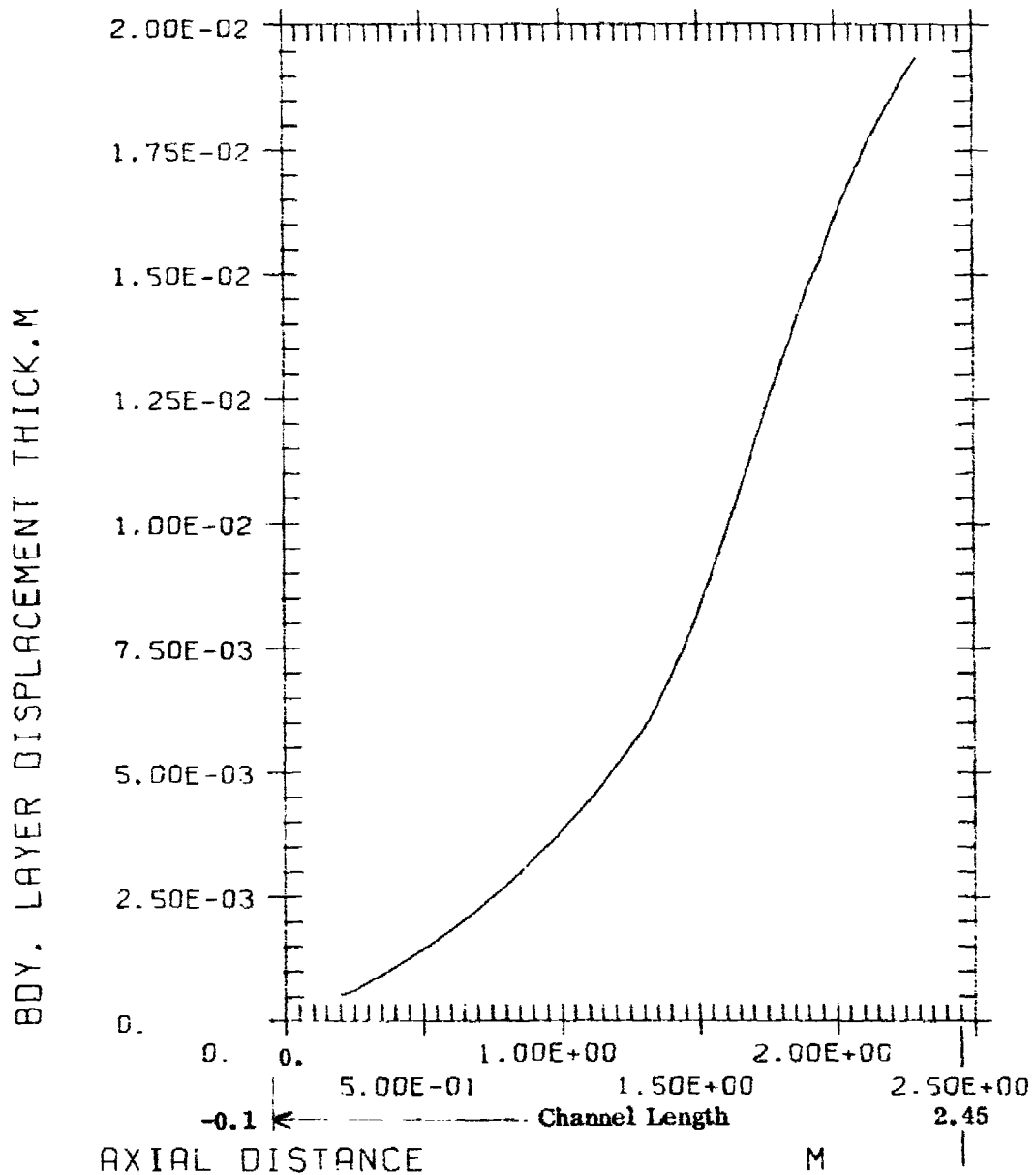
Figure 30.   Boundary Layer Displacement Thickness

80

PREDICTION OF 30 MW DIAGONAL GENERATOR

CASE 1200.366Z=0366 AND I=6KA,SF=.B,PLOT
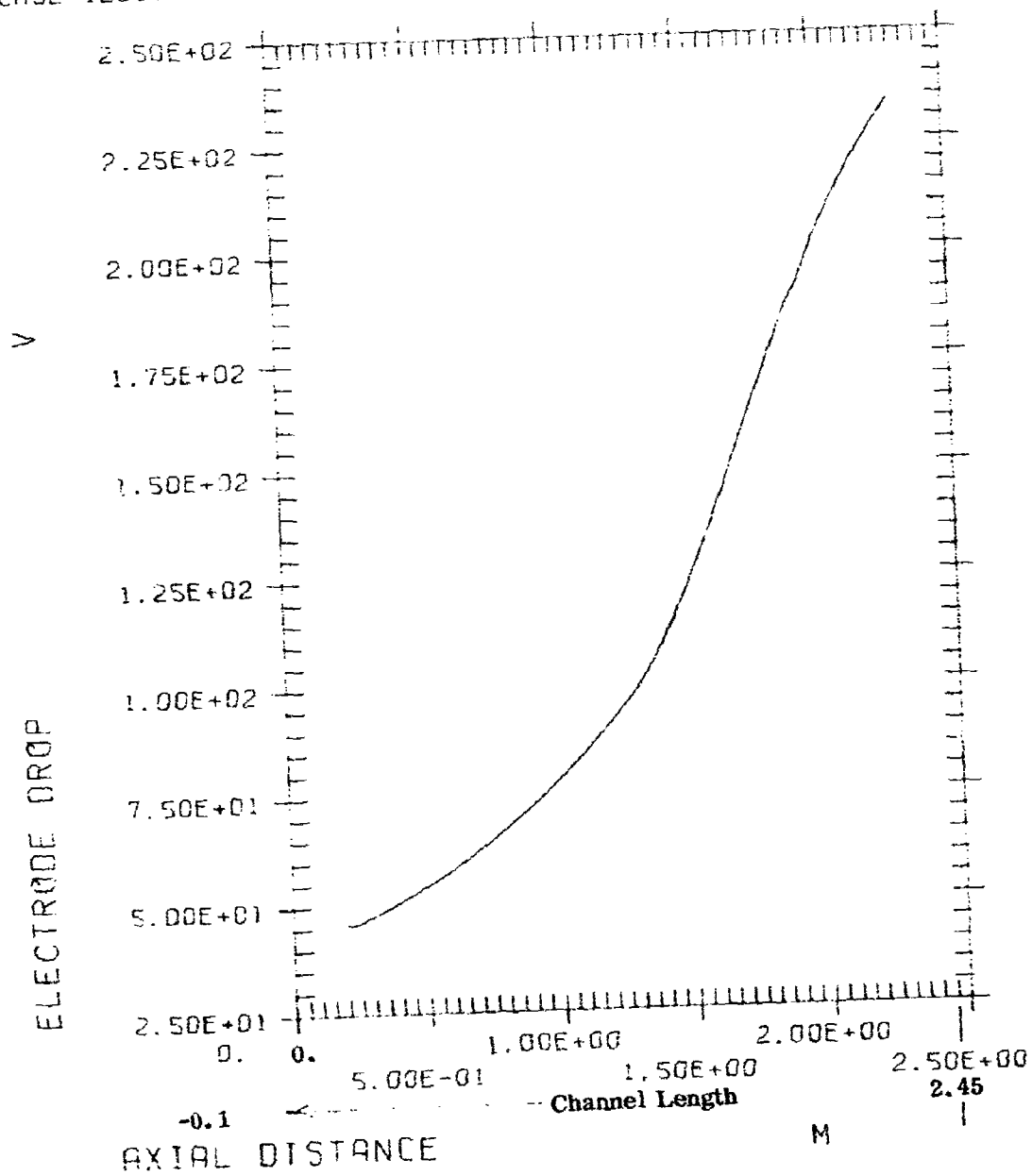
Figure 31. Electrode Voltage Drop.

81

PREDICTION OF 30 MW DIAGONAL GENERATOR

CASE 1200.366Z=0366 AND I=6KA,SF=.8,PLOT
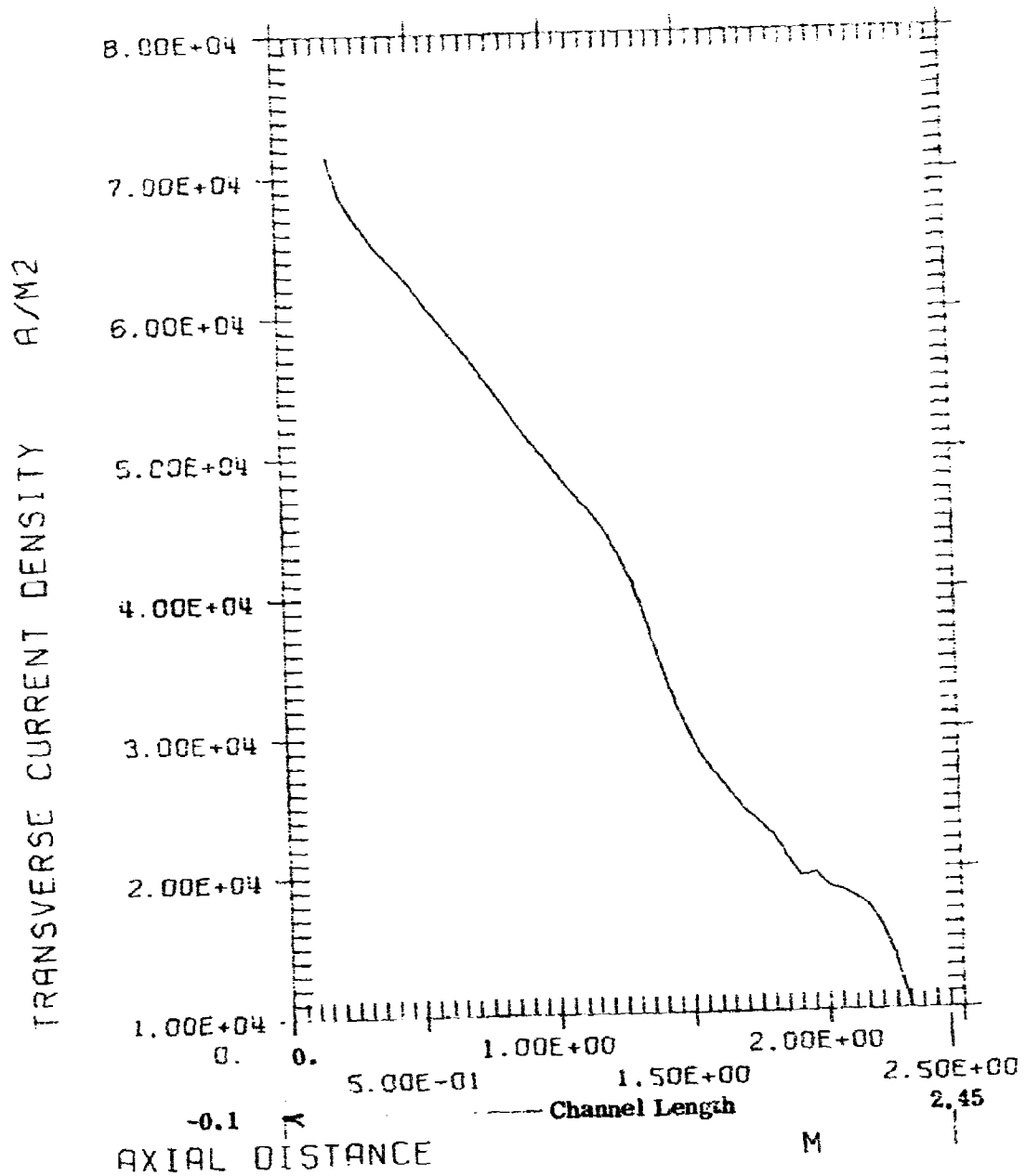
Figure 32.   Transverse Current Density.

82
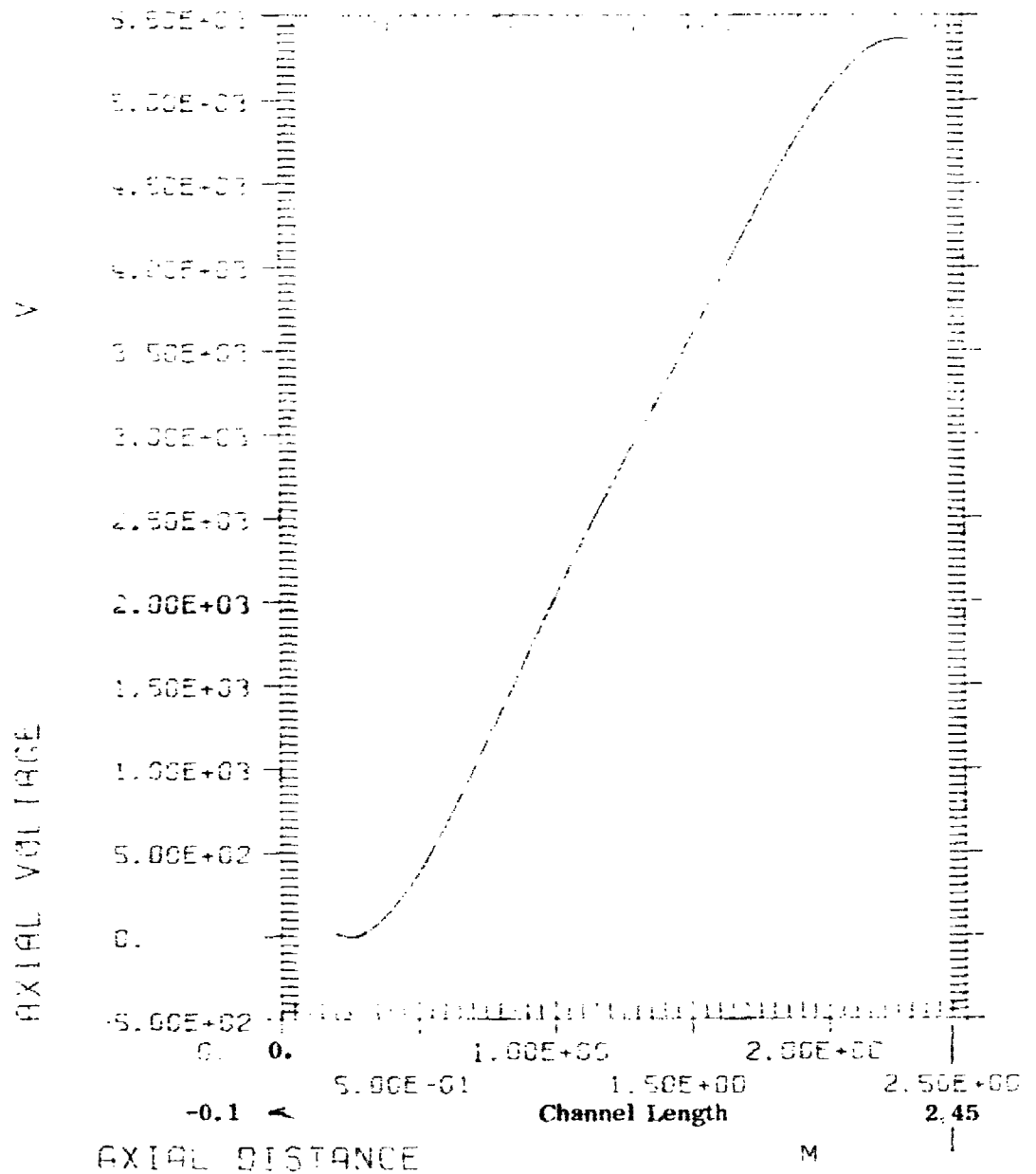
Figure 33. Axial Voltage Distribution.

83

PREDICTION OF 30 MW DIAGONAL GENERATOR

CASE 1200.366Z=0366 AND I=6KA,SF=.8,PLOT

Figure 34.   Gas Electrical Conductivity.

PREDICTION OF 30 MW DIAGONAL GENERATOR

CASE 1200.3662=0366 AND I=6KA.SF=.8.PLOT

Figure 35.   Total Power Output.

85

Figure 36.   Power Density.

86
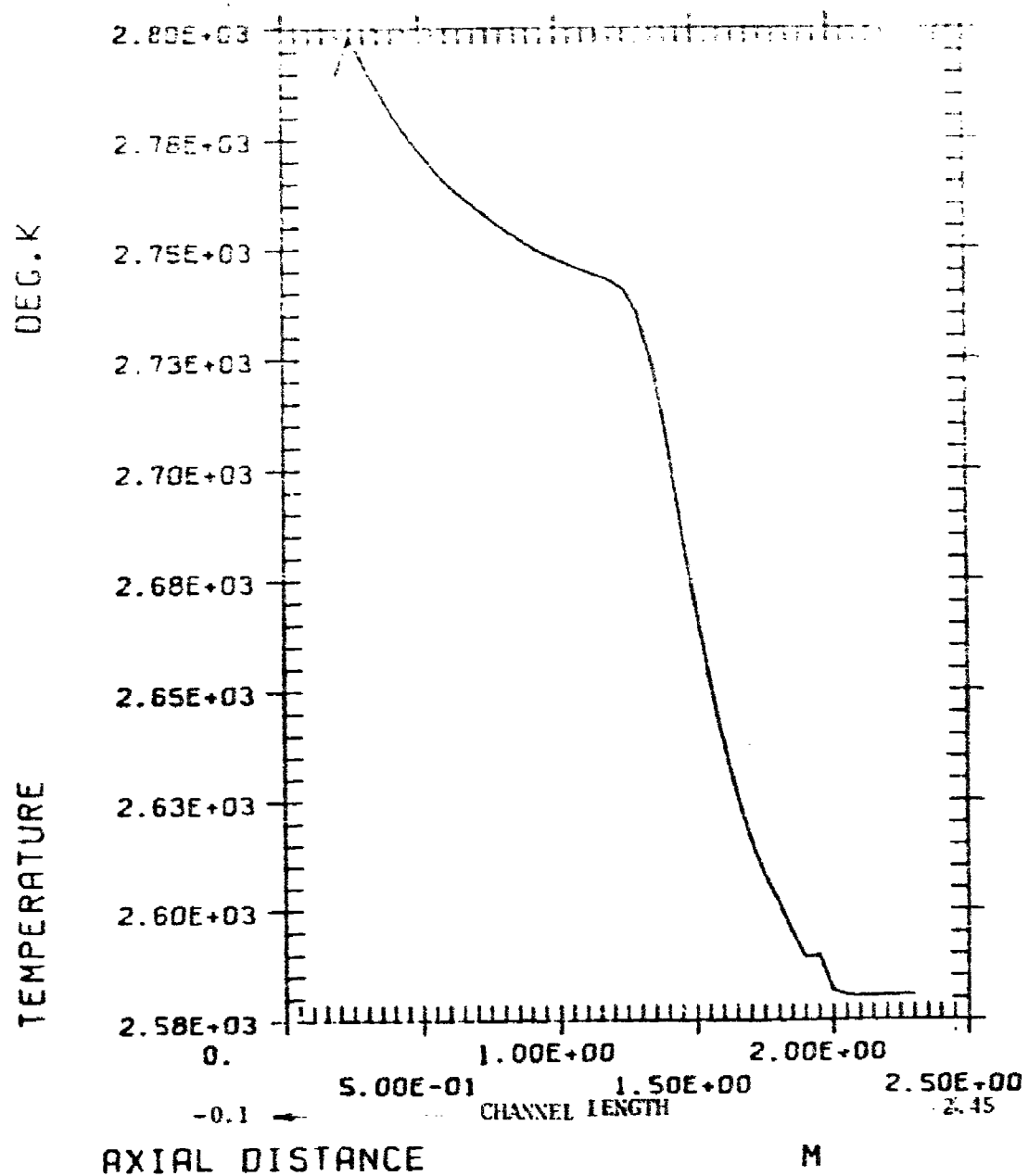
Figure 37. Static Temperature.

87

PREDICTION OF 30 MW DIAGONAL GENERATOR

CASE 1200.366Z=0366 AND I=6KA,SF=.8,PLOT
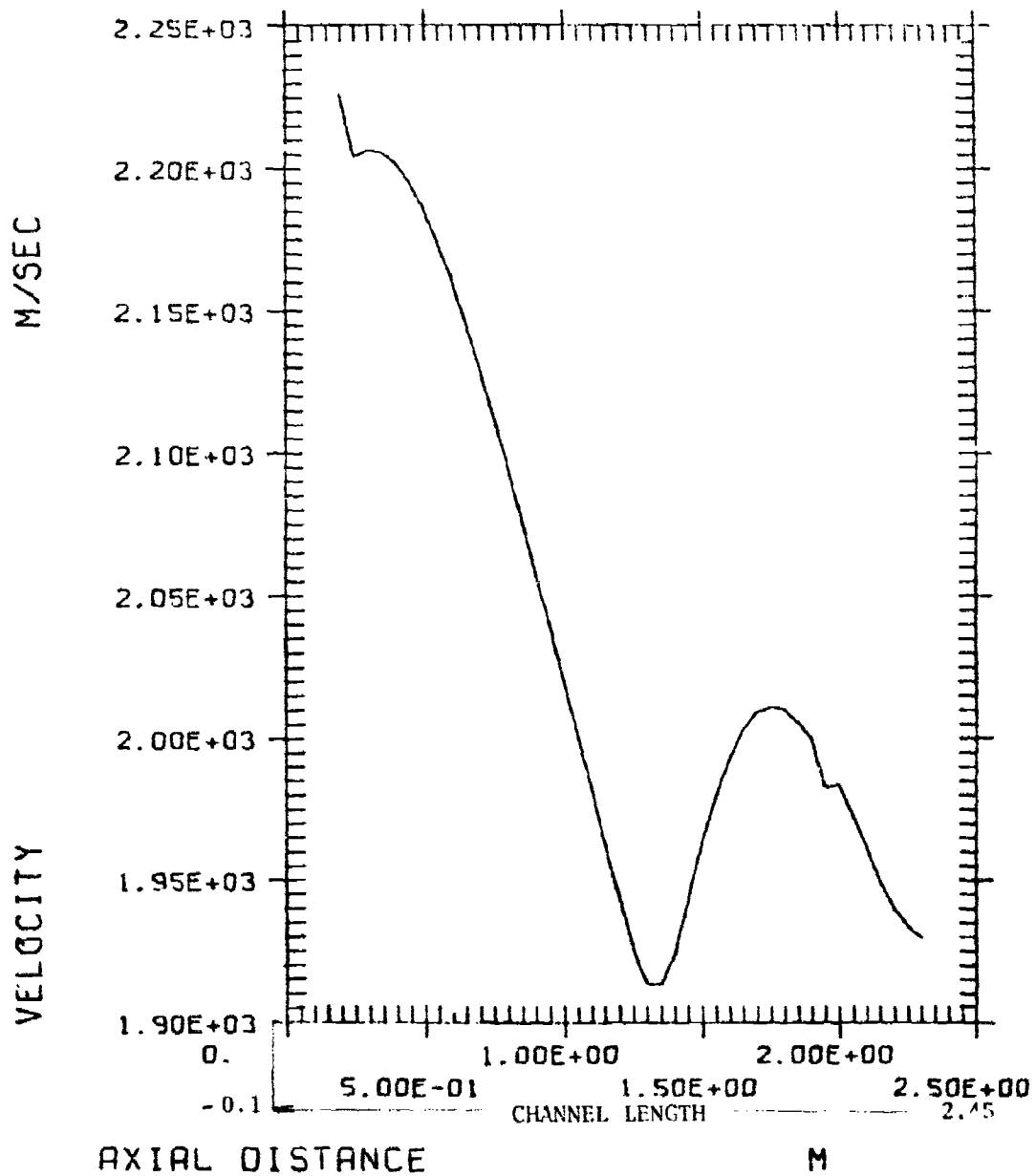
Figure 38. Velocity.
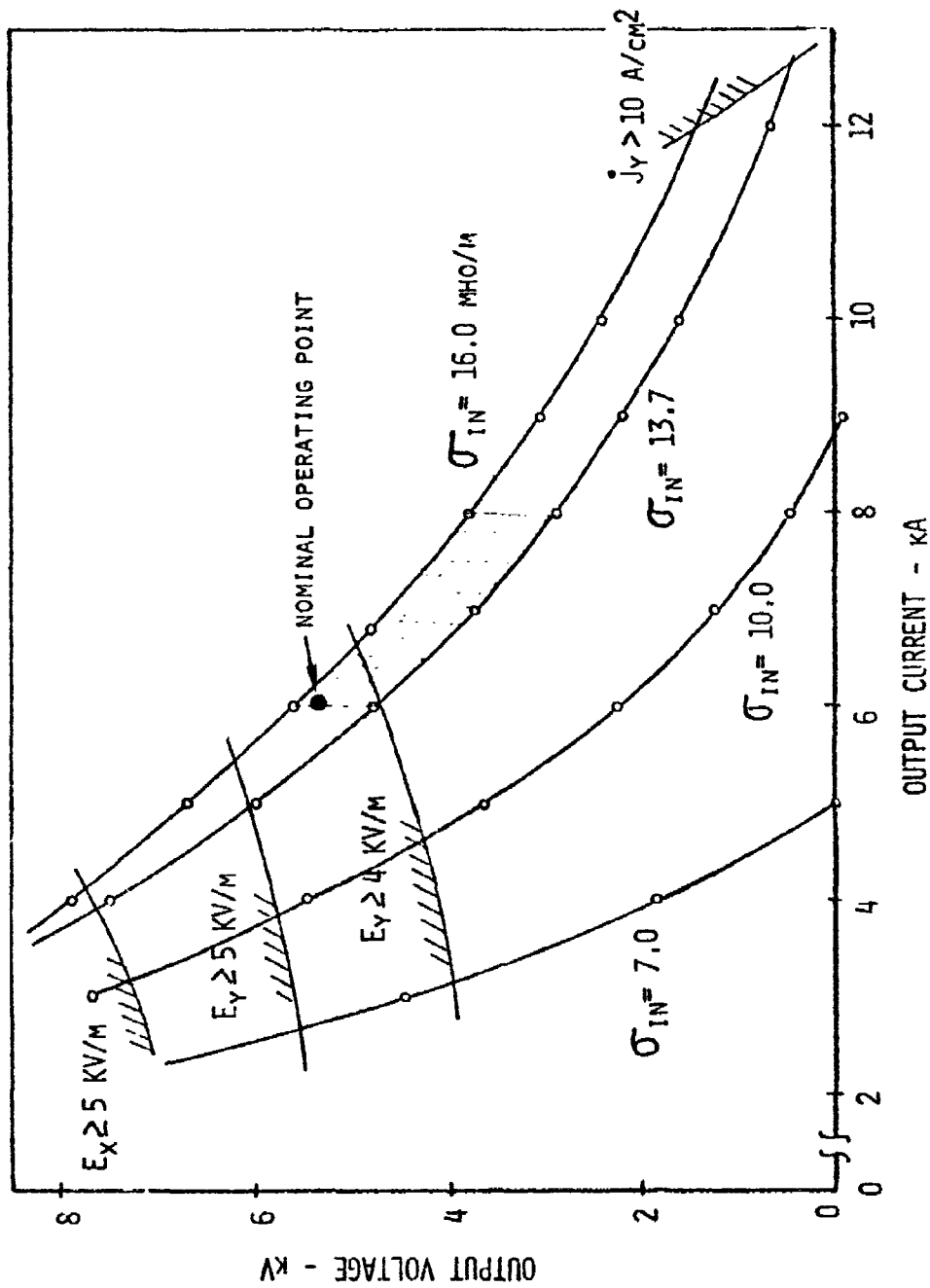
Figure 39. Channel/Diffuser Performance Summary.

89

TABLE 12. SELECTED PARAMETER VALUES FOR
LATEST PRELIMINARY DESIGN AND
OFF-DESIGN STUDY

Fuel	JP-4
Oxidizer	LO_2
Combustor Stagnation Pressure	30 atm
Combustor Stagnation Temperature	3450 K
Nominal Mass Flow	30 kg/sec
Channel Inlet Conductivity	15-16 mhos/m
Channel Inlet Mach Number	2.06
Generator Zone Diagonal Angle	50 deg, with respect to vertical
Peak Magnetic Field	4 Tesla
Hall Parameter (Maximum/Minimum)	2.0/0.5
Magnetic Field Distrubtion Over	
1.1 Meter Length	4-3 Tesla
Active Channel Length	2.55 m
Inlet Area	0.036 m^2
Area Ratio	10.0
Power Output	> 30 MW
Output Current at Design Point	6000 A
Output Voltage	5200 V

3. Thermal

a. Introduction

The thermal analysis of the lightweight channel was completed by recognizing the two competing thermal requirements. The zirconia surface temperature was required to be high enough to provide effective electrical current collection by each electrode, while at the same time the frame body temperature must remain low enough to maintain the integrity of the frame and the surrounding case. These two requirements required a careful design of the electrode frame details together with a practical cooling system operating under readily controllable flow conditions. Also, these coolant requirements had to be consistant with the AEDC facility capability. As a result of this restriction, a hydraulic analysis was also required. The hydraulic analysis is discussed in the following section. The thermal analysis included an investigation of the electrode frame and the case thermal behavior.

b. Electrode Frame Cooling Tube Analysis

The electrode frame cooling tube temperatures were obtained from preliminary estimates using various water flow rates and a simplified frame cross section model for a range of average gas side heat fluxes. The water/metal surface heat transfer coefficient was determined by:

$$h = 0.62 \; (1 + 1.29 \times 10^{-2} \, T - 2.47 \times 10^{-5} T^2)(v)^{0.8}(d)^{-0.2} \left[\frac{\text{watts}}{\text{cm}^2 \text{K}} \right]$$

where T was the mean water/metal temperature in Celsius, v was the water velocity in the tube in m/sec, and d was the tube i.d. in mm.[11] The approach used was to determine the required mass flow rate for a fixed bulk water temperature rise. This represented the minimum amount of water that was required for cooling. The heat transfer coefficient and the temperature distribution was then calculated. From these calculations the heat transfer coefficient required to prevent gas side overheating was computed. The velocity required to attain this heat transfer coefficient was then calculated and the resulting half-frame pressure drop was obtained. From these results the half-frame or full frame cooling loops were established.

---

[11] Kreith, F., Principles of Heat Transfer, International Textbook Co., 1961.

Table 13 provides the estimated axial heat flux distribution that was used for the high power MHD channel/diffuser thermal analysis. For this analysis the heat load was assumed to be low enough to permit two half-frame cooling loops to be connected in series to provide a frame cooling loop downstream of approximately 100 cm. The maximum design heat flux of $\sim$900 w/cm^2 occurred in the channel/diffuser entrance region while the minimum heat flux of $\sim$150 w/cm^2 was present in the channel/diffuser exit region. In all cases the required water pressure was less than the maximum pressure obtainable at the test facility.

c. Electrode Frame Temperature Distribution

Using the MITAS finite element heat transfer program, the electrode frame temperature fields were determined.[12] A typical electrode frame temperature distribution for an axial location with a heat flux of $\approx$500 w/cm^2 is shown in Figure 40. Temperature distribution plots for additional axial locations in the channel/diffuser were also completed. Figure 40 is for the electrode wall. Additional analysis was completed for the insulator wall, which utilized an oval cooling tube instead of the round tube used for the electrode wall. The resultant temperature distributions for the insulator wall were similar to the results shown in Figure 40. The critical regions of the electrode were the ceramic surface temperature, the Inconel screen temperature, and the screen/copper and the fin/cooling tube solder joints. Similar temperature distribution grids were also computed for other axial locations in the channel.

The most upstream region of the generator was the most critical from a heat transfer standpoint. The preliminary electrode design for the upstream electrodes were completed. Modifications, based on heat transfer data acquired during the SSFL development tests, are required before channel/diffuser fabrication. These test results verified the principle of the electrode frame design. The actual heat transfer data was 60%-70% lower than the design conditions. This will require the electrode ceramic depths to be adjusted from the original design value. In addition, some adjustment to the water cooling water flow rate could be made to adjust for variations in the heat transfer rates.

---

[12]User Information Manual for MITAS (Martin Marietta Thermal Analyzer System); Publication No. 86615000, Rev. A; Cybernet Service Control Data Network; September 1972.

TABLE 13. ELECTRODE COOLING DATA

Heat Load	w/cm^2	905	750	470	325	155
Station X	cm	-10	+10	73	120	190
Heat Load per Frame	kW	86.4	79.2	61.8	57.2	31.6
H Required to Prevent Gas Side Overheating	w/cm^{2}K	13	8.4	5.3	3.6	1.9
V (O/O)	m/sec	24/24	16/21	16/22	11/15	5/6
Cooling Flow per Half-Frame/Frame	liters/min	40/NA	47/NA	48/NA	NA/31	NA/13
ΔP for V Half-Frame/Frame	atm	10/NA	6/NA	7/NA	NA/8	NA/2
P Required to Prevent Boiling	atm	14	14	4	1	1
Required Pressure	atm	24	20	11	NA/9	NA/3
AEDC Systems Pressure	atm	27.2	27.2	27.2	27.2	27.2

NA = Not Applicable

93

INCONEL

Al2O3 | COPPER | Z_rO_2 | Z_rO_2

1523 1161 574 571 589 2027 2134 1677 2207 2249

1294	961	571	568	569	1852	1997	1654	2065	2199
1012	766	565	561	562	1570	1770	1520	1905	2021
755	646	554	551	552	1220	1458	1379	1617	1723
616	572	539	537	537	921	1129	1121	1267	1344
545	532	524	523	521	673	781	793	857	895
516	512	509	507	505	493	492	502	487	481

Silver
Solder

496	495	493	492	489	480	479	477	472	467
477	477	476	474	470	464	461	459	455	451
459	459	458	456	453	448	446 443 442	441 435	436

Copper

442	442	442	440	438	434	431	429	427	427
427	427	427	426	424	421	419	417	417	417
413	413	412	412	410	409	410	405	396	396

Solder
Copper

401	400	400	399	398	390	394	389 390	390
391	390	389	386	382	384	387		
386	384	382	372	375				

$q = 500$ w cm^2

367
361 357
347 345
336 334
327 326
321 321
317
316 316
316
315
315

$t = 310$ K
$v = 27.4$ m sec
$h = 8.4$ w cm^2 K

Figure 40. Temperature Distribution ~ 750 mm Downstream.

94

d. Case Temperature

The thermal shock temperature rise on the case was assumed to be the value at the outermost position of the cooling tube on a frame at the entrance region of the channel/diffuser. This rise was less than 49 K. For purposes of thermal shock analysis, the temperature rise was assumed, conservatively to be 55 K.

4. Hydraulic

a. Introduction

As the design description discussed earlier illustrated, there were two cooling paths per frame. In the channel entrance region the water flowed in parallel through each of the half-frame cooling loops. Downstream, where the heat flux was lower, two half-frames were connected together in series to form one cooling loop per electrode frame. Since the number of half-frame cooling loops controlled the final temperature at the coolant/frame interface, the connection arrangement was critical to maintain the desired temperature distribution. The hydraulics requirement, therefore, consisted of achieving a reasonable balance between the total flow requirements and the temperature distribution. The goal of the cooling system design was to maintain the cooling water flow requirements below the maximum water flow rate at the HPMS AEDC facility and to minimize the electrode frame temperature rise.

b. Flow Analysis

The calculations of the pressure drops through the cooling tubes were completed using the data on the measured pressure loss as a function of the flow velocity for the type of tubing used in the high power MHD channel/diffuser. The experimental measurements for 6 mm tubing are shown in Figure 41 for straight tubes. The data for curved tubes, orifices and changes in section were available from various publications.[13]

The total head loss in a flow path between the feed and drain manifolds consisted of the following components: (1) inlet manifold exit to flexible hose; (2) flexible hose friction loss; (3) flexible hose entrance loss to frame: (4) frame friction loss including bends; (5) frame exit loss to flexible hose; and (6) flexible hose to exit manifold. For half-frames which were connected in series, further pressure losses were caused by the return loops between the half-frames.

---

[13]Anon., "Flow of Fluids Through Valves, Fittings, and Pipes," Crane Company Technical Paper No. 410, 1976.
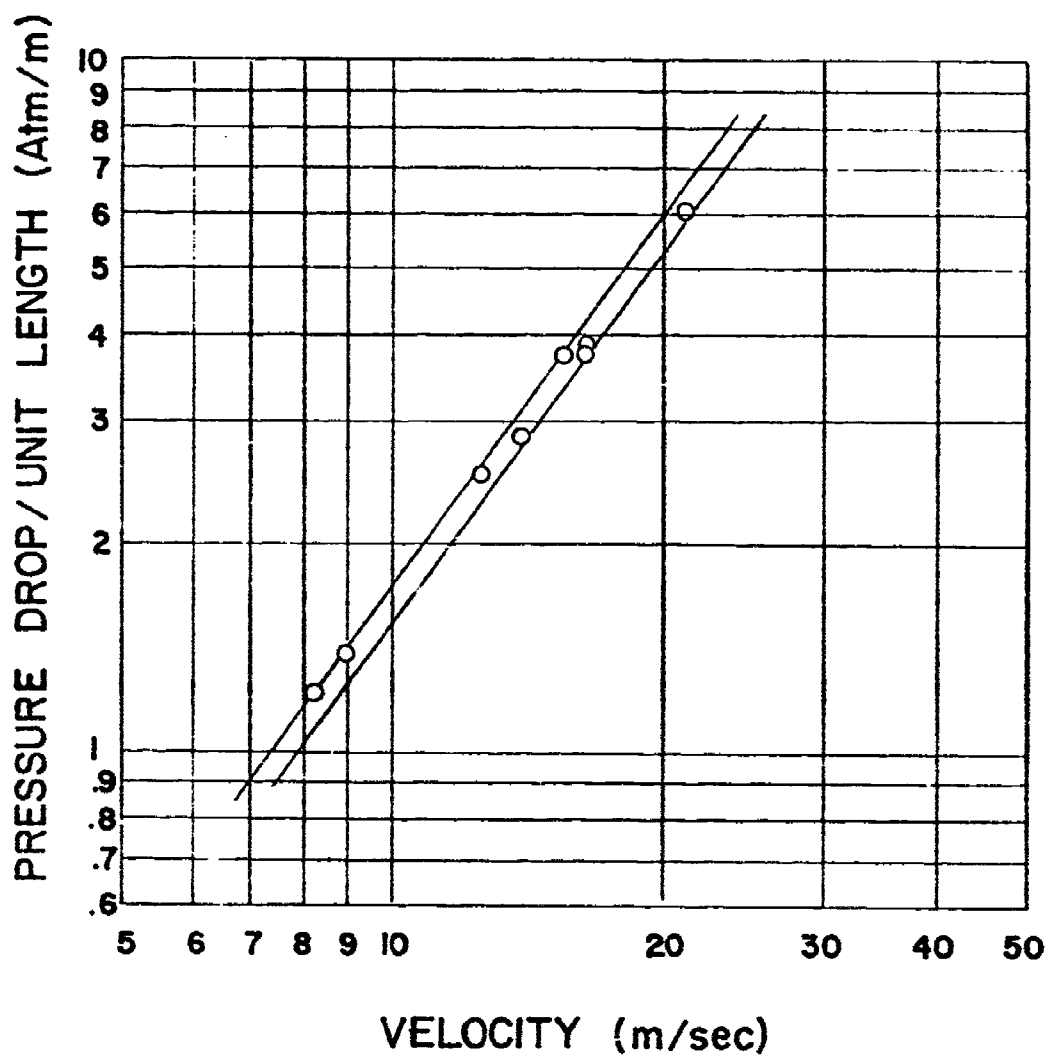
Figure 41. Pressure Loss for 6 mm I.D. Copper Tubing.

As a result of applying the data generated to the analysis of the entrance region and various other regions downstream from the entrance, the information shown in Table 9 was obtained. The difference in flow velocities resulted from the parallel and series cooling loops through the entrance and downstream electrode frames. To assure a balanced cooling water flow distribution, the velocities and cooling loop pressure drops were determined for the channel half-frames. This pressure drop data along with the pressure drop data for the connections, etc. was then used to determine the cooling loop connection scheme.

Since each of the 159 frames had two cooling loops, 318 parallel cooling loops were theoretically possible. However, the water flow requirements for cooling with all of the half-frames connected in parallel was excessive. In addition, the pressure drop required across each half-frame would not have been equal, thus requiring a more complex orificing of the manifolds; and the electrode temperature distribution would not have been satisfactory. A summary of the total cooling system requirements is given in Table 14.

5. Structural

a. Introduction

The structural analysis of the high power MHD channel/diffuser included an investigation of the electrode frames and the fiberglass case. First, the analysis of the copper electrode frames is presented. Then, the results of the analysis of the filament wound fiberglass are discussed. Finally, the manifold and mandrel analyses are presented.

b. Materials

Structural analysis of the electrode frames required the thermal and mechanical properties of oxygen-free high-conductivity (OFHC) copper. Figure 42 shows the coefficient of thermal expansion and the modulus of elasticity for OFHC copper. In Figure 43, the ultimate tensile strength and yield strength of OFHC are given. The thermal expansion, Young's modulus of elasticity and strength data were obtained from Copper Data Association (CDA) data sheets. The fatigue curve for combined strains for OFHC copper is shown in Figure 44. [14,15]

---

[14] Coffin, L. F., "Internal Stresses and Fatigue in Metals," G. Rossweiter and W. Grube, Elsevier Publishing Co., 1959.

[15] Majors, H., "Comparison of Thermal Fatigue with Mechanical Fatigue Cycling," ASTM STP 165, 1954.

TABLE 14. COOLING SYSTEM SUMMARY

Heat Load, Channel, MW	10.73
Cooling Water Temperature, In	21 C
Cooling Water Temperature, Out	38 C
AEDC System Water Pressure, atm	1.88
Minimum Flow Rate, liters/min	2760

Actual Flow Rate

Frames in Parallel, liters/min	5850
Half-Frames in Parallel, liters/min	11,730
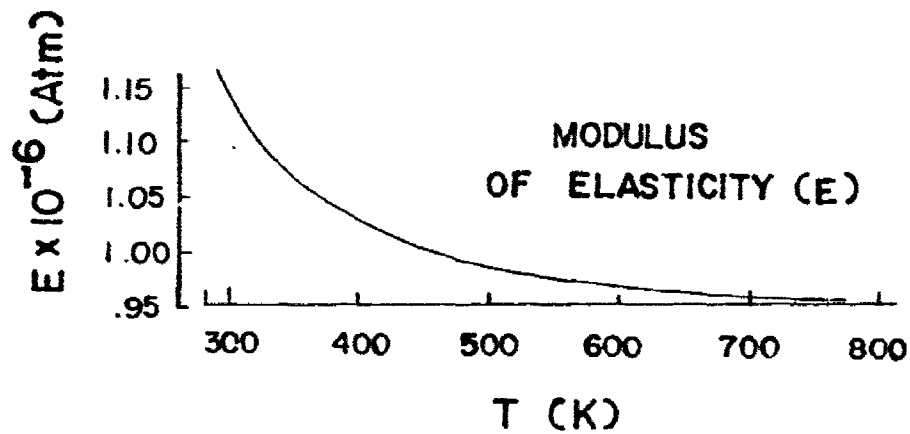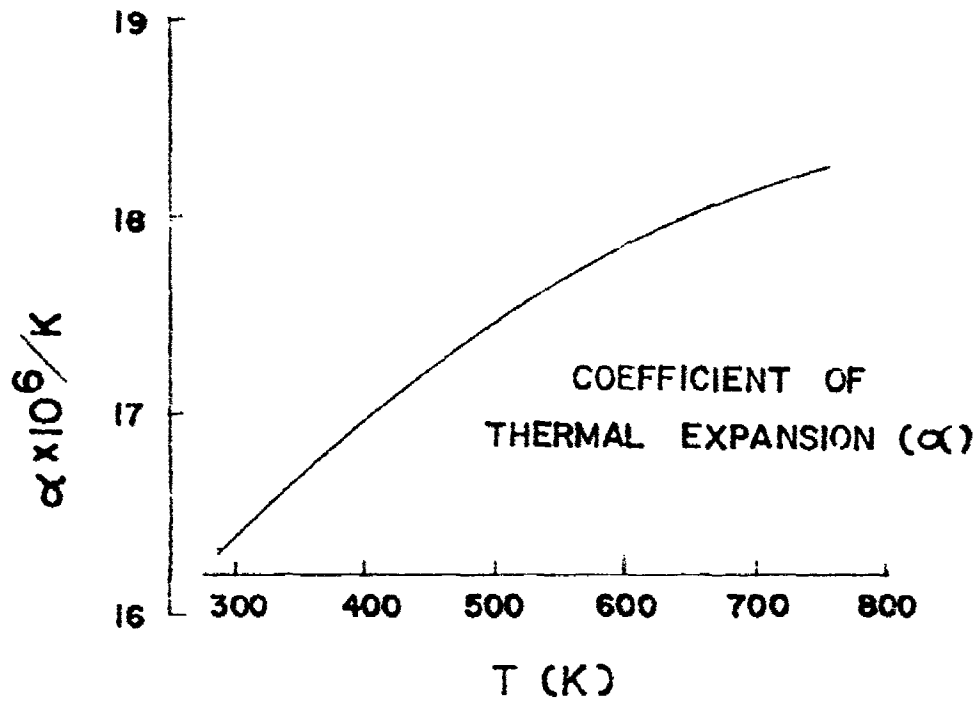
Figure 42. Coefficient of Thermal Expansion and Young's Modulus of Elasticity for OFHC (CDA-102).

99
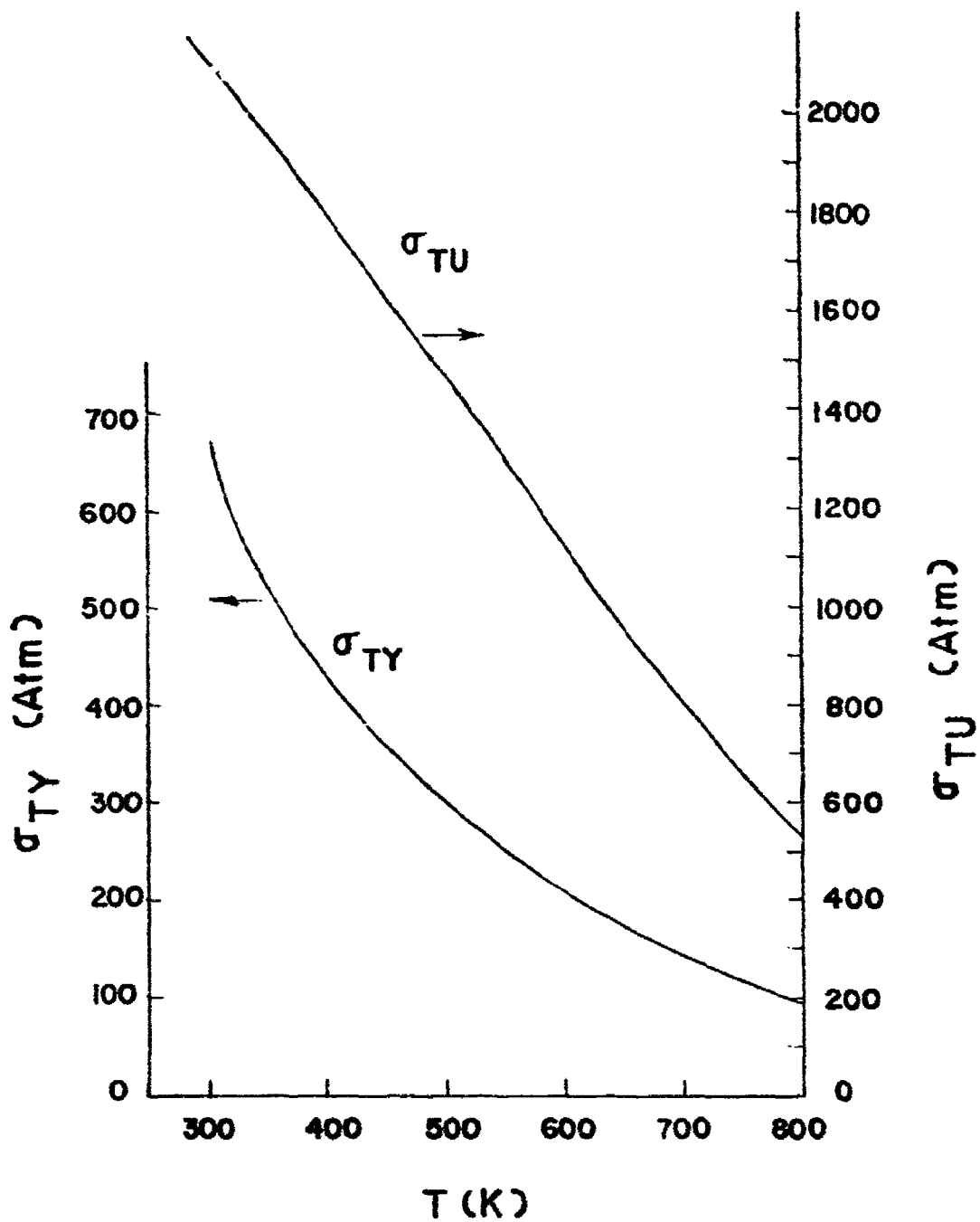
Figure 43. Yield Strength and Ultimate Tensile Strength of Annealed OFIIC (CDA-102).

100
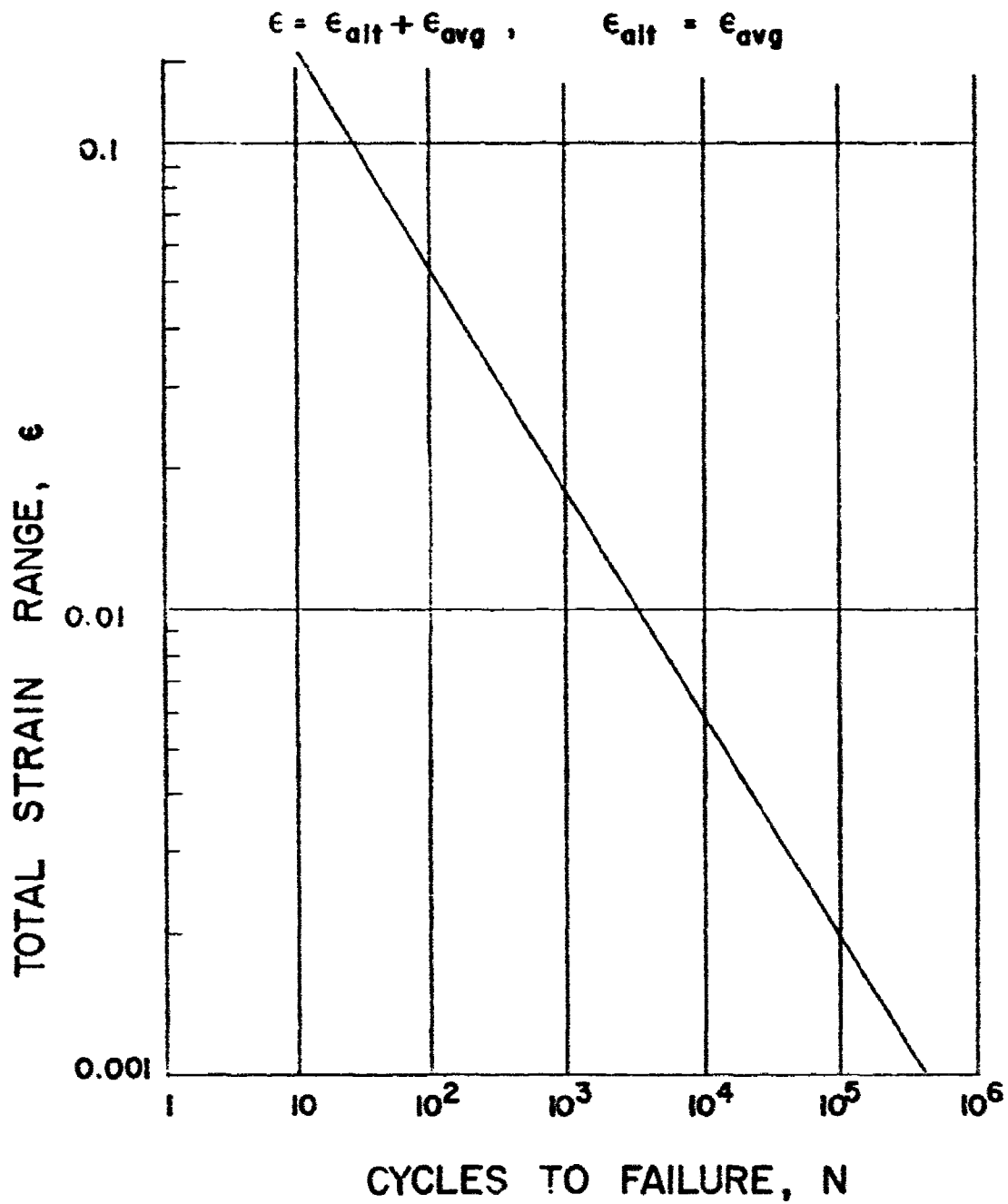
Figure 44. Fatigue Curve for Annealed OFHC (CDA-102) for Combined Thermal and Mechanical Strains.

Theoretical analyses of stresses in the interframe alumina and the zirconia in the gas face cups indicated stress levels greater than values which might be considered usable for the life of the channel. However, the compositions of those materials have been developed especially for MHD generators. They were spongy in nature. The properties were not those usually tabulated in the literature for ceramics. The survivability of the ceramics to be used in the high power MHD channel/diffuser has been substantiated through past experience.[3,4]

c. Electrode Frames

Introduction.   The calculation of the frame fatigue life under combined loads was performed by adding the strain components and entering the appropriate fatigue curve. In the curve of Figure 44, use was made of the fact that repeated thermal loading on a restrained bar will have a lower life than an applied mechanical strain at the maximum temperature of the thermal loading. Some conservatism resulted from the demonstration that the combination of thermal and mechanical effects followed an interaction relation which yielded longer life than the simple added strains method.[16]

Pressure in Coolant Tubes.   The maximum pressure deliverable to the critical coolant tubes with a 7.94 mm o.d. x 0.79 mm wall thickness was assumed to be 55 atm. The resultant circumferential membrane stress, σ_1, was 222 atm. The axial stress, σ_2, was less than $\sigma_1/2$ because of the presence of the electrode frame. The maximum tube wall temperature was assumed to be 395 K at the circumferential location where the tube was not in contact with the frame. Therefore, the circumferential membrane strain, ϵ_1, was 2.12×10^{-4}. This calculation was on the conservative side because the lateral shrinkage of the wall, $\nu \sigma_2/E$, was neglected.

Based on the static loading, the factor of safety was 8.4, while for fatigue, with $N_{all} > 10^6$ cycles, the factor of safety was greater than 100 if 1000 loadings were assumed for design purposes. These conditions existed close to the bending neutral axis of the frame/tube combination. At the extremes of the cross section, thermal stresses and longitudinal bending at the gas face controlled the factors of safety.

[16] Manson, S.S., "The Challenge to Unify Treatment of High Temperature Fatigue," ASTM STP 520, 1973.

<u>Frame Bending.</u> All upstream and intermediate frames were supported by anchors with a maximum span between anchors of 140 mm. Downstream, where the channel gas pressure was low, the anchor spacing was as great as 200 mm.

The bending moment, M, considering continuous beam behavior, was assumed to be one-tenth of the product of the electrode frame loading and the electrode frame length. The span between the anchors did not attain 140 mm until approximately 0.5 m downstream from the channel/nozzle interface, where the net pressure was 2 atm. Then, with a width of 11.3 mm, the moment was 4.4 N-m. The section modulus, Z, for the gas face, as shown in Figure 45, was 108 mm^3, and the bending stress, σ, was 402 atm.

The upper surface temperature is 589 K. Consequently, the modulus of elasticity, E, was approximately 10^6 atm, and the theoretical elastic strain, ϵ, was 4.24×10^{-4}. The bending deflection, δ, which was approximated by 0.017 pwL^4/EI_{xx}, was 0.65 mm. At the entrance the span was 90 mm, and the pressure was 3.4 atm. As a result the bending stress was 296 atm, and the bending strain was 3.0×10^{-4}.

<u>Thermal Strain.</u> The critical frames were in the region of the entrance where the transverse temperature gradients were the greatest. Each frame was assumed to be completely restrained internally against curvature because of these transverse temperature gradients. At the entrance the frame transverse temperature difference was 393 K for which the thermal strain, ϵ, was $\alpha \Delta T/2$, or 3.53×10^{-3}. At 0.5 m downstream from the channel/nozzle interface, the temperature gradient across the frame was 222 K. Consequently, the thermal strain at the gas face was 1.97×10^{-3}.

Analyses were conducted to determine stresses in the diagonal frames beyond the 0.5 m location. The frame anchors and cooling tube connections restrained those frames against the tendency to deform and overstrain under the linearly varying transverse gradients and out-of-plane thermal fields. Therefore, thermal stresses in those frames were less than those nearer the entrance where the heat load was higher.

<u>Combined Strains.</u> The total strain range, ϵ_{tot}, for pressure-induced bending and thermal strains at the entrance, was 3.83×10^{-3}, for which the total number of thermal cycles was 3.0×10^4, and the factor of safety was 30. The total strain range, ϵ_{tot}, for pressure induced bending and thermal strains 0.5 m downstream from the channel/nozzle interface was 2.39×10^{-3}, for which the total number of thermal cycles was 7.1×10^4, and the factor of safety was 71.

NOMINAL O.D. = 7.9 mm
NOMINAL I.D. = 6.4 mm
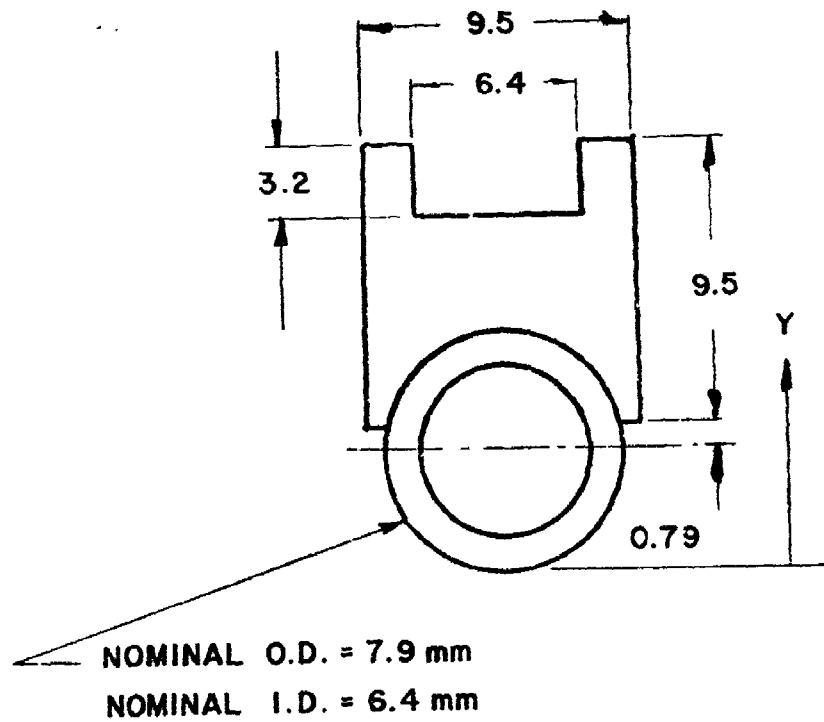
$A = 66.6$ mm^2

$\bar{y} = 7.95$ mm

$I_{xx} = 859$ mm^4

$Z_{xx} = 108$ mm^3

$\rho = 3.6$ mm

Figure 45. Frame Section Properties Assumed for Stress Analysis.

104

These factors of safety pertained to the continuous portions of each frame. The brazed joints have strength and elongation comparable to OHFC copper. In addition, there were filler blocks in the cup regions which raised the section modulus by 50% and reduced the possibility of local failure.

Vibratory Stresses.   The vibratory response was assumed to be 25 g at all frequencies. This was equivalent to a pressure on each frame of approximately 0.15 atm. This induced approximately a 10% increase in the bending stress, which corresponded to less than a 2% increase in the applied total strain. The influence on frame life was small enough to keep the factor of safety greater than 25.

Buckling Resistance.   All frames were supported by the anchors in a manner that permitted freedom of axial movement on each side. Axial forces were induced by the anchors which acted normal to the axial thermal growths. However, those forces were small compared to the column buckling load over the maximum span between anchors. The axial stress was found to be less than 6.7 atm while the Euler column stress was yield-controlled, and consequently, the factor of safety was greater than 40.

d. Case

The structural analysis of the filament wound, fiberglass epoxy case required the fatigue life properties of the fiberglass material shown in Figure 46.[17,18] Since this fatigue curve included   the effect of stress concentrations, even though none was present in the regions of the composite where the stresses were the greatest, the calculations resulting from this curve were conservative.

Pressure Effects.   The filament wound, fiberglass epoxy case had a cross section on each wall as shown in Figure 47.   An analysis was conducted to determine the forces and deflections on the varying wall section. In the critical regions, the inner cross section of the channel was approximately square. From beam theory, the central deflection, δ, edge moment, $\overline{M}$, and the edge bending stress, σ, were:

$$\delta = 0.23 \, pL^4/Et^3 \, [mm]$$

$$\overline{M} = He + M_o = 0.078 \, pL^2 [N\text{-}m] \quad \text{where p is in atm, L is in mm}$$

$$\sigma = 0.416 \, \overline{M}/t^3 \, [atm]$$

---

[17] Dietz, A.G.H., "Composite Engineering Laminates." MIT Press, 1969.

[18] Broutman, L.J. (Ed.), "Composite Materials, Vol. 5," Academic Press, 1974.

TOTAL STRESS $= \sigma = \sigma_{alt} + \sigma_{avg}$

$\sigma_{alt} = \sigma_{avg}$
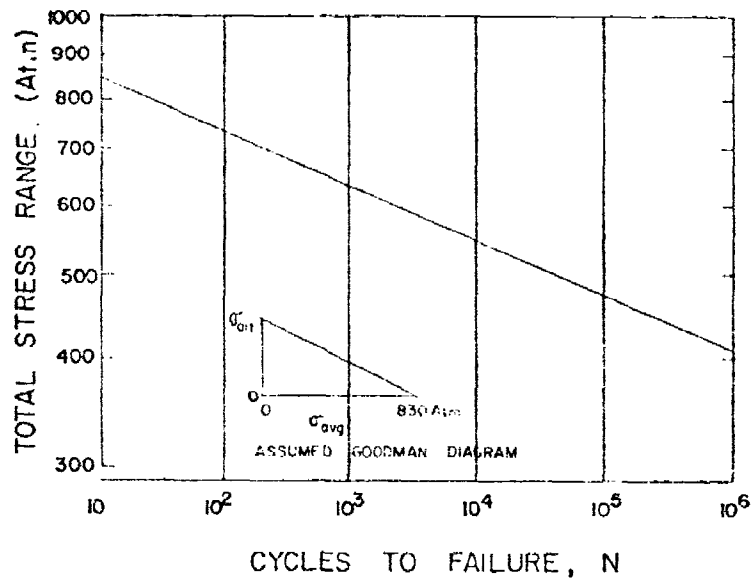
Figure 46. Composite Case Fatigue Curve.
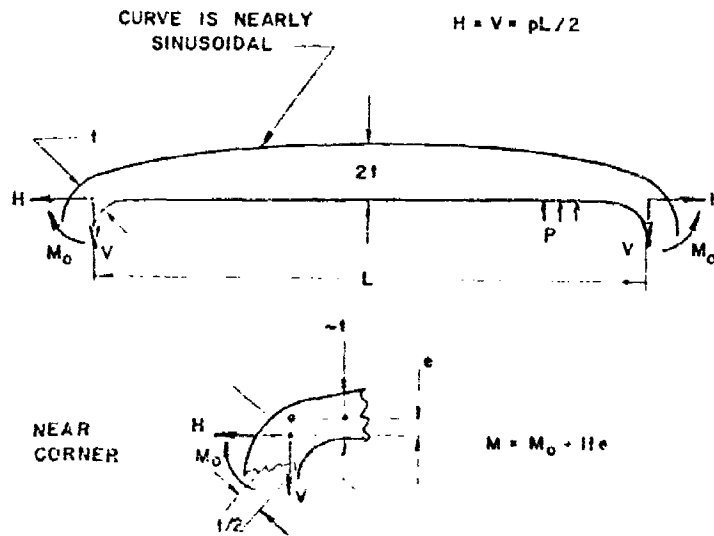
Figure 47. Composite Case Wall Analysis.

106

The primary transverse strength and stiffness arose from the circumferential roving. The case was analyzed as a series of parallel thin frames for this reason. The two-to-one thickness ratio has been found to occur on several test cases of various sizes.

From case pressure tests, the modulus of elasticity was 17×10^4 atm. The inward center deflection, for the largest span of 530 mm, at the peak negative pressure difference of 0.9 atm and with the corner thickness equal to 28.3 mm, was 0.17 mm. The corner transverse bending stress was 110 atm. Since $R/h = 1.6$, the stress was increased by 41% at the inner fiber because of the curved beam effect. [19]

The membrane stress was 7.9 atm. Thus, the total stress range was 118 atm. Therefore, with a fatigue life greater than 10^6 cycles, the factor of safety for fatigue was over 100. For static loading, the factor of safety was 9.5.

Thermal Shock. The entrance region of the case was assumed to be subjected to a 57 K temperature rise at the inner surface because of a "thermal shock." For the case material, the unit restraint stress per unit temperature rise, was $\alpha E = 3$ atm/K. Therefore, for a Poissons ratio of 0.33, the stress caused by thermal shock was 260 atm.

Vibration. The equivalent pressure on the combination of the 19.1 mm thick case and the nominally 9.5 mm thick frame at the entrance was 0.29 atm. The bending stress was 23.7 atm.

Combined Transverse Stresses. The sum of bending and thermal stresses, σ_{tot}, near the entrance was 400 atm. This stress level allowed a fatigue life of greater than 10^6 cycles with a factor of safety greater than 100.

Longitudinal Strength and Stiffness. The case provided the beam bending strength and stiffness of the channel. An analysis was conducted to determine the distribution of internal forces and moments in the channel when attached to the copper diffuser at the channel exit. This represented the current expected configuration during testing at AEDC. The analysis was conducted through the use of basic variable section beam theory employing numerical integration. The constraints were assumed to be the vertical support system at the entrance and exit ends of the channel and at the exit of the diffuser. In addition, the belleville spring system was taken into account to determine the interface moment at the combustor/nozzle exit. The calculations employed the well known equations:

---

[19] Timishenko, S., "Strength of Materials - Part I," D. VanNostrand, 1968.

$$\varphi = \int (M/EI)dx$$

and

$$\delta = \int \varphi \, dx$$

The 0.5 m long diffuser was assumed to be a constant, rectangular section copper tube with a wall thickness of 9 mm. The dimensions were chosen to match the exit end of the channel. The calculations showed that under the combination of channel mass and magnetic force loadings, the maximum bending and shear stresses occurred at the exit end of the channel. The magnitudes were 17.6 and 7.9 atm, respectively, which were negligibly small. The test cycle fatigue factor of safety exceeded 1000 and was greater than 50 for static strength.

The maximum deflection of the channel was 0.06 mm. The corresponding lowest bending frequency was:

$$f = 5\pi \, (\delta_{static})^{-1/2} = 64 \text{ Hz.}$$

The channel mass was one-eighth of the total transverse load applied during operation. Therefore, if a steady vibratory input were to induce 25 g of oscillatory motion in the channel, the loading would be 4.2 times as great as during static conditions. The resulting maximum stresses still would correspond to a virtually infinite fatigue life, according to extrapolation of the curve in Figure 43.

e. Manifolds

The 347 steel manifolds operated at less than 366 K at a maximum pressure of 53.3 atm. The stress in each manifold wall at the nipples for the connecting tubing was 69 atm. This included a factor of 2.5 for the biaxial stress concentration at each hole. The minimum stress for infinite life was 1086 atm.[16]

f. Mandrel

The numerical value of the mandrel bending stiffness was obtained from measurements of the mechanical properties of the interframe alumina. A large factor of safety was included to avoid low cycle fatigue of the alumina during the winding and curing stages. The local wall rigidity was determined on the basis of minimization of frame deflections into the channel resulting from the tension in the fiberglass roving.

The remainder of the specifications related to dimensional stability and handling for control of the components during assembly and curing. Specifying a quantity relating to removability of the mandrel from the cured channel was determined to be difficult. The meeting of that requirement was inherent in the ability to disassemble the mandrel sections for section by section removal.

Mandrel Structural Integrity. The design specifications identified certain structural requirements to be met by the mandrel. Table 15 summarizes those properties and shows the factors of safety which the mandrel design displays for those conditions.

The allowable interframe strain was determined from in-house tests on samples of ceramic. Assuming that the full channel mass was effective, the applied strain was that which could be induced during cure by bending of the mandrel as determined from elementary beam theory.

F. DESIGN VERIFICATION

1. Purposes

The design of the high power MHD channel/diffuser incorporated many significant features that either had not previously been fabricated or for which there was insufficient technical data available to satisfy the design requirements of the high performance MHD channel/diffuser. In addition, the greater size of the high power MHD channel presented the possibility of encountering new problems. Consequently, various design verification tasks were performed to reduce the risks of encountering costly and time-consuming delays during actual fabrication. These tasks are discussed in detail in the following sections.

2. Design Verification

Five design verification tasks were completed. These were: (1) case stiffness; (2) the modulus of elasticity for RTV-12; (3) copper properties; (4) pressure drop in the cooling tubes; and (5) ceramic testing. The electrode frame development, which was also a design verification task, is discussed in Appendix C.

a. Case Stiffness

A section of fiberglass composite case was subjected to internal pressure to determine the effective modulus of elasticity. The modulus was determined to be 17×10^4 atm.

TABLE 15.   MANDREL STRUCTURAL INTEGRITY

Condition	Applied	Allowable	FS
Strain In	$\epsilon = 0.0004$	0.001	2.5 (Static)
Interframe Ceramic	$N = 10^4$ cycles	$N > 10^6$	> 100 (Fatigue
Bending Deflection of Sides Because of Winding Tension	0.0086 mm	0.025 mm	3.0

Theoretical Basis. A theoretical relation was derived for the deflection of one wall of the case on the assumption that the case cross section was square. This was a reasonable approximation in the zones where the highest internal pressures were applied or the largest deflections occurred. The basis for the analysis appears in Figure 47. The expression for the deflection in terms of the case section dimensions and Young's modulus are presented in the section on structural analysis.

Test Procedures. The first step in determining the behavior of the case was the measurement of the wall thickness at several spanwise locations. The result appears in Figure 45 which shows that on the average, the center thickness was twice the corner thickness. The data were taken from all four sides of a case section 360 mm square and 360 mm long. Figure 48 shows how the data are encompassed reasonably well by a pair of parabolas representing the extremes of the data scatter band. This type of thickness variation also was used in the theoretical analysis mentioned previously.

The testing was conducted by placing the two cross section faces of the case between thick aluminum alloy plates to enclose the cubic interior of the case section. This zone was then evacuated to various pressure levels and the wall deflections were read with a resolution of 0. 0025 mm. A thin layer of vacuum grease was applied to the case edges to seal the interior.

The dial gauges were employed in pairs on opposite faces of the case at the centers of the square sides. Each gauge was read individually. There appeared to be rigid body movement of the case during testing. Therefore, the gauge readings were added algebraically for averaging to remove this effect.

Test Results. A set of data from one gauge pair appears in Figure 49. The slope of the mean line through the test points was employed in the deflection relation used in the structural analysis discussion.

$$\delta = 0.23 \ pL^4 / Et^3 \ [mm]$$

The modulus of elasticity for the case composite material as fabricated was then obtained and found to be 17×10^4 atm.

b. Young's Modulus for R TV-112

Tests were conducted to measure the Young's modulus in compression of the sealing material, RTV-112 used in the fabrication of the MHD channels.
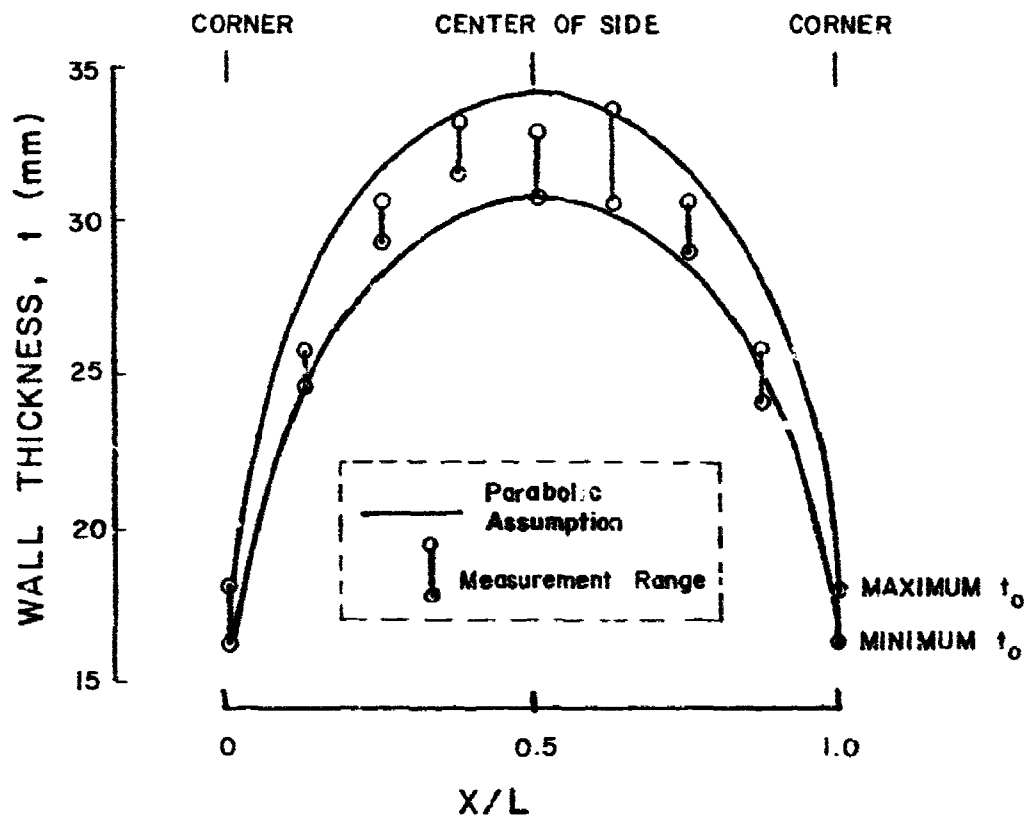
ASSUMPTION: $t = t_o \left[1 + (4X/L)(1-X/L) \right]$

Figure 43. Case Wall Thickness Distribution.

112
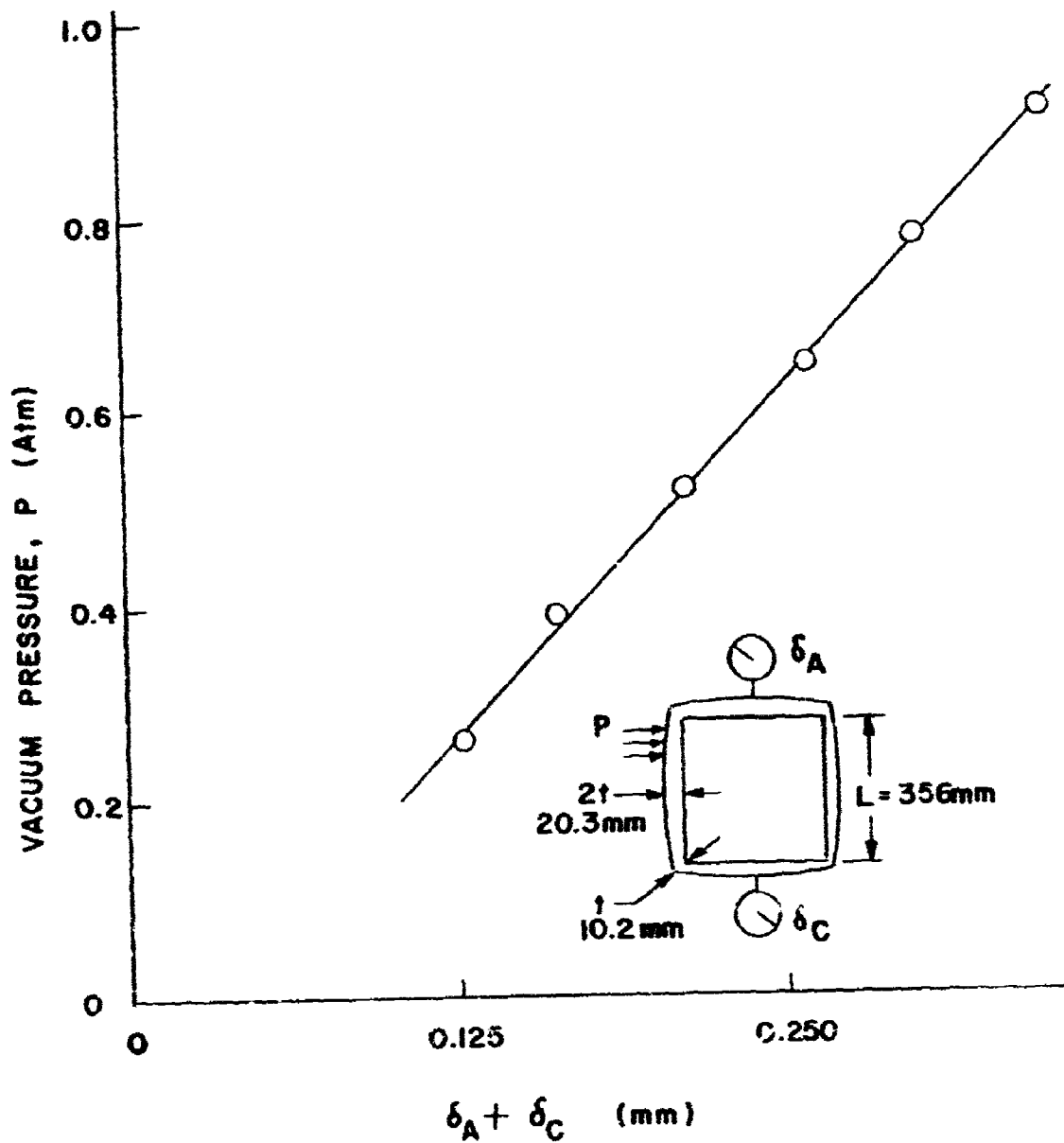
Figure 49.   Case Stiffness Test.

113

Procedure. The composite case was sealed with RTV-112 which had a small but finite Young's modulus. The magnitude of the modulus of elasticity was required in order to design the high power MHD channel.

The tests were conducted by applying a layer of RTV-112 on one face of an aluminum cube and curing the sealer. The assembly was then compressed in the manner shown in Figure 50. The deflection of each block was measured separately and then added algebraically to remove rigid body movement from the data.

The large strain that was observed before the application of significant amounts of load was because of the non-uniform cured surface between the blocks. After the application of the indicated small pressure, the bearing became uniform, which is shown by the linearity of the data.

Results. An average curve was drawn through the test points as shown in Figure 50. The slope of the line yielded an indicated Young's modulus of 65 atm by using the relation:

$$E = \Delta\sigma/[\Delta L/L]$$

where

$$\Delta L = (\delta_1 + \delta_2)$$

c. Copper Properties

Preliminary tests were conducted to obtain estimates of the material properties of the OFHC copper from which the frames was to be made. The results were found to agree reasonably well with published data. A pilot pressure test was performed on a flattened tube. The bare tube (no fin) sustained 47 atm with no significant deformation.

Material Properties. The test arrangement of Figure 51 was used to check the yield strength, σ_y, and the Young's modulus, E, of the OFHC copper for the electrode frame tubing. The small load in the test data table was used to obtain an estimate of E. The large load, which was found to initiate deformation, provided data for estimating σ_y. The equations, $M = FL[N-mm]$, $\sigma = 10M/Z$ [atm] and $E = 10FL^3/3I\delta$[atm], were used for these estimates which led to $\sigma_y = 470$ atm and $E = 1.3 \times 10^6$ atm. These compared reasonably well with reported room temperature values of 544 atm and 1.2×10^6 atm, respectively.

114
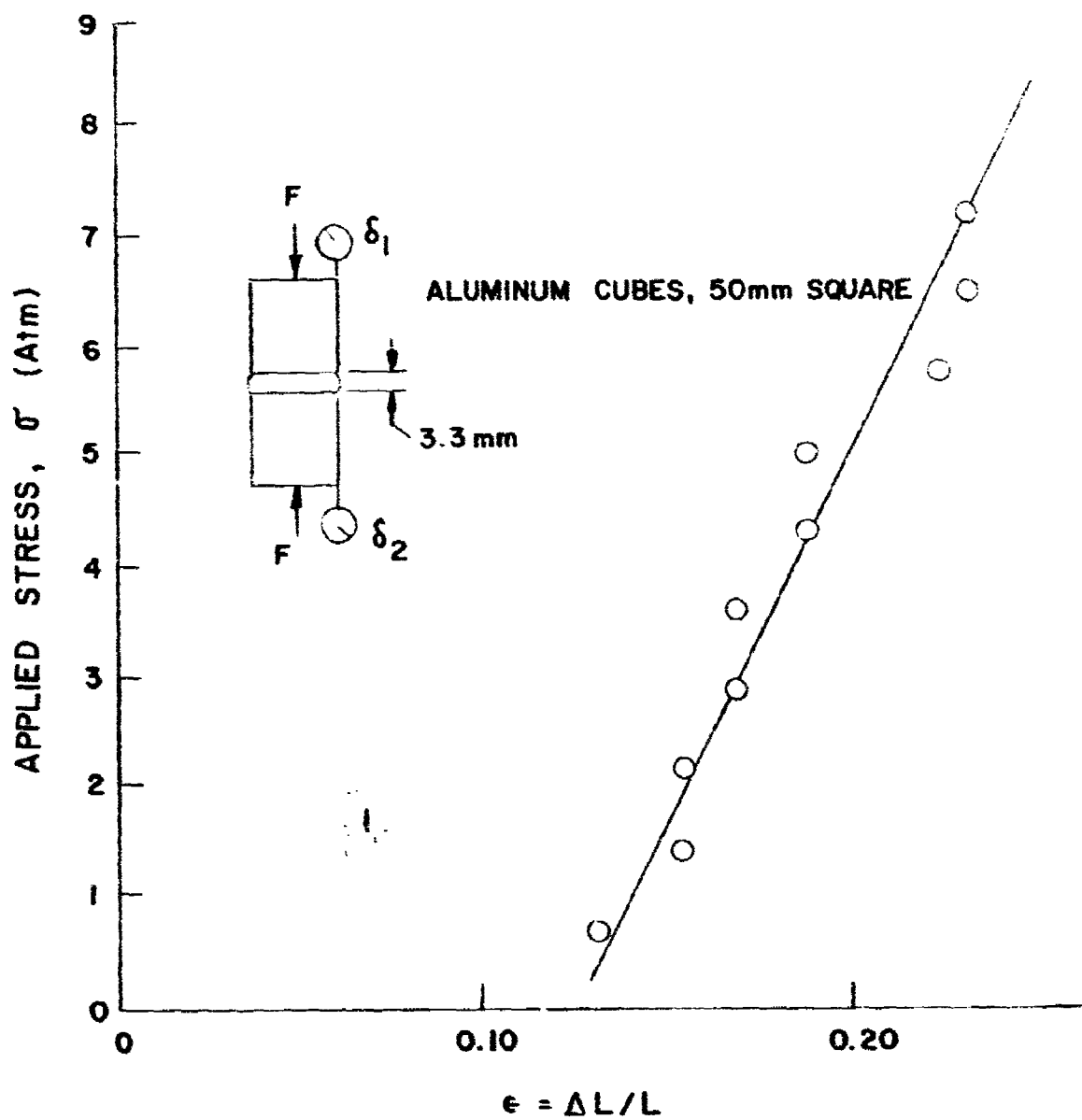
Figure 50.   RTV-12 Young's Modulus at Room Temperature.

115

LAST-WORD DIAL GAUGE

VISE

L = 150 mm

F (N)
δ (mm)

OFHC COPPER TUBE, 8 mm O.D., 0.64 mm WALL

$I = 98 \text{ mm}^4$, $Z = 25 \text{ mm}^3$
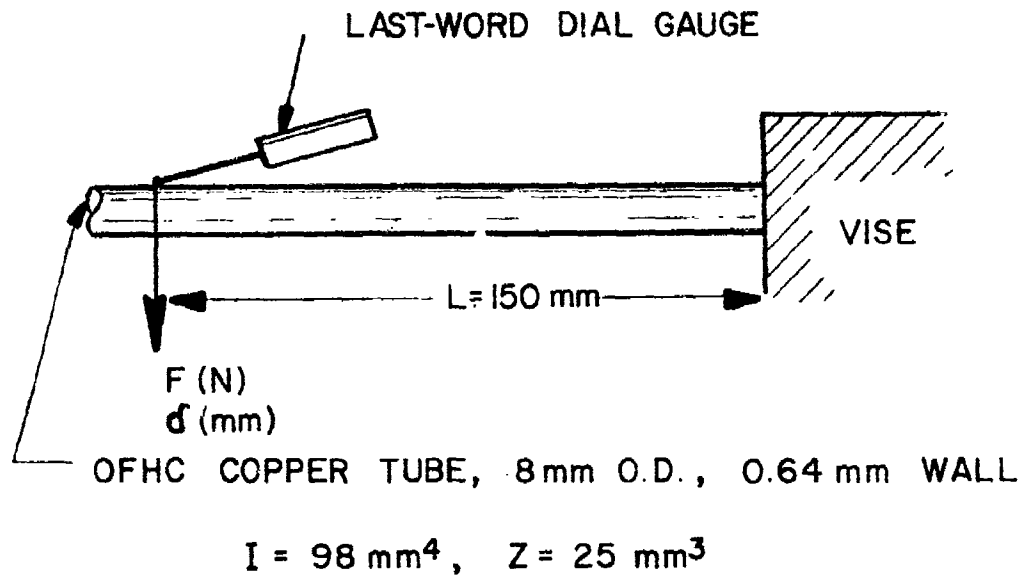
$$M = FL \; [\text{N-mm}], \quad \sigma = 10 \; M/Z \; [\text{Atm}]$$

$$E = 10 \; FL^3 / 3 \; I \delta \; [\text{Atm}]$$

DATA

Run	F (N)	δ (mm)
1	2.22	0.20
2	7.78	0.69 (Set = 0.025 mm)

$$E = 1.3 \times 10^6 \quad \text{Atm} \qquad \text{from Run 1}$$

$$\sigma_y = 470 \quad \text{Atm} \qquad \text{from Run 2}$$

Figure 51. Copper Tube Test.

Pressure Test. A short time pressure test was conducted at room temperature on a 250 mm length of flattened tube with a cross section as shown in Figure 52. The tube was crimped closed at one end. Pressure was introduced at the other end using a hand pump with a gauge direct reading to 6.8 atm. The tube depth, D (nominally 4.9 mm), was read with a micrometer during and after each pressurization up to a maximum of 680 atm. The test data are shown in Figure 52.

The results indicated that the tube sustained 47 atm before significant set was observed. If the flat walls were assumed to be clamped bars, the bending stress, σ, would be: $(P/2)(L/t)^2 = 1000$ atm. This was within the range of data for biaxial flexural yielding.

d. Pressure Drop in Cooling Tubes

Tests were run on round and flattened copper tubing to determine the head loss for use in the design and to check the diagnostics channel after fabrication. The test data, in conjunction with guidance from established hydraulics information, were used to generate curves of pressure drop per unit tube length as a function of flow velocity.

Procedure. The testing was performed using the system shown in Figure 53. Nitrogen gas under pressure was used to control the upstream pressure in the system. The valves controlled the tank vent and the inlet to the flow loop. The first gauge read the upstream pressure and the second gauge provided the downstream pressure. The downstream valve was used to initiate and terminate the test run. The elapsed time was recorded along with the total mass of water collected. Flow velocity through the tubing was calculated from the relation, $v = 0.0315 \, (\Delta \dot{m}/\Delta T)$, where $\Delta \dot{m}$ = the mass of the water collected in grams, and ΔT = the time interval in sec. For these tests the tube i.d. was 6.3 mm.

Results. The pressure loss information was obtained on a straight length of tubing 1060 mm long. After that had been obtained, an 800 mm tube consisting of four, 90 deg bends was tested. The pressure loss per bend was found to be approximately equal to a tube of length equal to 10 dia. These results were consistent with predictions.

A double frame was tested to compare predictions with the experimental data. Figure 54 shows the agreement of the predicted loss at 21 m/sec with the upper bound of the scatter band.

The frames of the diagnostics channel were checked out by first calculating and then testing a representative clean frame. The calibration band and the frame checkout bands are shown in Figure 54.

117

t = 0.74 AVE

4.9

3.4

P

D

L = 8.2

9.7

D/2
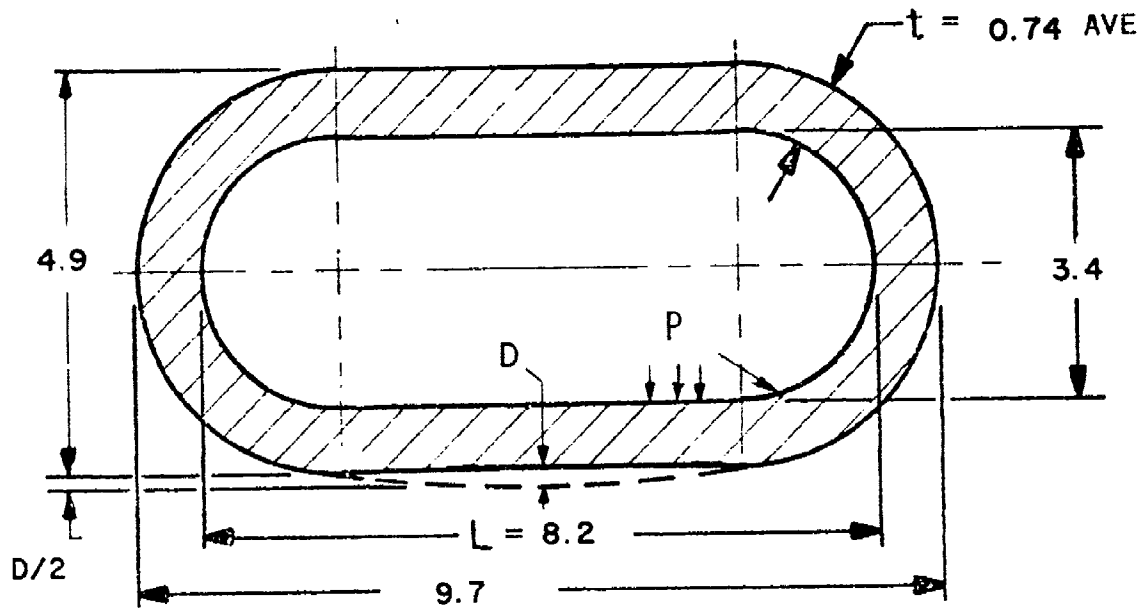
ALL DIMENSIONS IN mm

TEST DATA

P (ATM)	D (mm)	P (ATM)	D (mm)	P (ATM)	D (mm)
0	4.88	2.07	4.90	4.83	4.97
1.38	4.90	3.45	4.91	6.90	5.16
2.07	4.91	4.83	4.95	0	5.11
2.76	4.93	0	4.91		
3.45	4.93				
0	4.89				

Figure 52. Flattened–Tube Pressure Test Data.

118
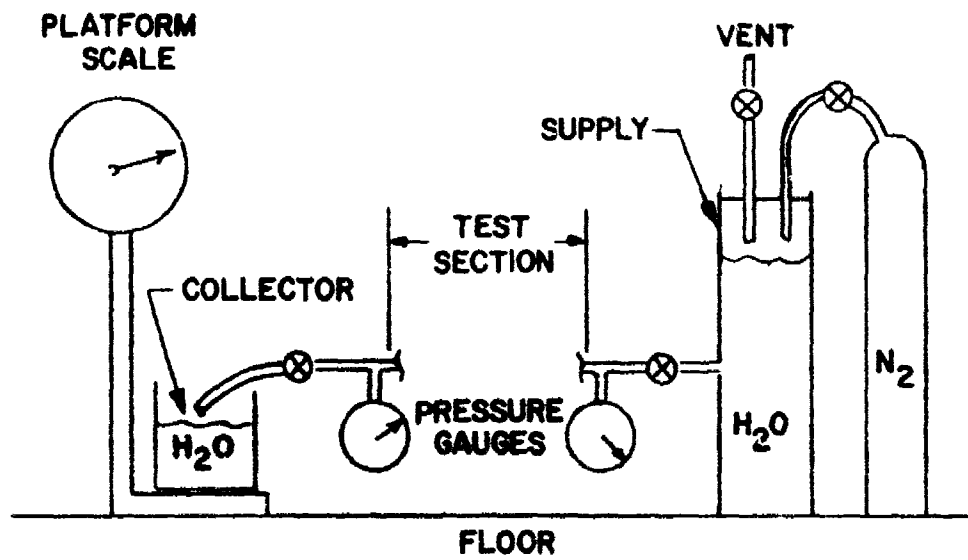
Figure 53.   Cooling Tube Pressure Drop Test Arrangement.
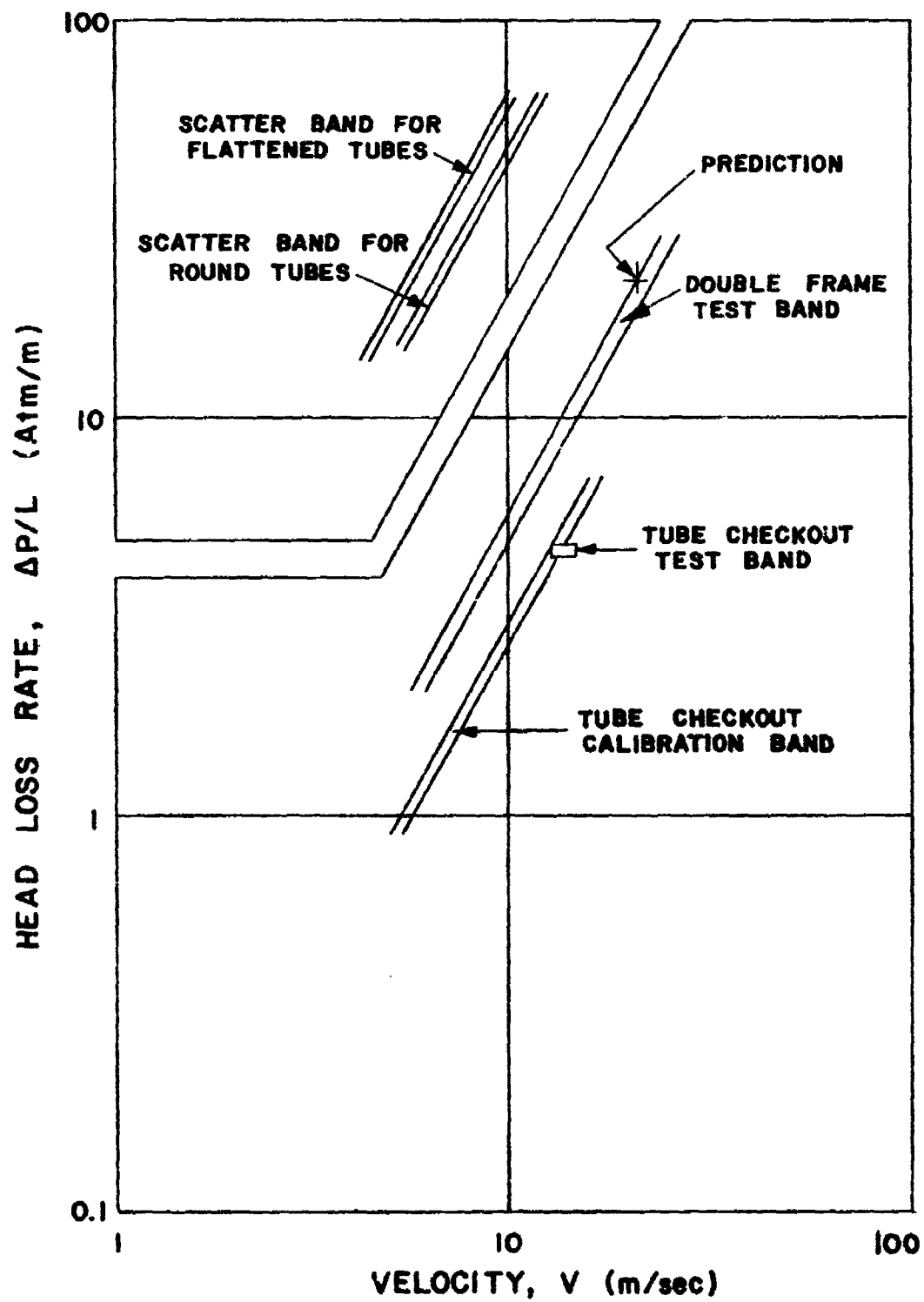
Figure 54. Head Loss Data From Tests With 6.3 mm I.D. Copper Tubing.

A theoretical analysis predicted a head loss for the flattened tubes of the high power MHD channel/diffuser to be 1.4 times the loss for round tubes. The bands in Figure 51 show reasonable agreement with the prediction.

e. Ceramic Testing

Preliminary tests were conducted on interframe alumina ceramic to determine the uniaxial compressive stress strain curves, crushing strength and compressibility.

Test Procedure. Samples of interframe ceramic were prepared in disk form. Seventy-five grams of alumina powder were mixed with 15 ml of bonding agent, which consisted of waterglass and water in several ratios. The mixture was cast in disk form, nominally 5 mm in diameter and 1.6 mm thick. The disks were cured at 350 K for four hours. The thickness and diameter of each disk were measured and recorded.

Each disk was compressed in a testing machine. The load was applied in 450 N increments. The thickness was measured after each load application until crushing occurred.

Results. Stress–strain curves, crushing stresses and maximum strains were measured. The data appear in Figure 55 for various values of the water-glass/water volume ratio, WG/W. The large scatter bands were typical for this type of material. Greater precision in load application was not warranted for these preliminary tests.

G. COMPONENT DESIGN DETAILS

1. Channel/Diffuser

a. Electrode Frames

The proposed electrode design, as shown in Figure 56, has been used in the fabrication of a previous lightweight channel.[4] In that design the cooling tubes served as the main structural member to which the screen and cooling fins were attached. The main advantages of that design were the minimal cross sectional material, hence, minimal mass; and the minimal length of thermal conduction path from the hot gas surface to the cooling water, hence, a maximum rate of heat removal for a given temperature gradient. But during the fabrication process,
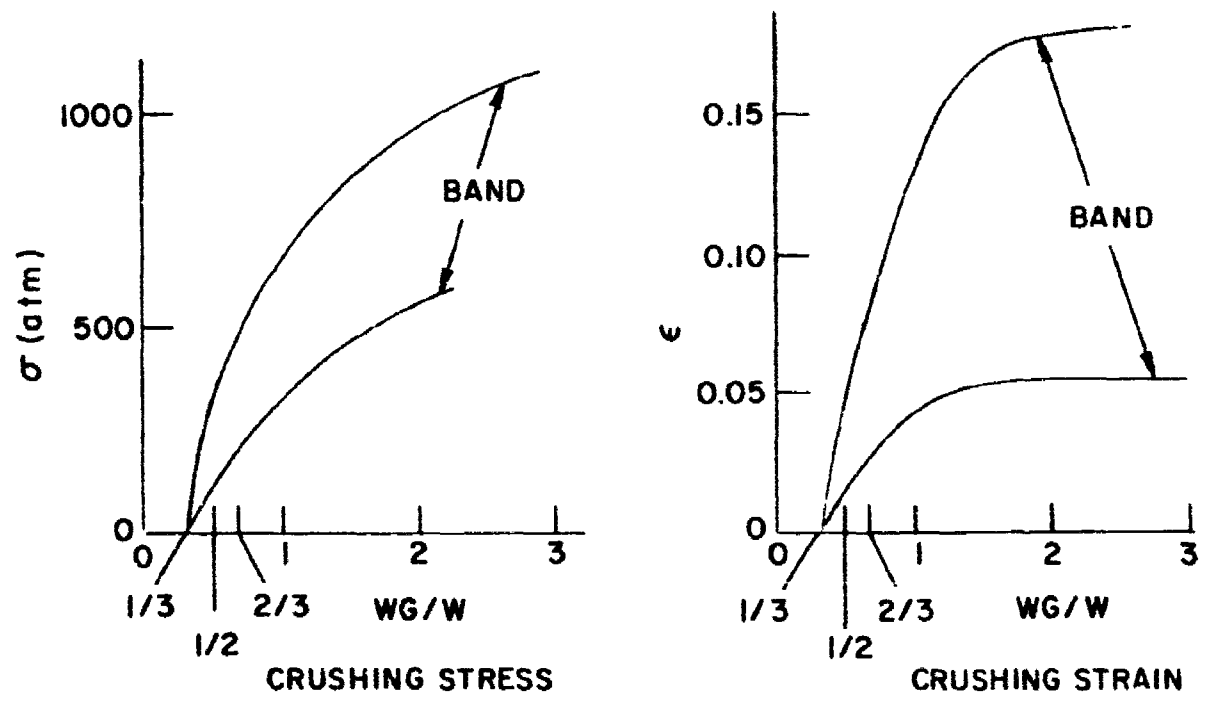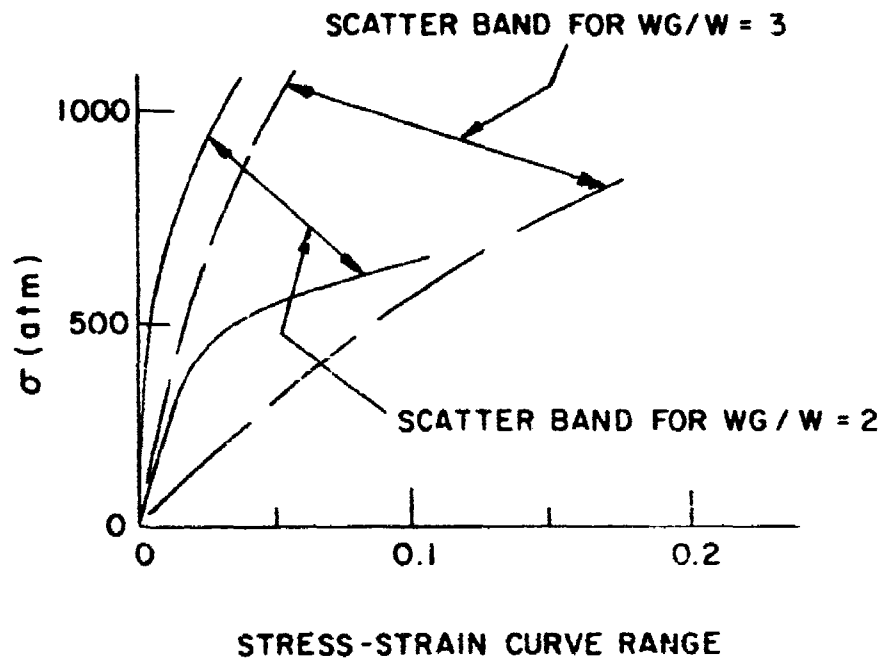
Figure 55. Ceramic Test Data.

122
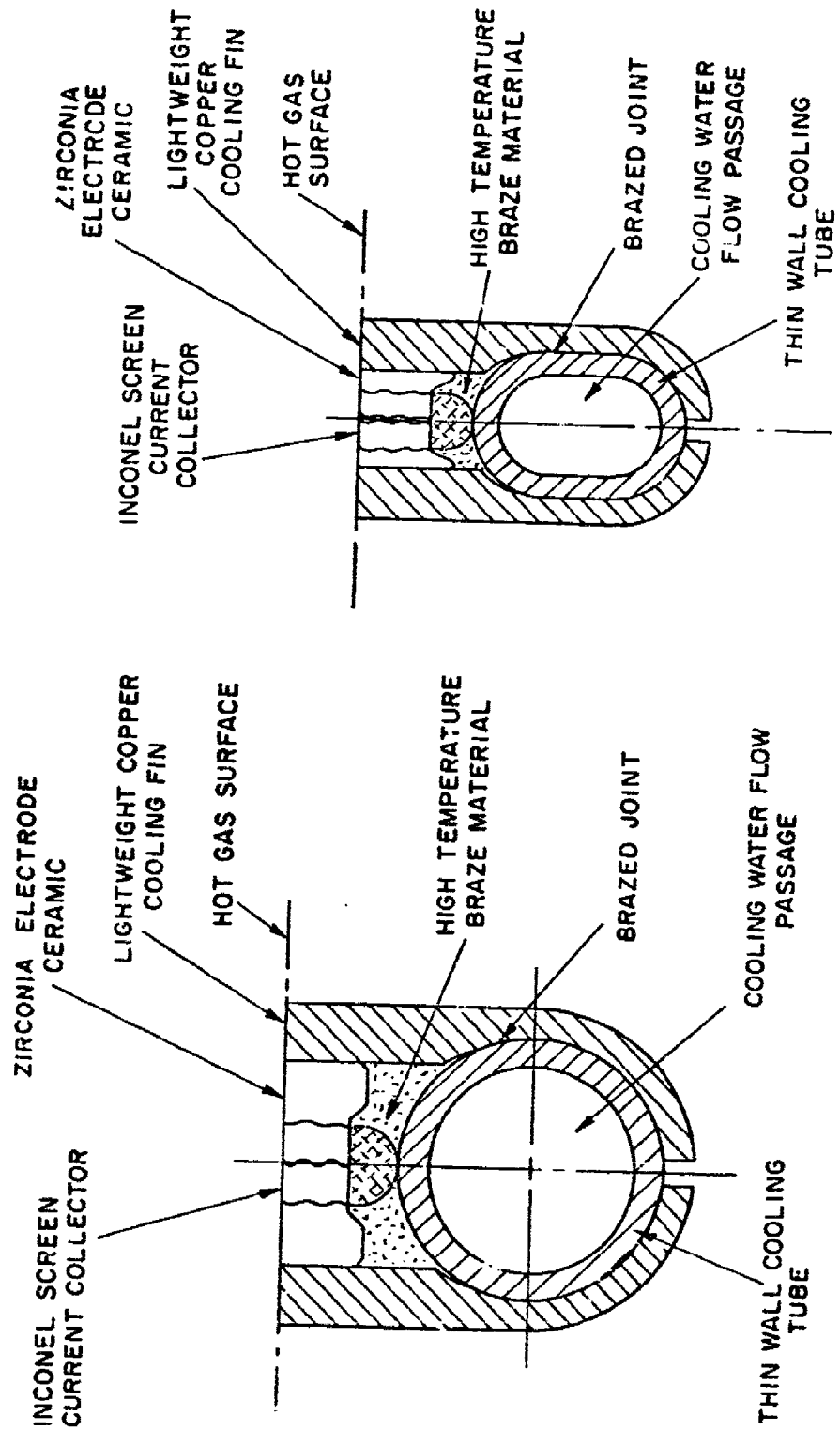
Figure 56. Proposed Electrode Design.

123

certain disadvantages became obvious – the major problem was the difficulty of holding close dimensional tolerances because of the irregularities of the tubes, the cooling fins, and the Inconel screens. The tolerancs affected both the width and height dimensions such that the final dimensions were not within the desired tolerance range.

The final electrode design is shown by Figure 57 and was used in the fabrication of the diagnostics channel. In this design the straight copper side and cross rails were brazed together at the corners with special copper corner blocks, thereby forming a continuous frame. Then continuous cooling tubes were soldered to the outside of the frames. The precision rails, which contained the screens, served as the main structural members. The main advantages of this design were the much closer dimensional tolerances that were achieved in the screen/groove geometry, the interframe spacing, and the smoothness of the internal hot gas surfaces of the channel. The main disadvantages of this design were: (1) the increased cross sectional material which contributed to an increase in the mass; (2) the increased length of the thermal conduction path; and (3) an additional solder joint between the screen and the cooling tube.

The high power generator channel consisted of 159 frames. These included three basic types: perpendicular, transition, and diagonal. All three frame types shared the same basic design with side and cross rails containing the screens, corner blocks, and continuous cooling tubes soldered to the outside of the continuous frames. Special electrode frame anchors secured the frames to the glass epoxy case while allowing for thermal expansion. A key feature of all the frames was the fact that there were no joints in the continuous cooling tubes in the regions of heat transfer from the hot gas to the cooling water. This feature significantly increased the reliability of the MHD channel because previous experience with MHD generator channels has shown that coolant passages with joints that were exposed to high rates of thermal expansion and contraction were very prone to develop leaks.

Perpendicular Electrode Frames. The perpendicular electrode frames are illustrated by Figure 58. The rails and corner blocks were joined to form a continuous frame that had a rectangular hot gas area opening. Continuous cooling tubes were soldered to the outside of the rails and corner blocks, and frame anchors were attached to the tubes. The hot gas surfaces diverge from the channel axis as required by the internal contour of the channel at that location. The basic frame lay in a plane that was perpendicular to the channel axis.

Upstream Transition Electrode Frame. The majority of the electrode frames were inclined to the axis of the channel at a constant angle and were called "diagonal" frames. At both ends of the channel, a transition from diagonal frames

124

INCONEL SCREEN
CURRENT COLLECTOR

HIGH TEMPERATURE
BRAZE JOINT

COPPER RAIL

RAIL/TUBE
SOLDER JOINT

COOLING TUBE
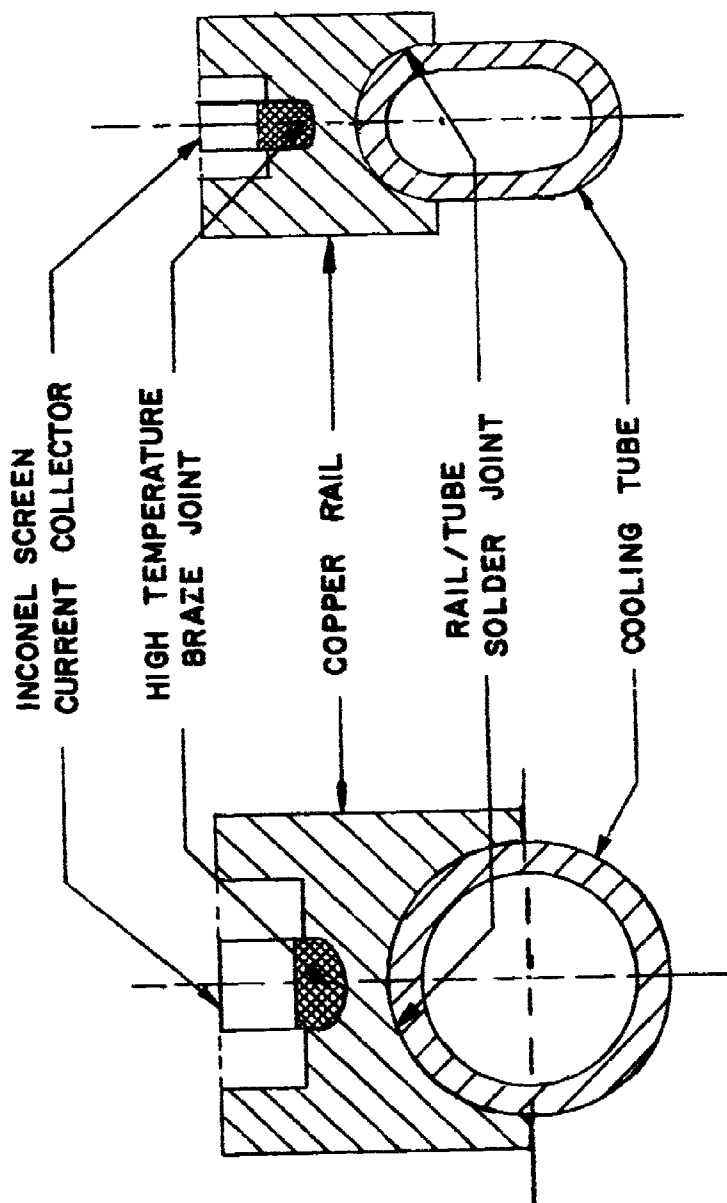
(A) WIDE SECTION

(B) NARROW SECTION

Figure 57. Final Electrode Design.

125

COOLANT
CONNECTIONS

CORNER
BLOCKS

FRAME
ANCHORS
(TYPICAL)

ASSEMBLY MANDREL

SIDE RAILS WITH SCREEN
AND COOLING TUBE

CROSS RAILS WITH SCREEN
AND COOLING TUBE
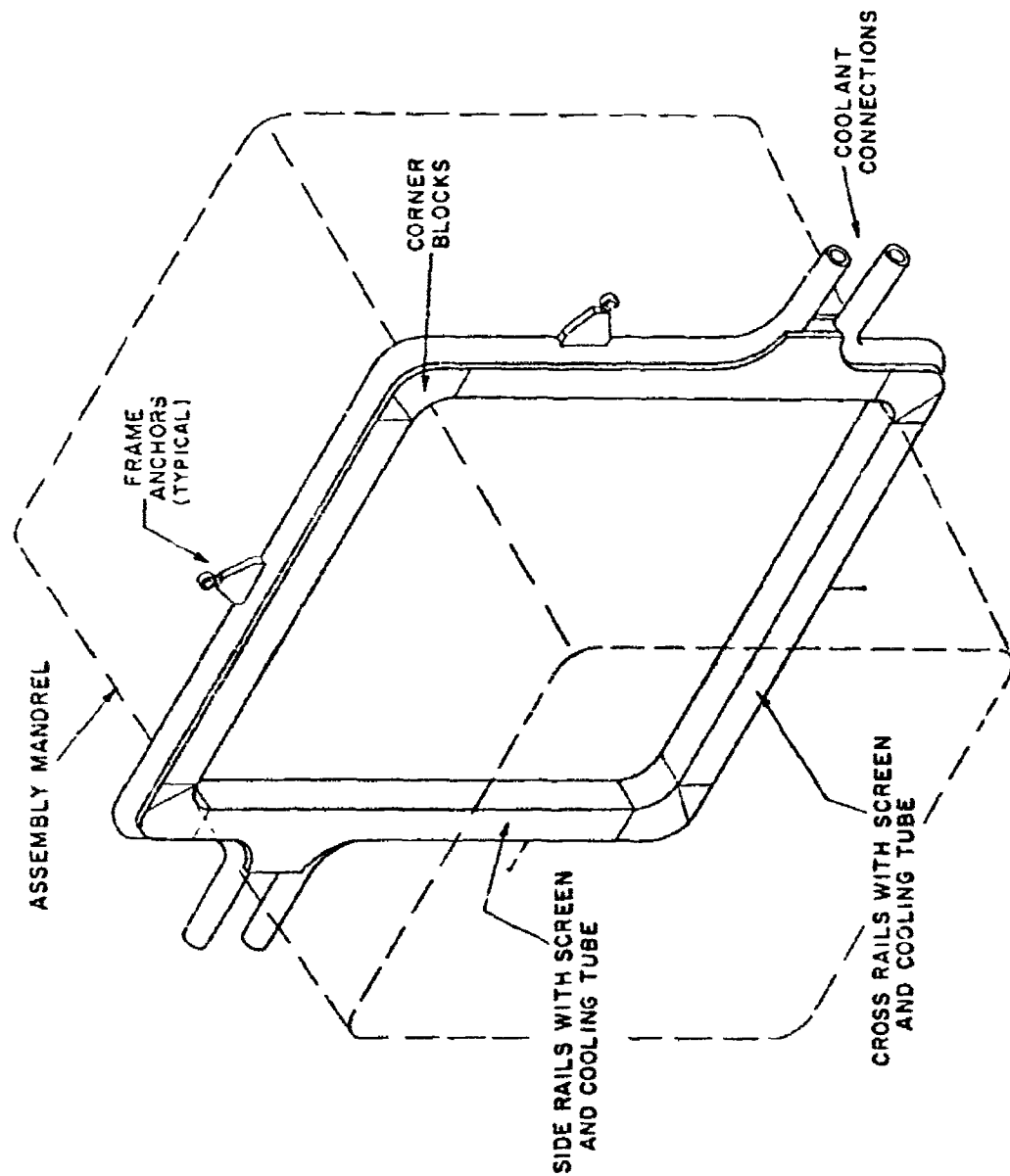
Figure 58.   Perpendicular Electrode Frame.

to perpendicular frames was required. This was accomplished with a set of wedge-shaped "transition" frames. The upstream and downstream transition frames served the same performance functions, but they are described separately because of the slightly different details of construction.

A typical upstream transition frame is shown by Figure 59. The most obvious difference was the configuration of the side and cross rails. Each frame had a single bottom cross rail, wedge-shaped side rails, and multiple top cross rails. The multiple cross rails served to distribute the effects of thermal expansion over a longer region and the side rails had corresponding expansion slots. Another difference was the lack of separate corner blocks. Instead the corners were integral parts of the cross rails. This design improved the cooling and simplified the assembly process in these regions of complex geometry. Another feature of the side rails was the way that the cooling tubes overlapped each other as they converged. This was done to provide adequate cooling of all areas. Again, the cooling tubes were continuous and frame anchors were attached to the outsides of the tubes.

Diagonal Electrode Frames. The diagonal frames are illustrated by Figure 60. Narrow side rails with single screens and wide cross rails with double screens and corner blocks were joined to form a continuous frame that had a trapezoidal hot gas area opening. Continuous cooling tubes were soldered to the outside of the frame, and the anchors were attached to the outside of the tubes. The basic frame lay in a plane that was diagonal to the channel axis.

Downstream Transition Electrode Frames. The downstream and upstream transition electrode frames were essentially the same, except that the downstream frames as shown by Figure 61, had separate corner blocks because of the lower heat transfer rates and the greater sizes involved at the downstream end of the channel. Each frame had a single top cross rail, multiple bottom cross rails, and wedge-shaped side rails that were provided with thermal expansion slots. The rails and corners formed a continuous frame to which continuous cooling tubes were attached. The frame anchors were attached to the cooling tubes.

b. Electrode Frame Anchors

Successful channel performance required a smooth internal hot gas surface at all times. Adjacent electrode frames were required to act in unison to maintain the smooth surface. The long, slender side and cross rails of the frames were not sufficiently rigid themselves to withstand the differential rates of thermal expansion and the gas pressure loading distribution. Consequently, the frames were required to be attached to the glass epoxy case which was designed to be the primary structural member of the channel.

FRAME ANCHORS (TYPICAL)

COOLANT CONNECTIONS

ASSEMBLY MANDREL

SIDE RAILS WITH SCREEN AND COOLING TUBE

CROSS RAILS WITH SCREEN AND COOLING TUBE
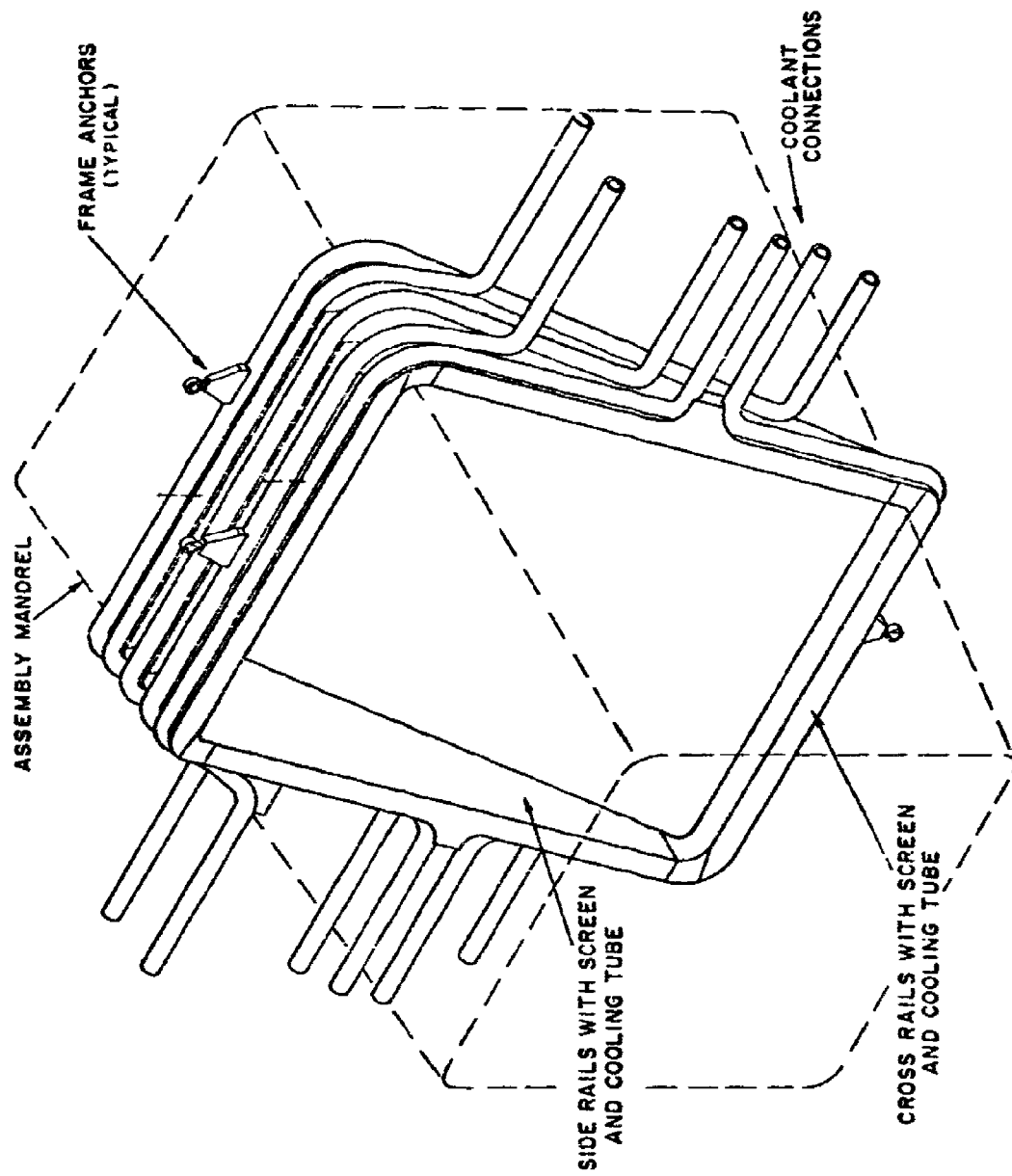
Figure 59. Upstream Transition Electrode Frame.

FRAME ANCHORS

CORNER BLOCKS

COOLANT CONNECTIONS

SIDE RAILS WITH SCREEN AND COOLING TUBE

ASSEMBLY MANDREL

CROSS RAILS WITH SCREEN AND COOLING TUBE
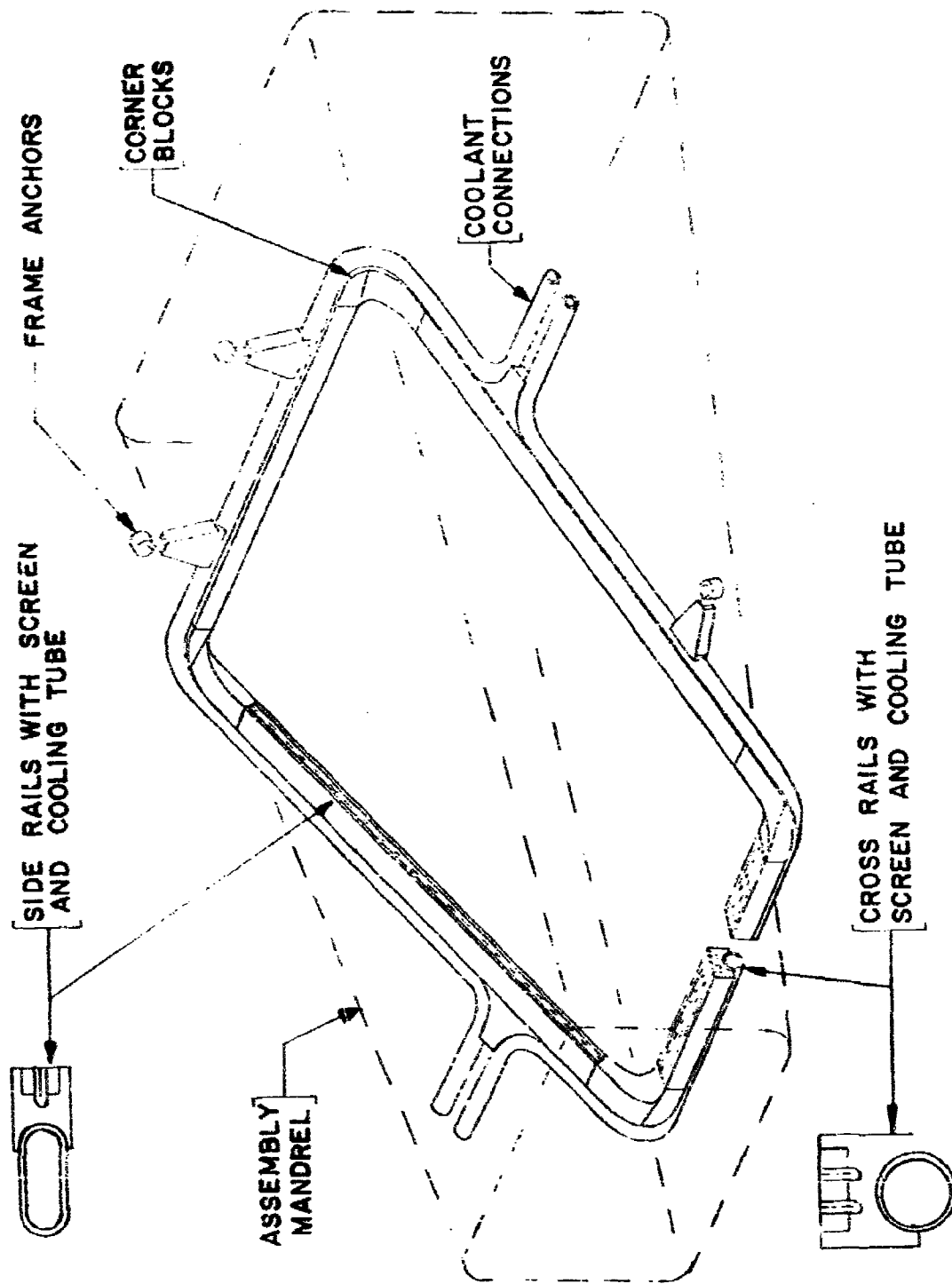
Figure 60. Diagonal Electrode Frame.
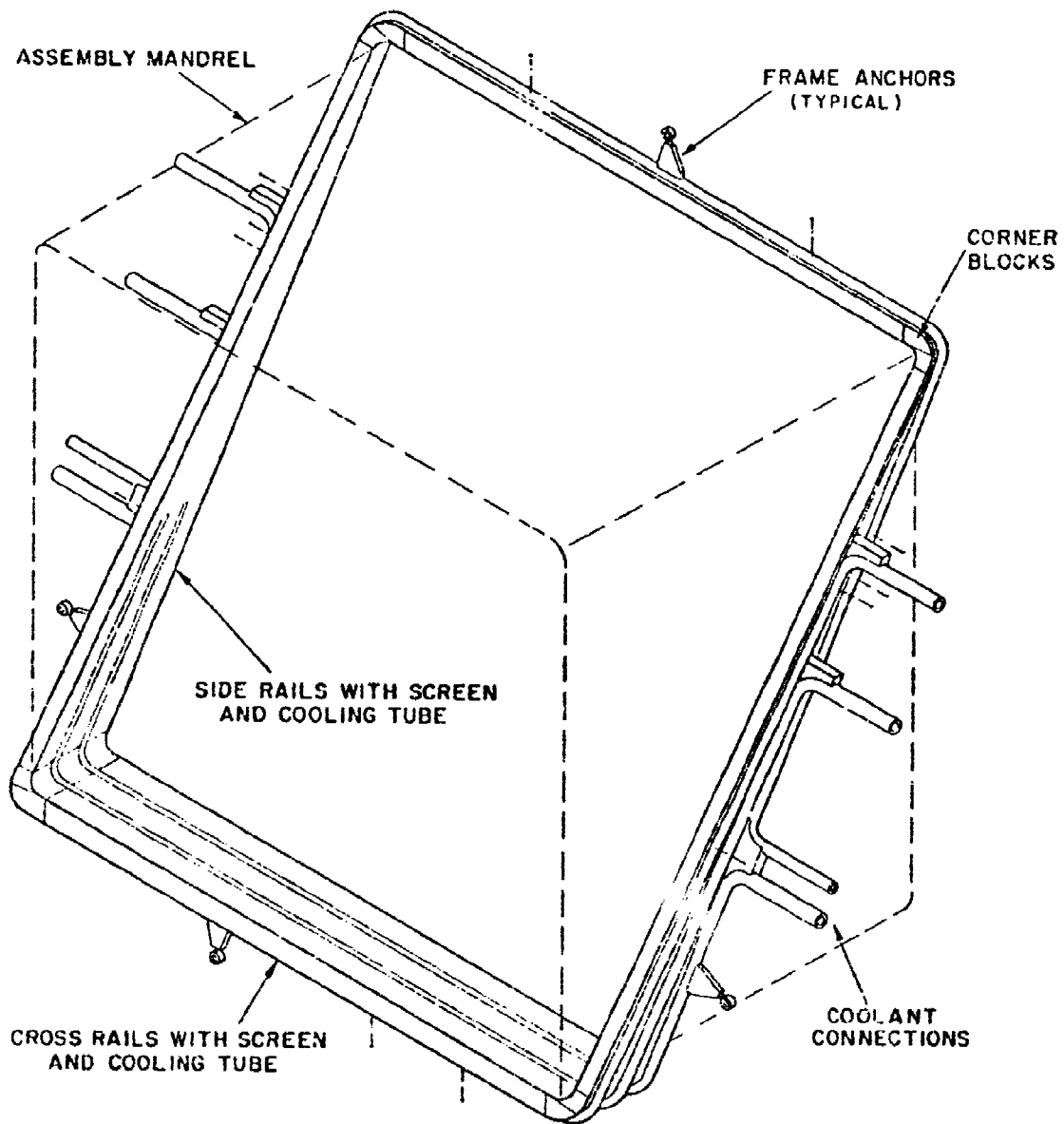
Figure 61. Downstream Transition Electrode Frame.

130

The anchors, as shown by Figure 62, consisted of a flexible beryllium-copper clip that was brazed to a rigid copper base which was soldered to the cooling tube. A flexible rubber boot was placed over the anchor clip before the glass epoxy case was fabricated in place over the frames. When the case cured, the anchor loop was rigidly embedded in the case while the rubber boot prevented the glass epoxy case from forming a rigid cavity which prevented movement of the frame. The anchor clip was stiff in the transverse and perpendicular directions and was only flexible in the longitudinal direction of the frame. This action, coupled with the resilience of the rubber boot, allowed sufficient longitudinal movement of the frame to accommodate the differential thermal expansion between the frames and the case while limiting the transverse and perpendicular motion of the frames.

c. Electrode Screen and Frame Brazing

The two most critical electrode frame brazing details were the current collector screens to rail joints and the rail to cooling tube joints. The screen/rail joint was primarily a thermal requirement; that is, there must be a reliable heat transfer path which requires a void-free, minimum thickness, adequate area braze joint. At the same time the exposed regions of the screen must be kept free from excess braze material which would interfere with the screen/ceramic current collection action. The rail/tube joint was primarily a thermal requirement, requiring a void-free, minimum thickness joint. In order to withstand the operating temperatures, the screen joint was made with a braze material that melted at 890 K. Since the cooling tubes were joined to the rails after the screens were attached, a lower melting temperature solder (610 K), which was still high enough to meet the operating requirements, was used.

d. Room Temperature Vulcanizing (RTV) Silicone Rubber Layer

The RTV silicone rubber layer was fabricated in place over the outside of the electrode frames and under the inside of the glass epoxy case as shown in Figure 63. This layer of rubber first served as a barrier that prevented liquid epoxy resin from penetrating the interframe insulating ceramic during the fabrication of the glass epoxy composite case. The epoxy resin was an organic material which could have carbonized and contributed to the electrical breakdown between frames if the resin was exposed to the elevated operating temperature between the frames near the hot gas surface. The rubber layer served as a thermal barrier to protect the glass epoxy case against any hot gas that might penetrate the interframe ceramic. The layer also prevented direct contact between the case and the cooling tubes, which at some regions may have operated at temperatures above the recommended epoxy glass service temperature. The final function of the rubber barrier was to serve as a stress distribution member by permitting some differential thermal expansion between the frames and the case without high stress concentrations at localized points.

131

ANCHOR LOOP

FLEXIBLE CLIP

FLEXIBLE RUBBER BOOT

RIGID BASE

SOLDER JOINTS
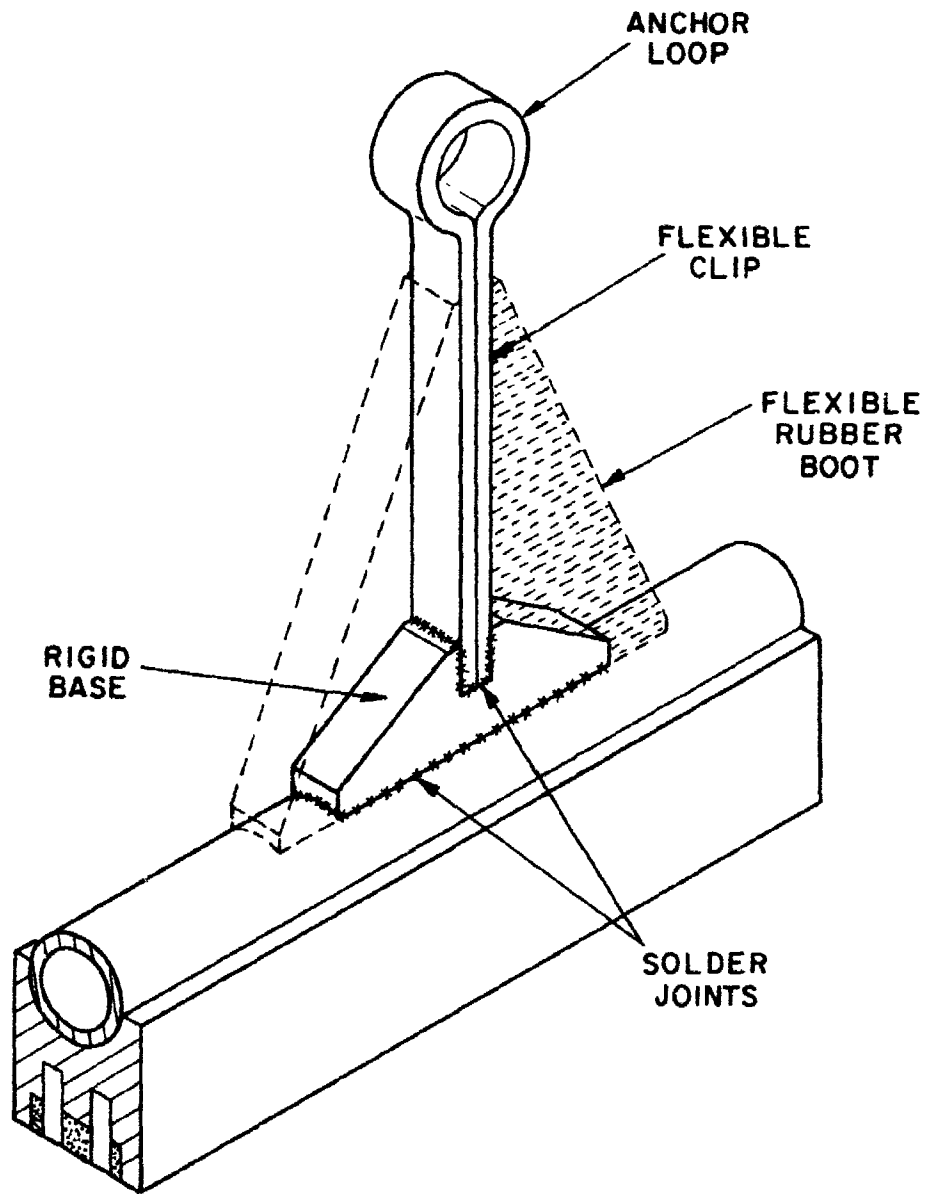
Figure 62.   Electrode Frame Anchor.

132

COMPOSITE CASE CONSTRUCTION

"A" = FIBERGLASS ROVING

"B" = FIBERGLASS FABRIC

A
B
A
B
A
SILICONE RUBBER

CHANNEL/DIFFUSER

COMPOSITE
CASE

SILICONE
RUBBER

ELECTRODE
FRAMES
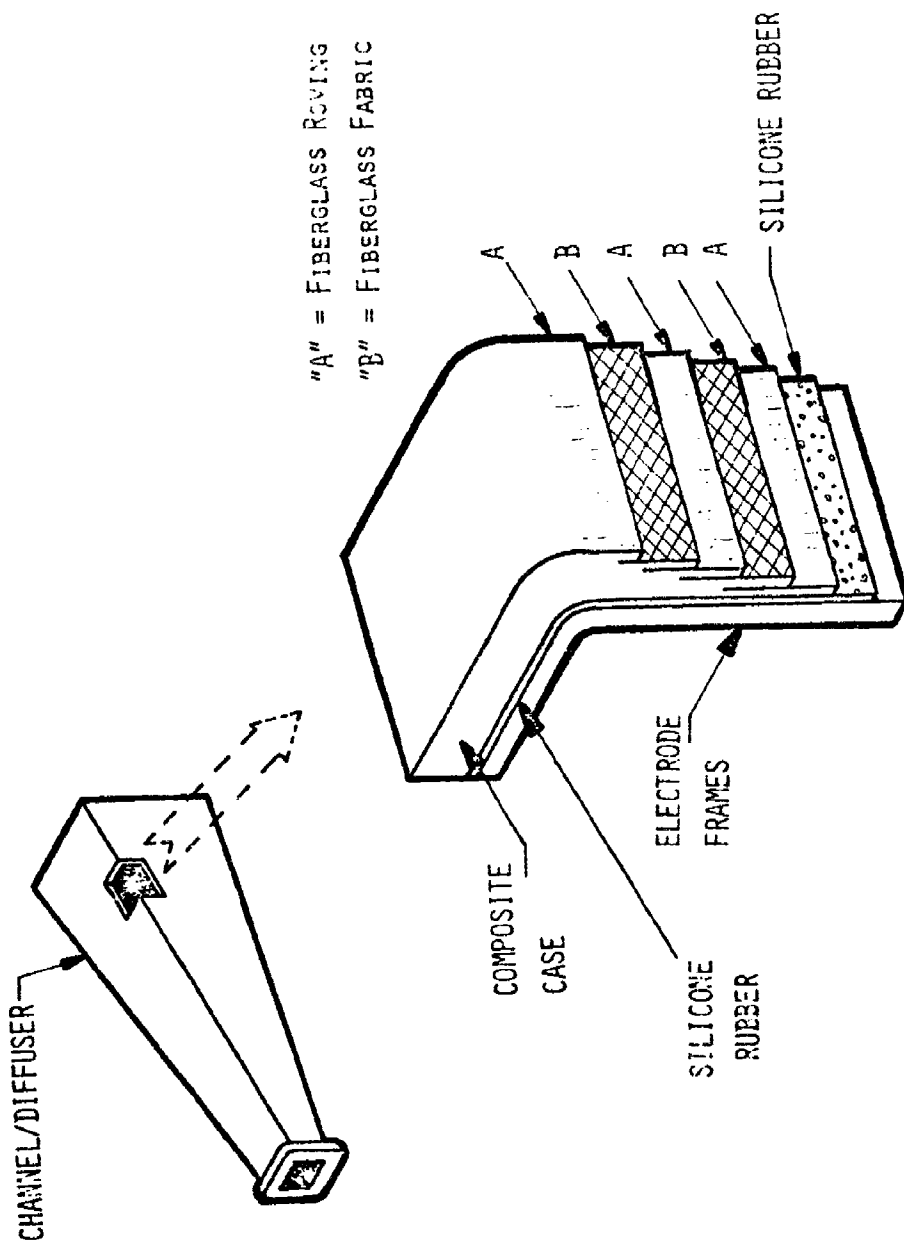
Figure 63.   Composite Case Construction.

133

e. Case Winding and Construction

The glass epoxy composite case was the primary structural member of the high power MHD channel/diffuser. The case was designed to carry the combined effects of the hot gas pressure, the thermal expansion of the frames, any vibrational loads, and the magnetic forces resulting from the interaction of the flowing plasma with the imposed magnetic field. The composite consisted of two components – fiberglass reinforcement material of various forms and a matrix of a thermo-setting epoxy resin. Alternate layers of fiberglass roving and fabric as shown by Figure 63 were wet-wound with liquid epoxy resin, and then cured at an elevated temperature to produce a high strength-to-mass ratio structure. The glass fibers were oriented so the fiber strength contributed the maximum reinforcement to the case. The selection of the various forms of the glass reinforcement materials, as well as their orientations was chosen to achieve a wide variation of case wall distributions. The wall thickness increased as a function of the distance from the nozzle interface because of the increasing length spanned by the walls and because of the hot gas static pressure distribution along the axis of the channel. The thickness also varied around the circumference of the channel wall at any given plane that was perpendicular to the axis. During the wet-winding process an excess of liquid epoxy resin was applied to the glass filaments to ensure a void-free composite wall with thorough wetting of the glass fibers. The excess epoxy was squeezed out by the tension force applied to the filaments during winding. This squeezing action was approximately twice as strong at the corners; consequently, the walls tended to be one-half as thick at the corners as they were at the mid-spans. The case thickness was also increased at both ends of the channel to accommodate the loads and fastening hardware associated with the combustor nozzle and the diffuser extension.

f. Electrical System

During this phase, the details of the electrical power take-off system were not completed. Power take-off designs for the diagonal generator are fairly simple when the power can be extracted in the fringe field region of the magnetic field. However, for test configurations where the electrical power is extracted in regions of high magnetic field, care must be taken in the design of the power take-off configuration to avoid current and voltage concentrations and the associated breakdown and arcing. For this program the magnetic field in part of the power take-off region is expected to be large enough to warrant careful design of the electrical power take-off system. Allowance for the use of balancing resistors to compensate for voltage gradients between individual frames in the power take-off section has been made.

The MHD generator channel design completed during this phase is a "two-terminal" device; i.e., the power is extracted by one terminal at each end of the channel. Since the level of power extracted is expected to greatly exceed the capacity of a single electrode frame, the electrical load must be distributed over a group of eighteen electrode frames at the channel inlet end and twenty-two frames at the exit end. The electrode frames at each end are connected through a balancing resistor, if required, to a common bus bar which serves as the terminal at that end.

134

2. Mandrel

a. Useage for Channel Assembly

The channel/diffuser consisted of an array of electrode frames held together by interframe ceramic and the external fiberglass-epoxy case. The frame spacing and alignment requirements imposed close tolerances upon the fabrication of the channel. Experience has shown that an excellent method for the control of the channel components during construction was to use a stiff frame shaped accurately to the inner surface contour of the channel. This frame was termed a "mandrel."

The mandrel served a variety of purposes from the initial layout of each frame to the final curing of the epoxy resin matrix material for the composite case. A list of the major functional requirements of the mandrel is presented in Table 16.

b. Structural Design

Before the design of the mandrel could be initiated, the design criteria from which the specific design conditions were established were required to be defined. The design criteria have been previously defined in the Design Criteria section of this chapter. A large variety of design possibilities could have been selected to meet many of the criteria. Since bending rigidity was needed throughout 360 deg of rotation of the mandrel, the need for stiffness was considered to be achieved best through the use of the configurations shown in Figure 64. Torsional rigidity was a minimal requirement since start up and shut down times were relatively "long". This minimized the torque loading.

The requirement of dimensional stability influenced the choice of materials. For example the use of wood would have involved some risk because of the long curing time and the presence of the fumes from the hot epoxy. These might have combined to change the wood dimensions in a manner which would lead to shifting of the electrodes, which could lead to cracking of the interframe ceramic. The design criteria were used to establish the design specifications, which have been previously discussed in the Design Specifications section of this chapter.

The numerical value of the mandrel bending stiffness was obtained from measurements of the mechanical properties of the interframe alumina. A large factor of safety was included to avoid low cycle of fatigue of the alumina during the winding and curing stages. The local wall rigidity was determined on the basis of minimization of frame deflections into the channel resulting from the tension in the fiberglass roving.

135

TABLE 16.   MANDREL REQUIREMENTS

1.   Reference for Assembly of Each Frame From Components.

2.   Reference for Checking Each Frame After it is Assembled.

3.   Support for Frame Array During Remainder of Channel Fabrication.

4.   Control of Depth of Interframe Ceramic During Application.

5.   Support for Frame/Ceramic Array During Application and Cure
     of RTV Hot Gas Barrier.

6.   Tool for Winding Fiberglass Case.

7.   Tool for Supporting Channel During Case Cure.

8.   Tool for Supporting Channel During Repair Procedures.

9.   Support for Channel During Shipment in Protective Areas.

136
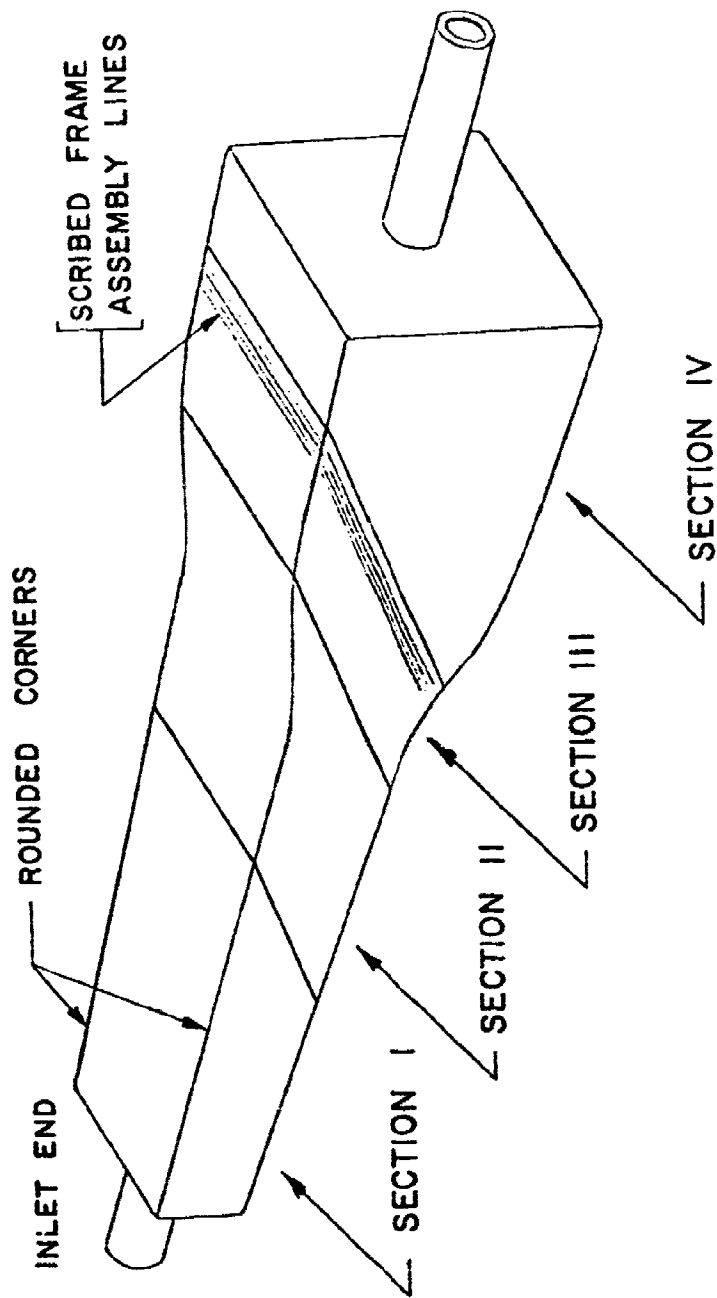
Figure 64. Mandrel Configuration.

137

The remainder of the specifications related to the dimensional stability and handling for control of the components during assembly and curing. Specifying a parameter to quantify the removability of the mandrel from the cured channel was difficult. The meeting of that requirement was inherent in the ability to disassemble the mandrel sections for piecemeal removal.

The design specifications identified certain structural requirements to be met by the mandrel. Table 15 summarizes those design properties and provides the factors of safety for the mandrel design. The allowable interframe strain was determined from experimental tests on samples of the ceramic. The applied strain was that which would be induced during the cure by the bending of the mandrel. This was determined from elementary beam theory by assuming that the full channel mass was effective. The winding tension induced inward pressure on the mandrel faces. The applied deflections were estimated from elementary beam theory. The allowable deflection was the amount considered tolerable to avoid local overstrain of the interframe ceramic.

c. Assembly Details

The four-piece mandrel design is shown in Figure 65. The mandrel was designed in four sections to facilitate a multistation assembly process. The mandrel consisted of aluminum alloy plates bolted together into four box sections that were then bolted together to form the overall assembly mandrel. The combined assembly provided for the processes of electrode frame fit-up, interframe ceramic emplacement, and the winding of the case as illustrated by Figure 66.

The mandrel was designed to be removed from the completed channel by collapsing one section at a time, beginning at the large end. The corner brackets were removed first and then the individual surface plates were removed.

3. Manifolds Assembly

a. Manifolds

The design objective for the manifold was to minimize the coolant pumping power requirements by maximizing the cross sectional flow area. The flow was divided into six supply and six return manifolds because of the limited space between the channel/diffuser and the magnet. Figure 67 shows the channel/diffuser inlet and outlet manifolds above and below the channel, respectively.

SIDE PLATE (TYPICAL)

CORNER BRACKETS

SECTION TIE BOLTS

TOP PLATE

CROSS SECTION
(TYPICAL)

BOTTOM PLATE
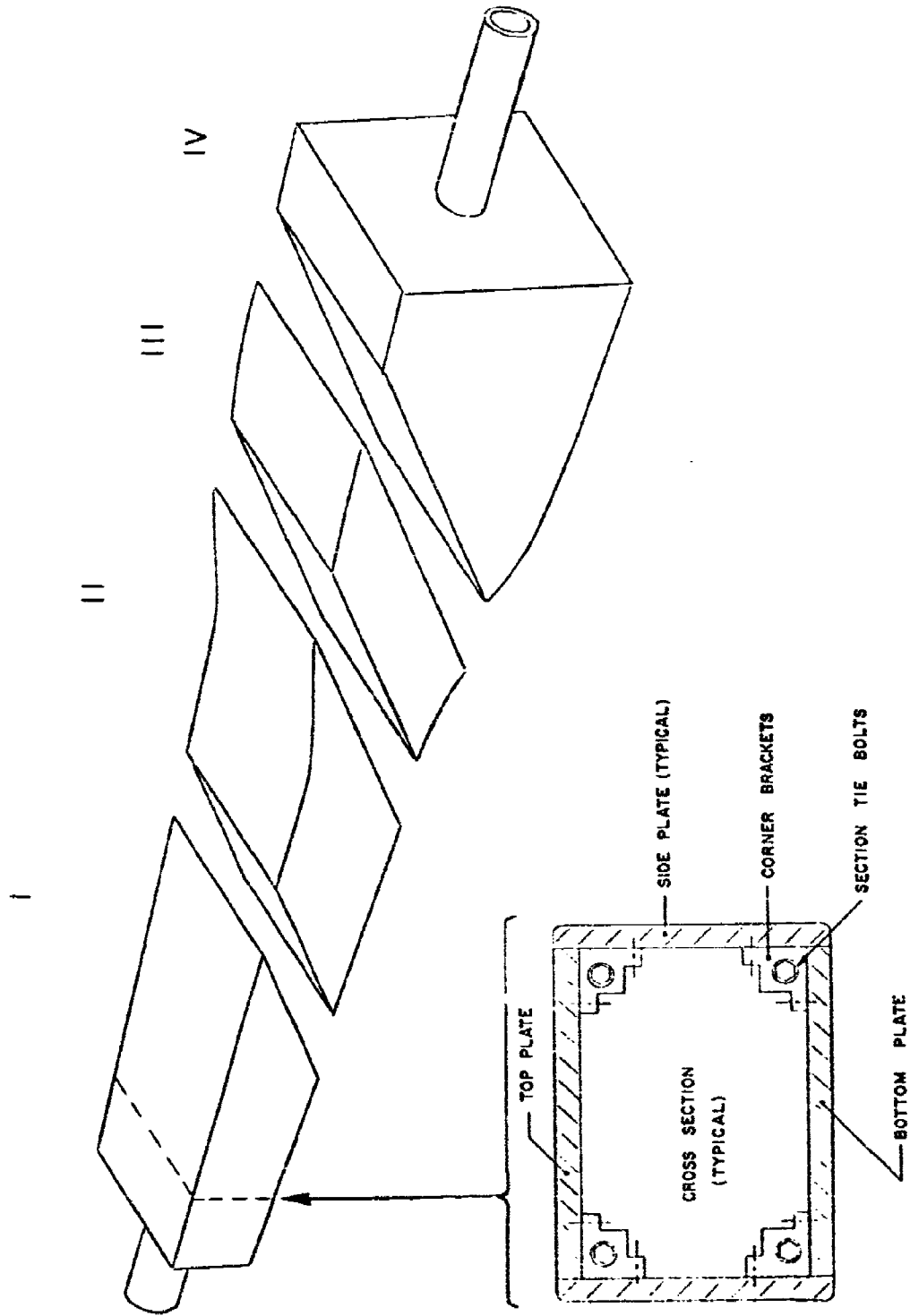
Figure 65. Mandrel Sections.

139

Figure 66. Mandrel Useage During Fabrication.

140

CONNECTING TUBING
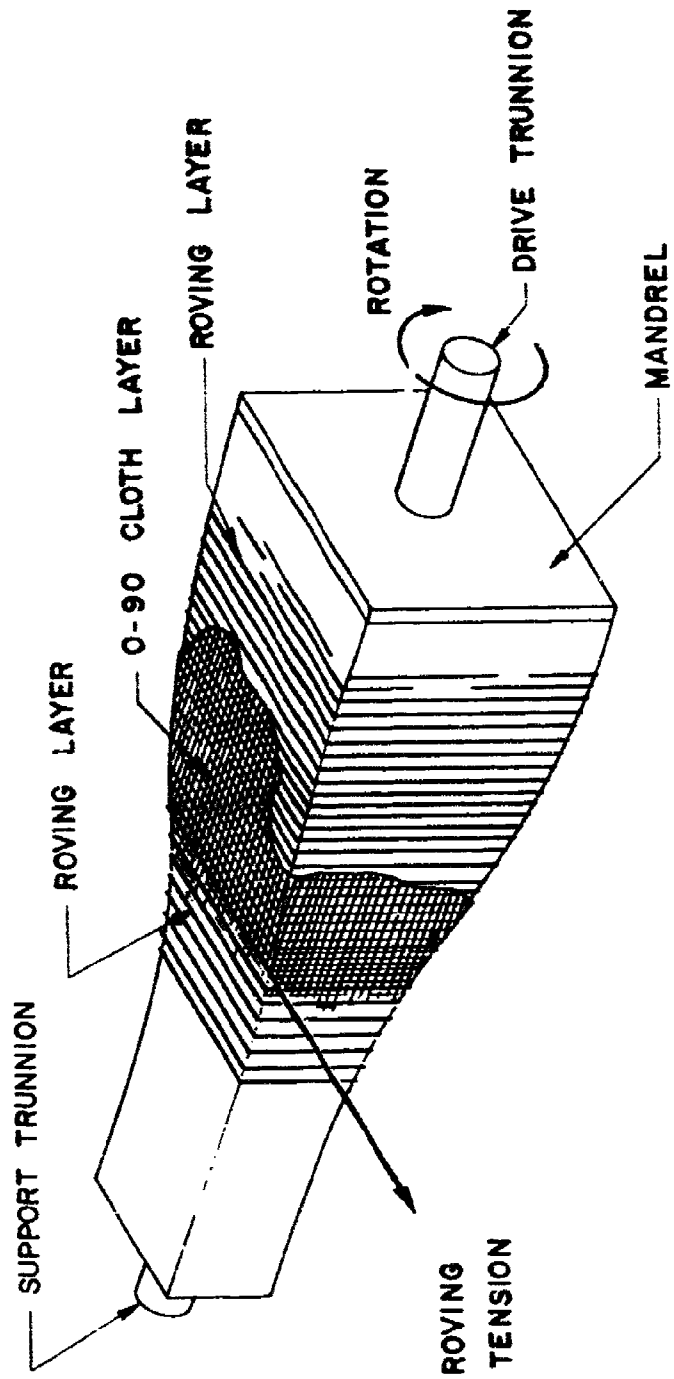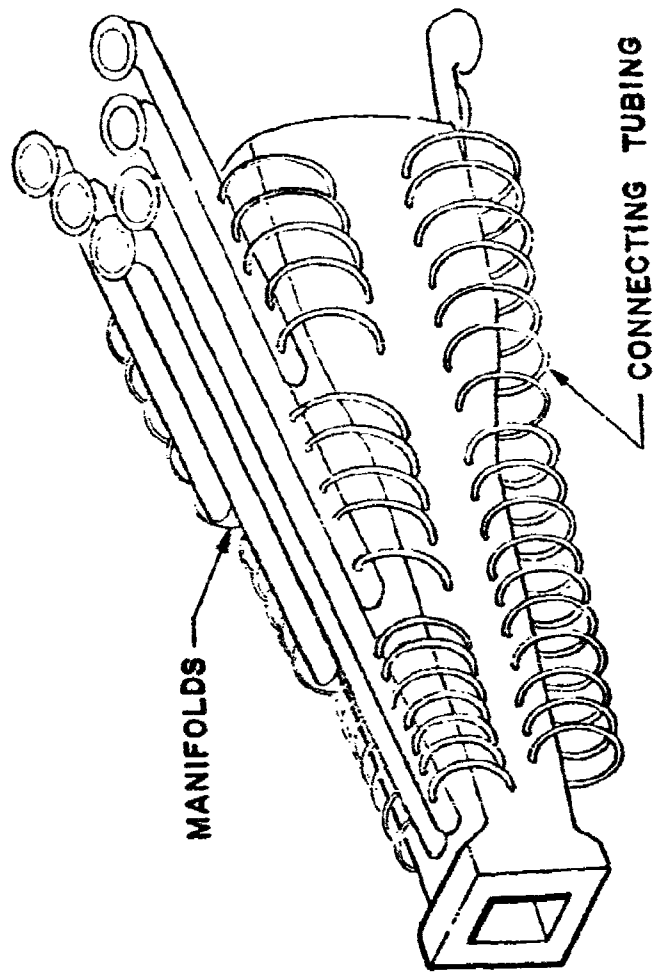
MANIFOLDS

Figure 67. Water Manifolds Assembly.

141

Three different lengths of manifolds were designed. The long manifolds served the upstream third of the channel, the intermediate manifolds served the central third of the channel, and the short manifolds served the downstream third of the channel. The manifold design each consisted of 102 mm diam Schedule 40 non-magnetic stainless steel pipe. The design specified that on one end of each pipe an end cap was to be welded in place, and a 90 deg elbow and a connecting flange were to be welded on the other end. Drilled and tapped holes were to be provided in each manifold to accommodate the cooling tube fittings. A drain valve was also to be provided in the end cap of each of the supply manifolds.

The supply and return manifolds were designed to attach to each other with a temporary steel frame structure that attached the manifolds to the channel while the cooling tubes were installed between the manifolds and the electrode frames. After the channel/manifold assembly was installed in the magnet and the manifold flanges were bolted to the facility cooling line flanges, the temporary frame structure was designed to be removed. The manifold design required that the manifolds be supported by the facility cooling lines and by the magnet spacer blocks so that no manifold loads were transferred to the channel assembly.

b. Connectors

The tubing between the manifolds and the channel was designed to be with two types of non-magnetic metal fittings. At the channel the connectors were soldered to the electrode frame cooling tube terminations, and at the manifolds pipe thread connectors were used. Some of the frame cooling tube "half-loops" were designed to be connected in series with a copper tubing reverse-bend loop.

c. Connector Tubing

Since there was a voltage gradient along the channel, the electrode frames must be electrically insulated from each other. Consequently, the design cooling water lines from the electrode frames to the manifolds were non-conductive materials and the tube lengths were selected so that the water passages had sufficient length to prevent current leakage through the coolant. The coolant lines consisted of a very rugged flexible tubing with a polyamide core, a glass braid liner, and polyurethane jacket. Special attention was necessary to ensure that the tubing did not contain any metallic or high carbon content material that would conduct electrical current when exposed to the high voltage gradients between the channel frames and the coolant manifolds during operation.

A cooling water flow schematic drawing is required to define the exact interconnections that are required. This schematic would be based on the electrode frames heat transfer and hydraulics analyses. However, the actual physical location of the lines would be determined at assembly because of the large quantity of lines and the limited space between the channel and the magnet.

4. Instrumentation

Diagnostic instrumentation to measure the important performance parameters of the high power MHD channel/diffuser was incorporated in the final channel/diffuser design. This instrumentation was utilized to measure the electrical, thermal, structural, and gas dynamic behavior of the system during the performance test program at the HPMS test facility at AEDC. Section IX presents the performance test plan. The diagnostic instrumentation for the high power MHD channel/diffuser is shown in Figure 68.

Since the gas conductivity had been measured previously during the development test program, instrumentation to determine this important parameter was not included in the performance test program. The development test program hardware is described in Section VII, and the results of the development test program are presented in Section VIII.

a. Voltage and Current

In the design of the high power MHD channel/diffuser, voltage measurement connections were provided for each of the non-power takeoff electrode frames. This was accomplished by soft soldering a voltage tap to the electrode frame cooling tube outlet or inlet. The inlet and exit power takeoff electrode frames had voltage taps attached to the electrode frame power takeoff terminals. Voltage measurements were also provided for at both the high voltage and low voltage side of the load by the test facility instrumentation.

Current measurement instrumentation, while not a part of the high power MHD channel/diffuser design, was required for each of the power takeoff electrode frames. In addition, the total current flowing through the electrical load was required. These current measurement devices were also provided by the test facility instrumentation.

b. Pressure

Pressure taps for the measurement of the gas static pressure were provided at thirteen different axial locations in the high power MHD channel/diffuser. These taps were located in the side spacer blocks between the electrode frame cooling tubes.
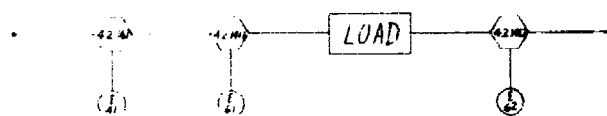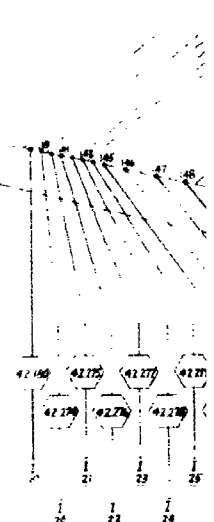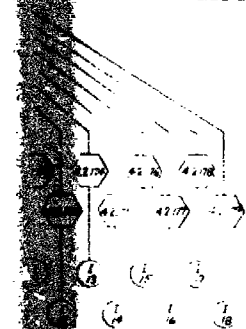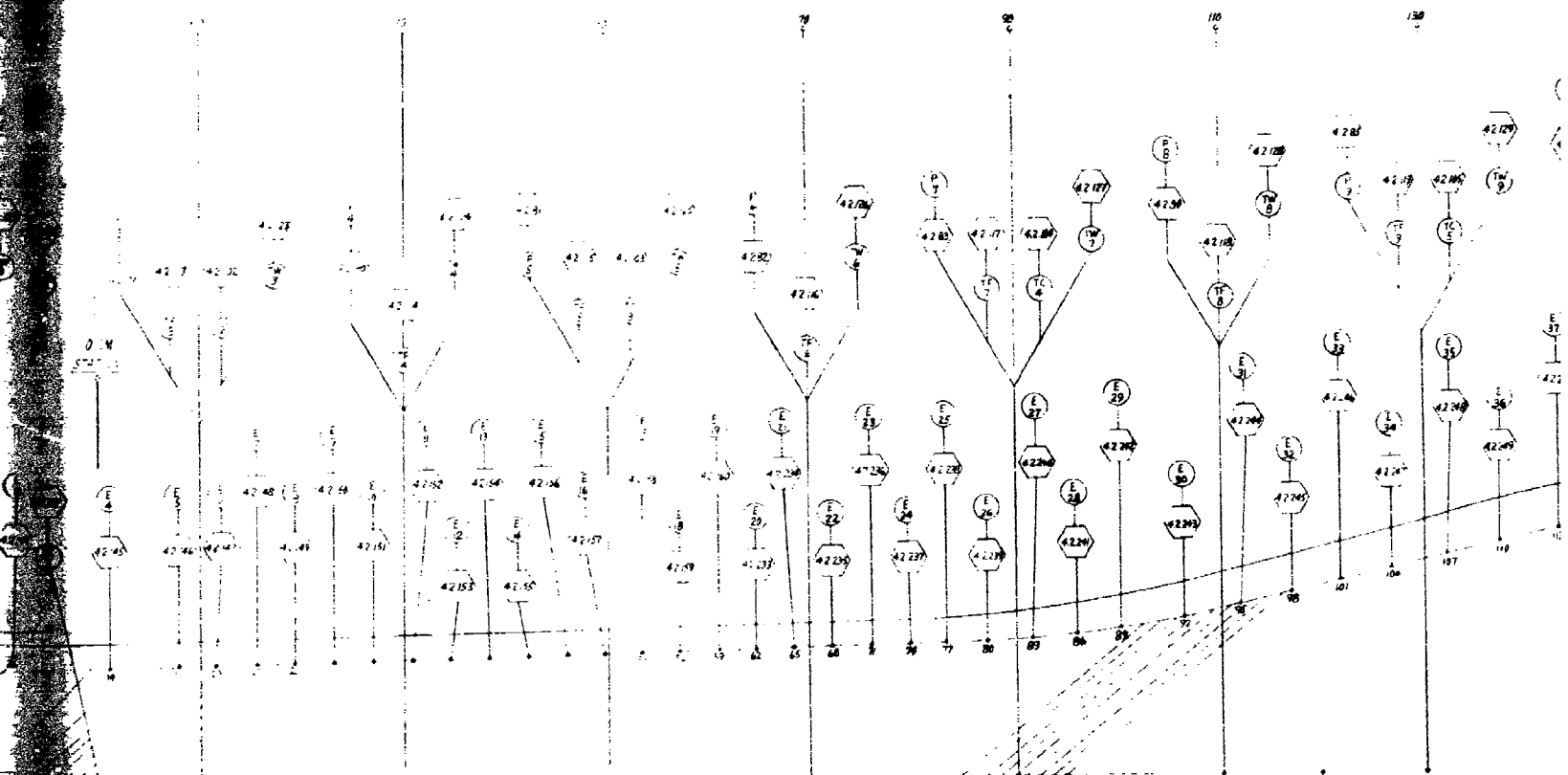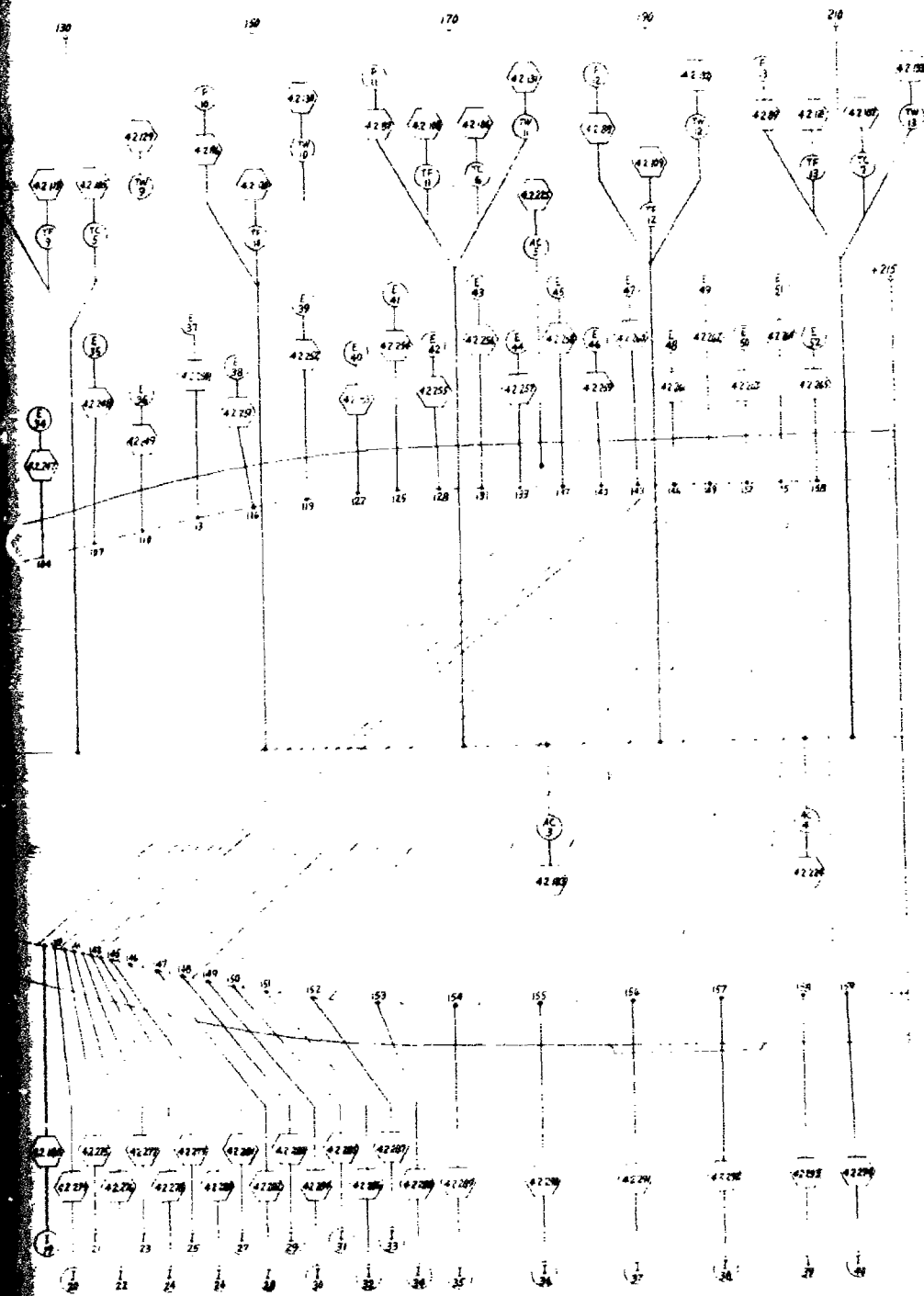
143

LOAD

Figure 68. High Power MHD Channel
Diagnostic Instrumentation

145

The pressure transducer assembly was mounted as close to the channel as was possible to minimize the gas volume between the pressure transducer and the interior of the channel; and hence, maximize the frequency response of the pressure measurement system.

The pressure transducers, which were selected, were required to operate properly while exposed to a magnetic field strength up to four Tesla. A frequency response from d.c. to a few hundred Hz was also required along with reasonable cost and availability. These requirements led to the selection of a semiconductor strain gauge type pressure transducer which could function in the high magnetic field and meet all of the additional requirements.

c. Temperature

Thermocouple temperature measurements were required in three different areas of the channel: (1) case temperature, (2) electrode frame copper temperature, and (3) electrode frame water temperature. The case temperature measurements were made at seven different axial locations. These thermocouples were designed to be located at depths in the case ranging from the case surface to 2 cm into the case. The thermocouples were mounted by drilling small holes into the case during the finishing operation and using epoxy to permanently attach the thermocouples to the case.

Electrode frame copper temperature measurements were made on thirteen electrode frames. These thermocouples were mounted on the electrode frames prior to the case fabrication and the application of the RTV layer. Since these thermocouples were attached directly to the electrode frames, they were used only during the thermal checkout tests and were disconnected uring the MHD performance tests. The use of these thermocouples during the high power MHD performance tests would have required voltage isolation amplifiers which were not expected to be available during the period of time when the performance testing was expected to occur.

Electrode frame outlet water temperature measurements were also made on thirteen electrode frames. These thermocouples were mounted in the outlet electrode frame cooling loops at the connecting tube/manifold connection. A street "T" with a standard "water immersion" thermocouple and fitting was used.

d. Vibration

In order to assess the structural performance of the high power MHD channel/diffuser system during operation, five accelerometers were provided for the measurement of channel/diffuser vibrations. The accelerometers were

required to function properly when exposed to magnetic fields as high as four Tesla. In addition, the accelerometers must be small in size and provide a frequency response from a few Hertz to several thousand Hertz for loadings of up to 100 g's. A piezoelectric semiconductor type accelerometer was selected for this application.

H. FABRICATION

1. Introduction

Since the actual high power MHD channel/diffuser and manifolds fabrication was not part of this phase of the HPMS program, the following discussions present the details of the planned fabrication approach instead of reporting the actual results of the fabrication process.

The planned fabrication of the high power MHD channel/diffuser was based on the previous successful fabrication and performance testing of three lightweight hot gas flow channels which have been completed for the Air Force. The first channel was a small, lightweight flow model shown in Figure 69.[3] The second channel was a 200 kW, lightweight MHD channel, which is shown in Figure 70.[4] The third channel was the diagnostics channel completed during this program. This channel is shown in Figure 71. The designed high power MHD channel/ diffuser is illustrated by the sketch of Figure 72. This figure shows the composite case wall structure and a cutaway of the interior of the channel, while Figure 73 shows the electrode frame design concept.

All of these channels utilized a common fabrication process which involved three major steps: (1) fabricate the individual electrode frames; (2) assemble the frames on a contoured mandrel; and (3) fabricate the contiguous composite case. However various modifications in the fabrication process evolved during the construction of these channels. The lightweight flow model had an oval interior cross section with electrodes which were not perpendicular to the flow axis. The 200 kW lightweight MHD channel was rectangular in cross section with electrodes which were perpendicular to the flow axis. Both of these channels, however, did have diagonal electrode frames while the diagnostics channel consisted of electrode

148
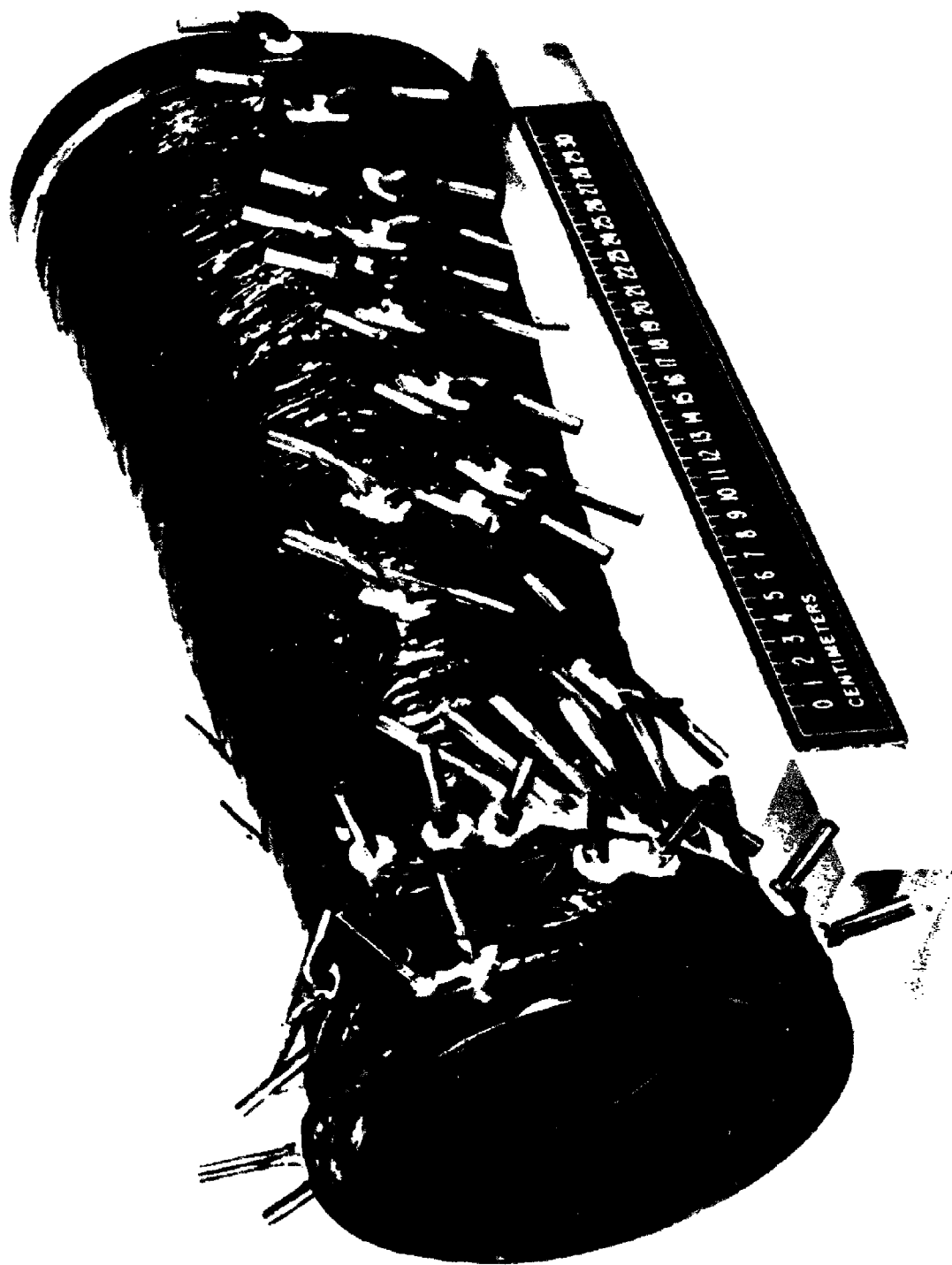
Figure 69.   Lightweight Gas Flow Channel.
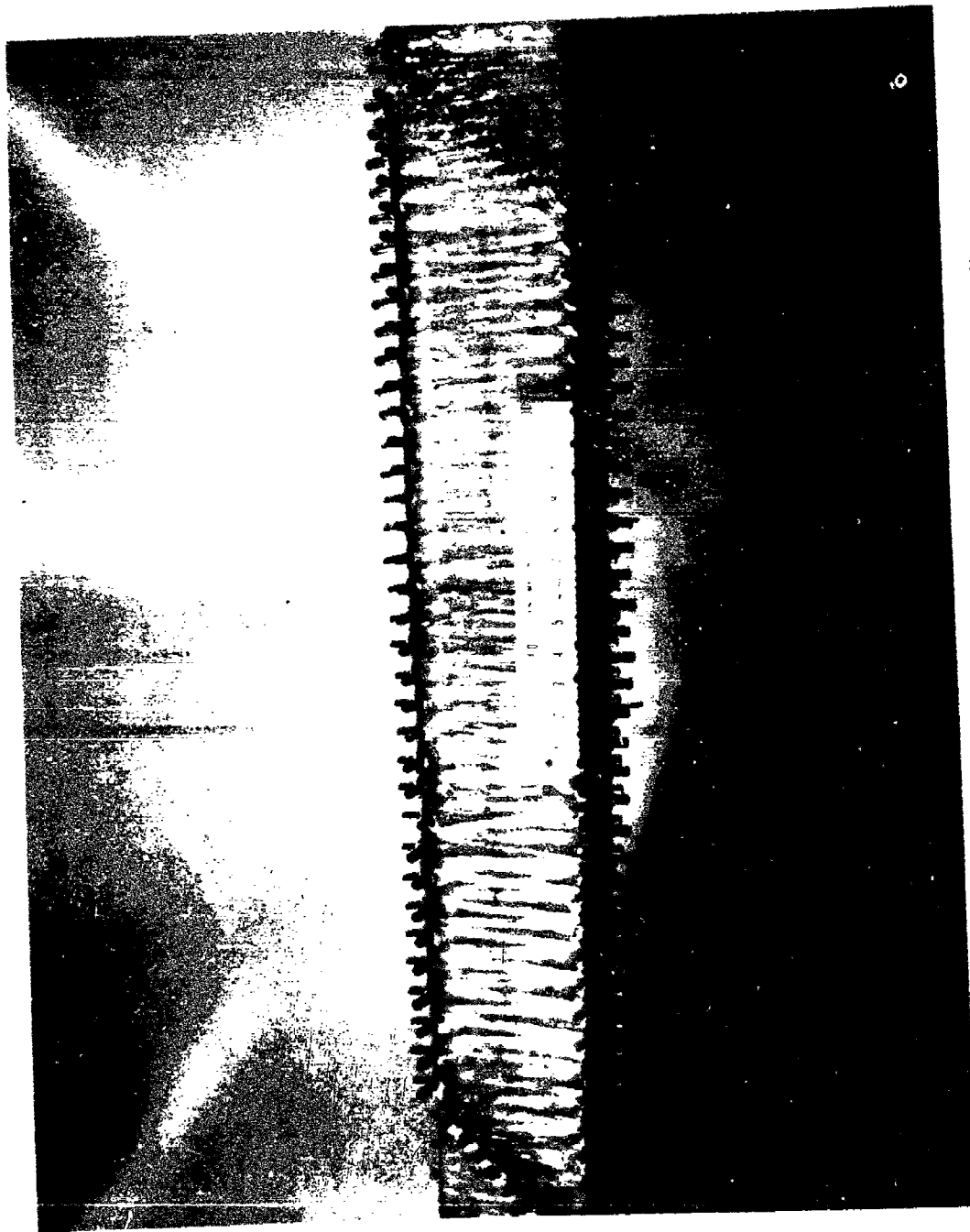
Figure 70.　Lightweight 200 kW MHD Channel After Filament Winding.

DIAGNOSTICS CHANNEL SYSTEM

Diagnostics Channel

Water Manifold

Diagnostics Channel

Static Pressure Taps
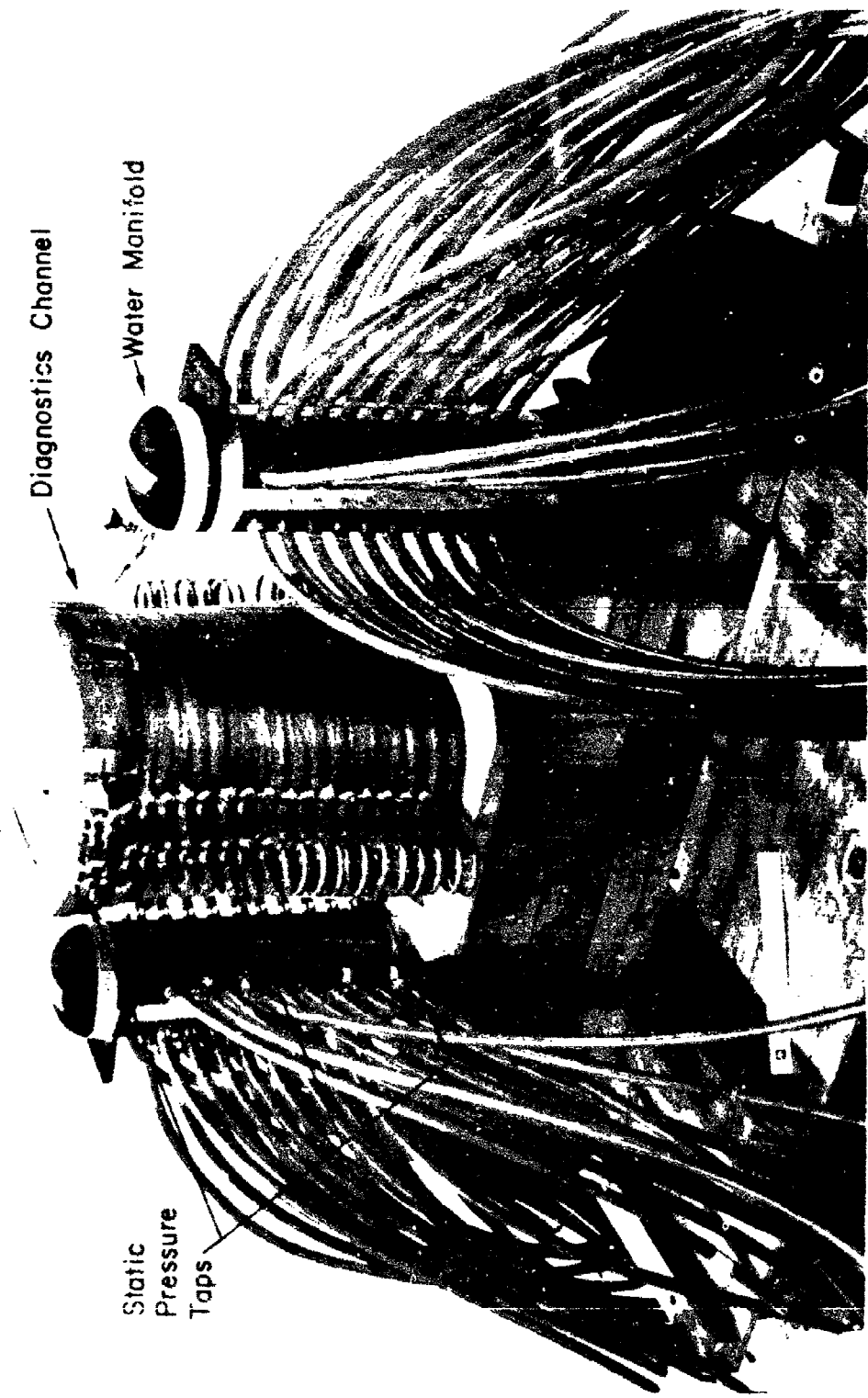
Figure 71. Diagnostics Channel.

DIFFUSER SECTION

WALL STIFFENING RIBS

COOLANT MANIFOLDS

POWER TAKE-OFF SECTION (BOTTOM WALL)

DIAGONAL ELECTRODE FRAMES

FIBER REINFORCED COMPOSITE WALL STRUCTURE

GENERATOR ELECTRODE SECTION

POWER TAKE-OFF SECTION

TRANSITION REGION

NOZZLE FLANGE
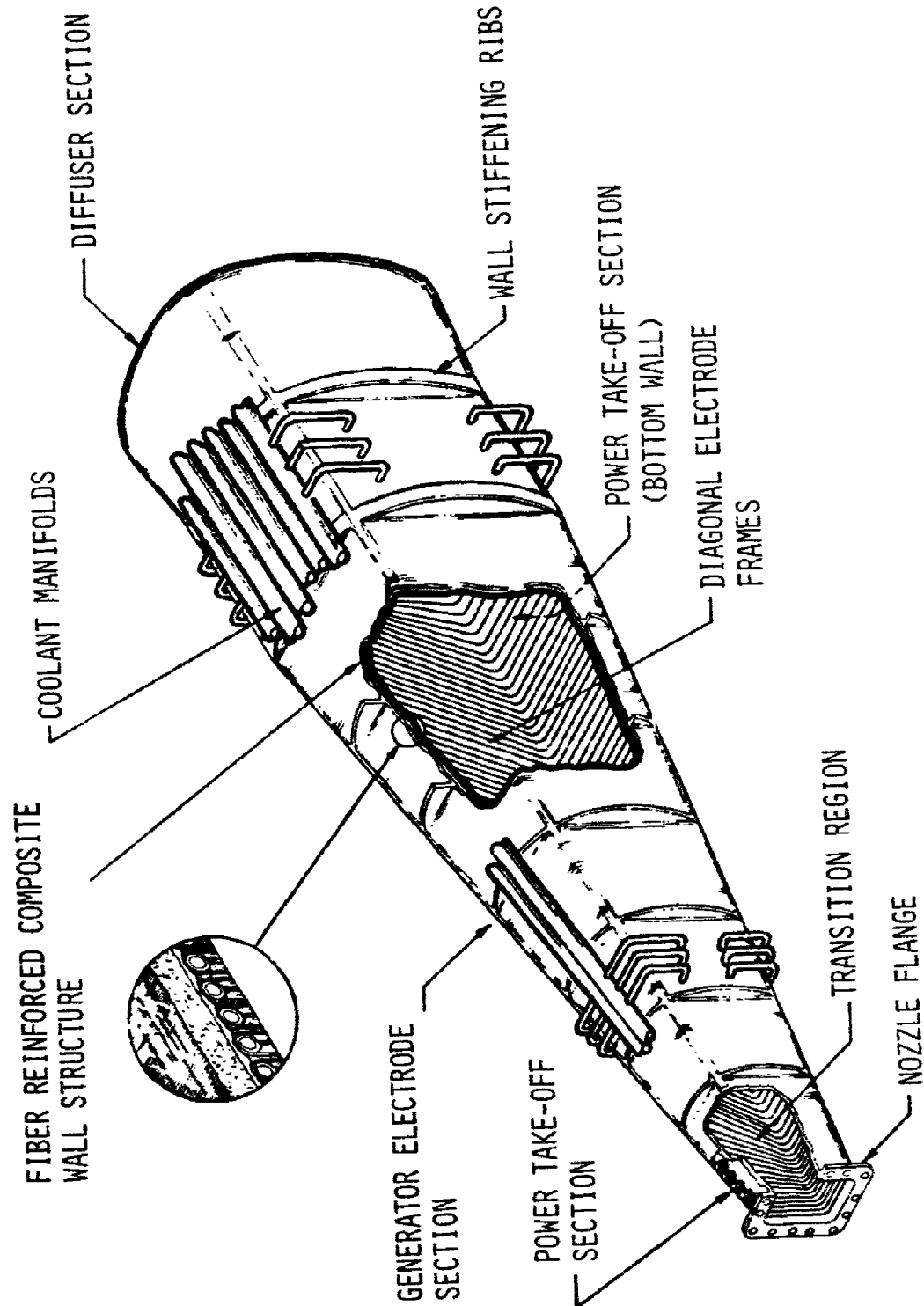
Figure 72. High Power MHD Channel/Diffuser Concept

152

CORNER REGION

CONNECTIONS REGION

ROUND, STRAIGHT SECTION

FLATTENED, STRAIGHT SECTION

SIDE RAILS WITH SCREEN AND COOLING TUBE

CROSS RAILS WITH SCREEN AND COOLING TUBE
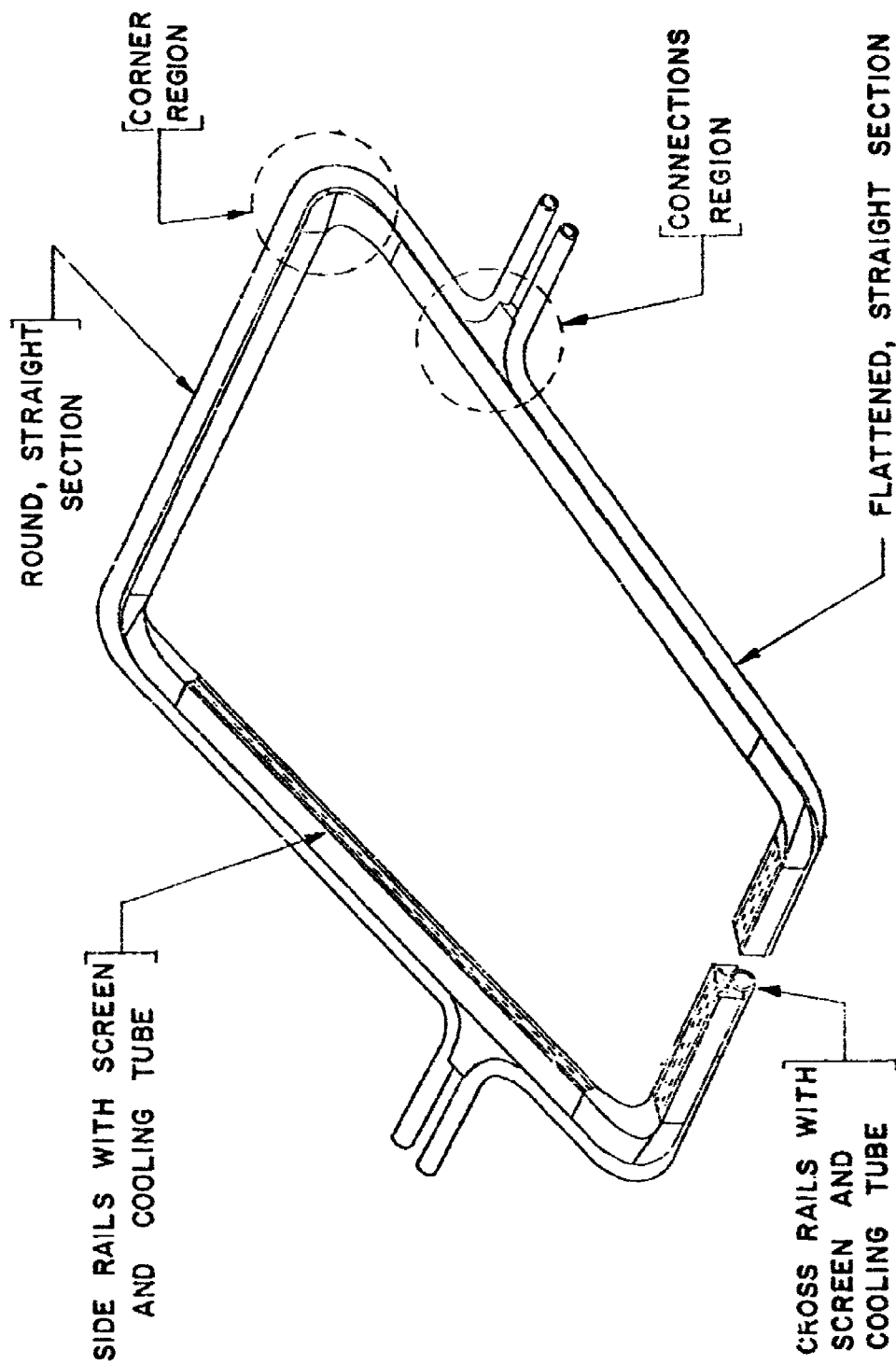
Figure 73.   Electrode Frame Design Concept.

frames perpendicular to the flow axis. Further refinements to the diagnostics channel included building the electrode frame around copper rails instead of the cooling tubes.

Three key features contributed to the successful fabrication of the high performance, lightweight gas flow channel: (1) the use of a contoured assembly mandrel; (2) the design of a minimum weight, efficiently cooled electrode frame; and (3) the use of a contiguous, fiberglass reinforced epoxy filament wound composite case.

The contoured assembly mandrel,which had an outer surface that matched the internal geometry of the channel/diffuser hot gas surface, served two critical functions: (1) a master sizing gauge on which the electrodes were fabricated to the required dimensional accuracies; and (2) a positioning fixture which located and aligned all of the frames in relation to each other while fabricating the contiguous composite shell which then retained the electrodes in their proper positions. These mandrel functions of sizing and positioning the electrode frames ensured a smooth internal channel surface contour which was necessary for high performance operation.

The second key feature was the fabrication of the electrode frames. The frame cross section consisted of the minimum mass of metal that was required for the electrical-thermal-mechanical functions involved. The frame structural requirements were minimized by supporting the frames on the composite shell which was the primary structural member of the channel. The frame cooling passages were highly efficient and reliable because of the use of continuous cooling tubes which did not have any joints in the region of severe thermal expansion and contraction. The successful fabrication of the complex contoured geometry of these tubes was possible with the use of special forming tools that were developed on this program.

The third key feature was the fabrication of the composite glass-epoxy shell. The cost and mass of the shell were minimized because of its contiguous construction, i.e., fabricated around the outer surfaces of the electrode frame array by winding the shell in place. This process eliminated all extensive precision machining operations and minimized the mass by eliminating all bolted joints at the corners of the channel walls. The winding process readily conformed to the varying channel geometry contours and to the structural thickness distribution requirements which would have required much higher costs and greater weight to accomplish with machined, rigid channel wall materials.

154

During the process of planning and scheduling for the high power MHD channel/diffuser fabrication phase, an analysis of the overall fabrication schedule revealed that the mandrel related tasks were the critical path items. A study of the relation between the sequence of electrode frame fabrication operations and the method of constructing and utilizing the assembly mandrel revealed that a significant shortening of the fabrication schedule was possible by constructing the mandrel in four sections. The time saving was achieved by separating the mandrel into the four sections which were used simultaneously for fabrication of four groups of frames. Upon completion of the electrode frames, the mandrel sections would be combined into one full length mandrel assembly for fabricating the glass-epoxy case. The use of a sectional assembly mandrel was a new concept which was adopted for this program in view of the scheduling goals at that time.

2. Facility Description

The channel subsystem fabrication process required a number of common commercial fabricating facilities. None of these were by themselves uncommon or unique. What was uncommon was the combination of facilities that were involved in fabricating a single device such as the channel/diffuser. The major fabrication processes were the machining, brazing, fiberglass epoxy filament winding, and ceramic casting. In the following sections the various facilities are described in relation to the channel fabrication process steps for which they were required.

a. Machining Facilities

The mandrel external surface contours involved close tolerances and the interface between sections required precision alignment features to prevent any mismatch of adjacent surfaces. The electrode frame components manufacture required a machine shop with capability for mass production of many complex parts of a similar but not always identical nature. Other various hardware items required conventional machining facilities.

b. Welding, Brazing, and Soldering Facilities

A Heli-Arc welding process was required for temporarily fastening the electrode frame components together until they were permanently joined by brazing. The electrode frame rails required very precisely controlled brazing of the Inconel current collector screens to the copper rails. Previous experience had indicated that a manual torch brazing operation was required to successfully braze the screens to the rails. Appendix C contains a more complete discussion of this operation.

155

The cooling tubes were soldered to the frames with a medium temperature solder. This process required a skilled, manual torch soldering operation because the tube to frame solder joint was a critical heat transfer path and the only means of quality control was through dependence on close operator control. The materials and geometry of the electrode frames were such that a quality control program for the inspection of the tube to frame solder joint was difficult to implement.

c. Specialized Assembly Facilities

The electrode frames were assembled by fitting their components to size on the assembly mandrel. This process required considerable work around the mandrel to handle the frames as well as adequate areas for in-process storage of the individual frames. Lifting and handling facilities were required for manipulating the mandrel and channel during the various assembly process steps. The estimated masses of the channel and mandrel were 580 kg and 295 kg, respectively.

The electrode frame cooling tubes were formed to fit the frame geometry while the frames were on the assembly mandrel. This process required facilities for cutting, annealing and forming copper tubing with specialized tooling and fixtures that were developed on this program.

d. Leak Detection Facilities

A source of pressurized gas such as dry nitrogen and leak detection fluids were required for leak-checking the frame cooling tubes, the coolant hoses, and the coolant manifolds. A vacuum pump with lines, valves and gauges was required for leak-checking the fiberglass-epoxy channel case.

e. Fluid Flow Measurement Facility

A facility was required for measuring the rate of water flow through the electrode frame cooling tubes and the associated pressure drops. A flow calibration curve was required for every coolant passage in order to balance out the total coolant flow through the supply and return manifolds.

f. Winding Facility

A positioning fixture was required to orient the mandrel for ease of fabrication during the various frame array fabrication process steps. Experience has shown that the fiberglass winding machine adequately serves this function.

The filament winding of the fiberglass-epoxy case required a fixture or machine to rotate the channel while winding on the fiberglass in a controlled configuration. Commercially available filament winding machines were ideal for this process but if they are not readily available, a large engine lathe could be readily modified to meet the specialized requirements of winding the channel case.

Lifting and handling facilities were required to move the channel and mandrel in and out of the winding facility. The combined mass was estimated to be 875 kg.

g. Surface and Component Cleaning Facility

The tube wall cavity surfaces and the electrode frame grooves required a facility for sandblasting the surfaces in preparation for bonding operations. A means of chemically cleaning the exterior surfaces of the electrode frames was also required.

h. Ceramic Emplacement Facility

The electrode and insulating ceramics required facilities for mixing and emplacing the castable ceramics in the electrode frame grooves and in the spaces between adjacent electrodes.

i. Elevated Temperature Facility

The application of the RTV hot gas barrier and the castable electrode and insulator ceramics required a facility for drying out the materials by means of circulating hot air. The oven for curing the fiberglass epoxy shell served this function very well.

The fiberglass epoxy case curing process required a facility for elevating the case temperature in a controlled, programmed process while the channel was being continuously rotated in the winding fixture. This oven should be a portable unit with automatic temperature indicating and controlling instrumentation which can be placed surrounding the channel while the channel remains in the winding machine.

3. Process Steps

The channel/diffuser fabrication process involved eleven major steps:

Step 1. Fabricate assembly mandrel.
Step 2. Fabricate frame components.

Step 3.   Assemble frame components.

Step 4.   Check out frame assemblies.

Step 5.   Fabricate frame array on mandrel.

Step 6.   Fabricate glass-epoxy case.

Step 7.   Channel finishing operations.

Step 8.   Check out tests on channel.

Step 9.   Fabricate manifold components.

Step 10. Assemble manifolds to channel.

Step 11. Check out tests on subsystem.

The required sequence of these steps is illustrated in Figure 74 for a one-piece assembly mandrel. If a four-section mandrel was used, the same eleven major steps were involved but Steps 2, 3, and 4 were subdivided into the four parallel steps shown in Figure 75. Each of these major steps are further broken down into the detailed tasks. These details are presented in more detail in Appendix H.

4. Schedule Plan

The proposed channel/diffuser fabrication schedule plan is presented by Figure 76. Approximately nine months were estimated to be required for the completion of the channel/diffuser. This estimate was based on the simultaneous fabrication of four groups of electrode frame assemblies utilizing a four section mandrel. The estimate assumed a normal, single shift operation. The use of a one section assembly mandrel was estimated to extend the schedule by approximately nine months unless more than a one shift operation was used.

START

Fabricate [1]
Assembly
Mandrel

Fabricate [2]
Frame
Components*

Fabricate [9]
Manifold
Components

Assemble [3]
Frame
Components*

Check--Out [4]
Frame
Assemblies*

Fabricate [5]
Frame-Array
on Mandrel

Fabricate [6]
Glass-Epoxy
Composite Case

Channel [7]
Finishing
Operations

Check-Out [8]
Tests On
Channel

Assemble [10]
Manifolds to
Channel

Check-Out [11]
Tests On
Subsystems

FINISH

* Includes Entrance
and Exit Flanges

Figure 74.   Channel/Diffuser Fabrication Process Steps

159
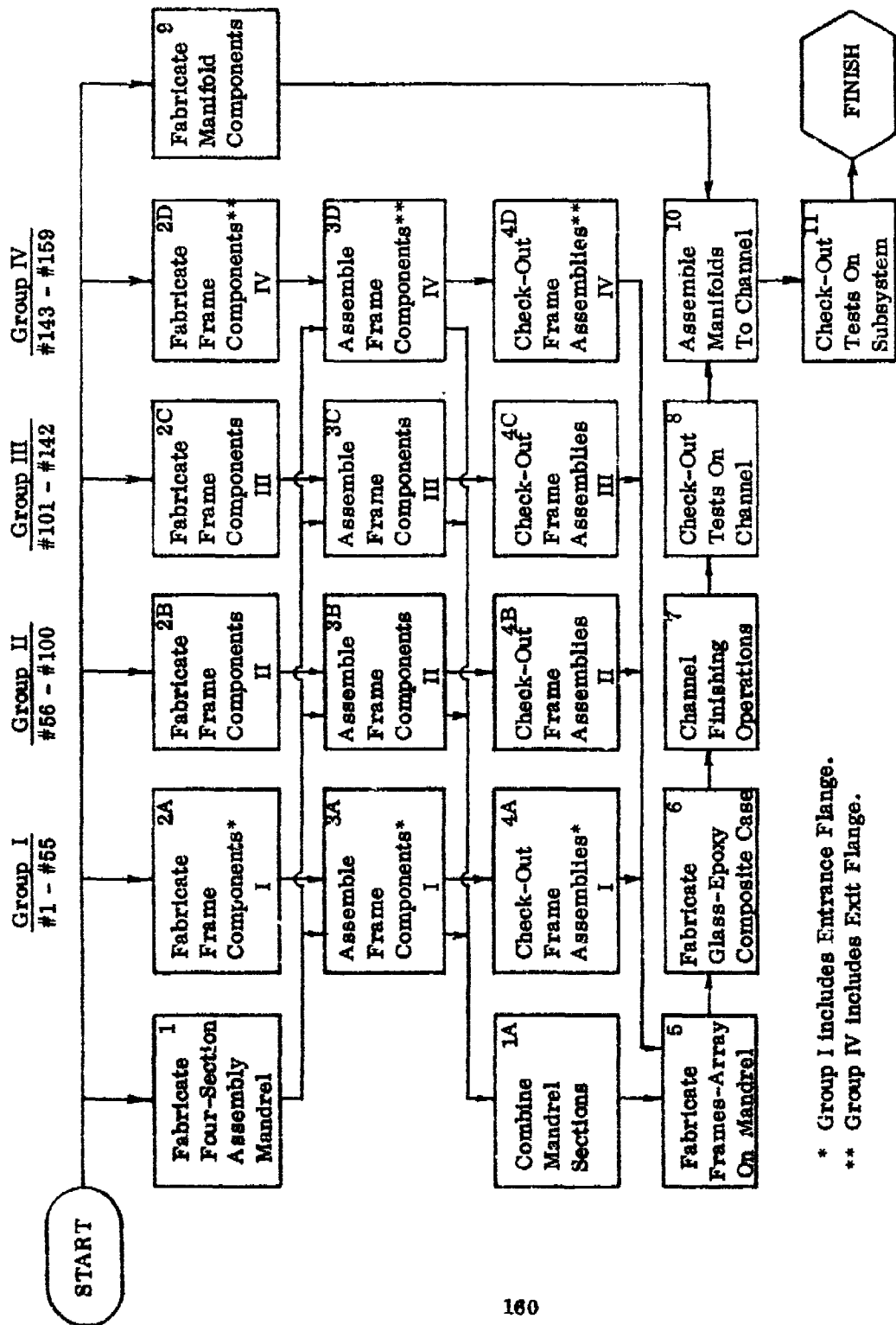
Figure 75. Four Group Fabrication Process Steps [Channel/Diffuser].

* Group I includes Entrance Flange.
** Group IV includes Exit Flange.

160

TASKS	ELAPSED TIME (MONTHS)								
	1	2	3	4	5	6	7	8	9
• Four Section Mandrel									
Fabricate Complete	▭								
Separate Into Sections			▭						
Reassemble Complete						▭			
• Electrode Frame Assemblies									
Fabricate Components									
Group I	▭								
Group II	▭								
Group III	▭								
Group IV	▭								
Assemble Components									
Group I				▭					
Group II				▭					
Group III				▭					
Group IV				▭					
Checkout Test Assemblies									
Group I						▭			
Group II						▭			
Group III						▭			
Group IV						▭			
• Frames Array on Mandrel Fabricate Complete							▭		
• Glass Epoxy Case									
Winding Operations							▭		
Curing Operations								▭	
• Channel Finishing Operations									
Fabrication								▭	
Checkout Tests									▭
• Coolant Manifolds									
Fabricate Components									
Assemble to Channel									▭
• Channel/Diffuser/Manifolds									
Subsystem Checkout Tests									▭
Pack and Ship									▭

Figure. 76. Channel/Diffuser Fabrication Schedule.

161

SECTION V

COMBUSTOR ASSEMBLY DESIGN AND FABRICATION

A. INTRODUCTION

A combustor assembly consisting of a cooled-wall combustor, injector and igniter was designed. The assembly delivered a supersonic, highly conducting gas at a nominal flow rate of 30 kg/sec to an MHD power channel. The gas was generated by the high pressure combustion of liquid oxygen and jet fuel (JP-4) to which cesium carbonate, a seed material, was added.

The combustor assembly was designed for use with the MHD power channel in power extraction tests. The injector and ignition system were fabricated and tested with a heat sink combustor in a series of development tests. The cooled wall combustor was partially fabricated to demonstrate key fabrication processes; complete fabrication will not be completed until after the development test data has been thoroughly evaluated.

Several design requirements for the combustor assembly are described in Table 17. The reactants (liquid oxygen, JP-4 [jet fuel] and cesium carbonate) were used because of their high performance potential and feed system compactness. In the design process a fourth reactant, SPAN 80, was selected to be mixed with the JP-4 to facilitate mixing of the Cs_2CO_3. The basis for use of this reactant is described in Section VI-B.

The combustor assembly was designed for a range of combustor pressures from 24-36 atm. This led to a variation in flowrate from 25.3 to 36.5 kg/sec. The combustor exit was designed to meet the flow conditions required by the power channel. These conditions were determined in a design trade-off study.

To provide high gas conductivity, a target temperature of 3450K was established. This required very efficient combustion with characteristic velocity efficiencies of 99% or higher. These efficiencies were 3-4% higher than contemporary LO_2/hydrocarbon combustors have achieved. In addition to the efficient reactant combustion, complete ionization of the cesium was necessary. This led to the requirement for the injection of small Cs_2CO_3 particles or droplets.

The design was directed to minimize spatial and temporal variations in gas characteristics at the exit of the combustor. This led to the requirement for the uniform injection of reactants and seed across the gas stream, tailoring the combustor cross section variations, and the avoidance of feed methods which would introduce time variations in reactant flow.

162

TABLE 17. COMBUSTOR ASSEMBLY DESIGN REQUIREMENTS

Reactants $LO_2/JP-4/Cs_2CO_3$

Nominal Operating Conditions

    Combustion Pressure   30 atm

    Mixture Ratio   3.34*

    Flow Rate   30.4 kg/sec

Variations

    Combustor Pressure $\pm$ 20%

    Seed Flow   0, 1-10%**

Exit Conditions

    Mach No.   2.06

    Geometry   19.69 cm x 18.10 cm

Target Performance

    Temperature   3450 K

    Seed Material Cs_2CO_3

    Spatial Distribution Uniformity

Pressure	– 2 to 5% (pk to pk)
Temperature	– 10 to 20 K (pk to pk)
Velocity	– 2 to 5% (pk to pk)
Species	– Uniform

Temporal Fluctuation: Pressure $\leq \pm 5\%$ of nominal combustor pressure

* $\dot{m}(LO_2)/[\dot{m}(JP-4)+\dot{m}(SPAN\ 80)]$

** Based on percent by weight of the total flow

163

B.   COOLED-WALL COMBUSTOR ASSEMBLY

A cooled-wall combustor assembly was designed to provide uniform flow
of hot gas to the power channel while minimizing energy losses because of cooling
and aerodynamics. The combustor interfaced with the reactant injector at one
end and the MHD channel at the other. Provisions for a reactant ignition system
were made near the injector end of the combustor. The combustor was designed
to be cooled to permit steady state operation.

1.   Requirements/Design Approach

The cooled-wall combustor was designed to the requirements and target
performance goals summarized in Table 18. The major factors in determining
combustor size were the nominal flow rate, combustor pressure, and the rec-
tangular cross section required at the entrance to the channel. The combustor
length was largely determined by the target values for the characteristic veloc-
ity efficiency (η_{c*}) and gas uniformity at the nozzle unit. The combustor cooling
and structural design were primarily influenced by the $\div 20\%$ flow rate and cyclic
life goal.

The high conductivity copper alloy liner was used for the inner, hot gas
wall. The cooling passages were machined as grooves into the four sides of this
liner. The coolant grooves were closed with nickel, which also formed part of
the structure that resisted the combustor pressure. This nickel was applied using
an electroforming (ELF) process developed by Rocketdyne. This approach has
been used to fabricate numerous lightweight combustors and was particularly
appropriate for the two-dimensional geometry of the MHD combustor. An aluminum
backup structure was used to support the combustor. To avoid inducing loads into
the MHD channel, the combustor was designed to be structurally mounted at the exit.

The combustor construction was designed to be lightweight. While there was
potential for further weight reduction (e.g., in the manifold and line area), the
basic construction provided a combustor that was relatively lightweight for the
design operating pressure and flow rate.

2.   Performance Analysis

The series of analyses was conducted to define the combustor geometry.
These analyses included nozzle geometry, combustor cross section, combustor
length, and cooling method.

164

TABLE 18. COMBUSTOR DESIGN REQUIREMENTS

Nozzle Geometry (at exit)

Width, cm	18.10 ± 0.01
Height, cm	19.69 ± 0.01
Side Wall Exit Angle, rad	0
Contour Exit Angle, rad	0.095
Corner Radius (at exit), cm	1.27

Nozzle Performance

Nozzle Exit Gas Uniformity

Velocity, %	2 to 5 (pk to pk)
Temperature, K	10 to 20 (pk to pk)
Pressure, %	2 to 5 (pk to pk)
Species	Uniform

Nozzle Exit Boundary Layer Thickness, mm

Displacement Thickness	~1
Energy Thickness	~7
Thermal Thickness	~7

a. Nozzle Geometry

The expansion nozzle was designed to match the rectangular exit geometry and flow uniformity requirements summarized in Table 18. This geometry was selected based on an MHD channel design and performance evaluation.

A new nozzle contour design was developed to meet the uniformity goals. Truncation of conventional nozzle contours to the specified exit angle resulted in flow gradients near the wall which exceeded the uniformity goals. Consequently, a new design procedure was incorporated that generated source flow conditions at the nozzle exit.

The resulting nozzle contour is shown in Figure 77. Several iterations between the inviscid characteristics solution and the boundary layer analysis were required before the inviscid core dimension and the boundary layer displacement thickness totalled 8.48 and 18.1 cm at the nozzle throat and exit, respectively. The inviscid edge flow angle was 0.095 rad, while the wall contour had an exit angle of 0.096 rad because of boundary layer growth. The specified area ratio resulted in an exit Mach number of 2.062 and a nozzle throat-to-exit length of 23.35 cm.

After the contour was established, a separate analysis was performed to obtain the flow field at the nozzle/channel interface. The resulting flow profiles are shown in Figure 78. All properties are nondimensionalized with respect to sonic conditions. The difference in peak values was divided by the average value to give the variations shown in Figure 78. These differences are compared to other nozzle designs in Table 19. The table shows that gas uniformity was substantially improved by the current nozzle design.

b. Combustor Cross Section

A rectangular cross section was selected to match the MHD channel and avoid potential nonuniform flow. Both circular and rectangular cross sections were considered for the combustor. The circular cross section was the more conventional geometry, but required a transition section to match the rectangular cross section of the power channel. The rectangular combustor cross section matched the channel entrance section without transition. A comparison of the various geometries, including three transition methods, is presented in Table 20.

A rectangular cross section chamber was also preferred for this particular application because of the simplification in the machining of the delicate internal coolant slots. Because the exit of the nozzle must be rectangular, a circular-to-rectangular transition, regardless of where it was effected, would entail some risk in the fabrication procedure. This type of internal transitional geometry

166
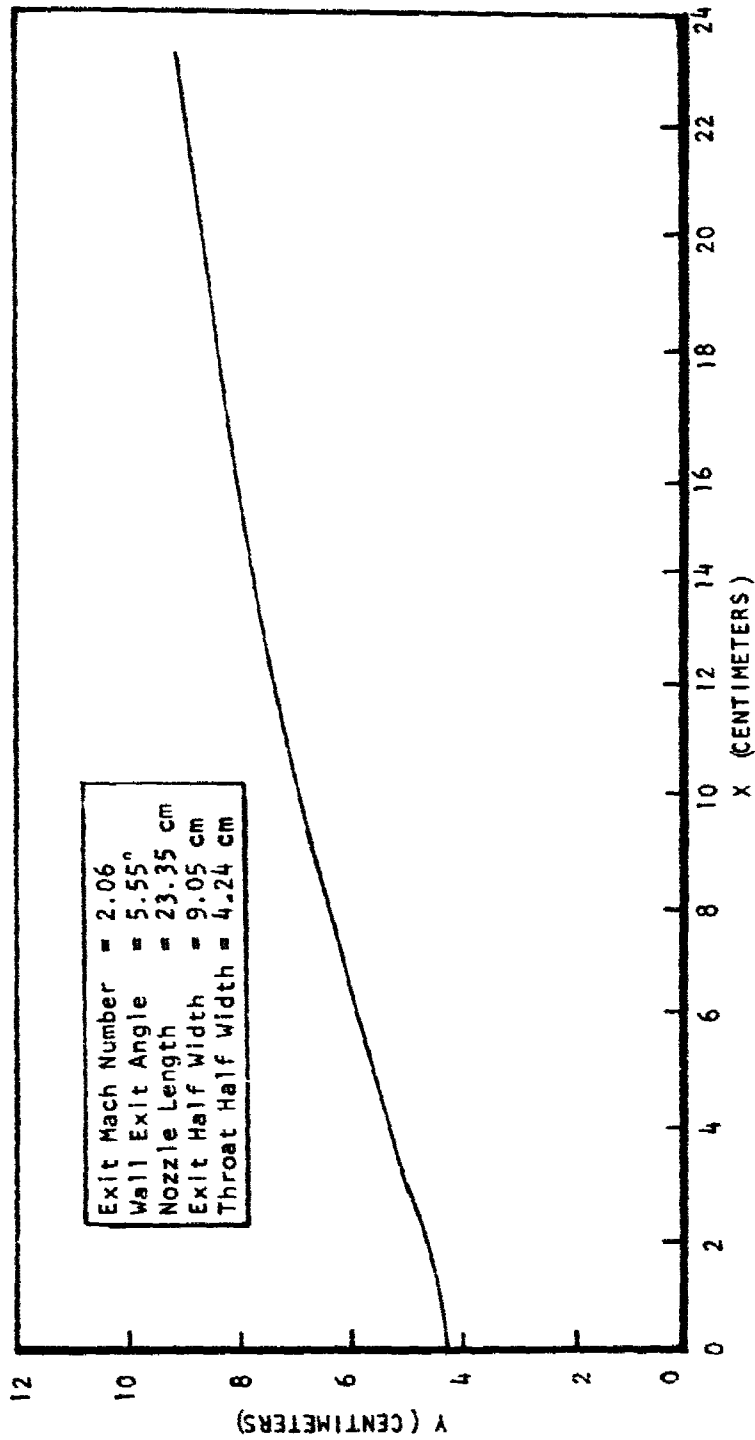
Figure 77. Nozzle Contour.

The legend on the figure reads:

Exit Mach Number   = 2.06
Wall Exit Angle   = 5.55°
Nozzle Length   = 23.35 cm
Exit Half Width   = 9.05 cm
Throat Half Width = 4.24 cm

X axis: X (CENTIMETERS)
Y axis: Y (CENTIMETERS)

167
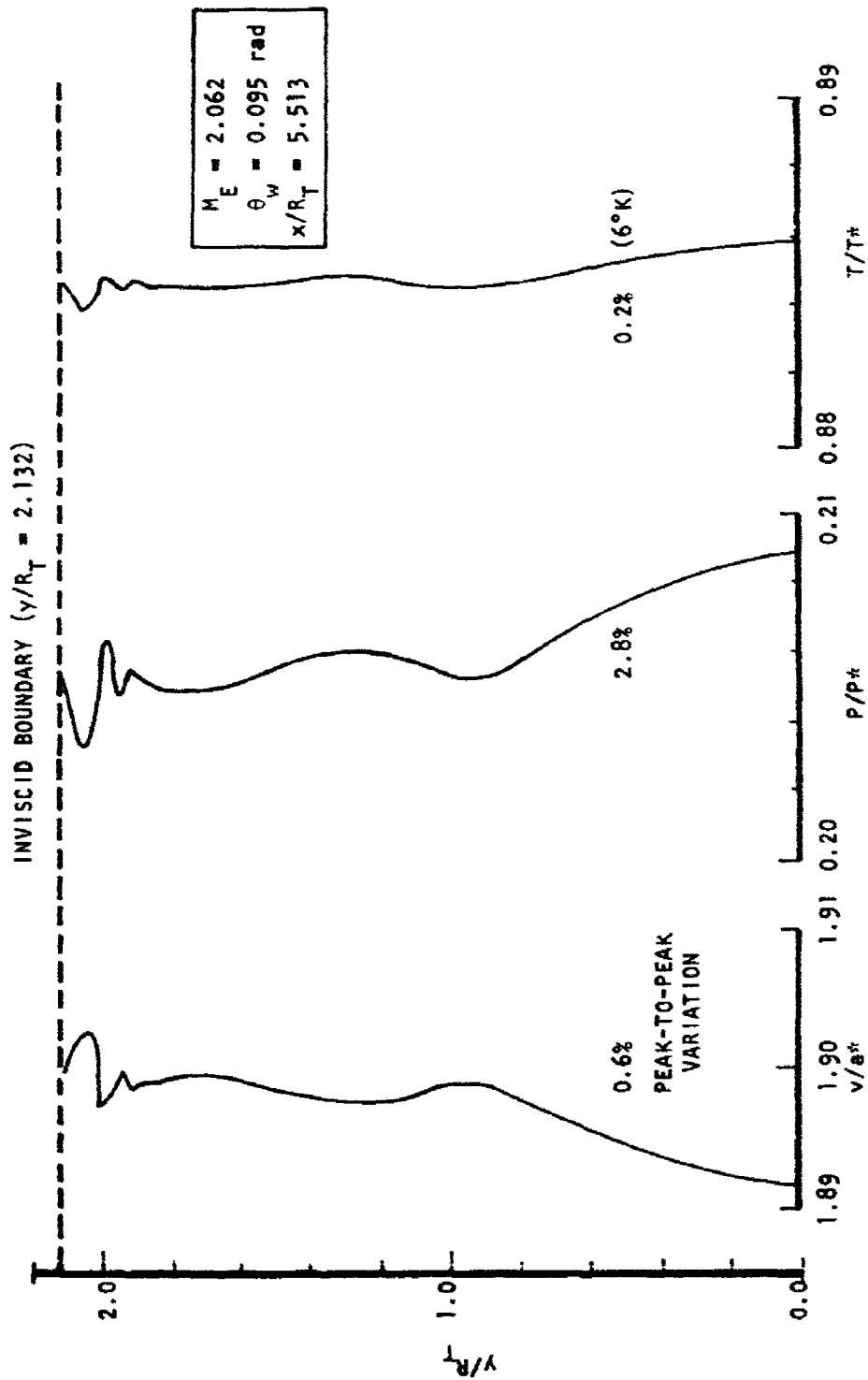
Figure 78. Nozzle Flow Profiles.

TABLE 19. NOZZLE DESIGN IMPROVEMENT

Nozzle Type	Ideal Bell*	MHD Nozzle*[5]	Improved Nozzle
Exit Angle, rad	0.052	0.052	0.052
Mach No.	1.9	2.1	1.9
$\Delta P/P$, %	12	18	1.6 to 1.9
$\Delta T/T$, %	1	1.5	0.1
$\Delta V/A$, %	3.5	3.6	0.4
Nozzle Length, L/R_T	4.5	6.8	4.5

* Truncated at 0.052 rad exit angle.

[5] O. K. Sonju, J. Teno, J. W. Lothrop, and S. W. Petty, "Experimental Research on a 400 kW High Power Density MHD Generator," AFAPL-TR-71-5, May 1971.

TABLE 20. COMPARISON OF VARIOUS COMBUSTOR GEOMETRIES

Geometry	Heat Transfer	Exit Flow Conditions	Fabrication
No Transition (rectangular)	• Maximum Combustor Surface Area • Design Data Available	• Amenable to Analysis	• Combustors fabricated • Simple cooling channel fabrication
Supersonic Transition	• Minimum Chamber Surface Area • Potential Shock Formation in Nozzle	• Difficult to Analyze	• Combustion chamber easy • Nozzle difficult because of critical 3-D tolerance • 3-D cooling channel machining required
Subsonic Transition	• Minimum Surface Area for Net Heat Loss • Chamber Analysis Well Understood	• Difficult to Analyze	• Cylindrical portion easy • Coolant passage tolerance critical
Sonic Transition	• Excess Heat Transfer Area • Cooling of Throat Region Difficult	• Difficult to Analyze	• Hot gas seal difficult • Milling of cooling channel moderately difficult

also would lead to nonuniform flow and increase the complexities of precise flow analysis. Rectangular combustors have been fabricated on a number of occasions and did not represent any unusual fabrication difficulty.

c. Combustor Geometry

A contraction ratio of two and a combustor length of 68.6 cm were selected to provide confidence that high combustor performance would be achieved. Combustor performance was measured by the characteristic exhaust velocity, c^*, a common measure of the performance of rocket combustors:

$$c^* = \frac{P_{ns} A_t}{\dot{m}}$$

where

A_t = aerodynamic throat area

P_{ns} = nozzle stagnation pressure

$\dot{m}$ = total mass flow rate

The c^* efficiency, η_{c^*}, is the ratio of the measured c^* (derived from combustion pressure and reactant flow rate measurements) to the theoretical value. To achieve the delivered gas temperature goal of 3450 K, the target value of c^* efficiency for the current program was greater than 99%. This was 2 to 3% higher than has been demonstrated with previous LO_2/RP-1 combustors. To provide a combustor with the potential for the high c^* efficiency, the combustor geometry was based on both a theoretical analysis and a review of data from LO_2/RP-1 rocket engine tests.

A contraction ratio (injector area/throat area) of two was selected to assist in achieving high performance. A comparison of the performance of two combustors of equal characteristic length, but different contraction ratio, indicated a substantial improvement in c^* efficiency in going from a contraction ratio of five to a value of two.[20]

A performance analysis was conducted using an injector atomization model for impinging injector elements in combination with a Distributed Energy Release fuel droplet heating and vaporization model.[21] Results from the model are shown in Figure 79. These results indicated that 99 to 100% c^* efficiency, based on vaporization rates, can be obtained with combustor lengths in the 0.3- to 0.5-meter-range with an injector producing a JP-4 mass-mean droplet diameter (D_{30}) of 100 μm or less.

[20]"Chamber Technology for Space Storable Propellants," 4th Interim Report No. R7985, Rocketdyne, Division of Rockwell International, September 1969.

[21]M. D. Schuman and D. G. Behosse, "Standardization Distributed Energy Release (SDER) Computer Program", 13th JANNAF Combustion Meeting, CPIA Publication 281, Vol. III Dec. 1976, pp 79-91 (Also, AFRPL-TR-77-1, AFRPL).
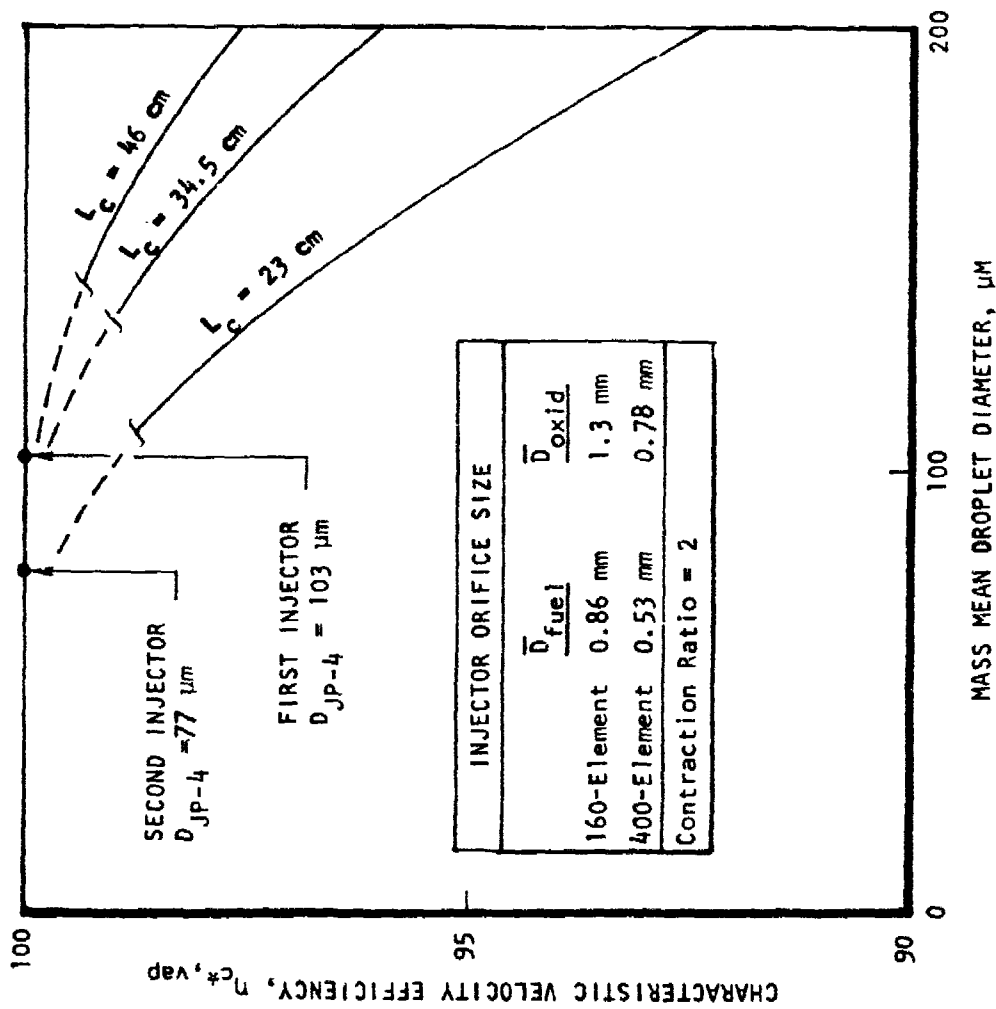
Figure 79. Injector Atomization Model Results.

172

As described in Section V-C, two inj   rs were designed to produce D_{30} values of 103 and 77 μm, respectively. The lower droplet size was limited by injector fabrication considerations which restricted the fuel orifices to a diameter greater than 0.5 mm.

Combustor performance attained in previous testing of this type of injector was reviewed for LO_2/RP-1 reactants and several other reactant types. LO_2/RP-1 test experience is summarized in Figure 80 where the fuel injector orifice diameter and characteristic length, L*, of the combustor are presented. The characteristic length is defined as:

$$L^* = \frac{\text{combustor volume}}{\text{throat area}}$$

This parameter was a measure of the hot gas stay time in the combustor. Combustor performance of these LO_2/RP-1 combustors is indicated in parentheses following the identification. As the figure shows, the recommended injector design has smaller fuel orifice diameters and, therefore, smaller fuel dropsize than the previous LO_2/RP injectors. In addition, the mixture ratio bias near the walls frequently used on the previous LO_2/RP injectors has been eliminated. Both of these factors led to improved combustion performance. However, to achieve the characteristic length values comparable to these previous combustors, combustor lengths of 60 cm or greater must be used.

The results of tests of a F_2-O_2/hydrocarbon combustor using a self-impinging doublet injector element are illustrated in Figure 81. Although not directly applicable to the LO_2/JP-4 combustor, these test results illustrated the performance improvement that can be achieved with increased L*.

In summary, the theoretical analyses indicated that the target performance could be attained in a relatively short combustor. However, the target performance level had not been demonstrated and existing data indicated that improved performance can be achieved with longer combustors. Because of this, a combustor length of 68.6 cm was selected.

d. Combustor Cooling Method Selection

Water cooling was selected for the combustor. The combustor was initially analyzed for regenerative cooling with the JP-4 fuel. The fuel regenerative cooling approach was attractive since no additional system coolant was necessary and the energy transferred to the fuel returned to the combustion process when the fuel was injected. Water cooling of the combustor was also considered for the current combustor design because of uncertainties in several areas.
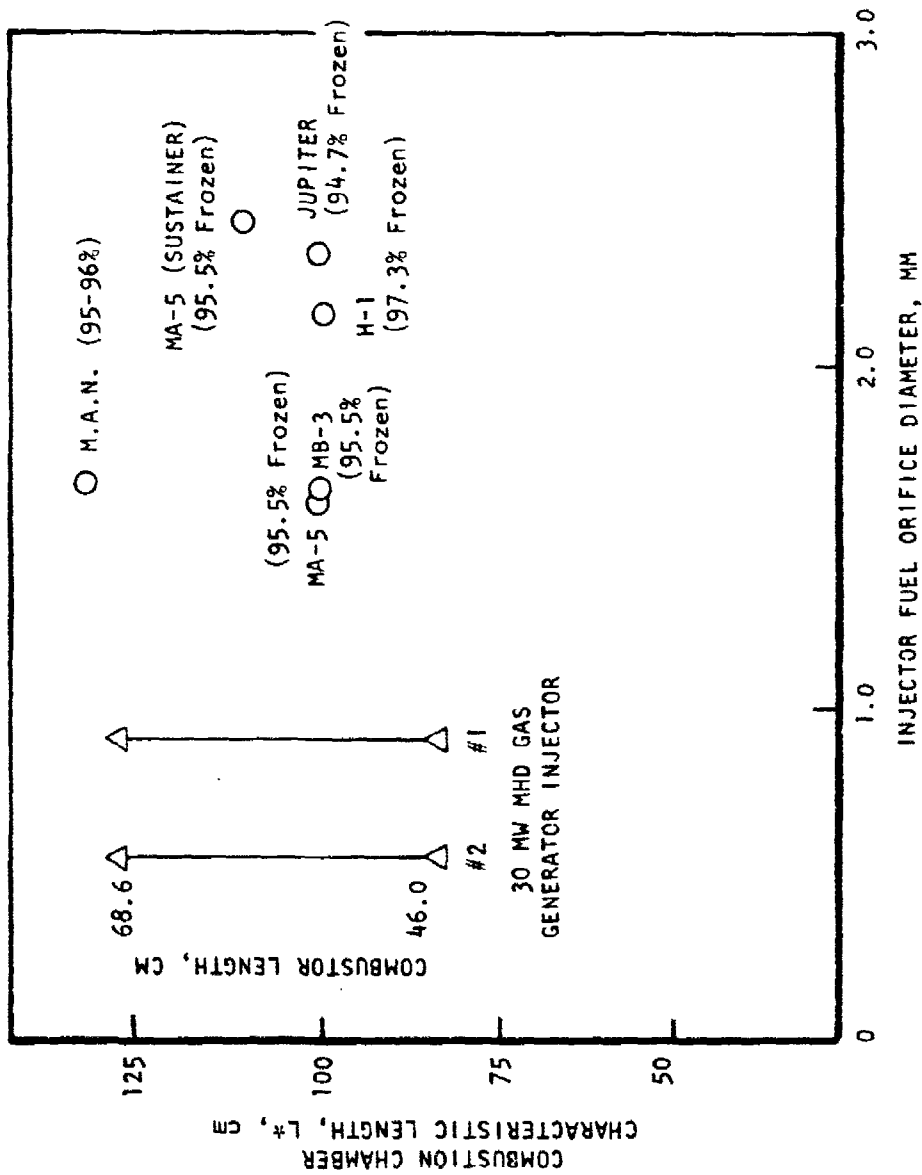
Figure 80.   LO$_2$/RP-1 Combustor Performance.
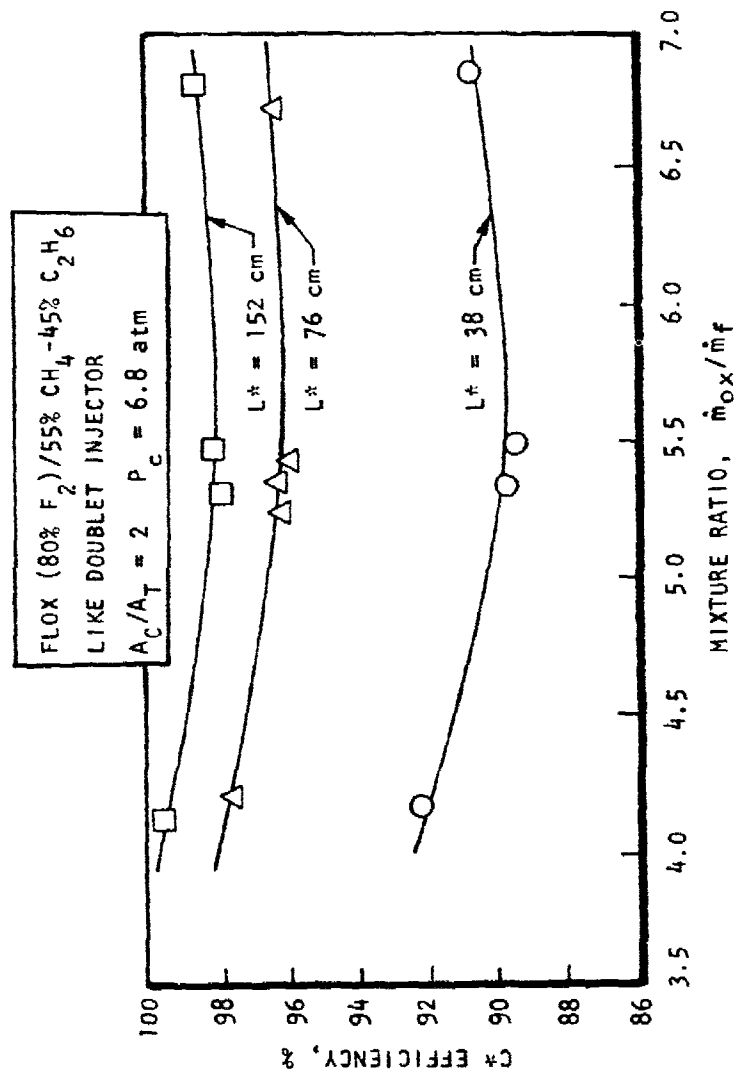
Figure 81. Characteristic Length Effect on Efficiency; Reactants (80% F_2-20% O_2/55% CH_4 -45% C_2H_6).

175

Fuel regenerative cooling at the current operating point (stoichiometric mixture ratio) was more difficult than typical rocket combustors which operated at a fuel-rich mixture ratio of 2.4:1 or less. At the stoichiometric mixture ratio of 3.4:1, the heat flux was greater because of the high combustion temperature, and in addition, there was less fuel available as coolant because of the high mixture ratio.

Another consideration during the design was the prediction of the expected heat flux. In typical LO_2/RP-1 rocket combustors, which operate fuel rich, a surface carbon layer is obtained which acts as an insulator and reduces the heat flux. There has been no applicable testing conducted with LO_2/JP-4 combustors operating at stoichiometric conditions where, at high combustion efficiency, theoretically all of the carbon may be consumed and no insulating carbon layer would be formed. Although some indication of seed material deposition on the combustor walls has been observed in testing with potassium seed, no experimental information on cesium seed deposition was uncovered.

The initial combustor heat transfer analysis was based on an empirically determined gas-side film coefficient corrected to the combustion pressure and gas properties of the current LO_2/JP-4 combustor. Because of its importance, the cooling analysis was also conducted for a range of carbon layer deposition values. Evaluation of the effect of wall carbon deposition was based on a carbon resistance correlation empirically determined in extensive LO_2/RP-1 testing.

The fuel heat transfer coefficient was based on experimental work conducted with RP-1 at Rocketdyne. (No forced convection data were available for JP-4 in the 35 to 55 atm pressure range.) The primary restriction on regenerative cooling was the bulk temperature of the JP-4. An inlet temperature of 294 K was assumed. Based on RP-1 data, a maximum allowable JP-4 temperature of 477 K was selected. At higher temperatures the JP-4 is prone to coking on the coolant channel wall. This coking would greatly reduce the effectiveness of JP-4 as a coolant and subsequently lead to excessive combustor wall temperature.

The thermal analyses were conducted at the nominal operating point and for a range of combustor lengths. The final bulk temperature of the JP-4 coolant is presented in Figure 82 as a function of combustor length and the extent of the carbon layer. With no carbon layer the JP-4 reached the maximum bulk temperature of 477 K at a combustor length of about 0.1 m. For a 68.6 cm length combustor, the bulk temperature was 728 K, much too high for safe operation. The presence of even a thin carbon layer dramatically reduced the fuel bulk temperature rise and would have allowed regenerative cooling of longer combustors.
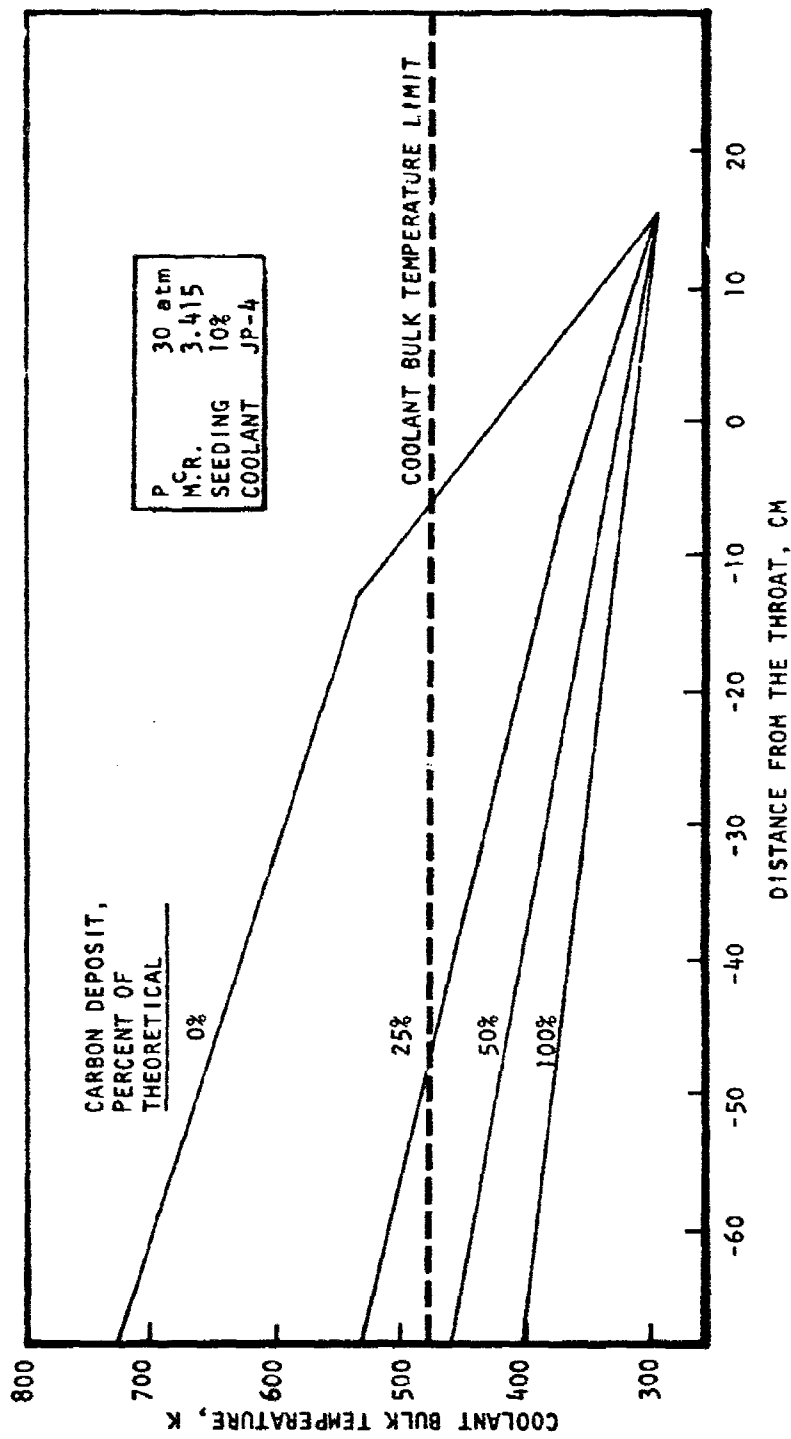
Figure 82. JP-4 Bulk Temperature Change With Length.

177

A plot of the allowable combustor length for regenerative cooling as a function of carbon layer thickness is presented in Figure 83. Since the current combustor cooling circuit has not been completely optimized, some potential for extending the range of regenerative cooling beyond the current analyses is illustrated. As shown in Figure 83, a carbon layer some 50% of the thickness of low mixture ratio LO_2/RP carbon layers allows regenerative cooling combustor lengths of 60 to 80 cm. With no carbon layer, combustor lengths on the order of 20 to 30 cm could potentially be regeneratively cooled.

The combustor cooling decision was, therefore, essentially a decision on the extent of the carbon or seed material layer deposited on the wall. In the absence of data and for operation at the stoichiometric mixture, the carbon coating was not expected to be sufficient to allow regenerative cooling of a 68.6 cm long combustor. A regenerative cooling method would, therefore, have been a higher risk approach. Cooling with water was evaluated as a reasonable approach for the entire operating range, and consequently, this method was selected.

The presence of a combination of three factors would allow regenerative cooling: (1) operation at lower than stoichiometric mixture ratio (near maximum electron density) would increase the likelihood of a carbon layer, (2) seed material deposition, and (3) a shorter combustor length. Each of these require experimental confirmation.

3.   Design

The combustor assembly (Figure 84) consisted of the liner, electroformed nickel closure, inlet and exit flange/manifolds, and the backup structure. The combustor design and supporting analyses are summarized in the following sections.

a. Description

Liner. The combustor liner, shown in Figure 85, was designed to provide a high combustor performance, a relatively uniform gas flow field, and coolant passages to maintain an acceptable hot gas wall temperature.

The combustor internal contour began with a 19.69 cm by 15.54 cm rectangle with 0.64 cm radii in the corners at the injector end. These radii became 1.27 cm at the throat and combustor exit. The throat was a 19.68 cm by 8.48 cm rectangle, and the exit was a 19.68 cm by 18.10 cm rectangle. The combustor was 91.95 cm long and 68.6 cm from the injector end to the throat.
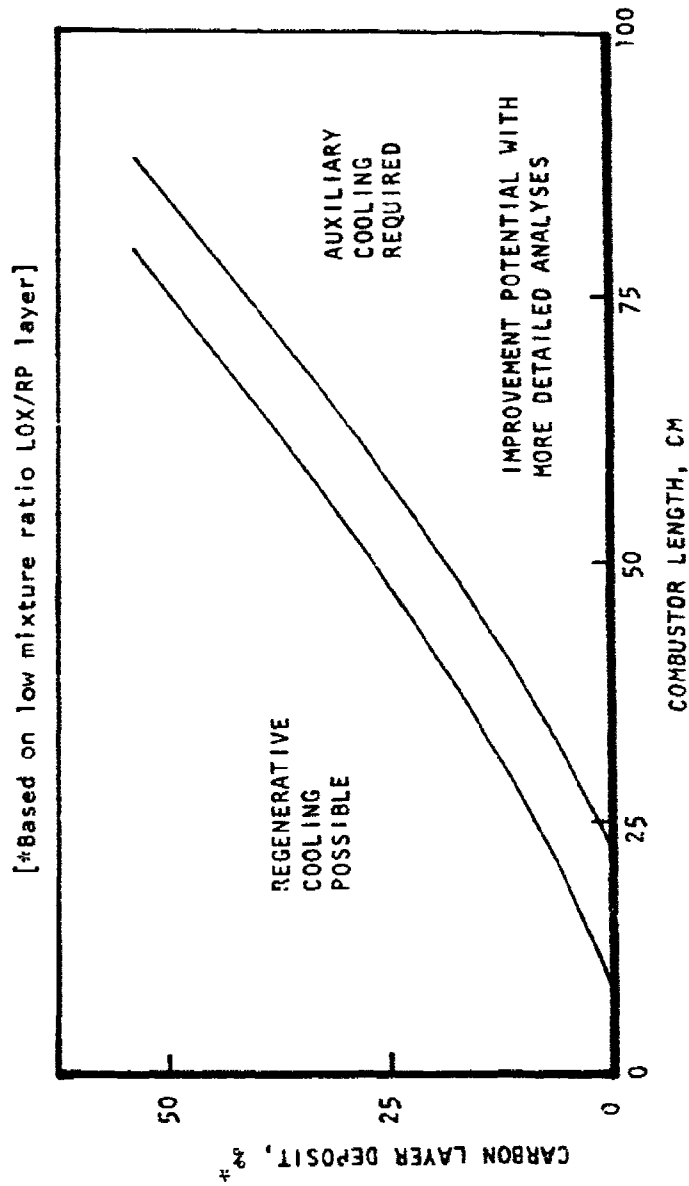
Figure 83. Carbon Deposit Influence on Combustor Length.

179
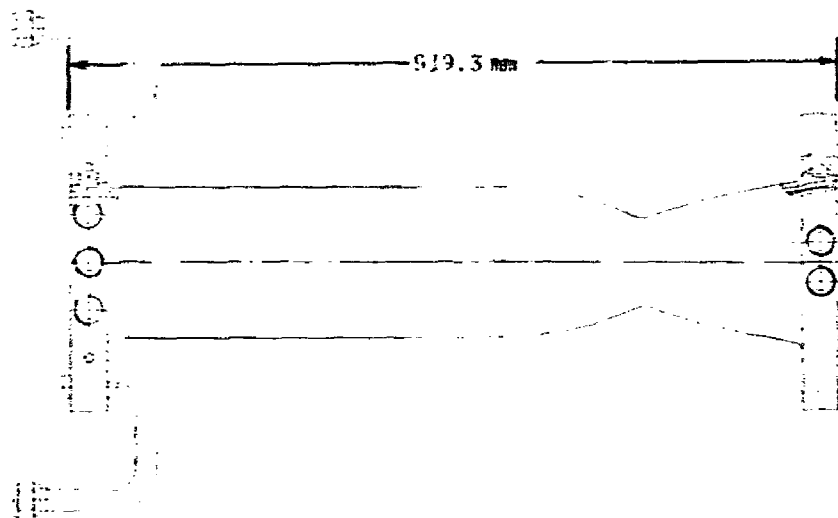
LINER WITH MANIFOLDS ATTACHED
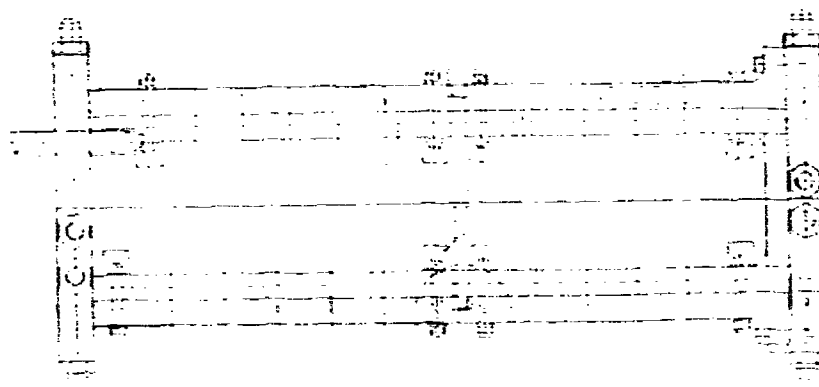
COMBUSTOR ASSEMBLY, SIDE VIEW
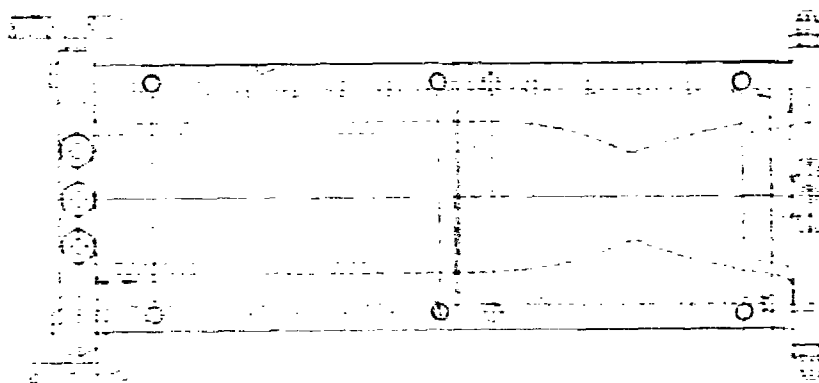
COMBUSTOR ASSEMBLY, TOP VIEW

Figure 84. Combustor Assembly.

NICKEL CLOSURE

AMZIRC

84.8 mm

155.4 mm

EXIT MANIFOLD PASSAGES

(A) CONTOUR WALL

COOLANT PASSAGE

IGNITER PORT

196.9 mm
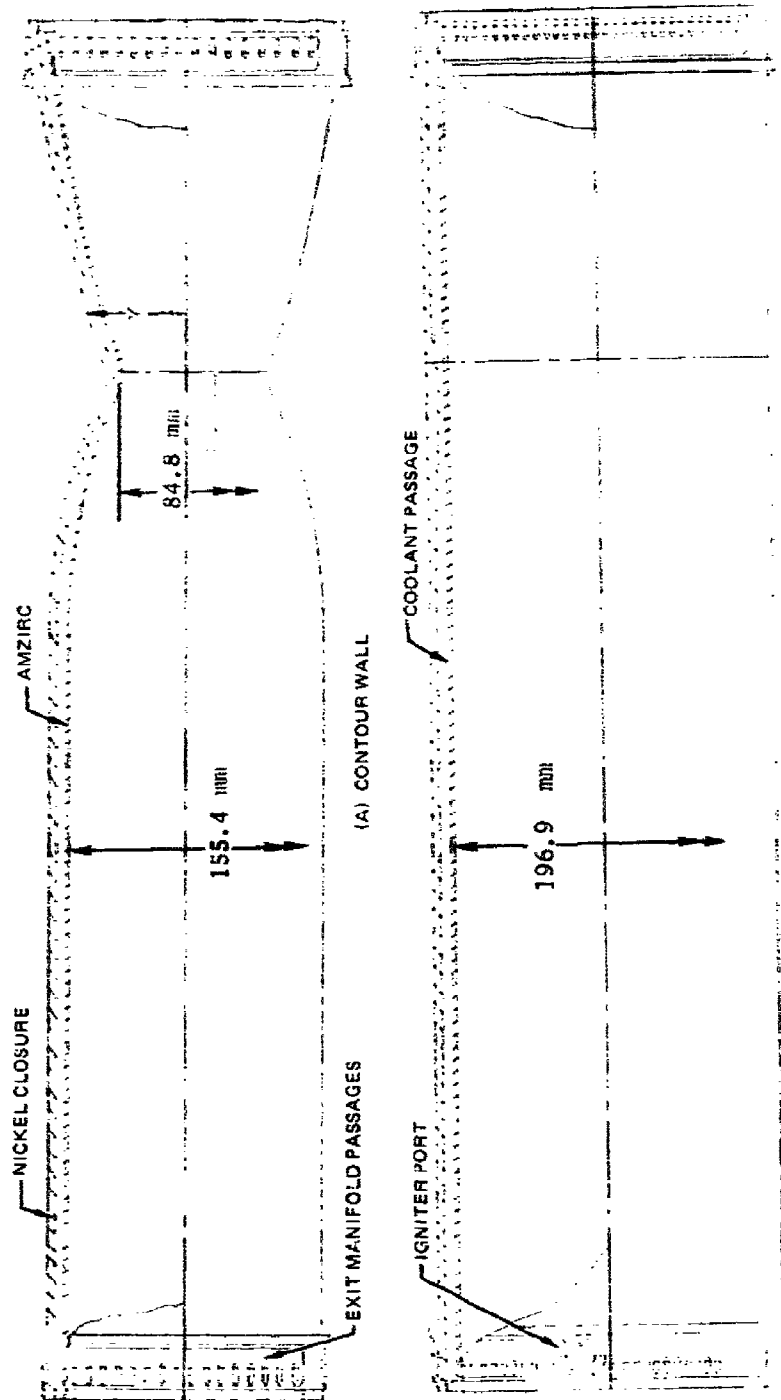
(B) FLAT WALL

Figure 85. Combustor Liner

The sides bounding the 19.68 cm dimension were flat, while the other sides were contoured. The subsonic and throat sections of the contoured wall consisted of two constant radius sections which met where each has the same tangent. A wall radius of 4.24 cm, which was equal to the throat half-height, was used at the throat. The subsonic section joining the combustion chamber straight section to the throat had a 42.20 cm radius. This section started from a tangent point 17.8 cm upstream from the throat and joined the throat radius at a point where each had the same tangent.

The exterior of the liner was slotted with a series of coolant passages. There were 16 slots on the flat wall and 30 slots on the contoured wall. In the region of the ignitors, the coolant passages terminate in an annulus around the ignitor port and subsequently flow in the manifold. A variation in slot depth occurred at the throat region where the velocity was increased to compensate for the higher heat input.

The liner was made of Amzirc, a copper alloy. The coolant passages were closed with an electroformed nickel layer. Electrodeposited nickel coolant passage enclosure design has been successfully demonstrated on numerous combustor configurations. The deposited nickel thickness of 0.51 cm nominal overall, illustrated in Figure 84, was determined by a tradeoff study considering fabrication schedule, backup structure, strength, and stress requirements.

Manifolds. The outlet and inlet manifolds, shown in Figure 86, were designed to withstand the coolant flow rates and pressure requirements. The inlet manifold maximum design pressure of 109 atm and the outlet maximum design pressure of 75 atm dictated the basic geometry. The high pressure requirements were initiated by the high coolant passage pressure drop and the requirement to have the pressure in the coolant passage higher than chamber pressure at all operating conditions. The manifold velocities were chosen to be 1/2 the coolant passage exit - velocity and all manifold cross velocities were designed to be 9 m/sec. The resultant inlet velocities were 25.5 m/sec into the flat wall section and 21.6 m/sec into the contoured wall section.

The manifolds were electronbeam (EB) welded to the electrodeposited nickel closure. The manifold/flange envelope was primarily dictated by the weld width and depth required and the injector and power channel bolt patterns. The coolant feeder and discharge lines also were dictated by the respective bolt patterns. The manifolds were made of Inconel 625, a material chosen for its strength and excellent welding characteristics with the nickel closure.

Structure. The aluminum backup structure with the nickel closeout was selected based on fabrication schedule and weight. By retaining only a 0.51 cm nickel closeout on the liner to reduce fabrication time a substantial backup structure was required. The structure (6061 aluminum) was 3.8 cm thick on the contoured wall and 3.19 cm thick on the flat wall. The design incorporates an expansion gap to permit axial thermal growth while restraining perpendicular movement.

IGNITER PORT

(A) INJECTOR-END MANIFOLD

355.6 mm

COOLANT INLETS
(2 ON EACH SIDE)

568.3mm

(B) NOZZLE EXIT MANIFOLD
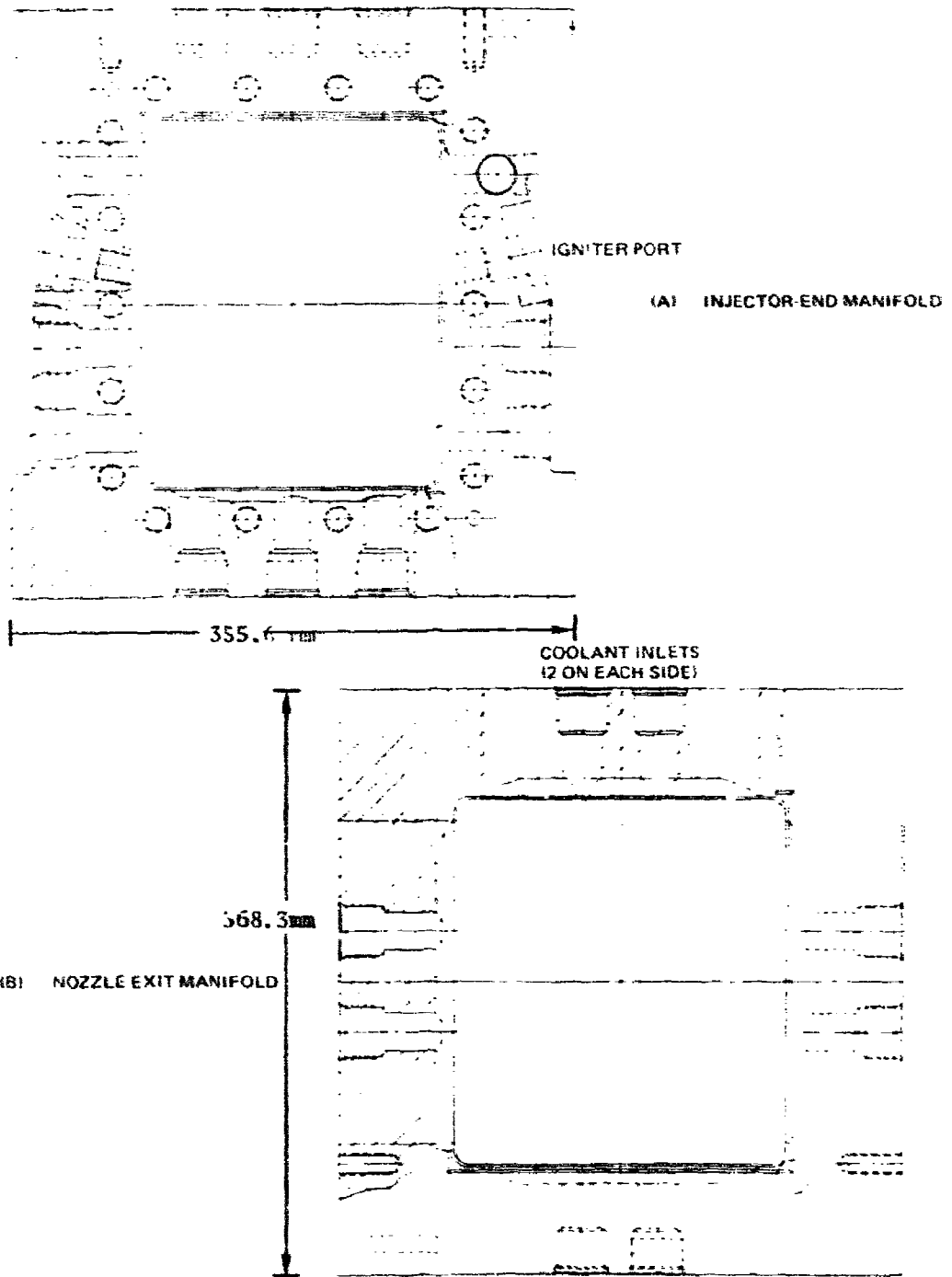
Figure 86. Combustor Inlet and Outlet Manifolds

Instrumentation. Because of the cooling passages, instrumentation mounted on the combustor wall was very limited. In the design provisions were made for a pressure measurement near the injector and at the nozzle exit to measure combustor gas pressure. No additional instrumentation was directly associated with the combustor. The cooling flow measurements were associated with other components.

b. Combustor Wall Thermal Analyses

The combustor cooling passage geometry was designed to the requirements listed in Table 21. The following ground rules were established to determine these requirements: (1) deionized water coolant; (2) 300 K water inlet temperature; (3) water bulk temperature rise less than 67 K; (4) uppass cooling circuit; (5) 44 atm water exit pressure; (6) passage geometry limits; and (7) a design goal of a maximum liner wall temperature of 625 K.

The gas side heat transfer coefficient was selected based on a boundary layer heat transfer analysis. Additional heat input from the gas radiation was assumed. This analysis is presented as Appendix G. The design gas-side film coefficient is presented in Figure 87. Deionized water was used as the coolant to avoid buildup of scale in the copper liner. The coolant side heat transfer coefficient and the properties of water were taken from Reference 22.

The water inlet temperature was selected as the highest value anticipated for the open-loop water cooling system used in development testing. Following the design, additional information was received which indicated that the closed-loop cooling system used at AEDC could lead to inlet temperatures as high as 325 K. The impact of this was found to be small and is discussed in a later section.

The water exit bulk temperature was selected to be below 373 K with the 300 K inlet temperature. This avoided flashing of the water to vapor on being discharged to the atmosphere. The result of this design limit was a water bulk temperature rise of less than 67 K.

An uppass circuit, with the water inlet at the exit of the nozzle, was chosen so that the coldest water will cool the throat region where the heat fluxes are highest. A coolant outlet pressure at the injector end of 44 atm was chosen so that, if a possible crack should appear in the hot gas wall, the water will flow into the combustor and cool the cracked area. This damage could then be repaired posttest. The passage geometry (aspect ratio, band width, axial variation, curvature) was selected to avoid fabrication difficulty based on previous experiences in machining and electroforming.

---

[22]Hines, W. S.: "Turbulent Force Convection Heat Transfer to Liquids at Very High Heat Fluxes and Flow Rates" RR61-14, Rocketdyne, A Division of Rockwell International, 30 November 1961.

TABLE 21. FINAL DESIGN PARAMETERS FOR THE WATER-COOLED MHD COMBUSTOR

Propellants - LO_2/JP-4   Mixture Ratio - 3.415

$\eta_{c}*$ - 99.3%

Parameters	P_c = 30 atm		P_c = 36 atm	
	Contoured Wall	Flat Wall	Contoured Wall	Flat Wall
Maximum H_g*, W/cm^2 K	0.7768	0.786	0.879	0.879
Q, kW	2407	1737	2755	1987
Maximum Q/A*, W/cm^2	2230	2230	2540	2540
Maximum h_c, W/cm^2 K	20.50	20.78	24.3	24.7
Wall Thickness, cm	0.254	0.254	0.254	0.254
Material	Amzirc	Amzirc	Amzirc	Amzirc
Closeout Thickness, cm	0.254	0.254	0.254	0.254
Closeout Material	Nickel	Nickel	Nickel	Nickel
No. of Channels	30	16	30	16
Minimum Channel Height, cm	0.231	0.40	0.231	0.40
Maximum Channel Height, cm	0.51]	0.76	0.51	0.76
Channel Width, cm	0.325	0.259	0.325	0.259
Minimum Land Width, cm	0.33	0.27	0.33	0.27
Maximum Land Width, cm	0.33	0.869	0.33	0.869
Coolant	Water	Water	Water	Water
Coolant Flow Rate, kg/sec	9.1	6.8	10.9	8.2
Maximum Coolant Velocity, m/sec	40.5	41.1	48.5	49.4
Maximum T_{WG}, K	603	586	624	609
Coolant Inlet Temperature, K	300	300	300	300
Coolant ΔP, atm	14.4	20.1	20.2	30.1
Coolant Bulk Temperature Rise, K	63.3	60.5	60	57.8
Coolant Exit Pressure, atm	44	44	44	44

*Includes effect of radiation.

185
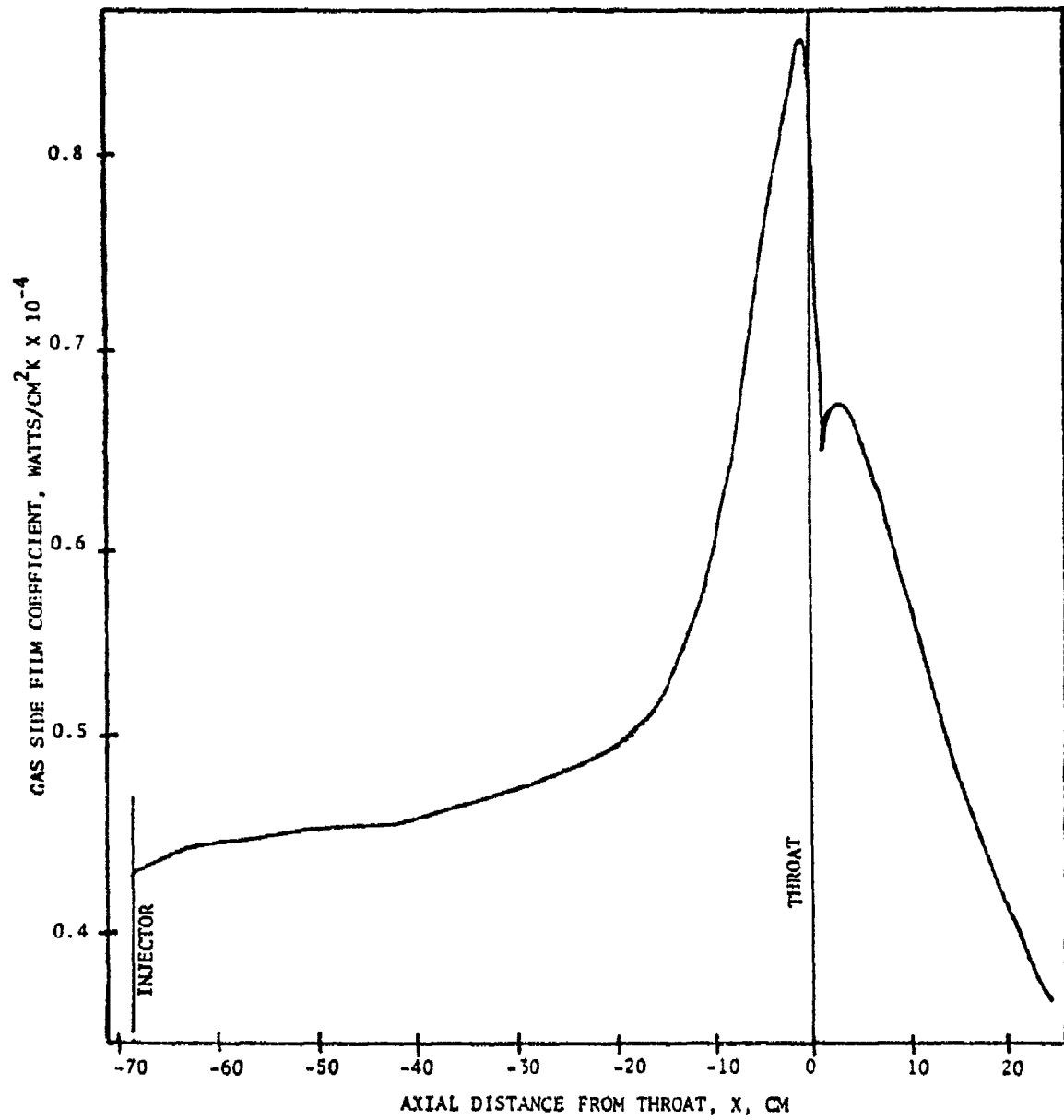
Figure 87. Gas Side Film Coefficient,
Contoured Wall, Pc = 30 atm.

186

A maximum liner wall temperature of 625 K was selected to provide 375 thermal cycles at the +20% combustion pressure condition. The design value of 375 full thermal cycles was established as a goal to guide the thermal design of the combustor liner. A full thermal cycle was defined as the variation from ambient temperature (294 K) to maximum operating temperature. The design cyclic life of 375 cycles was based on a full thermal cycle at the maximum heat load condition (+20%). There was a safety factor of 4 included in this value. Although the combustor will probably reach steady-state maximum temperatures in a run time of 3 seconds, the combustor wall temperature may not return to the ambient temperature between firings. Since the return to ambient conditions is very dependent on the duty cycle and the response time of the cooling circuit, short duration tests probably would not contribute "full thermal cycles."

Contoured Wall, Nominal Condition Design (30 atm). A parametric analysis of the cooling passage geometry was conducted based on a maximum one-dimensional wall temperature estimated to provide the desired cyclic life. The land thickness was not optimized in these analyses, but rather, a land width was chosen for the throat region to facilitate the electrochemical deposition process of the nickel closeout wall and to obtain a sound design so that the closeout wall can stand the pressure and thermal stresses without being detached from the lands. From the analysis a cooling passage geometry was selected. Design parameters are summarized in Table 21. The final design of the contoured wall was selected to have 30 channels of 0.325 cm width. The land width was established constant and equal to 0.33 cm. The channel heights calculated in the parametric design varied irregularly from station to station. These channel heights were plotted versus axial distance from the throat and a smooth curve was drawn through the points to facilitate the machining of the channels. The variation of the channel height as a function of axial distance for both the contoured and side-wall final designs is shown in Figure 88. The smoothed channel heights of Figure 88 were input to the analysis to determine the wall temperatures. These temperatures are presented in Figure 89. The minimum and maximum channel heights were 0.231 and 0.51 cm, respectively. The maximum two-dimensional gas-side wall temperature was 603 K.

The maximum total convective and radiative heat flux occurring near the throat was 2230 w/cm^2. A water velocity of 40.5 m/sec was required to maintain the gas-side wall temperature at 603 K. A water flow rate of 9.1 kg/sec was necessary for the contoured wall to maintain the exit bulk water temperature below 373 K. The coolant bulk temperature rise and pressure drop (excluding entrance and exit losses) were 63.3 K and 14.4 atm, respectively. The total calculated heat loss by the hot gas to the water was 8290 kW.
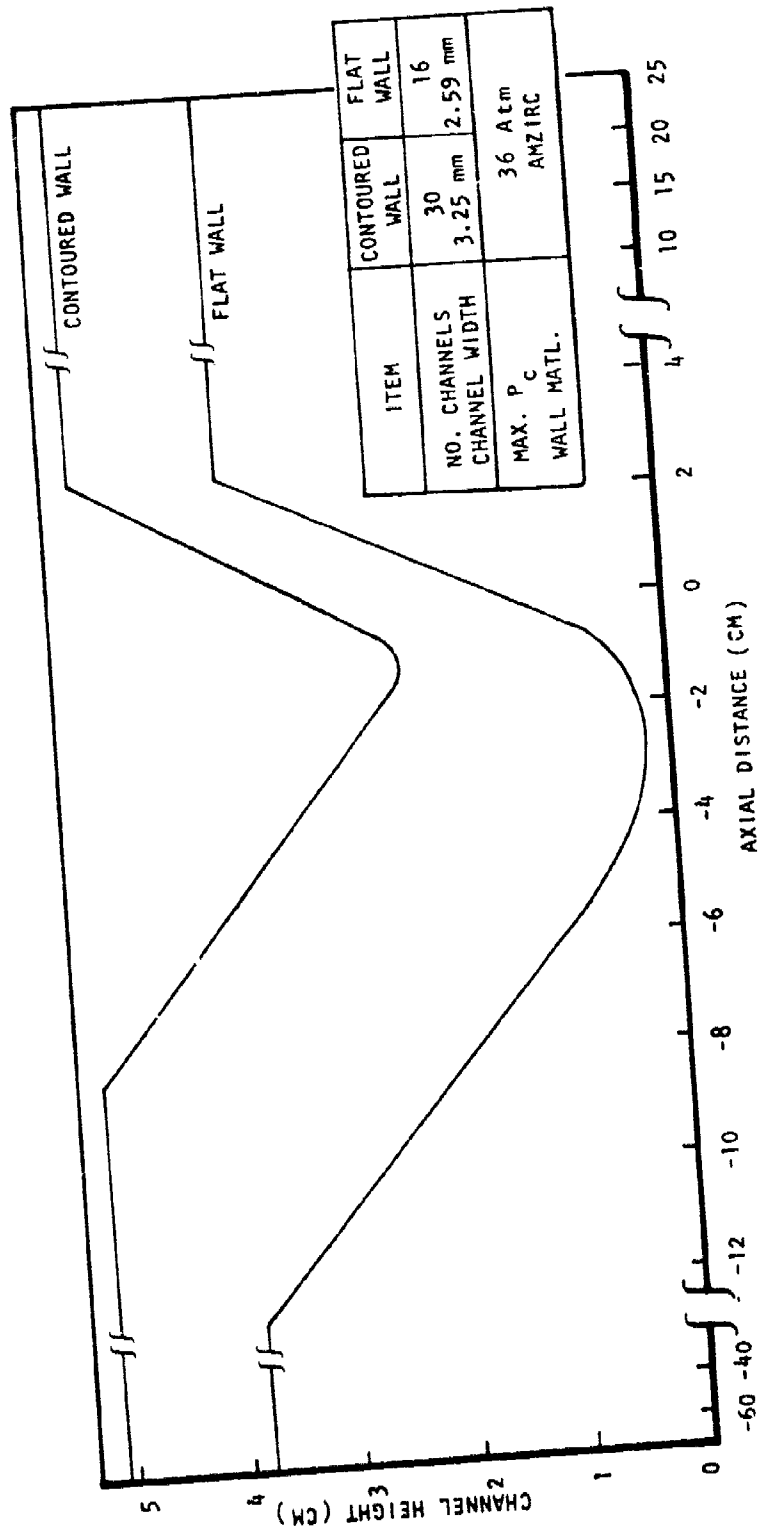
Figure 88. Cooling Channel Channel Height.

ITEM	CONTOURED WALL	FLAT WALL
NO. CHANNELS	30	16
CHANNEL WIDTH	3.25 mm	2.59 mm
MAX. P_c	36 Atm	
WALL MATL.	AMZIRC	
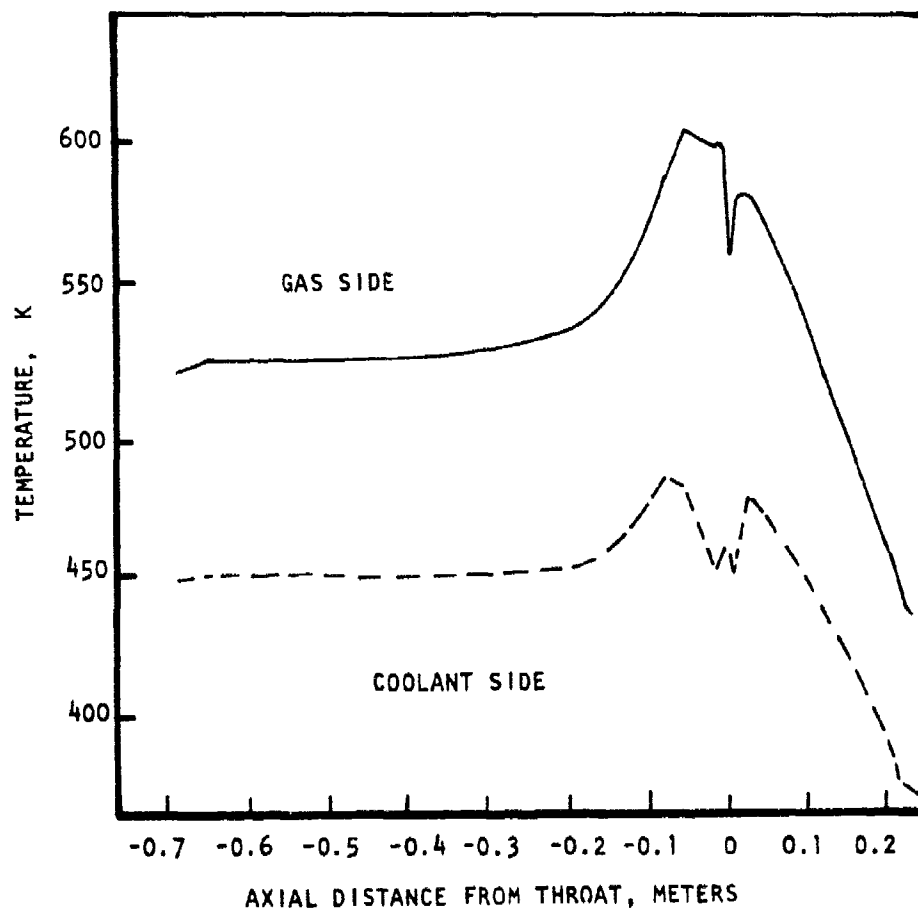
Figure 89.   Contour Channel Wall Temperatures.

Flat Wall - Nominal Condition Results.   The design and analysis approach
for the flat wall was similar to that of the contoured wall. A water flow rate of
6. 8 kg/sec per wall was selected to maintain the exit bulk temperature of water
below 373 K.   The gas-side heat transfer coefficients were assumed the same as
for the contoured walls.

A land width at the throat was selected that was wide enough for the electro-
chemical deposition of the closeout wall. This resulted in 16 passages, each having
a 0.259 cm width.   The number and width of the passages were kept constant for
the entire length of the flat walls. The channel height plotted against axial distance
from the throat is shown in Figure 88.   The minimum channel height at the throat
was 0.399 cm, and the maximum channel height at the exit and injector end was
0.76 cm.

Under these conditions, the maximum gas-side wall temperature was cal-
culated at 586 K corresponding to a heat flux of 2230 w/cm^2. The coolant pressure
drop, excluding the entrance and the exit losses, and the water bulk temperature
rise were 20.1 atm and 60.6 K, respectively.

Off-Design Condition.   The design of the contoured wall was analyzed at
36 atm to verify that the gas-side wall temperature did not cause a reduction in
cyclic life. For this purpose the gas-side heat transfer coefficients were increased
by 5.7%.   A water flow rate of 10.9 kg/sec per contoured wall satisfied the re-
quirement of exit bulk temperature. The maximum heat flux near the throat was
2540 W/cm^2, and the maximum gas-side wall temperature occurs 5 cm upstream
of the throat.   The maximum wall temperature is 624 K as shown in the two-dimensional
plot of Figure 90. The water pressure drop and bulk temperature rise were 20.1 atm
and 60 K, respectively.
A thermal analysis of the flat walls was also conducted and indicated that
the maximum gas-side wall temperature was 609 K, which was below that of the
contoured wall.   The throat heat flux was 2540 W/cm^2. Approximately 8 kg/sec
of water were required for the cooling of each flat wall. The water pressure drop
and bulk temperature rise were 30 atm and 57.8 K, respectively.

Increased Water Inlet Temperature.   The cooled wall combustor was designed
based on a water inlet temperature of 300 K. This value was selected based on the
open-cycle cooling system to be used in development tests. At AEDC a closed-
circuit deionized water cooling system will be used. The operating characteristics
supplied by AEDC indicated that the heat rejection capability of this system was
insufficient to maintain an inlet temperature of 300 K. Although the system would
start at an inlet temperature in the 300 K region, the steady-state inlet temperature
could be as high as 325 K.

HOT GAS SIDE

TEMPERATURE (K)

623	623	623	623	624	624
569	569	569	569	570	571
515	515	514	514	517	518
462	462	460	456	466	469
			383	439	444
			400	418	423
			384	401	406
			373	387	392
			364	377	381
			358	369	373
			353	364	368

COOLANT CHANNEL

NICKEL CLOSEOUT

328	329		348	361	365
339	340	334	346	351	353
342	347	343	346	349	351
		344			

C Land
C HOT GAS SIDE

P_c 36 atm
REACTANT LO_2/JP-4
M.R.   3.415
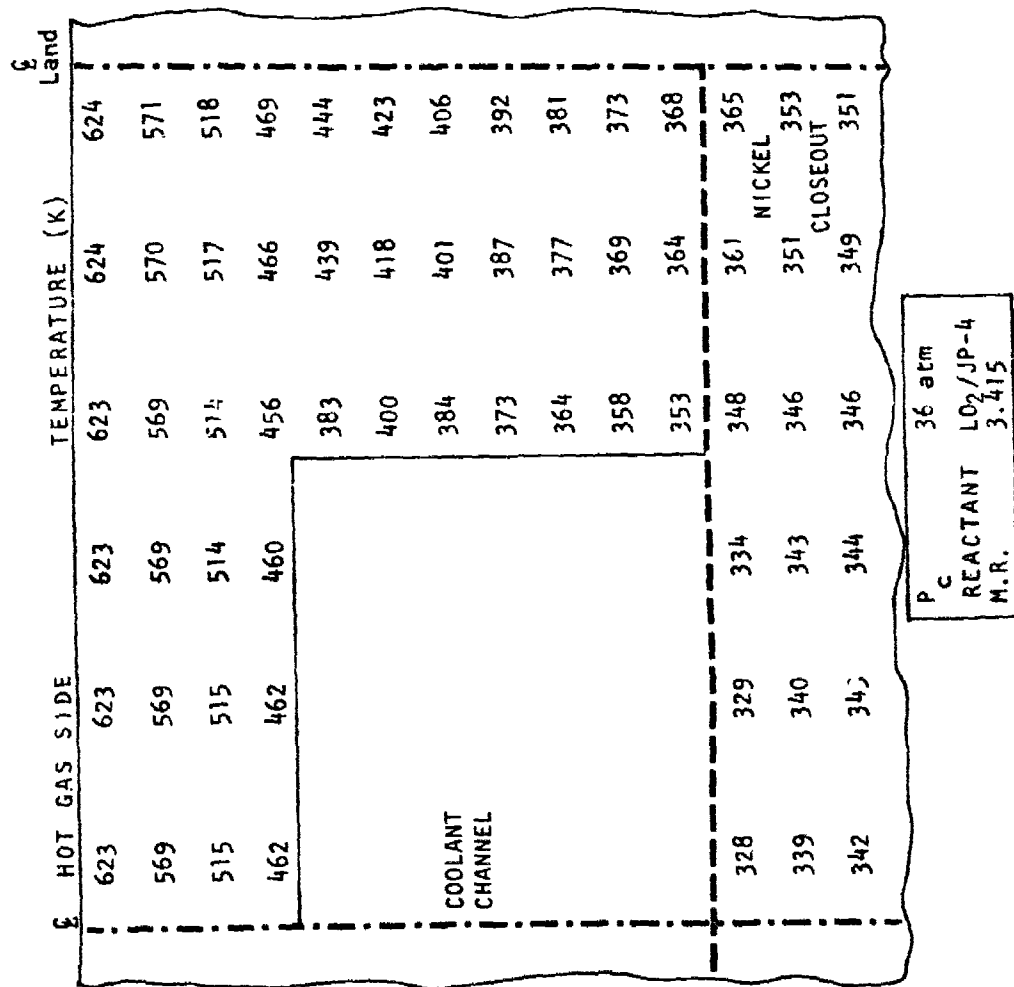
Figure 90. Channel Wall Temperature Distribution; Maximum Combustor Pressure; Maximum Wall Temperature Region (5 cm upstream of throat).

191

The thermal analyses of the contoured wall were repeated for the 36 atm condition. All design parameters were kept the same, except the water coolant inlet temperature was raised from 300 K to 325 K. The results indicated that the maximum gas-side wall temperature increased from 624 K to 631 K. Figure 91 shows that the higher wall temperature resulted in a slight decrease in cycle life, i.e., 355 cycles. However, this cycle life should be acceptable.

To describe the capability of the selected design to accommodate variations in heat flux level, a series of heat flux variations were analytically evaluated. These variations along with the results are summarized in Table 22. All of the cases were based on the current combustor design, a fixed cooling flow rate, and the maximum chamber pressure. Based on these analyses, the coolant passage design was shown to be conservative.

c. Nozzle Exit and Injector End Thermal Analysis

The nozzle exit and injector end were analyzed to determine the thermal characteristics. The gas-side boundary conditions remained unaffected, but the coolant side film coefficient was adjusted upward to include the entrance effect:

$$N_{NU} = 0.005(N_{Re})^{0.95}(N_{Pr})^{0.4}\left(1 + \frac{0.2N_{Re}^{0.25}}{L/D_H}\right)$$

Nozzle Exit. Results of the thermal analyses indicated that the maximum gas-side wall temperatures at the contoured wall nozzle exit were 488 and 511 K for 30 and 36 atm, respectively. The flat wall maximum temperatures were 514 and 541 K for the 30 and 36 atm, respectively. These temperatures were on the high side since the nickel wall, which closes the cooling passages, was not included in the thermal model. Also, the 541 K occurred at the very end of the nozzle where the coolant side heat transfer coefficient was much higher than the average value used in the analysis. Therefore, the nozzle exit maximum gas-side wall temperature was below 533 K for the range of combustor operating conditions considered.

Although the coolant side heat transfer coefficients for the flat wall were higher than those for the contoured wall, the gas-side wall temperatures for the flat wall were higher than those of contoured wall for the same gas side conditions. The reason for this was the wider land for the flat wall (0.87 cm) than for the contoured wall (0.33). Because of two-dimensional effects, the wider land caused higher gas-side wall temperature for cases where the other conditions were identical.

192
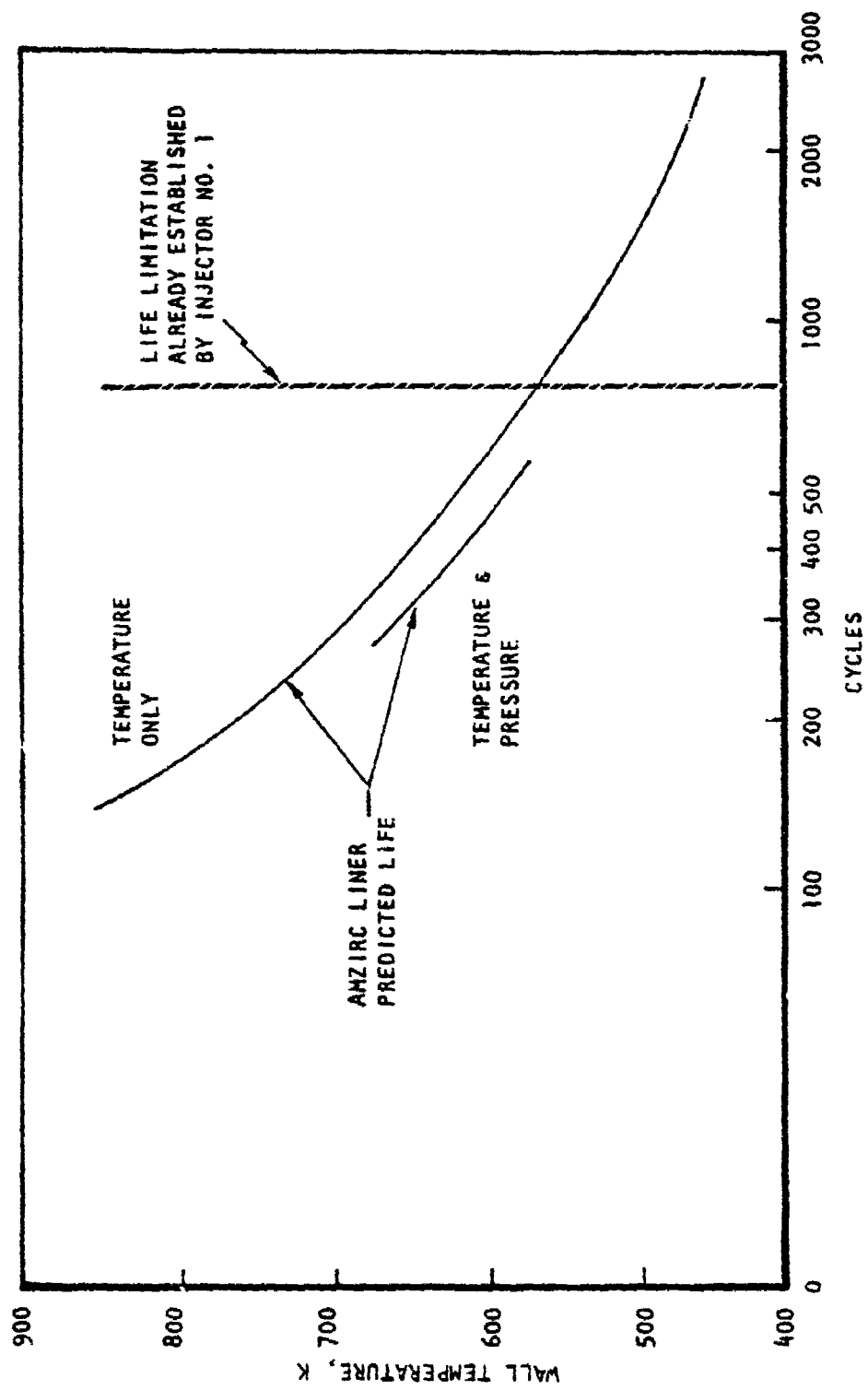
Figure 91. Amzirc Cycle Life.

193

TABLE 22. EFFECT OF INCREASED HEAT LOAD (CONTOURED WALL)

Basic: Fixed Cooling Passage Design; Constant Water Flow Rate
P_c = 36 atm; Inlet Water Temperature: 300 K

Case No.	Water ΔT, K	Water ΔP, atm	Maximum Wall Temperature, K			Case Condition
			X = -1.3 cm	X = -5 cm	X = -42 cm	
Nominal Design	60.5	20.2	623	625	536	
1	61	20.2	676	678	537	Film coefficient in throat region (-1 ≤ x ≤ 0.18) increased by 20%
2	60.5	20.2	600	625	536	Nominal design case except curvature effect on coolant-side film coefficient was included
3	61	20.2	652	652	537	Throat region gas-side coefficient increased by 20% side coefficient by 42% for curvature effect
4	72*	20.8	622	625	613**	Film coefficient in combustor increased by 36%; no curvature effect
5	76	20.8	622	625	637**	Film coefficient in combustor increased by 54%; no curvature effect

* Exit temperature is high for SSFL test; flow rate increase to 12.7 and 13.6 kg/sec, respectively will produce acceptable temperatures.

** Temperatures are at -68.6 cm, the injector end of the combustor.

Injector End. The thermal model of the combustor nozzle exit was modified by inputing the land, channel dimensions, and the boundary conditions at injector end. The coolant side heat transfer coefficients were increased by 50% to account for the curvature effect at this location where the coolant must make a 90 deg turn before leaving the channels and entering the exit manifold. The maximum gas-side wall temperatures for the contoured wall were 590 K and 612 K for 30 and 36 atm, respectively. These temperatures would be lower by 5 to 10 Kelvin if the nickel wall was included in the thermal model.

d. Materials Analyses

The following materials were used in the cooled wall combustor: Amzirc, Inconel 625, electrodeposited nickel, and aluminum. Inconel 625 was selected for the combustor manifolds because of weldability and material properties. Inconel 625 has better corrosion resistance than the stainless steels with 75% higher yield and ultimate strengths. It also has excellent weldability and is the preferred material for welding to ED nickel. These materials can be joined by either the GTA or EB welding processes without cracking or excessive porosity. The 2024-T351 aluminum was selected as the material for the support structure because of its lightweight, moderate strength and good corrosion and stress corrosion resistance.

Liner Material. Amzirc is a copper alloy with 0.15% zirconium and is used for the combustor liner. Amzirc was one of several copper alloys (Amzirc, NARLOY-Z, NARLOY-A, etc.) which have zinc or silver added and were processed in a specific manner to provide increased strength.

Investigation of Amzirc properties uncovered a body of low cycle fatigue data.[23,24] The data consisted of a total of 66 points which were applicable to the liner. The data were plotted and a best-fit curve was drawn. The cycles at each strain range from Reference 23 were divided by two to establish minimum curves. The expected minimum curves using other data sources were established by dividing the cycle life by three. The reasons for treating other sources' data more conservatively than those from Reference 23 were: (1) differences in failure criteria; (2) specimen geometry differences; and (3) unknowns in test procedures and measurements. In fact the Reference 24 data showed better life because the failure criterion was complete fracture, while Reference 23 used 10% drop in load as the failure criterion. At a strain value of 1.2%, these Amzirc data gave a predicted life of 1800 cycles. Amzirc was, therefore, a viable combustor material from the standpoint of cyclic life.

---

[23] "Investigation of Thermal Fatigue in Non-Tubular Regeneratively Cold Thrust Chambers Isothermal Fatigue Tests, Task III," No.SR-2112-7001, February 1972.

[24] "High Temperature Low Cycle Fatigue of Copper Base Alloys in Argon, Part II – Zirconium Copper at 482, 538, and 590C," No. NASA CR-121-260, August 1973.

To minimize the risk in the liner joining operation, the EB weld process verification tests were made using material from the liner billet. The evaluation consisted of radiographic inspection, metallographic examination, and tensile testing.

The X-ray inspection showed some porosity in the weld samples. Examination of the backup material revealed root porosity, which is common with copper-base alloys. The root porosity was minimized or eliminated by providing sufficient welding power to force the weld root porosity into backup material beyond the finished part's dimensions. The amount of porosity in the joints was deemed acceptable for the liner application.

Tensile tests of a weld joint resulted in slightly reduced yield and ultimate strengths when compared to the tests conducted for the billet forging certification. However, the strengths far exceed the minimum design properties. The ductility was also reduced. This resulted in an estimated 15% loss in low-cycle fatigue life.

Liner Closeout. Electrodeposited nickel was selected as the material for closing out the MHD cooled combustor liner. The electrodeposited nickel was a dense, essentially pure form of nickel. Because of the nature of the electro-deposition process, intricate contours can be readily and economically reproduced or covered with this form of nickel. ED nickel can be deposited in thicknesses ranging from thin films to an inch or more.

Mechanical properties of annealed ED nickel were comparable to those of wrought Nickel 200. The deposited nickel had excellent bonding action with the Amzirc (zirconium copper) liner material. Tensile tests have shown that the ED nickel bond was stronger than the base materials.

ED nickel was readily welded by GTA and EB weld processes, although a few precautions had to be taken. ED nickel is magnetic, and strong or non-uniform magnetic forces in the material can deflect the electron beam and cause lack-of-root fusion-type defects. Degaussing of the hardware just prior to welding reduces the tendency for beam deflection.

e. Structural Analysis

The cooled-wall combustor assembly was structurally analyzed. All safety factor requirements and cyclic life goals were met for the defined load components.

The safety factors for the pressure load at design temperature conditions are summarized in Table 23. Area 1 shows the weld safety factors when subjected to the chamber thrust load and the coolant pressures. Area 2 illustrates the

196

TABLE 23. COMBUSTOR STRUCTURAL SAFETY FACTORS (PRESSURE LOADS AT TEMPERATURE)

Area	(1) Flange/Manifold Weld			(2) Aluminum Support Structure		(3) Flange Area Nickel Closeout			(4) Exit Flange Manifold	(5) Nickel Closeout
Temperature, K	294	444	373	294	294	294	444	373	367	367
Material	Aluminum 2024	EDNI Weld	EDNI Weld	Aluminum 2024	Aluminum 2024	Aluminum	EDNI	EDNI	Inconel 625	EDNI
SF_{tu}	3.90	3.32	2.30	2.24	2.26	4.60	5.29	2.77	35.6	7.47
SF_{ty}	2.58	2.75	1.75	1.70	1.51	3.07	3.44	1.82	16.2	4.85

197

structural capability of the aluminum support structure which is primarily a pressure containment structure. The analysis of the aluminum system assumed no load carrying capability from the liner or from the closeout. During operation the liner temperatures lowered the liner yield strength and caused large enough thermal stresses to give the liner negligible stiffness against chamber pressures. The combustor assembly was designed with small thermal expansion gaps between the nickel closeout and the aluminum support structure. If no thermal gaps were provided, the closeout temperatures would result in large compressive loads which could have led to buckling of the walls. During fabrication and assembly, large tolerance stackups were possible. With large tolerance stackups, excessive bending could occur in the liner and closeout materials. Therefore, the tolerance must be controlled. By high tolerance shimming the nickel and aluminum during assembly and line reaming the bolt holes and using high tolerance bolts, the tolerance stackups were minimized and acceptable. Area 5 shows the safety factor of the nickel closeout from the pressure load not carried by the aluminum. Area 3 depicts the flange areas where the nickel closeout must carry the high water coolant pressures across the flange manifolding. Area 4 is at the water exit flange area between the bolt hole pattern and the flange manifolding where coolant pressure hoop stress occurs.

A summary of the life data for the combined load cases is shown in Table 24. Area A shows the fatigue capability of the Amzirc liner. Point 3 is the Amzirc EB weld area. The Amzirc weld area was predicted to have 15% lower life capabilities than the parent material. Therefore, life capabilities were adjusted for the 15% reduction. Area C shows nickel locations.

4.　Combustor Fabrication

The combustor was partially fabricated and set aside pending acquisition of actual heat transfer and performance data. The overall fabrication process is described in the flow diagram of Figure 92.

The fabrication process began by forging the liner material to the basic shape. The forged shape was then cut into two equal axial pieces. This was followed by machinging the interior of the liner in these two sections, joining the two sections, and machining the exterior and the coolant grooves.

The next major process was generating the nickel closure for the coolant grooves through an electroforming process. The coolant grooves were filled with wax and nickel deposited to a depth of about 0.5 cm. This deposition was done in three steps, with some degree of surface machining between the steps. Prior to the actual deposition, a verification of the process was conducted. In this verification the actual tooling and shielding was fabricated and a series of tests performed using a "dummy" combustor. These tests established the actual process parameters.

198

TABLE 24. COMBUSTOR LIFE DATA

Area	(A) Liner			(B) Nickel Closeout			(C) Flange Weld
Point	A	B	C	D	E	F	G
Temperature, K	630	511	635	443	353	400	611
Material	Amzirc	Amzirc	Amzirc	EDNI	EDNI	EDNI	Amzirc EB Weld
Efficiency, %	1.32	1.12	1.22	0.47	0.26	0.31	1.20
N_F	1500	2100	1800	3600	10^4	10^4	1565
$N_F \div 4$	375	525	450	900	2500	2500	391

199

Row 1

PROGRAM DEVELOPMENT·INTERNAL MACHINE → VERIFICATION (1) → PROGRAM DEVELOPMENT·EXTERIOR/PASSAGE → VERIFI...

Row 2

BILLET PROCUREMENT → FORGING → DRILL → CUT → MACHINE (REF.) → MACHINE INTERIOR (2) → WELD PREP → TOOL INSTA... AND (...

Row 3

EB WELD SAMPLE EVALUATION → EB WELD PARAMETER DEVELOPMENT (3) → EB WELD (4) → STRESS RELIEF

Row 4

TOOLING DESIGN FABRICATION

ELF SHIELD/NOZZLE ANALYSIS/DESIGN → SHIELD NOZZLE FABRICATION → ELF TANK PREPARATION → ELF CHECKOUT → ELF VERIFICATION → E...

ELF SHIELD/NOZZLE ANALYSIS/DESIGN → VERIFICATION MODEL FABRICATION → ELF CHECKOUT

Row 5

INLET MANIFOLD FABRICATION

EXIT MANIFOLD FABRICATION

STRUCTURE FABRICATION

PLUMBING FABRICATION

Figure 92. Com...
Pro...

Figure 92. Combustor Fabrication
Process Flow Chart.

201

Following electroforming, the outer surface is machined to match the inlet and exit manifolds and the backup structure. The manifolds and backup structure are machined in parallel with the electroforming process. The manifolds, which also serve as the flange for attachment of the injector and channel, are electron-beam welded to the nickel closure. The aluminum structure is bolted together around the combustor.

The combustor assembly is then subjected to proof and leak tests. These tests verify the capability of the cooling circuit and manifolds. The interior of the combustor cannot be proof tested without imposing loads significantly higher than those needed for operation.

The combustor fabrication was completed through assembly of the liner for coolant groove machining and through the electroforming verification.

a. Liner Machining Evaluation

A major factor, which influenced the fabrication process, was the combustor length. The long length also influenced the liner material selection and led to a two-piece liner fabrication approach.

Six approaches to the fabrication of the combustor liner were evaluated. In addition to a single-piece approach, five variations of two-piece fabrication were considered. Two of these involved a separation perpendicular to the flow axis. Three approaches used a separation parallel to the flow axis: (1) horizontal or flat-wall separation, (2) vertical or curved wall separation, and (3) corner separation. A qualitative assessment of these six approaches is presented in Figure 93. The primary tradeoff was the long machining time and cost associated with the single-piece construction versus the cutting and joining operations of the two-piece approaches.

An assessment of the joining operation was conducted; electron-beam welding was the recommended method. Basically, there was some risk associated with any method of joining two pieces relative to use of a single piece. Of the joining methods considered, however, the EB welding approach had the highest probability of achieving a reliable joint and was easily inspected and reworked if necessary. The use of EB welding in this case was facilitated by the fact that, for Case 4, the weld was linear, the material was constant thickness, and the two pieces were symmetrical.

Since the liner did not bear any loads (other than the pressure in the cooling channels), there appeared to be no unusual structural problems associated with alternatives 3, 4, and 5. The primary purpose of the weld was to seal the joint

Figure 93. Cooled-Wall Combustor Fabrication Alternatives
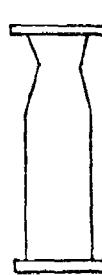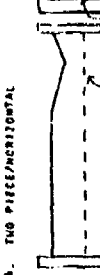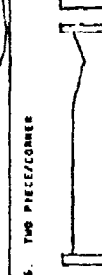
ALTERNATIVE	MATERIAL CUTTING	INTERNAL MACHINING	CHANNEL MACHINING	MATERIAL JOINING	E.L.F.	EXTERNAL MACHINING/ASSEMBLY	ADDED FABRICATION & MATERIAL	COOLING	STRUCTURAL	COMMENT	QUALITATIVE ASSESSMENT SUMMARY
1. SINGLE PIECE	NONE	36-inch machining depth; limited access to machines; long machining time	1 piece; 36 inch length	NO IMPACT	NO IMPACT	NO IMPACT	NO IMPACT	NO IMPACT	NO IMPACT		• Baseline approach • Impact machining time
2. TWO PIECE/AXIAL/WELDED	Cross-section cut (~70 in.²)	18-inch machining depth; moderate machining time	1 piece; 36 inch length	EB weld: a) 4 inches b) 32 inches c) 1-D d) const. depth; weld across channels (leak potential)					POSSIBLE	Sections must be welded prior to groove machining	• Potential for low risk schedule reduction
3. TWO PIECE/AXIAL/FLANGED	Cross section cut (~70 in.²)	18-inch machining; moderate machining time	2 pieces; 18-inch length; 2 setups; channels more complex	NO IMPACT	2 sections; 2 processes; may be easier		2 flanges/2 manifolds/2 sets of lines; flange/manifold weld; joint seal	Flange area of combustor difficult to cool; added analysis	Some reduction in cycle life; added analyses	Installation difficult due to flanges & manifolds; short length section operation more difficult	• No advantage over no. 2
4. TWO PIECE/HORIZONTAL	Longitudinal cut (~290 in.²)	Open-face machining; 2 identical pieces (except for A5 port); shorter machine time	2 pieces; 36 inch identical setup	EB weld: a) 2 setups b) 72 inches c) 1-D d) longer average land width	NO IMPACT	NO IMPACT	NO IMPACT	NO IMPACT	15% life reduction		• Potential for low-risk schedule reduction
5. TWO PIECE/VERTICAL	Longitudinal cut (~290 in.²)	Open-face machining; 2 identical pieces; shorter machine time	2 pieces; 36 inch length; identical setup	EB weld: a) 2 setups b) 72 inches c) 2-D d) variable depth					15% life reduction		• No advantage over no. 4
6. TWO PIECE/CORNER	Angled longitudinal cut (~400 in.²); difficult tooling setup	Open face machining; 2 identical pieces; unsymmetrical machining	2 pieces; 36 inch identical setup; unsymmetrical tooling	EB weld: a) 2 setups b) 72 inches c) 2-D d) variable depth					15% life reduction*		• No advantage over no. 4

*Units Are Not Metric

204

rather than provide a structural bond. There was concern about welding in alternative No. 2 because the weld would cross all of the cooling channels. Full penetration was required, and weld porosity could lead to leakage problems. In alternatives 4, 5, and 6, the weld was entirely within the land material between cooling passages. From a structural point of view, some reduction in cycle life could occur in alternatives 4, 5, and 6 because of the material properties in the weld.

Alternative No. 3 was unattractive because of the requirement for added flange, manifold, and line fabrication. This approach also increased installation difficulty at AEDC because the added flanges, etc., would crowd an already tight installation. The use of this concept as a variable length combustor would necessitate adding igniter ports in both sections. This resulted in additional complexity and cost.

Based on this review, only approaches 1 and 4 appeared to be of interest. Cost estimates for one- and two-piece fabrication were obtained. The cost and schedule for the single-piece machining was twice that of the two-piece fabrication. Based on this assessment, the two-piece fabrication approach was the preferred method.

b. Forging

Two Amzirc billets were forged to a length of 100 cm and a cross section of 22 cm by 20.3 cm at the exit. These dimensions provided material for the attachment of tooling. Following forging, the material was stress equalized by heating to 920 K and cooling in air. Test coupons were taken, and the material properties determined. The properties are summarized in Table 25. One of the forging was set aside as a backup. The other forging was machined as the liner.

c. Machining

The forging was split longitudinally, and the inner contour machined using numerically controlled machining. Machine control programs were developed for both the interior hot gas wall and for the coolant grooves. The coolant groove program was planned to be modified as necessary based on heat transfer data obtained in initial testing of the heat sink combustor (described in Section VII). The interior machining program was verified using a styrofoam model. Following this, the liner half was machined as shown in Figure 94.

One section of the machined combustor liner is shown in Figure 95. A pin and hole arrangement were used to ensure alignment when the two halves were joined. A surface was machined near the planned joint to facilitate

TABLE 25. AMZIRC PROPERTIES

Billet	Temperature K	Ultimate, atm	Yield atm	%Elongation
1	294	2300	1150	49
	811	1070	769	46
2	294	2390	1190	47
	811	1115	782	51

Figure 94. Combustor Liner Machining Process

4LC33-6/7/77-C2B

207
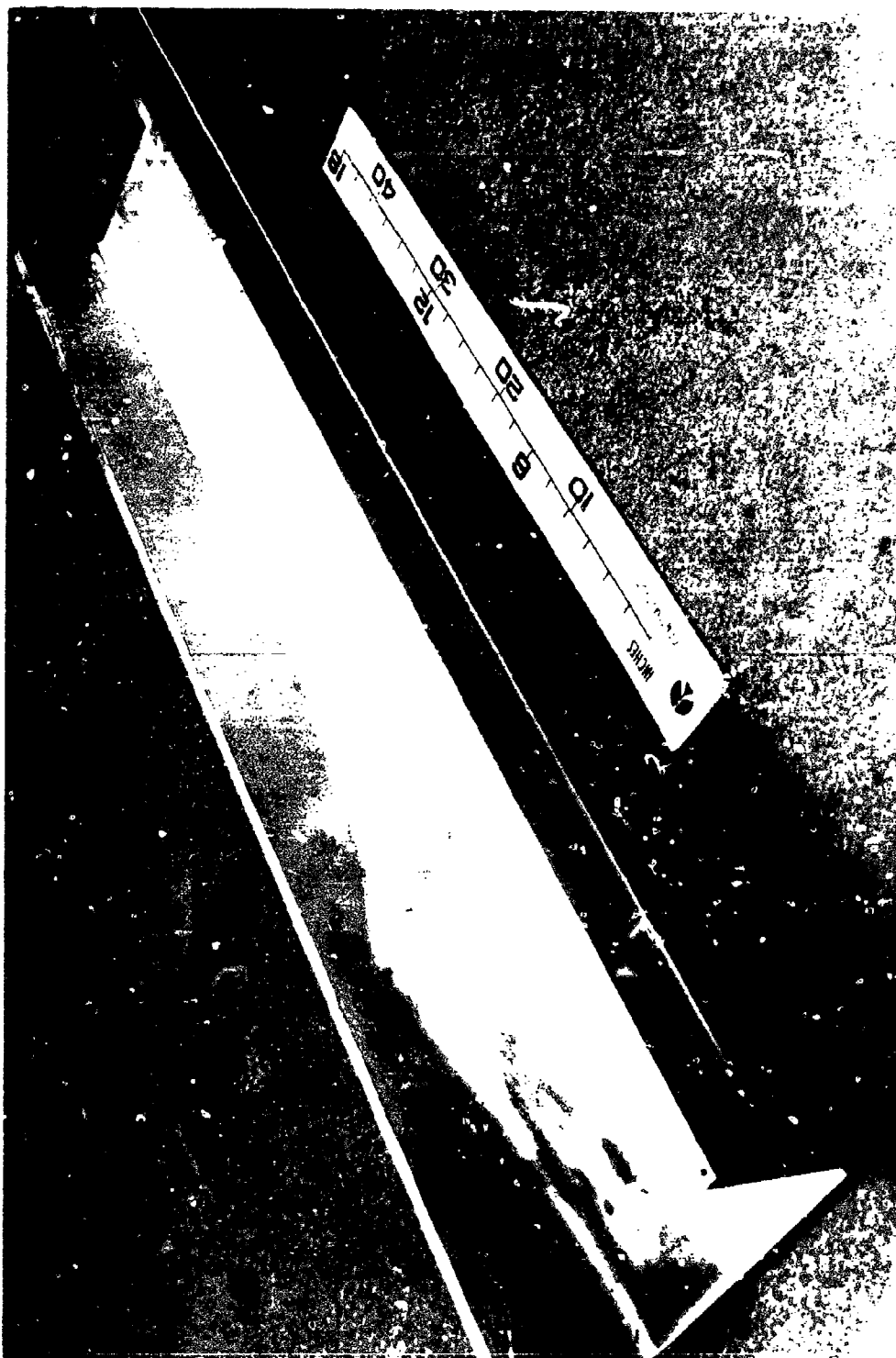
Figure 95 . Machined Combustor Liner

ultrasonic inspection following EB welding. Approximately 0.25 cm of material was left at the joint to allow for cleanup of the weld. Material was left at the entrance and exit to allow for machining and electroform tooling.

d. Welding

The two halves of the combustor were joined using electron beam welding. Prior to the welding, the two halves were assembled and a series of backup strips placed behind the joint. Electron beam welding was performed on each side. Ultrasonic test of the entire joint indicated that the weld had penetrated, and there were no unbonded areas. The backup strips were removed and X-ray inspection performed. This inspection revealed that the gross porosity was acceptable, but some voids existed in the weld. These were ground out and corrected with hand welding. The welded liner is shown in Figure 96.

e. Tooling

Tooling for the coolant groove machining and electroforming was fabricated as shown in Figure 97. The two plates fit the ends of the liner. The connector was a copper bar to provide an additional electrical path between the ends of the liner and ensure nearly equal electrical potential over the entire liner. This tooling was installed in the liner and the end plates welded to the ends of the liner. The interior of the liner was then pressure checked to ensure that no leaks would be encountered when the liner was immersed in the electroforming tank. At this point, the liner and tooling have been placed in storage.

5. Electroforming Verification

A standard procedure in the use of electrodeposition processes is the verification of the planned process using full size models. In this manner, key process variables can be specifically defined, fabrication risk reduced, and potential schedule delays for process development avoided.

a. Verification Model

The model used was assembled from two blocks of aluminum bolted together. The bolt pattern was finished flush with the surface contour with conductive fillers. This model, which is shown in Figure 98. duplicates the exterior dimensions of the liner following coolant groove machining. Since electrodeposited nickel will not adhere to aluminum without special pretreatment, the deposit could be removed for thickness measurements without damage to the aluminum substrate. The horizontal handling dolly and aluminum model are illustrated in Figure 98.

209
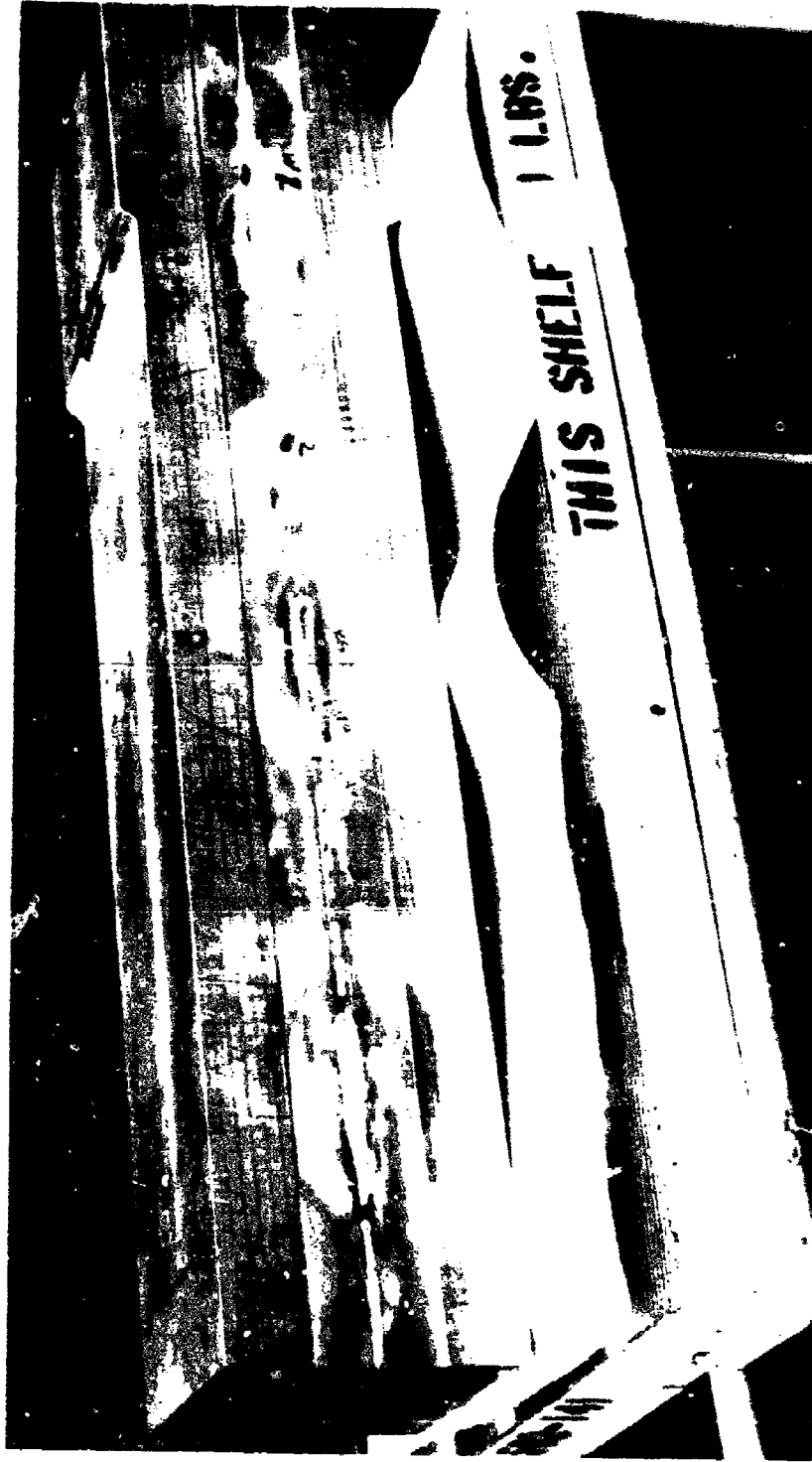
Figure 96 . Welded Combustor Liner

4LE33-7/9/77-C1A
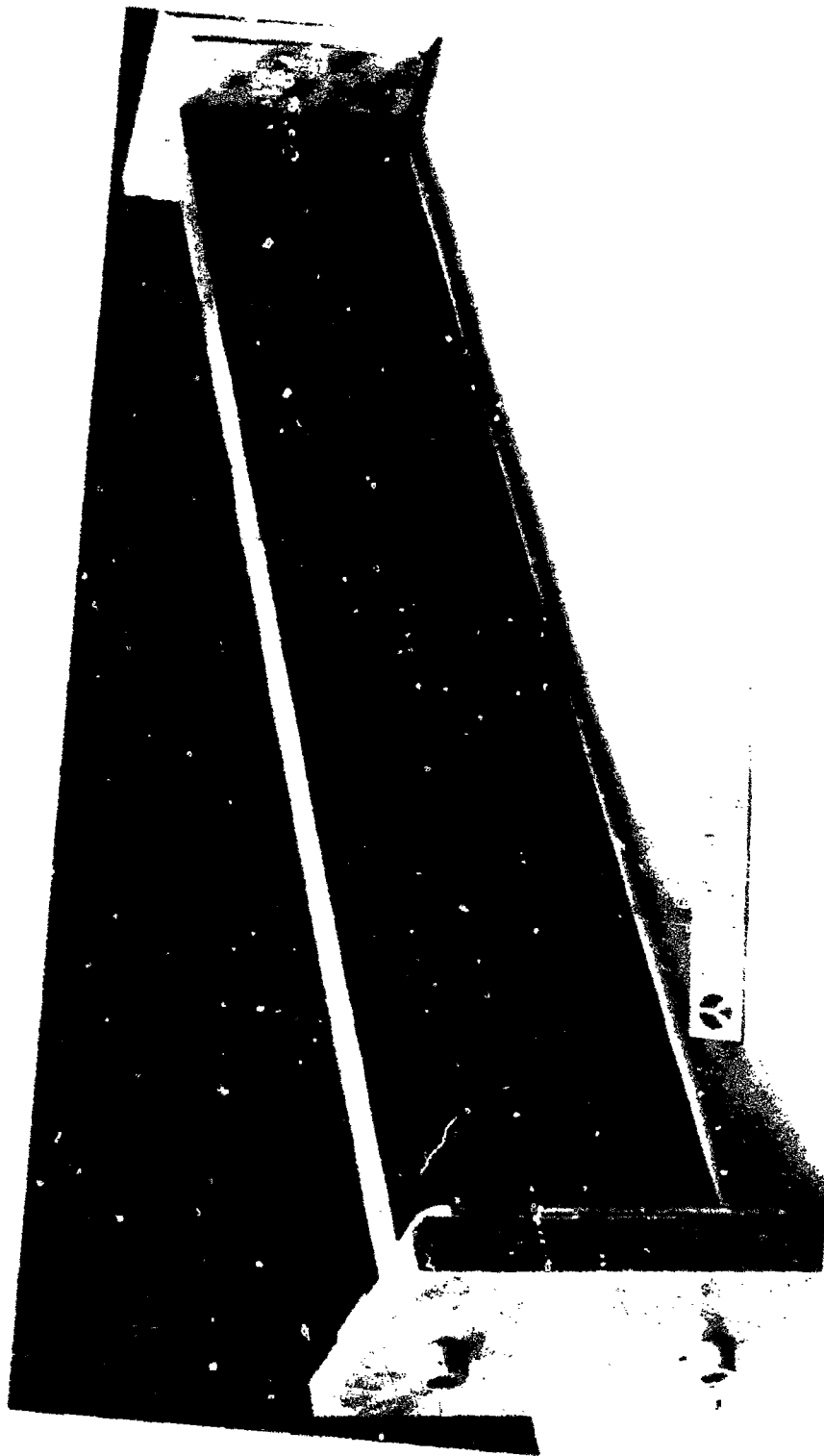
Figure 97 . Coolant Groove Machining and Electroforming Tooling

Figure 98 . MHD Model and Handling Cart.

4LE81-11/1/77-C1

b. Shield Design

The shielding for the MHD combustor electroforming effort was in four sets: one for each of the three principal pairs of plane surfaces, and one for the corners of the cooled walls. The shield sets, which were attached directly to the combustor, are illustrated in Figure 99. Shields for the top and bottom surfaces (injector and exit ends) were designed and modified to provide sufficient clearance for movement in the electroforming tank. Corner shields were designed by empirical methods. Shields for the contoured walls were designed with the aid of computer modeling to provide enhanced deposition near the throat by funneling additional current to this critical area. The shield set for the contoured wall was built in two sections, the throat funnel pair attached to the corner shields, and a tank shield which fits into place after starting the electrodeposition cycle. Electrolyte solution spray nozzles were installed in the tank shields to provide electrolyte replenishment. Shields for the relatively flat side walls were designed to hold deposition down to the same rate as on the contoured wall. The severe restriction in open surface area on the side walls might have limited solution replenishment, but this effect was corrected by tapering the openings in the side shields to provide a pumping action during agitation of the part in the electrolyte. The side shields were installed with hinges to permit rinsing during activation.

c. Installation

The combustor and complete shield set were installed in an empty tank to verify clearances and assembly procedures. The dry stacked configuration is shown in Figure 100. To ensure that different deposits could be compared, the surfaces of the part were identified as "front", "back", "left", and "right" when viewed in the tank from the center aisle of the facility. The model was always installed with the same orientation in the tank.

d. Process Tests

Three test runs were made to examine handling methods and verify deposition rates: (1) there was a five-hour run which provided a system shakedown and data on behavior during the critical first hours of deposition; (2) a seven day cycle to test shield effectiveness as the deposit thickness increases; and (3) a two stage cycle made up of a 48 hour closure deposit followed by a seven day structural deposit to model actual conditions in Phase II. Intermediate modifications were made in the tooling and shielding to optimize processing. A typical EDNi shell is illustrated in Figure 101.

This effort demonstrated that a 0.5 cm/min deposit over the combustor using a two to four day "short cycle," followed by an eight to twelve day "long cycle" could be accomplished without interstage machining. Deposition was enhanced in the throat region by adequate shielding.

213
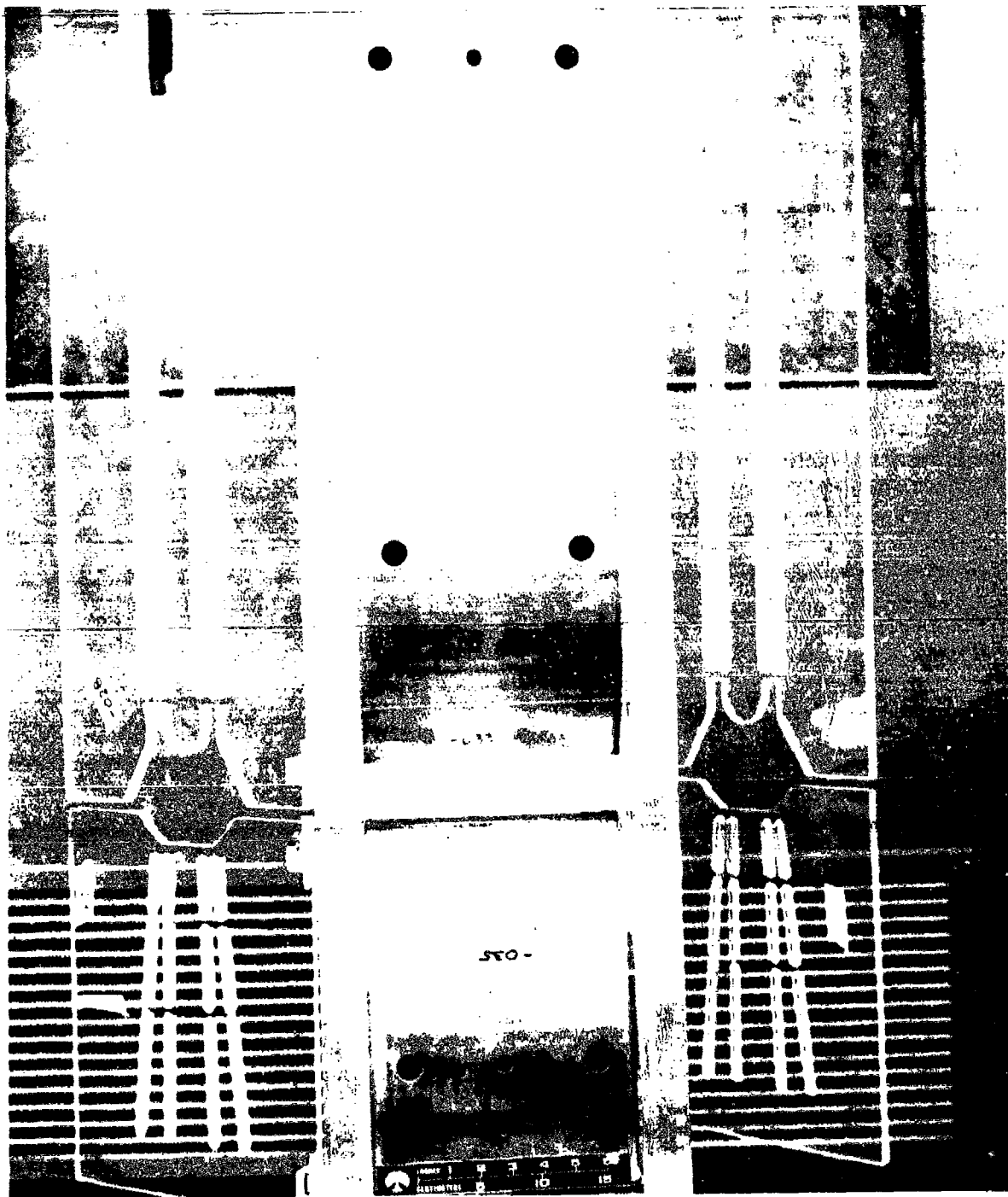
4LE43-7/21/77-C1D

Figure 99 . Model With Attached Shielding
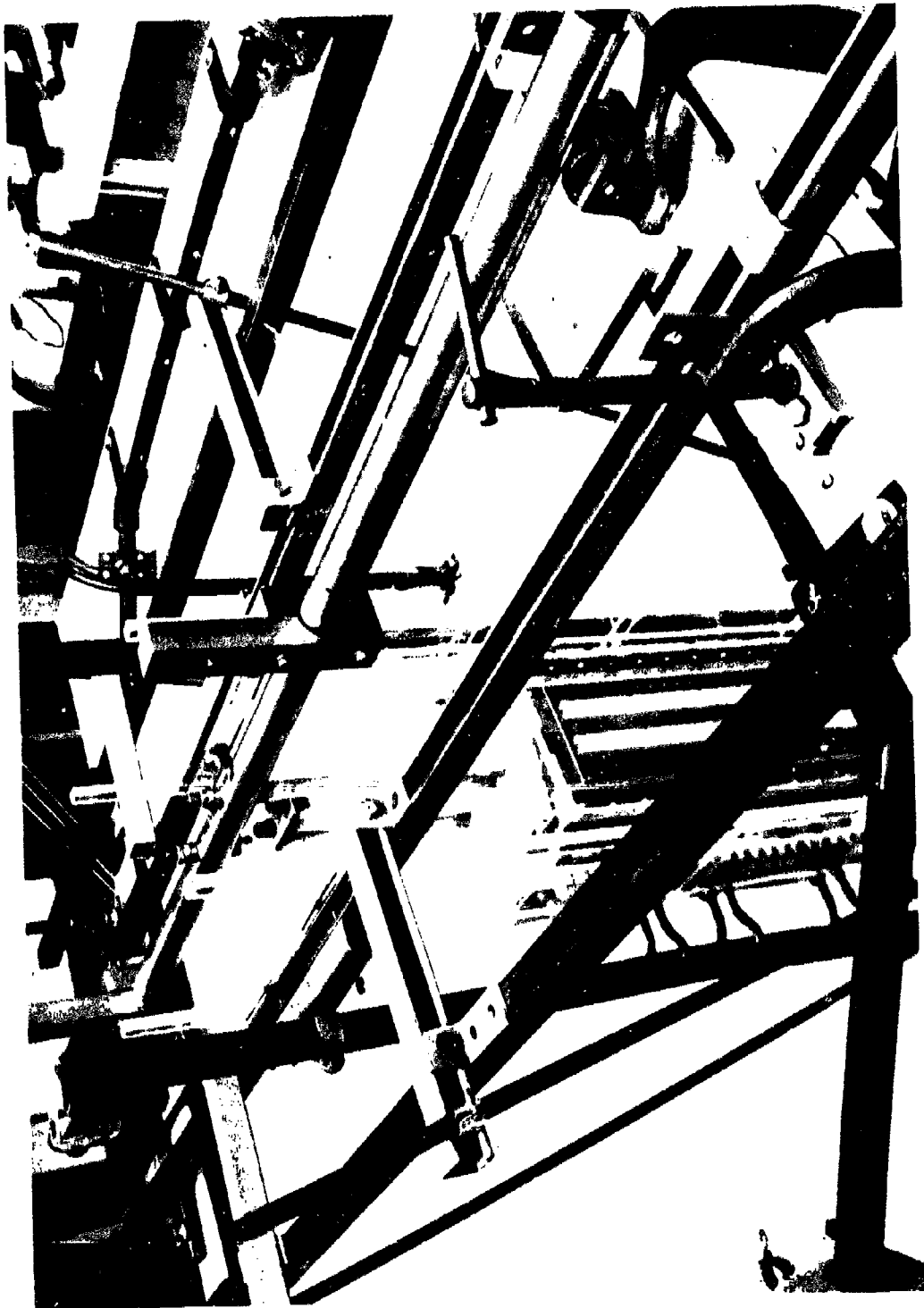
4LE13-9/16/77-CLA

Figure 100. Model and Shields Installed in Tank

215
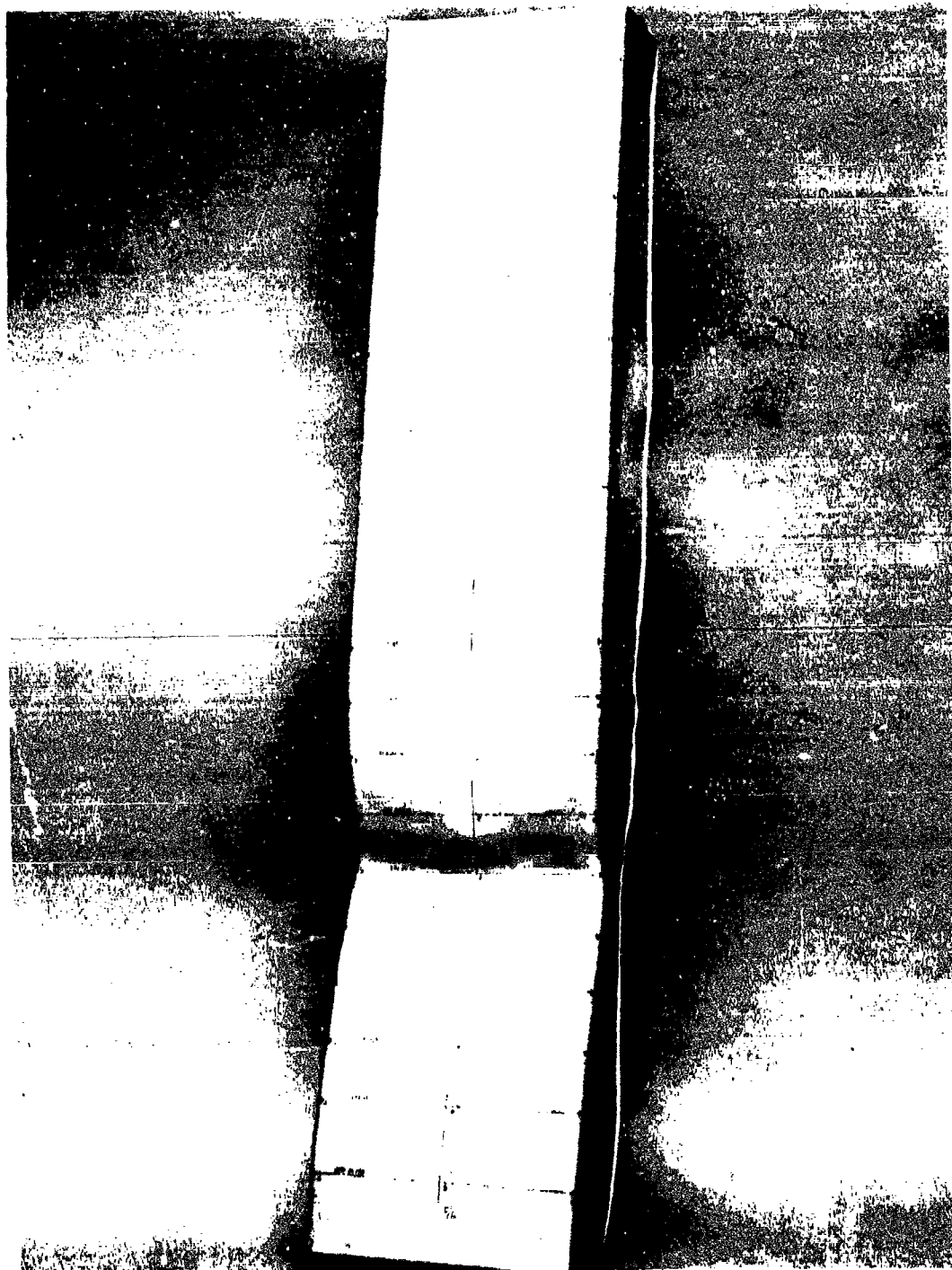
4LE31-9/26/77-C1

Figure 101. Ednt Shell From Cycle No. 1

C. INJECTOR

The injector distributed and atomized the reactants for combustion. The injector was designed to provide high combustion efficiency with uniform distribution of the combustion products. Since combustion instability has been a frequent companion of high performance LO_2/hydrocarbon combustors, provisions were made to include methods of damping the instabilities.

Two injectors were designed. The first injector was designed for high performance with a moderate increase in injector element density over current injectors. The second injector was designed for very high performance with a substantial increase in injector element density. The high performance, lower risk injector was fabricated.

1. Requirements/Design Approach

The injector was designed to meet the general and component specific requirements of Table 26. The characteristic velocity efficiency goal was 3-4% higher than has been demonstrated with LO_2/hydrocarbon reactants. No injector performance data were available in the mixture ratio range of interest. This, coupled with the requirement for uniform distribution, led to the use of a large number of small injector elements. Two injector designs were, therefore, generated: (1) 160 element injector, and (2) 416 element injector. Each injector was designed with the potential to perform higher than previous injectors. The 160 element injector used injector elements roughly one-half the size of previous injectors. With even smaller element size, the 416 element injector had the potential for higher performance. However, this fine element injector had a greater risk of fabrication and stability problems than the 160 element design.

A part of the design for stable, low pressure oscillation operation was the use of high pressure drops across the injector. Because of the flow variation, these pressure drops must be applied at the lowest flow rate conditions. With the liquid reactants this led to very high injector pressure drops at nominal and maximum flow conditions.

2. Configuration Selection

A review of liquid, bireactant injector design concepts was undertaken to select an injector type capable of satisfying the stringent design specifications for the MHD gas generator. The proven injector element concepts shown in Figure 102 were examined. Because of the high performance, uniformity, and short length requirement, "self-atomization" elements, such as showerhead elements, were rejected, and only impinging type elements were considered.

217

TABLE 26. INJECTOR DESIGN REQUIREMENTS/GOALS

Nominal Flow Rate, kg/sec

LO$_2$	21.7
JP-4/SPAN 80	6.4
Seed Solution	2.1

Flow Variation

Total	$\pm$ 20%
Seed	0, 1-10%

Performance

Characteristic Velocity Efficiency, η_{c^*}	$\geq$ 99%
Pressure Oscillations	Stable
	$\leq \pm$ 5%
Species Distribution	Uniform
Mixture Ratio Fluctuation	Small
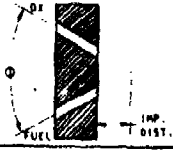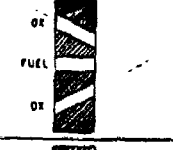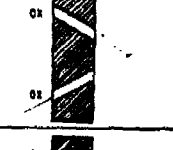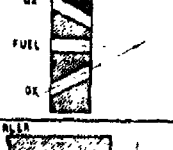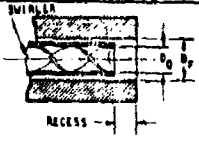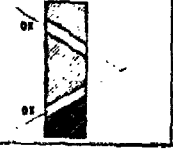
ELEMENT DESIGNATION	ELEMENT CONFIGURATION (FLOW DIRECTION)	ADVANTAGES	DISADVANTAGES	ENGINE APPLICATION
UNLIKE DOUBLET (1 ON 1) ● ○		1. Proven Dependability 2. Good Overall Mixing 3. Simple to Manifold 4. Extensively Studied	1. Subject to Blowapart with Hypergolic Propellants 2. Wall Compatibility Due to Mixture Ratio Gradients 3. Sensitive to Design Tolerances 4. Performance Sensitive to Continuous Throttling	1. Advanced Syncom (RCS), Virtually all RCS Engines, Saturn S-IIB Propellant Ullage. 2. Delta Launch Vehicle 3. Virtually all Space Storable Engines, Lunar Ascent Engine, Gemini (Maneuvering, Attitude Control, and Re entry Engine)
UNLIKE TRIPLET (2 ON 1) ● ○ ●		1. Good Overall Mixing 2. Resultant Spray Direction is Axial 3. Proven Dependability	1. Subject to Blowapart With Hypergolic Propellants 2. Unless Designed With Outer Orifice Flowing Fuel, Wall Compatibility Problems Occur. 3. Sensitive to Design Tolerances 4. Performance Sensitive to Continuous Throttling	1. Target Drone 2. AGENA Upper Stage, Gemini/AGENA Target Vehicles
UNLIKE QUADLET (2 ON 2) ○ ●● ○		1. Can be Used Near Chamber Wall for Compatibility 2. Resultant Spray Direction Axial 3. Proven Dependability	1. Subject to Blowapart With Hypergolic Propellants 2. Difficult to Manifold 3. Not Well Characterized	1. Space Vehicle Propulsion Engines. 2. Second Stage TITAN II, IIIA, B & C, Second Stage Gemini
UNLIKE PENTAD (4 ON 1) ● ● ○ ● ●		1. Good Overall Mixing 2. High Performance 3. Applicable to Extremely High or Low Mixture Ratios or Density Ratios 4. Well Characterized	1. Subject to Blowapart with Hypergolic Propellants 2. Difficult to Manifold 3. Wall Compatibility Problems 4. Performance Sensitive to Throttling 5. Injector Face Heating Problems	None Known
CONCENTRIC TUBE (WITH SWIRLER)		1. Good Mixing and Atomization 2. Low Pressure Drop Requirements 3. Proven Dependability	1. Difficult to Fabricate if Annulus Gap Excessively Small 2. Sensitive to Stability When Throttled	1. Russians Use This Element Extensively 2. Candidate Surveyor Vernier (MIRA 150A)
CONCENTRIC TUBE (WITHOUT SWIRLER)		1. Very Good Wall Compatibility 2. Low Pressure Drop Requirements	1. Very Poor Mixing for Liquid/Liquid Propellants 2. Difficult to Fabricate if Annulus Gap Excessively Small 3. Sensitive to Stability When Throttled	
LIKE DOUBLET (1 ON 1) ● ○ ● ○		1. Easy to Manifold 2. Excellent for Deliberate Control of Spray for Wall Compatibility 3. Good Mixing if Designed Properly 4. Very Stable Element 5. Not Subject to Blowapart 6. Well Understood 7. Proven Dependability	1. Requires Slightly Larger Axial Distance to Mix the Unlike Impinging Elements 2. Sensitive to Design Tolerances	1. Gemini First Stage, Satellite Launch Engine, TITAN I, II & IIIA,B,C First Stage 2. Upper Stage Engine (NOMAD), THOR, Atlas, Jupiter, F-1, H-1, Redstone 3. Upper Stage VEGA

Figure 102.   Typical Injector Element Design Concept
For Liquid Bireactants

219

The unlike, impinging type elements were rejected because of known unsuitability for LO_2/JP-4. Although potentially high performance with this element type was possible, there was a distinct tendency for "blow apart," as well as the formation of explosive fuel-oxidizer "gels" during the process of jet impingement and atomization. Concentric elements have been generally used where one of the reactants is a gas and in liquid oxygen/liquid hydrogen combustors. This concept was rejected for the LO_2/JP-4 combustor because of the long combustor length that would be required. The self-impinging doublet element was selected because this design had: (1) a high degree of atomization which promoted high performance; (2) better stability potential than unlike impinging elements; and (3) an extensive history of use with LO_2/hydrocarbon reactants.

A rectangular injector pattern was selected to match the combustor geometry. The injector was sized to fill the combustor cross section while leaving some area for acoustic damping devices. High combustion efficiency and reactant uniformity were promoted through the use of a large number of elements and uniform distribution of the elements across the injector face. Two injector configurations were evaluated: (1) 160-element injector, and (2) a 416 element injector. The first injector provided high performance with little fabrication risk while the second injector represented a very high performance potential with moderate fabrication risk and a greater degree of potential for combustion stability problems.

3. Performance Analysis

The injector elements were designed to promote high combustor efficiency and stable operation. The design approach was: (1) definition of reactant droplet size required to provide high efficiency; (2) determine element orifice to provide droplet size and meet pressure drop requirements; (3) orient element pairs to maximize mixing; (4) arrange elements to provide uniformity and compatible wall conditions; and (5) evaluate off-nominal operation.

Element Size. The degree of reactant atomization necessary was evaluated using a distributed energy release fuel droplet heating and vaporization model.[21] This model was selected based on the fuel being the combustion rate limiting reactant. As illustrated in Figure 79, a mass mean droplet diameter size of 100 μm was predicted to provide nearly 100% efficiency in a combustor length of 46 cm. A smaller droplet size would provide higher combustion efficiency in a shorter combustion length. The effect of the combustor length on adiabatic combustion temperature is illustrated in Figure 103. This example was based on the 160-element injector and assumed the heat loss to the combustor was recoverable.
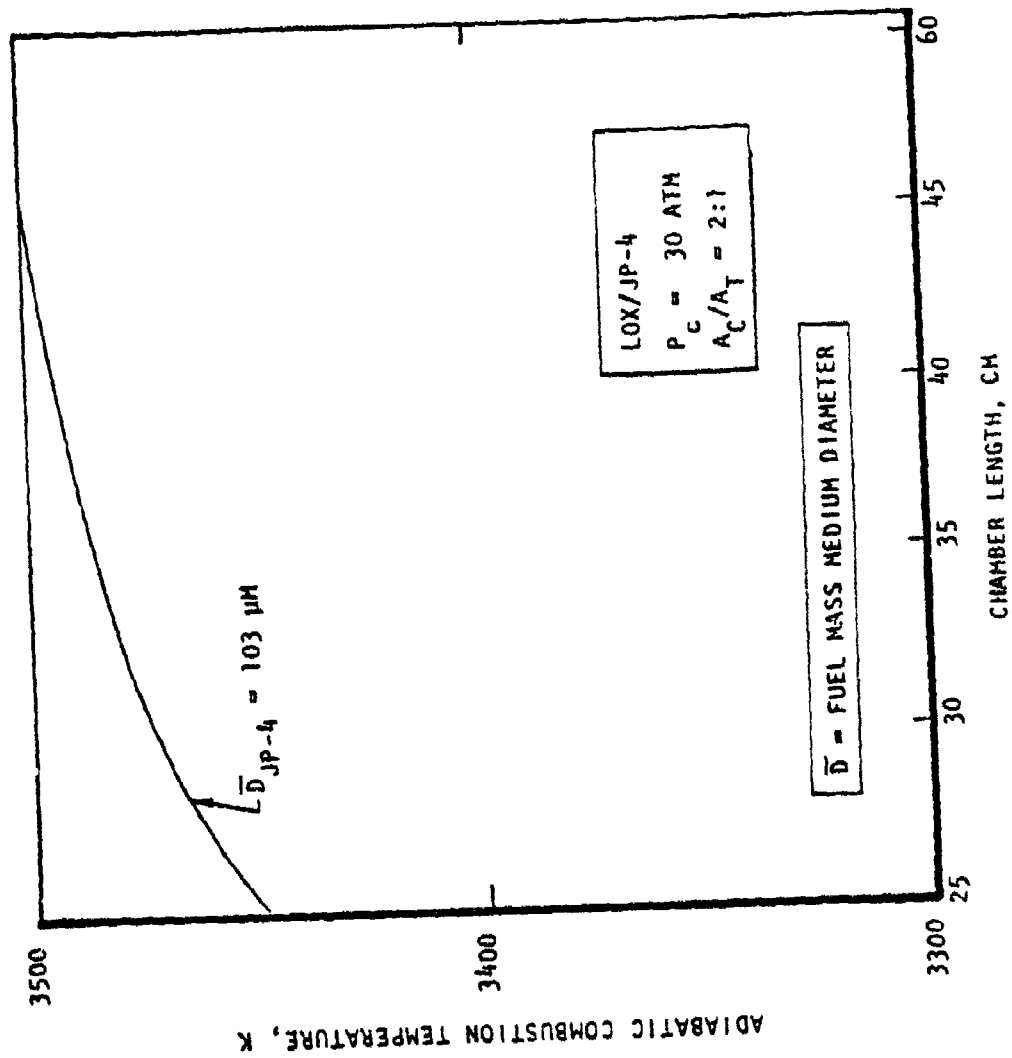
Figure 103. Effect of Chamber Length on the Adiabatic Combustion Temperature for Fuel Vaporization Limited System with Mass Mean Fuel (JP-4) Droplet Diameter of 103 Microns.

221

From the figure, the longer combustor lengths appeared to be necessary to attain the target gas temperature.

The 160-element and 416-element injectors produced mass mean fuel droplets of ~100 μm and 80 μm, respectively. Based on the theoretical calculations, both of these injectors were capable of producing near 100% efficiency in combustor lengths of 46 cm or less. As described in Section V-B, however, a longer combustor length (68 cm) was used because the program schedule allowed no chance for design iteration.

The injector orifice sizes were determined for the target fuel droplet diameters of 100 μm and 80 μm. The required injection characteristics were defined by

$$\bar{D} = 4.535 \times 10^3 \frac{D^{0.568}}{v^{0.852}} \times PcF$$

where

$\bar{D}$ = Mass-mean droplet diameter, μm

D = Orifice diameter, mm

v = Injection velocity, m/sec

PcF = Correction factor for reactant viscosity, surface tension and density

This relation was developed at Rocketdyne using the "frozen wax" atomization and measuring technique.[25]

The orifice size and injection velocity interaction are illustrated in Figure 104. With a fixed number of fuel and oxidizer elements, the relationship between the size of the orifices and the injection velocities (ΔP) was uniquely defined for a given flow rate. Based on the maintenance of a minimum pressure drop of at least 30% of chamber pressure, the corresponding fuel orifice diameter and injection velocity required for 160-element injector were found to be approximately 0.089 cm and 50.3 m/sec, respectively. For the less critical oxidizer elements, a nominal orifice diameter of 0.132 cm and a corresponding injection velocity of 47.6 m/sec were determined. For the 416-element injector, the fuel orifice was 0.058 cm, and the oxidizer orifice was 0.086 cm in diameter. The fuel orifice diameter was limited to avoid fabrication problems.

---

[25] "Correlation of Injector Spray Drop Size Distribution and Injector Variables", Final Report No. R8455, Rocketdyne, a Division of Rockwell International, December 1971.
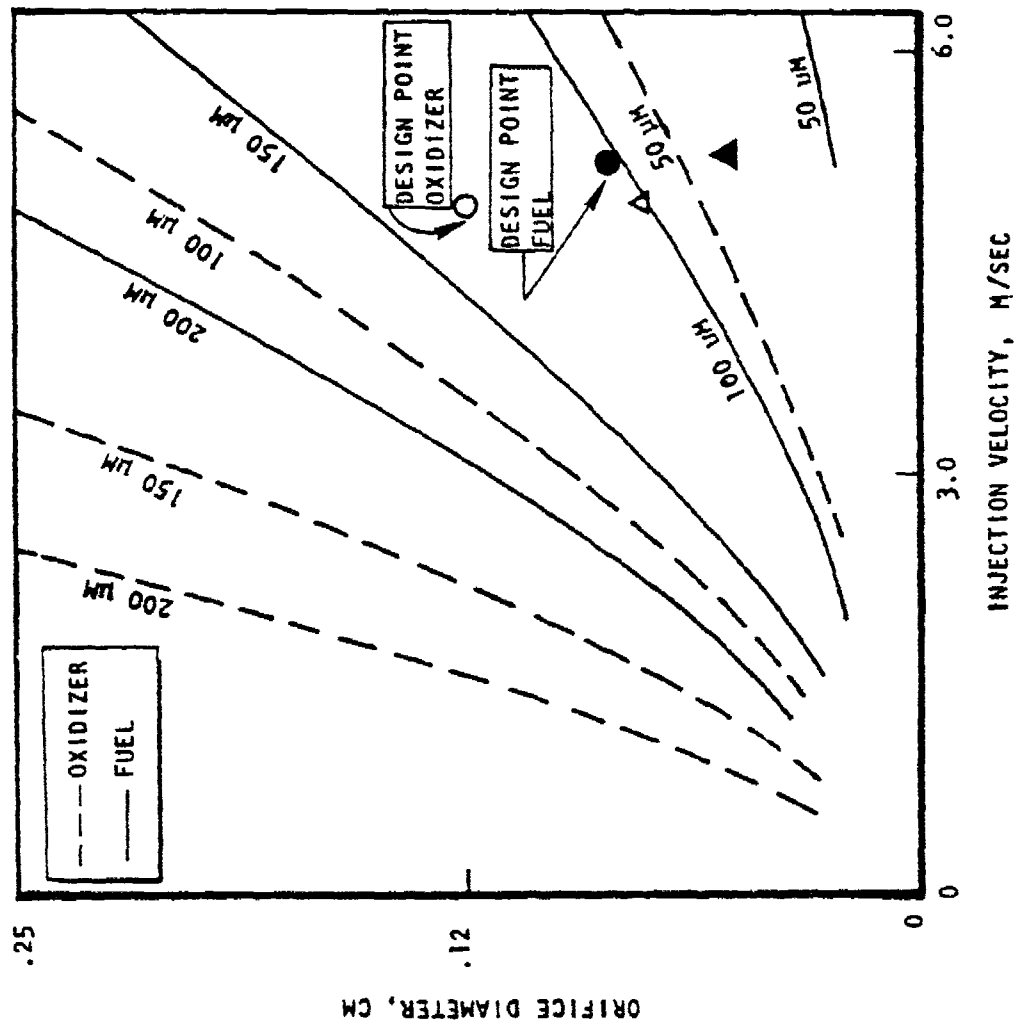
Figure 104. System Atomization Characteristics for LO_2/JP-4.

223

The combustion efficiency was dependent, to a large extent, on the local uniformity of the reactants about the injector face. In addition to providing the required small droplet diameters through the process of primary and secondary atomization, the elements must interact with each other to provide the concentration uniformity to ensure complete reaction between fuel and oxidizer. The importance of local uniformity is illustrated in Figure 105, showing the interaction of a single pair of fuel and oxidizer elements. The referenced figure illustrates the simple superposition of two spray fans to provide the interreactive mixing necessary for high combustion efficiency. In addition to the required lateral proximity for the fuel and oxidizer elements, experiments have shown that the optimum mixing was achieved when the fans were angularily inclined toward each other. The effect of inclination angle on the element spray mixing efficiency (Em) is shown in Figure 106 for an injection element similar to those selected for the MHD injector. An angle of 25 deg was incorporated into the injector designs to provide maximum mixing. The resulting element designs are summarized in Table 27.

Element Arrangement. The other aspect of injection design which was as equally important as the performance was the spatial distribution of reactants in the flow stream. Since the efficiency of electrical power generation was strongly dependent on the uniformity of flow, the design of the injector must at least provide for initial flow distribution uniformity. To a large extent, this was implied in the selection of the number of elements. In addition, a careful distribution of the fuel and oxidizer elements about the injector face was required so that each element provided a corresponding proportioned increment of flow area. The fully idealized case occurred when both the mass flux and mixture ratio distribution profile was "flat" across the entire chamber cross section. An exception occurred for the MHD injector where there was particular concern for chamber wall compatibility with highly reactive oxidizer at high temperatures. Since the MHD system used LO_2, there was direct concern for ensurance of compatible species concentration at the chamber wall. To preclude the possibility for localized oxidizer rich streams near the highly susceptible wall, the oxidizer elements near the wall are not canted so that a slight fuel rich biased environment would predominate the periphery of the flow field. This was not anticipated to cause any degradation of combustion efficiency since the peripheral regions near the wall were also designed for local mixture ratio conditions identical to elements near the core of the injectors; that is the local mixture ratio throughout the entire injector face was designed for operation at one common value.

Off-Nominal Operation. In addition to defining the injection characteristics at the nominal flow characteristics, computations were made to determine the operating characteristics at the other flow rates and Cs_2CO_3 seed concentrations.

224
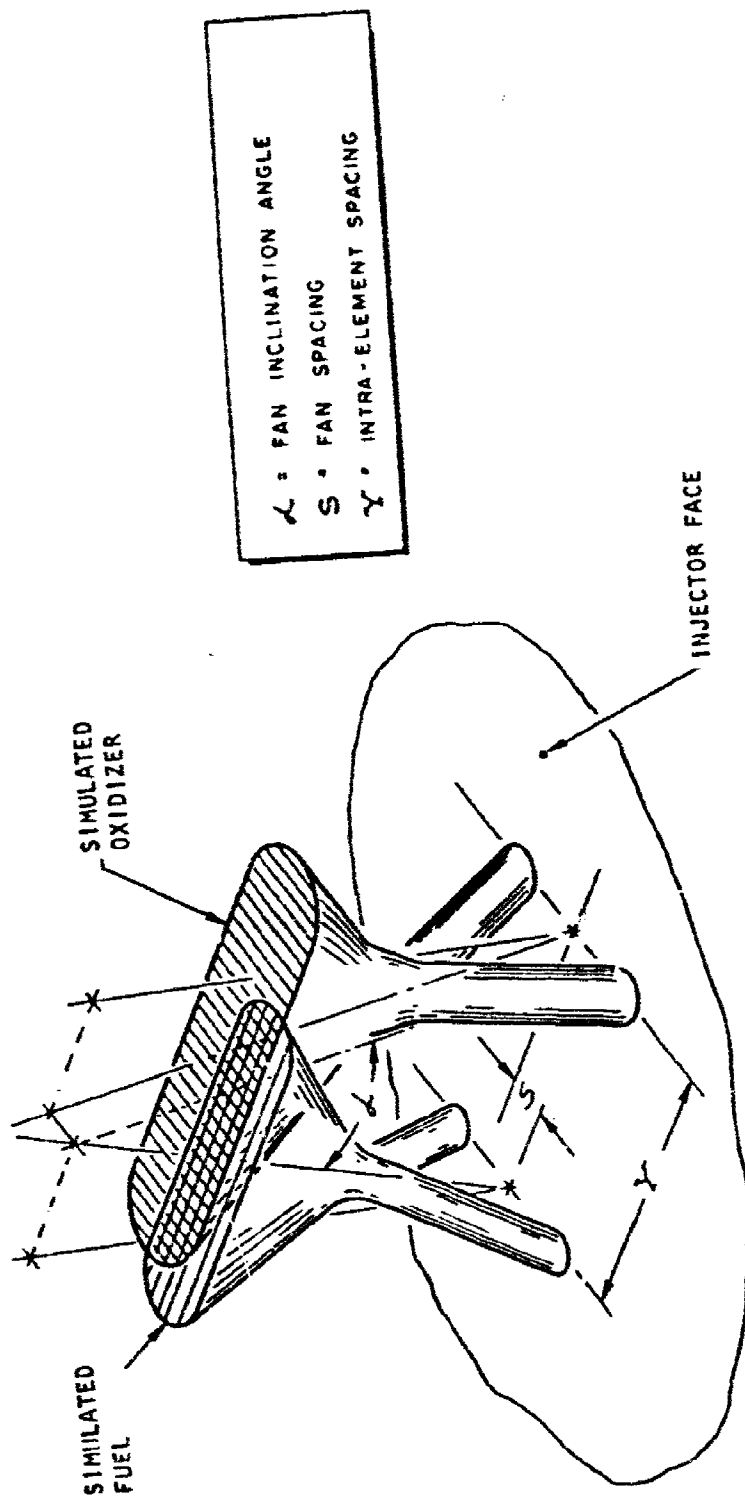
Figure 105. Geometric Factors Affecting Reactant Distribution for a Like-Doublet Injector Element.

FAN INCLINATION ANGLE, DEGREES
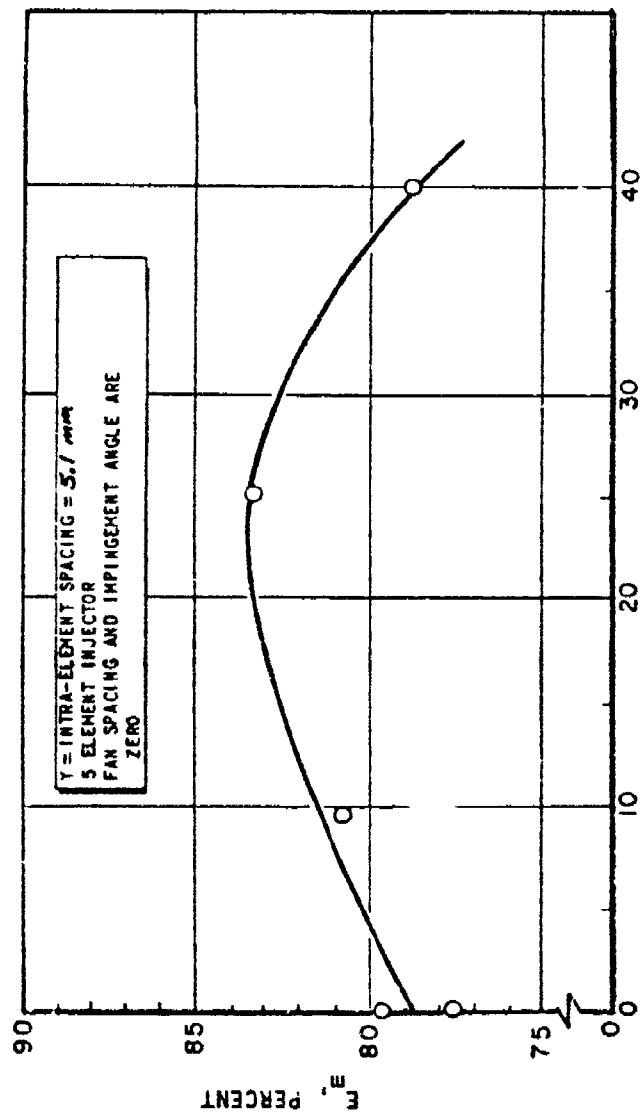
Figure 106.   Effect of Fan Inclination Angle on Reactant Mixing for a Like-Doublet Injector Pattern.

Ref. 26   Rupe, J. H. "A Correlation between the Dynamic Properties of a Pair of Impinging Streams and the Uniformity of Mixture Ratio Distribution in the Resulting Spray". Progress Report No. 20-209, JPL Pasadena, California 28 Mar 1956

TABLE 27. INJECTOR DESIGN SUMMARY

Number of Elements		160			416
Pattern		10x16			16x26
Element/Density, Elements/cm^2		0.6			1.64
Element Spacing, cm		1.37x1.10			.84x.68
Impingement Angle, deg		60			60
Cant Half-Angle, deg		12.5			12.5
	LO_2	JP-4		LO_2	JP-4
Orifice Diameter, cm	0.132	0.089		0.086	0.058
Injection Velocity, cm/sec	47.6	50.3		49.0	52.0
Impingement Point, cm	0.36	0.31		0.25	0.20

227

These characteristics are shown in Table 28 for seed concentrations of 0, 5, and 10% of total flow, and for flow variations of $\pm$ 20%. As the table shows, the maximum anticipated value for the fuel mass mean droplet diameter was of the order of 129 μm, while the injection ΔP fuel in oxidizer never dropped below a minimum value of 35% of chamber pressure. Thus, the results shown in Table 28 give confidence that high performance and stable flow conditions can be consistently maintained over the entire operating range of the MHD gas generator. The resultant fuel droplet diameter is shown as a function of the fuel mix-flow rate for the perturbation of seed concentration and flow rate in the curves of Figure 107. The curves clearly suggest that maximum performance, as determined by the minimum fuel droplet diameters, will occur at the increased mass flow rate conditions.

4. Combustion Stability Analysis

Numerous instances of combustion instability have been encountered in LO$_2$/ hydrocarbon combustors.[27,28] Combustion instability is defined as a sustained pressure oscillation of greater than 10% peak-to-peak magnitude of the mean combustion pressure.[2] These pressure oscillations can occur at one or more discrete frequencies. This level of oscillation can significantly damage combustor hardware. In addition, even lower pressure oscillations are desirable for efficient MHD power generation. The potential for instability is increased with injectors which provide the high efficiency targeted for the MHD combustor. An evaluation of the combustion instability was, therefore, performed.

Based on a review of combustion instability history, the injector element type, the orifice size, and the combustor dimensions all effect the potential for instability. The like-doublet injector element was much more stable than unlike type elements. The 15.5 cm by 19.7 cm dimensions of the combustor were smaller than the baffled compartments which have stabilized larger combustors (H-1 type combustor: 15.2 by 26.7 cm and F-1 type combustor: 17.8 by 38.1 cm). These two factors diminish the potential for instability. The orifice diameters of the MHD injector (0.089 cm fuel and 0.132 cm OX) on the other hand are much smaller than those employed on H-1 type combustors (0.161 cm fuel and 0.287 cm OX) and F-1 type combustors (0.714 cm fuel and 0.615 cm OX) and tend to increase the potential for instability. Consequently, specific stability aids were incorporated in the injector design to insure combustion stability.

The approach used in the stability aid design was as follows: (1) identify the most probable instability modes; (2) provide significant damping for the most probable modes; (3) limit stability aid complexity for the intital design i.e., avoid large cavities, baffles, etc., which would require cooling circuits ; (4) avoid stability aid designs which could accumulate reactants and potentially result in the formation of a shock sensitive gel; (5) provide a backup stability aid with increased damping and potential for resonant frequency adjustment; and (6) instrument the injector to provide temperature and pressure data for improved stability aid design.

---

[27] Oberg, C. L. , R. C. Kesselring, C. Warner III, and M. D. Schuman, "Analysis of Combustor Instability in Liquid Propellant Engines With or Without Acoustic Cavities," NAS9-12077, June 1974.

[28] 14th NASA F-1 Program Review, May 1964.

TABLE 28.   OPERATING CHARACTERISTICS OF MHD COMBUSTOR

COMBUSTOR SEED CONCENTRATION

	0%			5% (NOM)			10%		
	FLOW VARIATION			FLOW VARIATION			FLOW VARIATION		
	80%	NOM	120%	80%	NOM	120%	80%	NOM	120%
C^* – m/sec		1707			1659			1615	
Pc – atm	24.6	30.8	37.0	24.0	30.0	36.0	23.3	29.1	35.0
O_2 – kg/sec	18.8	23.5	28.2	17.3	21.7	26.0	15.9	19.9	23.9
JP-4 – kg/sec	5.5	6.9	8.3	5.1	6.4	7.6	4.7	5.8	7.0
Cs_2CO_3 – kg/sec	-	-	-	1.23	1.54	1.85	2.43	3.04	3.65
H_2O – kg/sec	-	-	-	0.47	0.59	0.71	0.93	1.16	1.39
SPAN-80 – kg/sec	-	-	-	0.17	0.21	0.25	0.34	0.42	0.50
TOTAL – kg/sec	24.3	30.4	36.5	24.3	30.4	36.4	24.3	30.3	36.4
P_{I,O_2} – atm %Pc	14.7 (60)	23.0 (75)	33.1 (90)	12.5 (52)	19.6 (65)	28.2 (79)	10.6 (46)	16.5 (57)	23.8 (68)
P_{Fuel} – atm %Pc	8.6 (35)	13.5 (44)	19.5 (53)	11.6 (48)	18.0 (50)	26.0 (72)	14.6 (63)	22.8 (78)	32.8 (74)
V_{Oxid} – m/sec	41.1	51.5	61.9	38.1	47.5	57.0	35.1	43.9	52.7
D_{Oxid} – μm	85	70	60	91	75	64	98	81	69
V_{Fuel} – m/sec	38.4	47.9	57.3	40.5	50.6	60.6	42.4	53.0	63.7
D_{Fuel} – μm	129	107	92	123	103	87	119	98	84
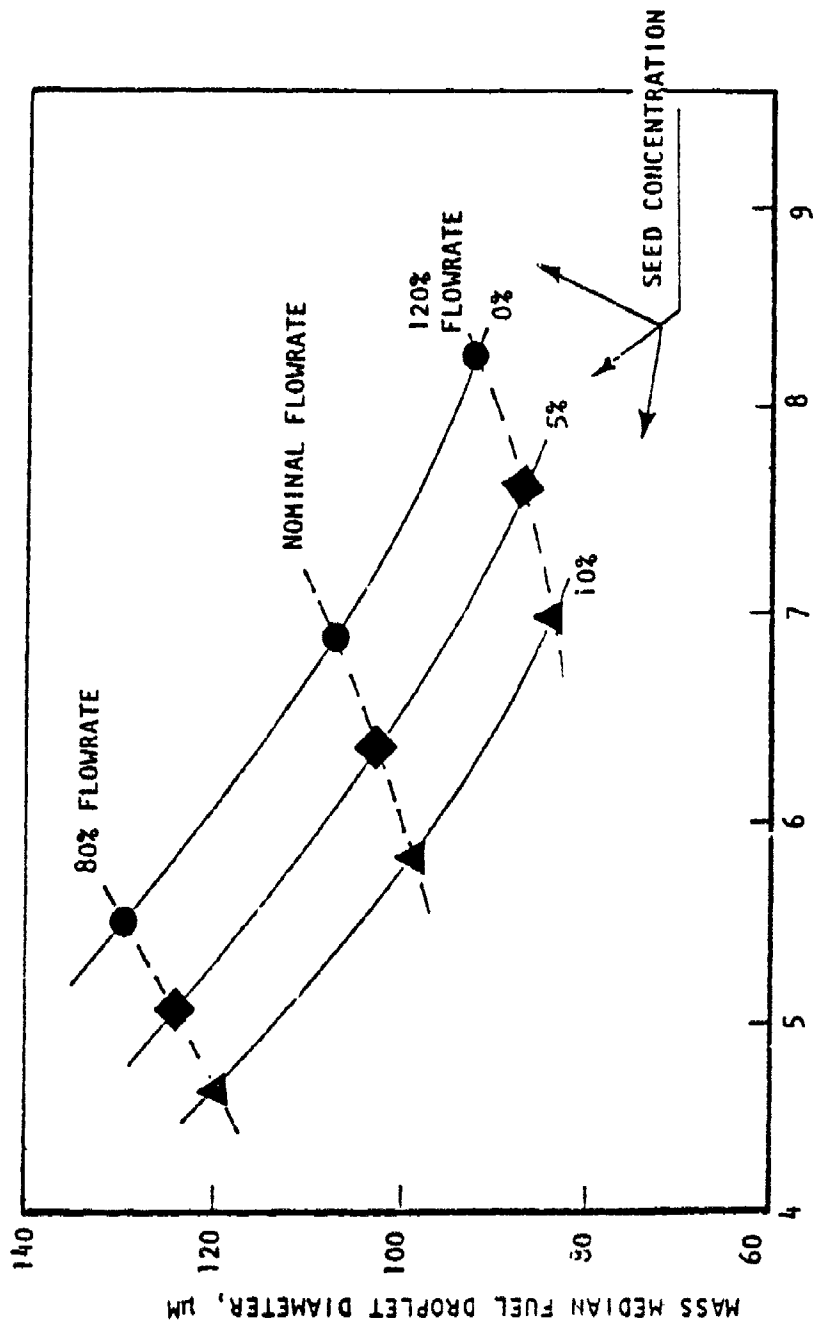
Figure 107. Mass Median Drop Size of Fuel Mix as a Function of Fuel/Seed Flow Rate and Seed Concentration.

The potential for instability in the two injectors was evaluated using a Dykema model (Reference 29). A correlating parameter, N_s, which represented a ratio of the characteristic molecular diffusion time to the characteristic acoustic time was determined. Values of N_s for the transverse modes are presented in Table 29. The region of instability was $6.4 \leq N_s \leq 30.25$ with the maximum potential at $N_s \sim 9$. As Table 29 shows, the second transverse mode in the 19.7 cm dimension was predicted to be most likely for the 160 element injector and the third transverse in the 19.7 cm dimension for the 416 element injector.

The analysis, in addition to historical considerations, indicated that provisions should be made for multiple mode stability aids. This was accomplished by designing for the lowest frequency and providing for frequency adjustment by reducing cavity depth.

a. Expected Instability Modes

The combustor was 15.5 cm between the two "sides" and 19.7 cm between the top and bottom. The most probable acoustic instability modes were the transverse modes. These modes were calculated from the equation $f = nc/2L$, where: f = frequency in Hz, n = integer, c = sound velocity in combustor, and L = distance in the transverse direction. The calculated frequencies for the various chamber acoustic modes are summarized below:

| | Mode Order | | |
Dimension	1st	2nd	3rd
19.7 cm	2819 Hz	5638 Hz	8457 Hz
15.5 cm	3570 Hz	7140 Hz	10710 Hz
Injector-to-Throat	910 Hz	1820 Hz	2730 Hz

The reactant injection fan orientation over the injector was a major consideration in selecting the "most likely" mode. For the injection shown Figure 108, there was an alternating (F-OX-OX-F-F-OX-OX) alignment of spray and in the 19.7 cm direction. Hence, instability waves in this direction might be more easily reinforced. Consequently, the 2819 Hz mode and/or its harmonics were the most likely modes because of the lower frequency and the alternating alignment of spray fans.

b. Absorber Design

To preclude the occurrence of reactant accumulation detonations, only axially aligned absorbers were considered for inclusion in the injector/chamber design. Helmholtz absorbers located in the chamber wall, especially on the

[29] Dykema, O. W., "An Engineering Approach to Combustion Instability," 2nd JANNAF Combustion Conference, CPIA No. 105, pp 205-223, May 1966.

TABLE 29. DYKEMA MODEL RESULTS

Combustor	Mode	N_s	Experimental Stability
160-Element Injector	1T (19.7 cm)	4.8	
	2T "	8.5	Most likely mode
	3T "	14.3	
	4T "	19.0	
	1T (15.5 cm)	6.0	
	2T "	12.0	
	3T "	18.1	
	4T "	24.1	
416-Element Injector	1T (19.7 cm)	2.9	
	2T "	5.8	Most likely mode
	3T "	8.7	
	4T "	11.6	
	1T (15.5 cm)	3.7	
	2T "	7.4	
	3T "	11.1	
	4T "	14.8	

INJECTOR PATTERN

SPRAY FAN

FUEL
0.089 CM DIAM.

OXID
0.132 CM DIAM.

15.5 CM

19.7 CM
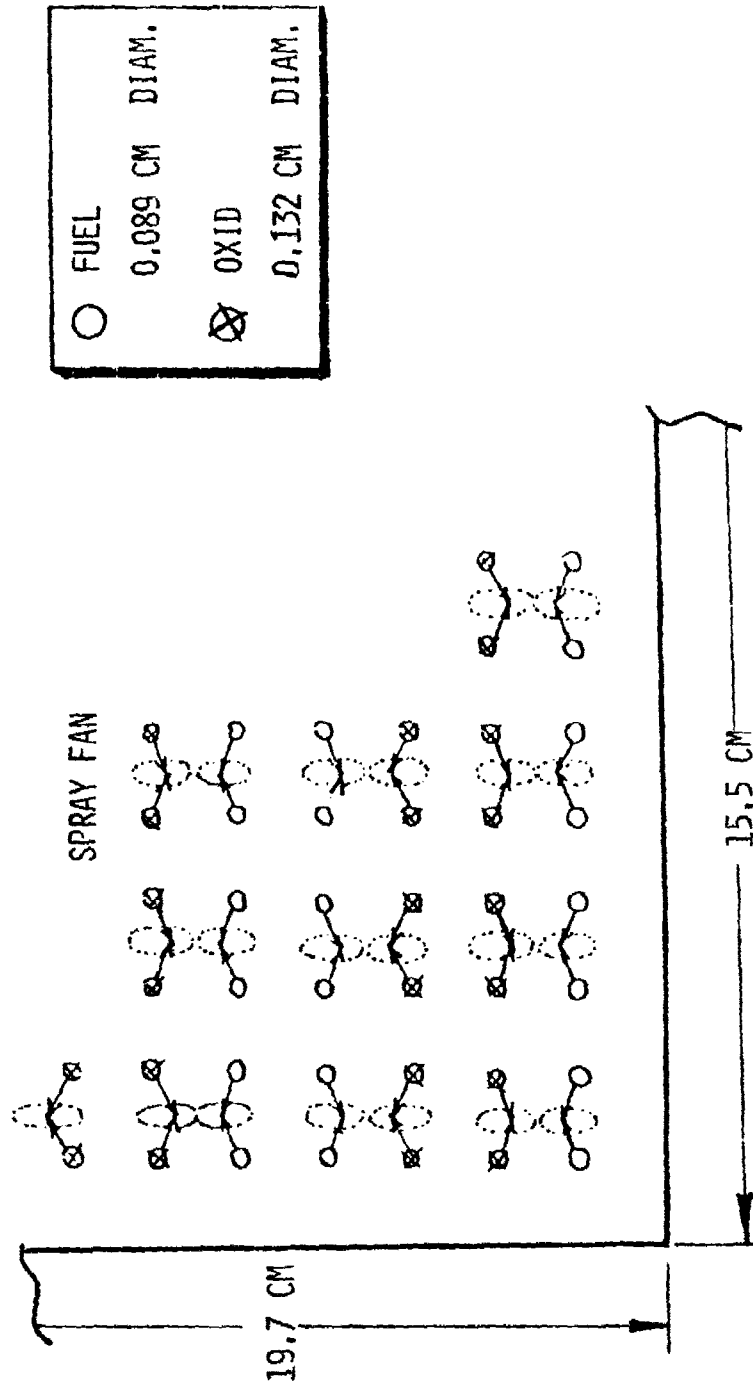
Figure 108. Fan Orientation Schematic.

233

bottom of the combustor, were specifically avoided. The maximum available aperture width around the periphery of the combustor was 0.64 cm to avoid radial winds and/or nonumiform flow near the injector face. This corresponded to 14.6% fractional open area.

For the transverse modes in the rectangular combustor, pressure antinodes existed at the walls perpendicular to the wave travel. Only at these pressure antinodes will the absorbers that are tuned to that particular mode be effective. Thus, the absorber placed at the top and bottom of the combustor was tuned to the transverse mode whose wave travel was between the top and bottom of the combustor. The absorber placed on the sides was tuned to the transverse mode whose travel was between the sides of the combustor. Because no significant volume existed for an axially oriented Helmholtz resonator, straight quarter wave slots were designed for inclusion around the injector periphery. These slots, positioned axially, as shown in Figure 109 should preclude the accumulation of reactant in the cavity and a possible subsequent detonation.

A generalized cavity damping model [30,31] was used to calculate values of the damping coefficient, α^*, as a function of both slot depth and sound velocity ratio ($c_{slit}/c_{chamber}$) and fractional open area for both the 2819 Hz mode and the 3750 Hz mode. These results are shown in Figure 110 and 111.

An estimation of the value of the sound velocity ratio to be expected was obtained from LOX/RP-1 acoustic liner test data. [32] Based on this data, a value of c_s/c_c 0.518 was assumed. Interpolation of the results in Figures 110 and 111 resulted in the selection of optimized slot depths of 5 cm (2819 Hz mode) and 3.9 cm (3570 Hz mode) for the two modes of interest.

c. Quarterwave Slot Design

The selected quarterwave slot absorber design incorporated axially oriented quarterwave slots on all four sides of the injector as shown in Figure 112. The slots on the sides were tuned to the 3570 Hz mode, and the slots on the top and bottom were tuned to the 2819 Hz mode. The slot width was maintained at 0.635 cm around the entire periphery to minimize radial winds and any performance detriment such winds might occasion. Thus, the fractional open area for the side absorbers was nominally 8.2% while the fractional open area for the top and bottom absorbers

---

* $\tilde{P} = Ae^{-\alpha t}$; Where $\tilde{P}$ = Oscillatory pressure,

         A = constant,

         t = time.

[30] Oberg, C.L., et al, "Evaluation of Acoustic Cavities for Combustion Stabilization," 7th JANNAF Combustion Meeting, CPIA No. 204, pp 743-756, February 1971.

[31] Oberg, C.L., and T.L. Wong, "Combustion Instability Suppression Devices," 8th JANNAF Combustion Meeting, CPIA No. 220, pp 781-794, November 1971.

[32] Kuluva, N.M., and C.L. Oberg, "Acoustic Liners for Large Engines," Final Report Contract NAS8-21345, (R7792), Rocketdyne, Division of Rockwell International, March 1969.

Injector Face

Chamber Wall
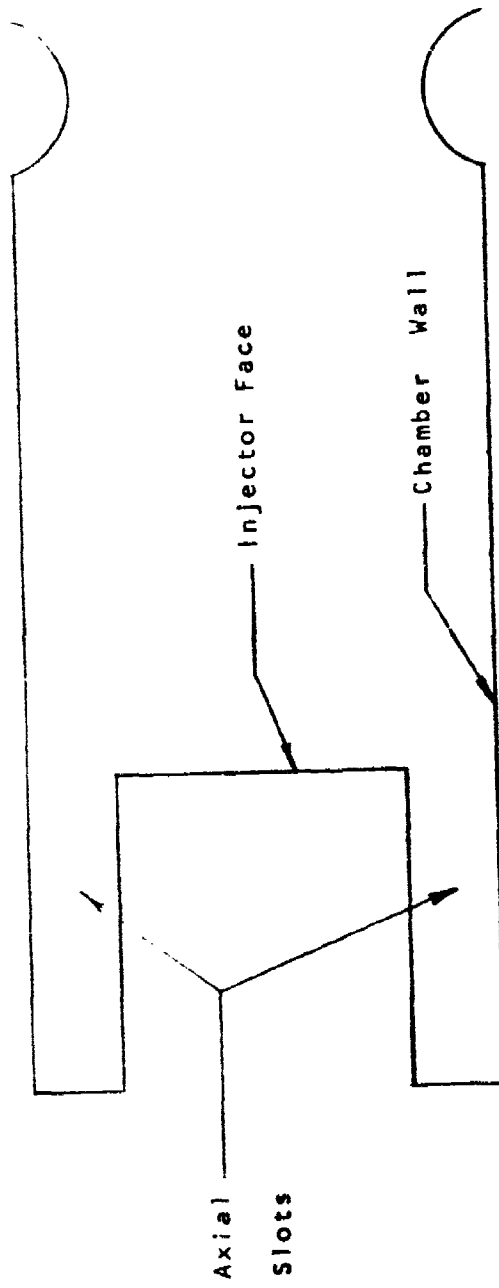
Axial
Slots

Figure 109. Axially Oriented Quarterwave Acoustic Slot.
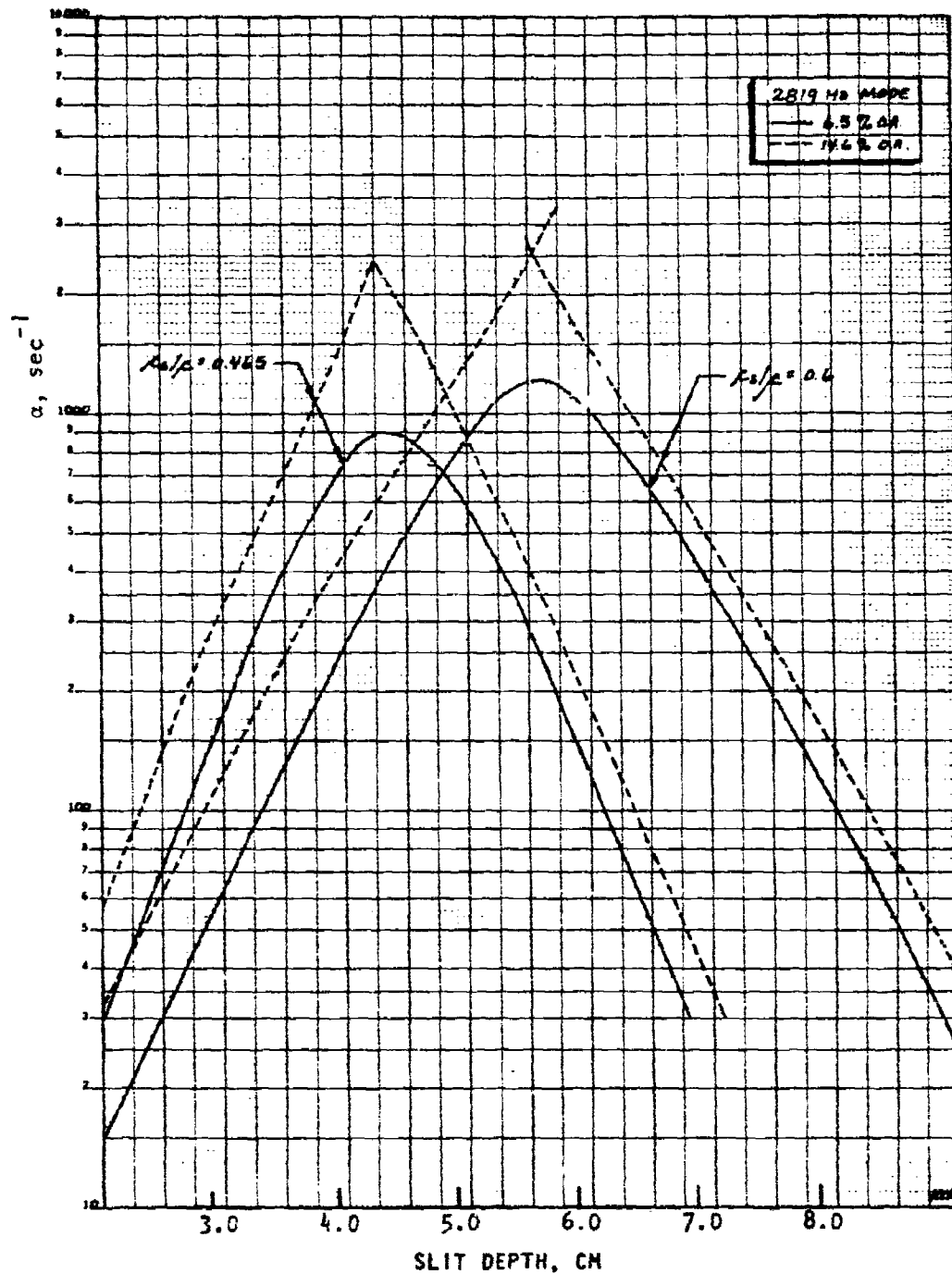
Figure 110.   Damping Characteristics for Quarterwave Slot.
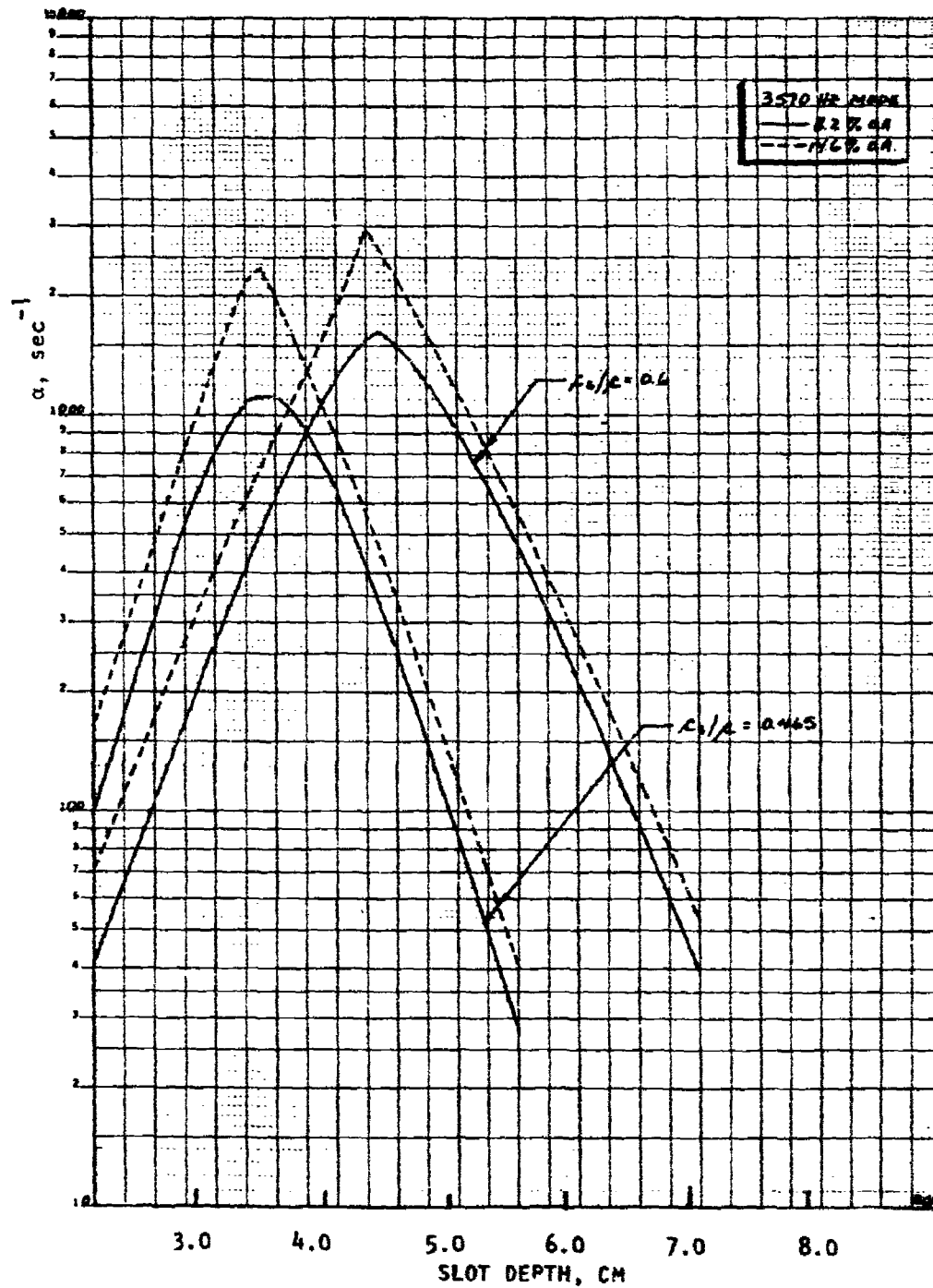
Figure 111. Damping Characteristics for Quarterwave Slot.
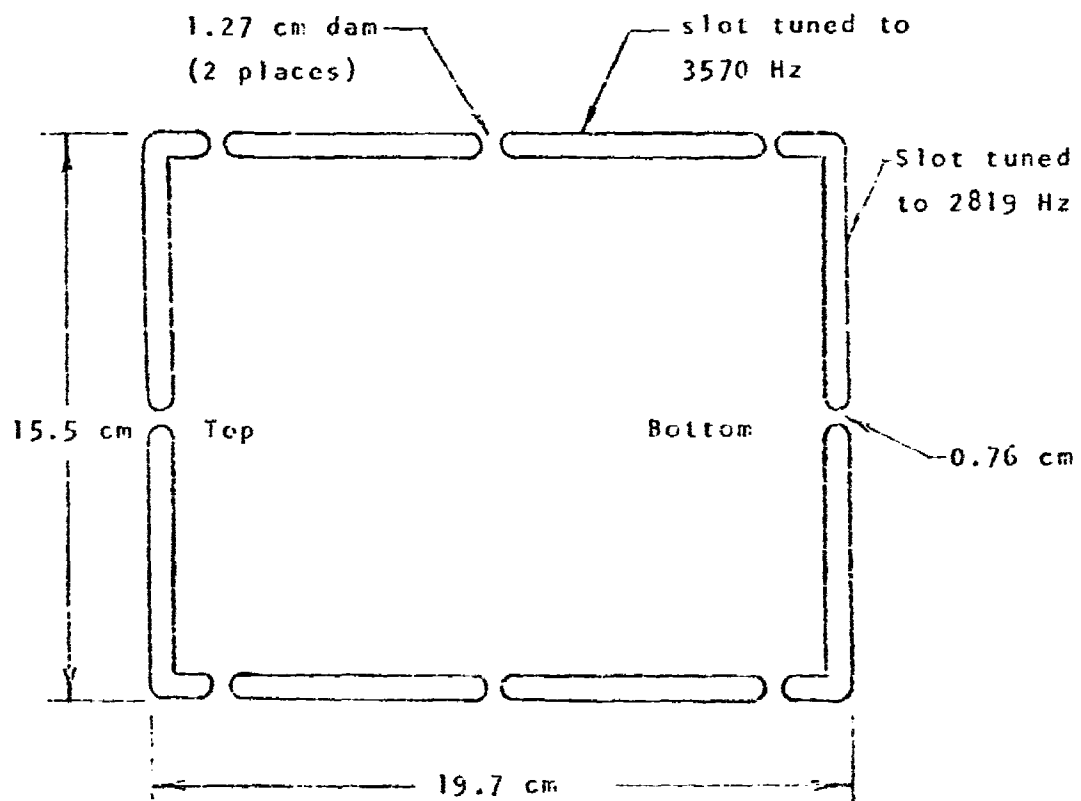
Figure 112.   Selected MHD Acoustic Slot Design.

was nominally 6.5%. Consequently, the deeper, side slots were continued around the corner as shown in Figure 112 at the expense of the shorter slot to provide additional protection against the more likely 2819 Hz mode. Dams were located as shown in Figure 112 to interrupt the circumferential slot in eight places. This was done to preclude the existence of instability modes in the slot itself. A distributed slot purge was provided at the base of each slot to further preclude accumulation of propellant in the slot.

The quarterwave slot design shown in Figure 112 utilized slot depths which were tuned to the first transverse mode.* If a second order transverse mode occurred, the slot depth could be decreased to a depth tuned to that second order mode. Slots tuned to the first transverse mode theoretically should be equally effective for the third transverse mode.

Additional analyses were conducted using the generalized cavity damping model to determine the predicted damping for the second transverse mode, 5638 Hz, in the 19.7 cm direction. This mode was predicted by the Dykema analysis to be the most probable mode of instability. Results from the computer model are shown in Figure 113. For a sound velocity ratio of 0.52 and using the dotted curves obtained by interpolation in Figure 113, the damping coefficients for both the first transverse and second transverse modes were determined for: (1) a slot depth tuned to the 1T mode, i.e., 4.95 cm; (2) a slot depth tuned to the 2T mode, i.e., 2.41 cm; and (3) a slot depth intermediate to the tuned depths for the 1T and 2T modes. These results are summarized in Table 30.

Table 30 and Figure 113 show that, assuming proper tuning, quarterwave slots designed for either the 1T (2819 Hz) or 2T (5638 Hz) modes resulted in damping coefficients which were reasonably high (i.e., good damping) for the respective mode for which the slot was designed. However, no broadband capability was apparent. A slot designed for the 1T mode would not be at all effective for the 2T mode nor would a slot designed for the 2T mode be at all effective for the 1T mode. Indeed, a slot whose depth was intermediate between the 1T and 2T slot depths was predicted to be relatively ineffective for either mode (see Table 30).

d. Absorber Backup

Provisions were made for a backup absorber through inclusion of a 3.8 cm spacer between the combustor and injector flange. Either a Helmholtz resonator for broadband damping or a larger acoustic slot for a more open area absorber,

---

* If the assumed sound velocity ratio ($c_s/c = 0.518$) is correct.
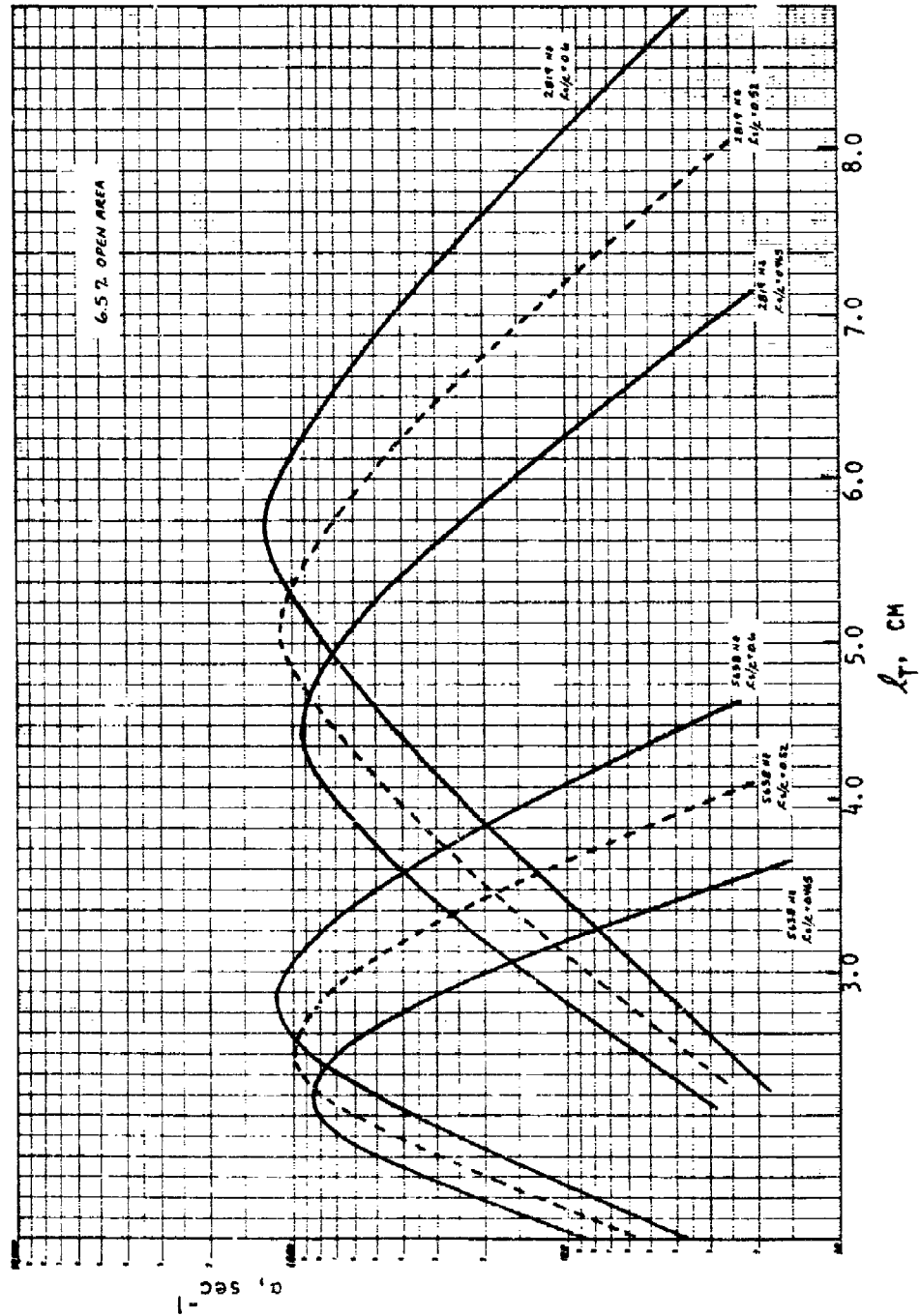
Figure 113. Damping Characteristics of Quarterwave Slot Placed at Ends of 19.7 cm Dimension.

TABLE 30. DAMPING CHARACTERISTICS

Damping Characteristics for QWL Slot

Slot Depth (cm)	$\alpha_{2819}(\sec^{-1})$	$\alpha_{5638}(\sec^{-1})$
4.95	1100	10
2.41	38	1000
3.68	280	60

Damping Characteristics for Spacer Absorber

Absorber Depth, (cm)	$\alpha_{2819}(\sec^{-1})$	$\alpha_{5638}(\sec^{-1})$	$\alpha_{8457}(\sec^{-1})$
3.94	2300	170	<10
1.65	140	2000	730
2.79	900	740	75

as shown in Figure 114, could be incorporated into the spacer. Absorber modification was based on the actual acoustic data. Section VIII describes the test results and the subsequent acoustic absorber modifications.

To assess the damping capabilities of the "spacer absorber", the generalized absorber damping model was run for a Helmholtz resonator with the maximum aperture width, minimum aperture length, and the maximum area ratio. As shown in Table 30, assuming proper tuning, a resonator designed for 1T (2819 Hz) mode, was predicted to have a damping coefficient of 2300 $\sec^{-1}$. This value was more than twice that predicted for the current quarterwave slot. Similarly, a resonator designed for the 2T (5638 Hz) mode, was predicted to have a damping coefficient of 2000 $\sec^{-1}$. In addition, a resonator having a total absorber depth of 2.8 cm was observed to have predicted damping coefficients of 900 $\sec^{-1}$ for the 1T mode and 740 $\sec^{-1}$ for the 2T mode. The backup absorber, therefore, has the potential for significantly increasing damping. By adjusting the depth the damping can be tuned to the desired frequency. In the test program a backup absorber, described in Section VIII-C, was incorporated in the hardware to provide increased damping.

5. Design of 160 Element Injector

The 160 element injector assembly illustrated in Figure 115 consisted of the face place, mounting flange, LO_2 manifold and fuel manifold. Additional components which were inlcuded in the overall injector were the acoustic spacer and the LO_2 manifold line. These were mechanically connected to the injector assembly.

a. Manifolds

The LO_2 and fuel manifolds distributed the reactants from the control valves to the injector body. The primary distribution system for the fuel side was external to the injector body. The fuel manifold was aligned with the central axis of the combustor so that axial motion caused by thermal expansion, for example, would not generate off-axis loads. Distribution for the LO_2 was accomplished internal to the injector body. The LO_2 manifold line was designed with two bends and sufficient flexibility to absorb off-axis motion without excessive loading on the brazed injector connections. Both manifolds were constructed of corrosion resistant steel. The component elements were welded and brazed together.

b. Face Plate

The injector face plate is illustrated in Figure 116. The face plate was machined from a solid piece of OFHC copper. A total of 160 element pairs were provided for reactant injection.

(a) SLOT DESIGN

(b) HELMHOLTZ RESONATOR
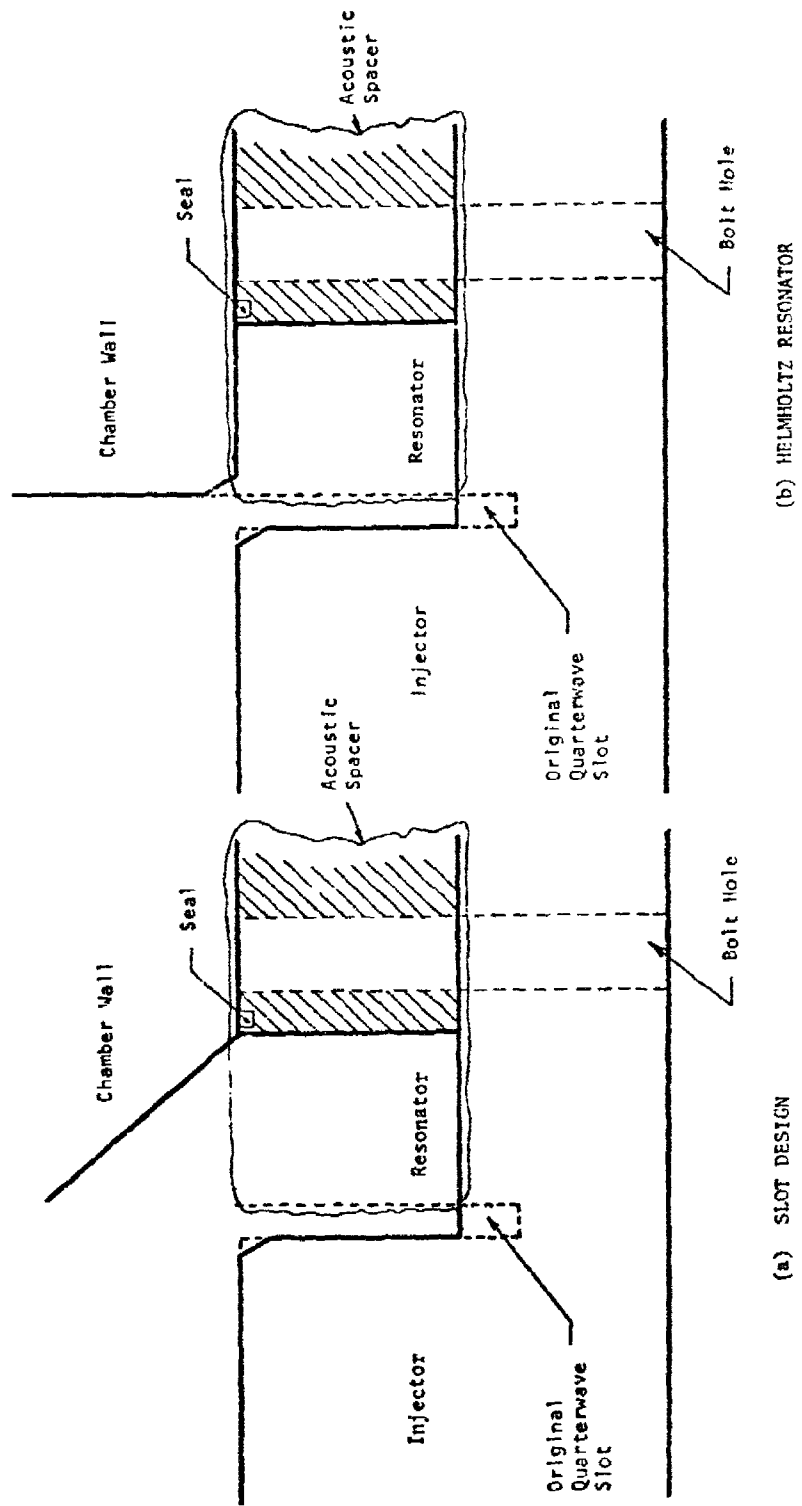
Figure 114. Acoustic Spacer Configurations.

243

FUEL MANIFOLD

LOX

LOX MANIFOLD

FACEPLATE

FLANGE
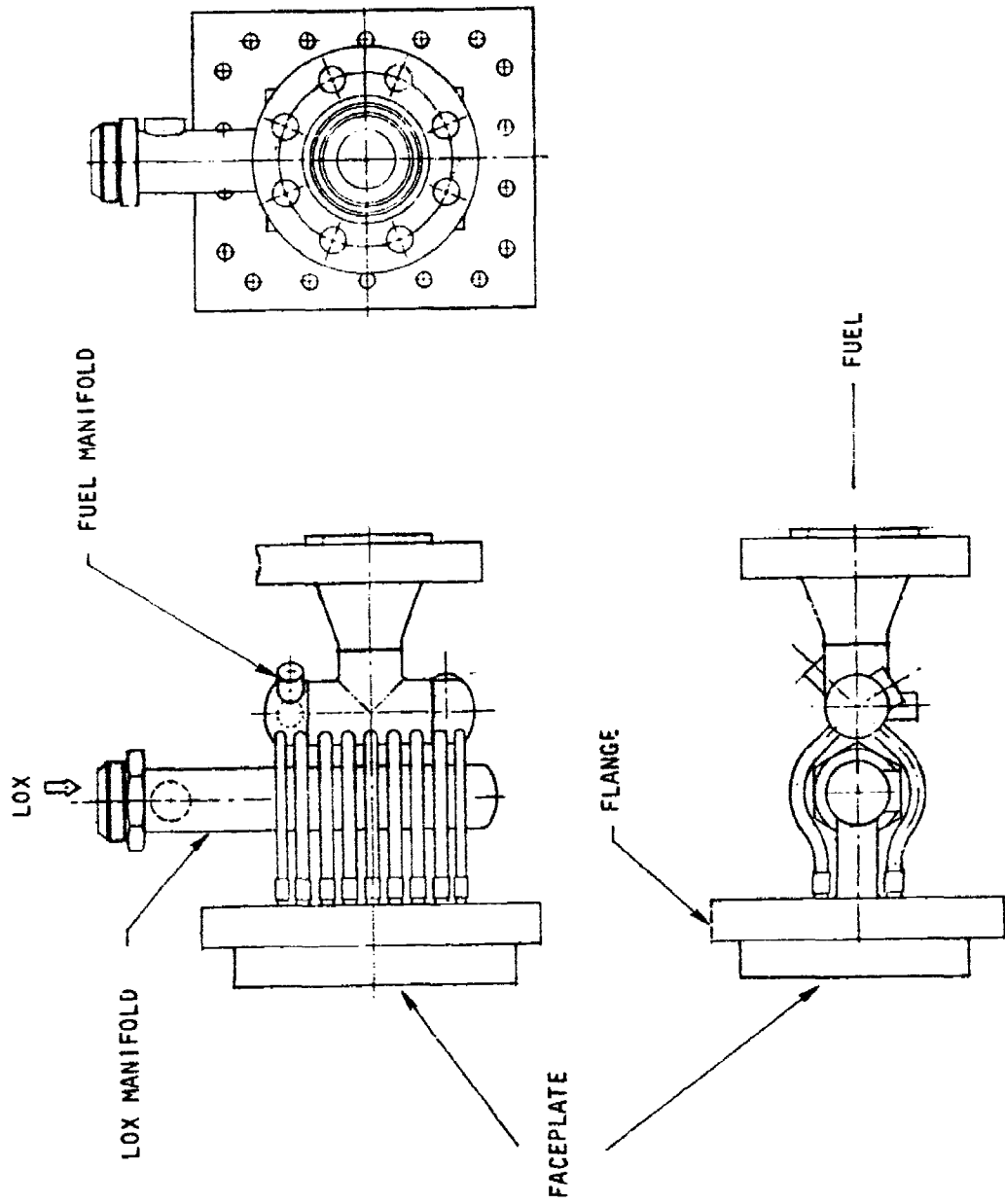
FUEL

Figure 115. 160-Element Injector

244

FUEL ELEMENT

30°TKR

13.6mm

12.5° TYP

FACEPLATE

FUEL DISTRIBUTION

FUEL

LOX ELEMENT

30°TYP

12.5° TYP

LOX DISTRIBUTION

LOX
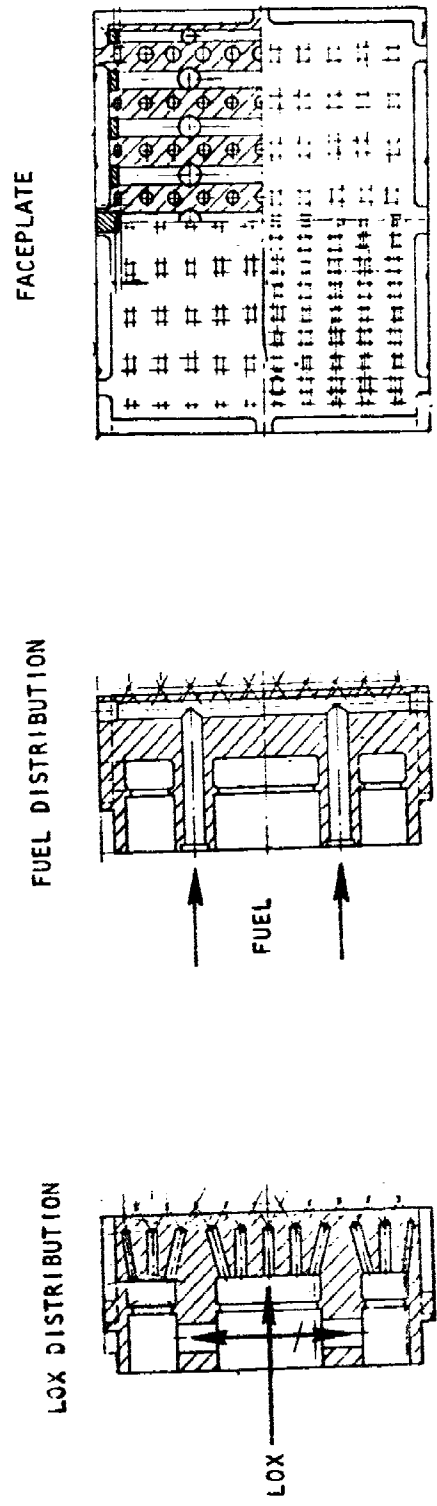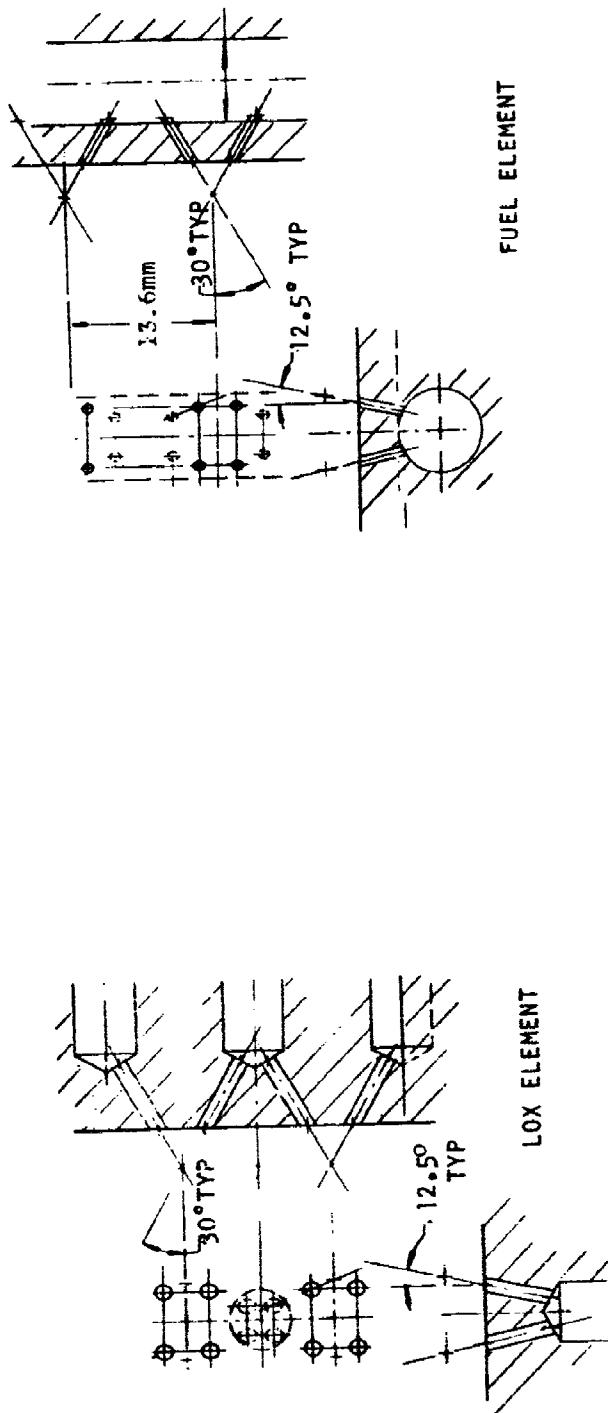
Figure 116. 160-Element Injector Faceplate

245

The fuel flows from the eighteen manifold feeder tubes into nine horizontal distribution passages which in turn fed a series of individual injection orifices. Typical fuel orifices are illustrated in Figure 116. The orifices were 0.089 cm in diameter and had an impingement angle of 30 deg. The orifices were canted to provide overlap of the fuel and oxidizer fans. The 160 element design led to 320 individual fuel orifices. The fuel distribution passages at the top and bottom of the injector were fed only a single row of orifices and were, therefore, small in diameter. As illustrated in Figure 117, the outer orifices were canted inward to avoid wall impingement.

The oxidizer flowed from the five inlet passages into a central manifold. From this manifold the oxidizer was distributed to outer distribution manifolds and to the orifice feeder passages. Restrictor plates were used between each manifold and the orifice feeder passages to assure uniform distribution. As illustrated in Figure 116, each feeder passage delivered oxidizer to four oxidizer injection orifices. These orifices were 0.132 cm diameter and impinged at a 30 deg angle. The outer series of oxidizer orifices were directed axially to avoid wall impingement. See Figure 117.

The periphery of the injector face plate was machined to provide an acoustic slot approximately 0.64 cm wide. A series of eight dams were provideu to separate the individual slots and avoid recirculation.

c. Injector Body

The face plate and flange were brazed together to form the injector body, see Fig. 118. The flange was machined from corrosion resistant stainless steel. The flange contained eighteen holes for the combustor assembly bolts. Four feeder passages were provided for distribution of a gaseous purge into each acoustic slot. Four purge sources were provided on the top and bottom, and six were provided on each side. These purges were used at start and shutdown of combustor operation to prevent accumulation of liquid reactants in the slots. Locating pins were provided to assist in assembly.

d. Priming and Distribution

The injector manifolds and distribution passages were analyzed for priming time and distribution uniformity. The volume of the LO_2 manifold was 1800 cm^3 and the fuel manifold was 970 cm^2. With the nominal flow rates, the oxidizer manifold was primed in approximately 90 msec and the fuel manifold in approximately 100 msec. In reality, the manifold priming time should be shorter because the initial fluid flow rate will be much higher than the steady state flow rate.
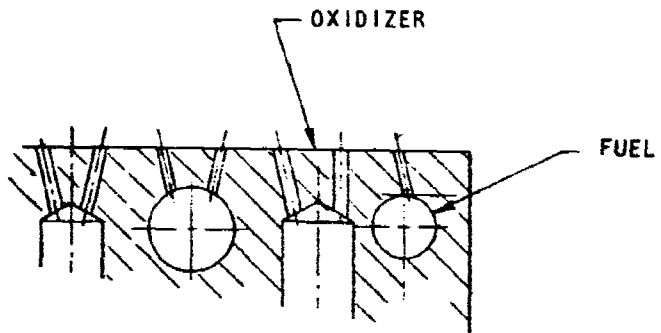
Figure 117.   Edge and Corner Elements.

SLOT
PURGE

DAM
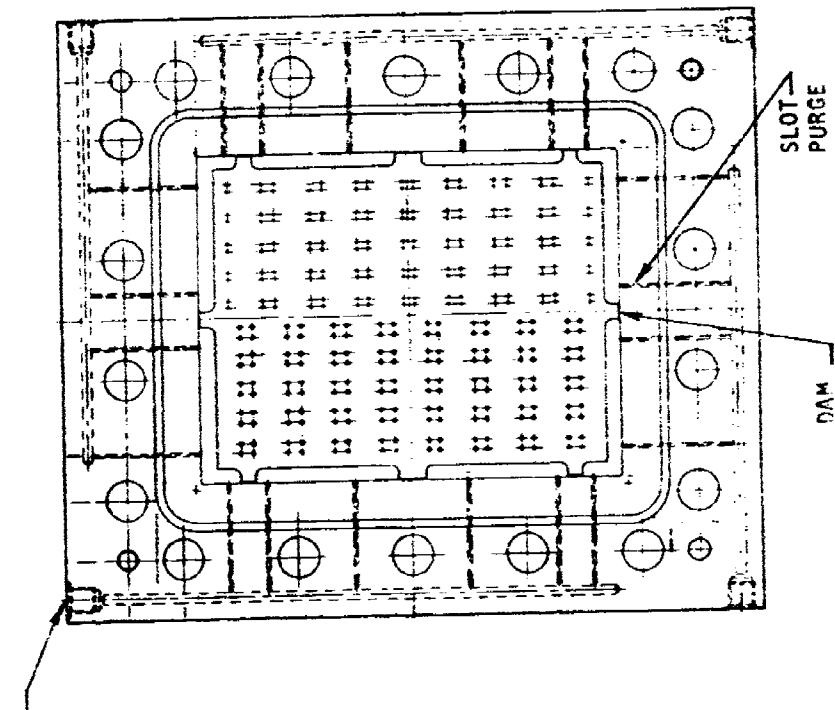
SLOT PURGE
DISTRIBUTION
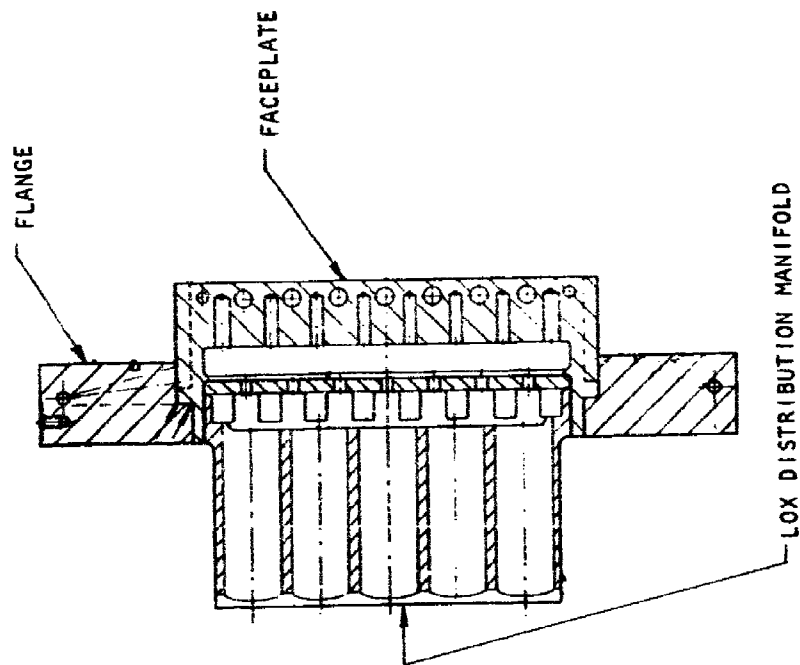
FLANGE

FACEPLATE

LOX DISTRIBUTION MANIFOLD

Figure 118. Injector Body

248

The injector manifold was analyzed for flow distribution characteristics. Manifold distribution effects were primarily related to dynamic pressure heads resulting from manifold flow velocity. The design specification required that any local manifold velocities which exceed one-fourth of the orifice injection velocities be avoided. With an oxidizer injection velocity of 43 m/sec, and a fuel injection velocity of 46 m/sec, the maximum manifold velocities were 10.8 and 11.5 m/sec, respectively. The injector manifolds and flow passages, with maximum computed velocities of 7.3 m/sec in the oxidizer system and 9.3 m/sec in the fuel system, easily met this requirement.

The predicted flow distribution by orifice, numbered from left to right in a transverse section, are shown in Figure 119. These represented worst case sections, which in the oxidizer case was located directly under the openings in the distribution plate. The level of predicted maldistribution from manifold flow effects was quite low, being on the order of 2.1% for the oxidizer side and 4.2% for the fuel side as maximum deviations. Flow variations of less than 5% could not be readily separated from random orifice fabrication effects, and efforts to further reduce manifold effects produced very little improvement in the overall distribution picture.

e. Material Analysis

The materials used in the injector were OFHC copper and corrosion resistant stainless steel (CRES). The copper face plate material was selected because the high thermal conductivity permited the use of reactant cooling. The copper could be brazed readily and was compatible with the reactants. The CRES material was used for the manifolds and flanges because of good strength and ability to be brazed. The CRES thermal expansion matched that of the copper. This reduced the thermal strains and contributed to the long cyclic life.

f. Thermal Analysis

The injector was analyzed to determine the steady-state temperature distribution. In the analysis the injector was subjected to a heat input at the face surface from the combustor. Cooling was provided by the reactants flowing through the injector.

Previous rocket engine injector face thermal data have shown that the injector face heat flux was approximately equal to one-half the value of the combustor heat flux. This results in a heat flux level of 410 w/cm^2. Heat transfer coefficients used for the reactants were developed from tests previously
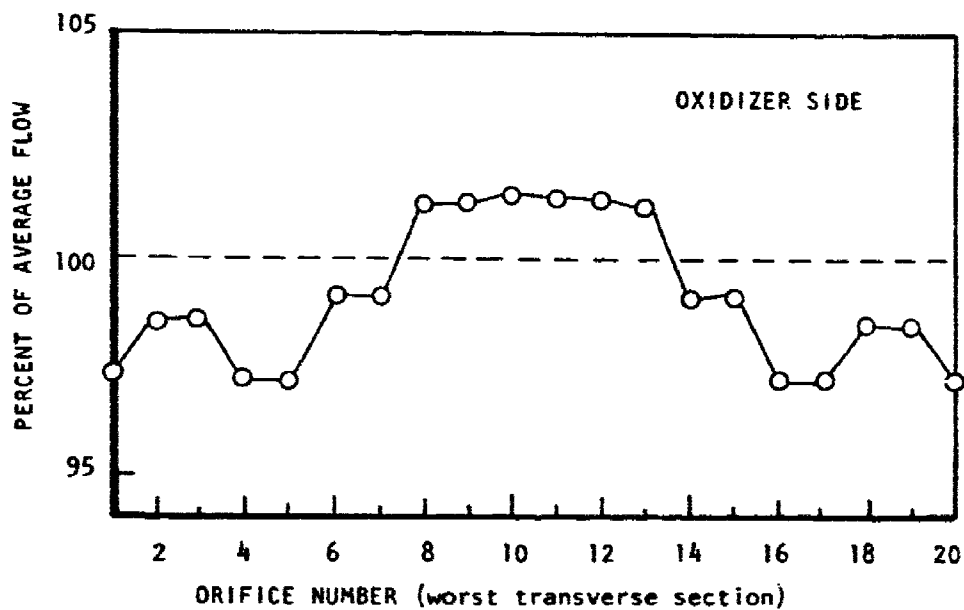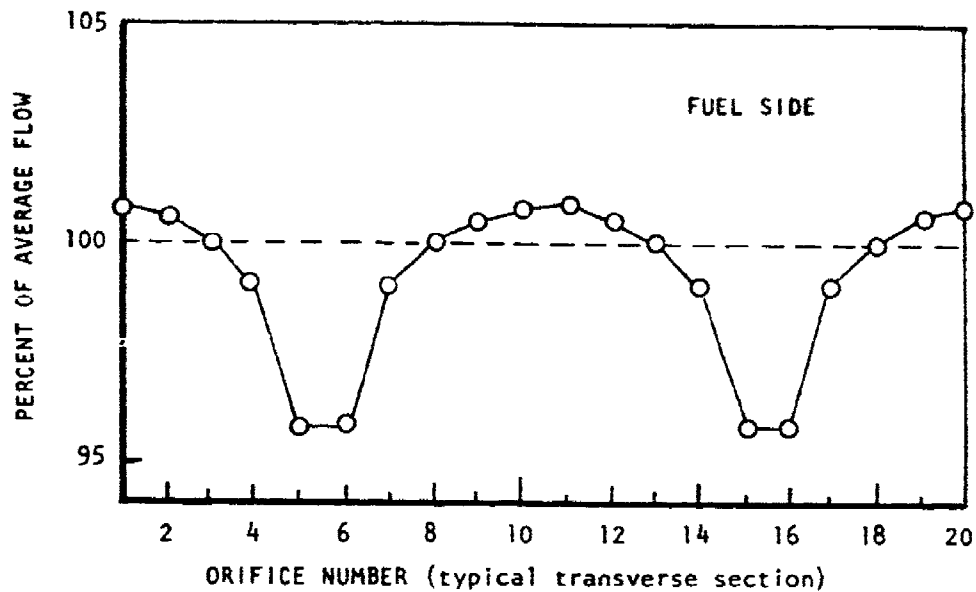
Figure 119.   Predicted Manifold Effects on Flow Distribution.

conducted by Rocketdyne.[33]

1. Oxidizer - O_2

$$h_c = 75 \frac{G^{0.8}}{d^{0.2}} (\frac{278}{T_w})^{1.2} [\frac{w}{cm^2 K}]$$

2. Fuel - JP-4

$$N_{Nu} = 0.0055 (N_{Re})^{0.95} (N_{Pr})^{0.4}$$

where

$$G = \frac{\dot{m}}{A}, \text{ in } kg/(mm^2 sec)$$

$$d = \text{orifice diam, mm}$$

$$T_w = \text{wall temperature, K}$$

A two-dimensional model of a typical injector section was analyzed. This model, which is illustrated in Figure 120, included both fuel and oxidizer orifices and distribution passages. The injector was analyzed for both copper and nickel face materials. Based on the cyclic life considerations, a copper face material was selected. The copper face was analyzed for fuel inlet temperatures of 422 K and 294 K. These corresponded to fuel which had passed through a regenerative-cooling jacket and fuel which was at ambient temperature. The temperature distribution in the injector element is illustrated in Figure 121. Maximum injector face temperatures were 385 K for ambient temperature fuel and 432 K for a regenerative coolant fuel. These temperatures were well within the allowable values for copper.

The transient analyses indicated that the injector reached steady-state temperature in approximately five seconds. In the three seconds typical of operation with a solid wall combustor, approximately 80% of maximum steady-state temperature was attained. Since the LO_2 preceded the fuel in the combustor start-up operation, the injector temperature dropped to 170 K and then rose to the steady-state values.

---

[33] Hines, W.S., "Turbulent Forced Convective Heat Transfer to Liquids at Very High Heat Fluxes and Flow Rates," RR61-14, Rocketdyne, Division of North American Aviation, November 1961.

251
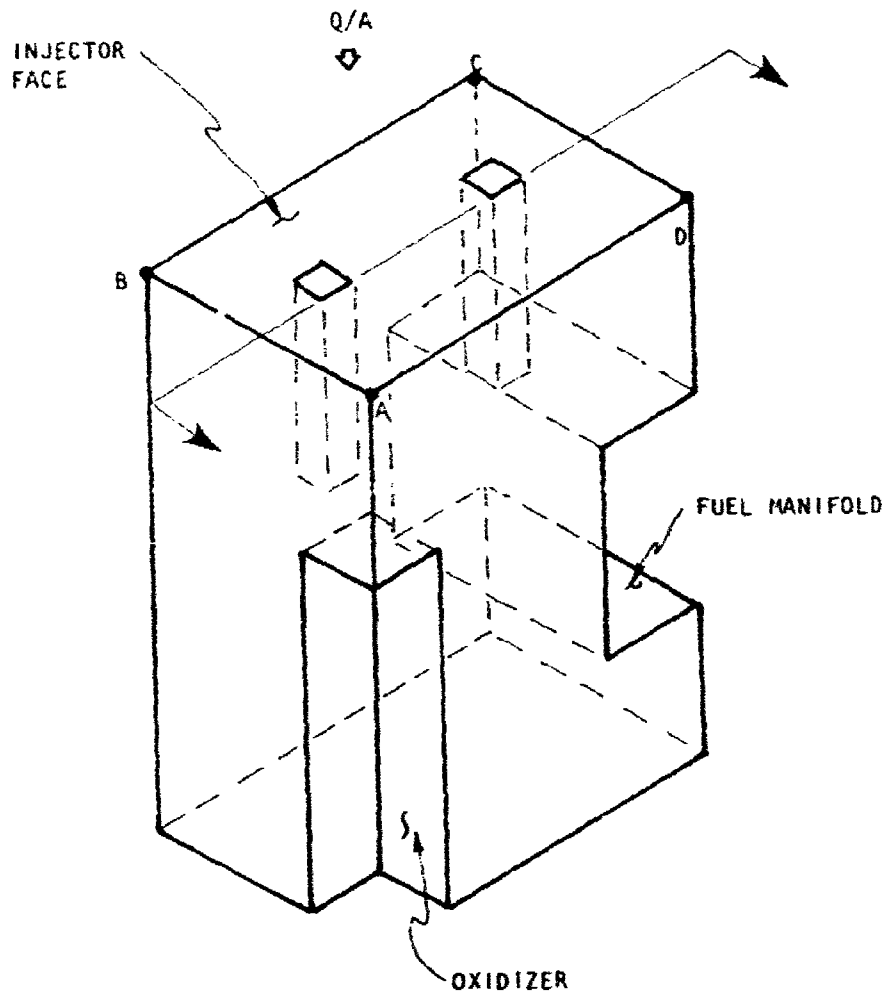
Figure 120. Injector Model Identification.
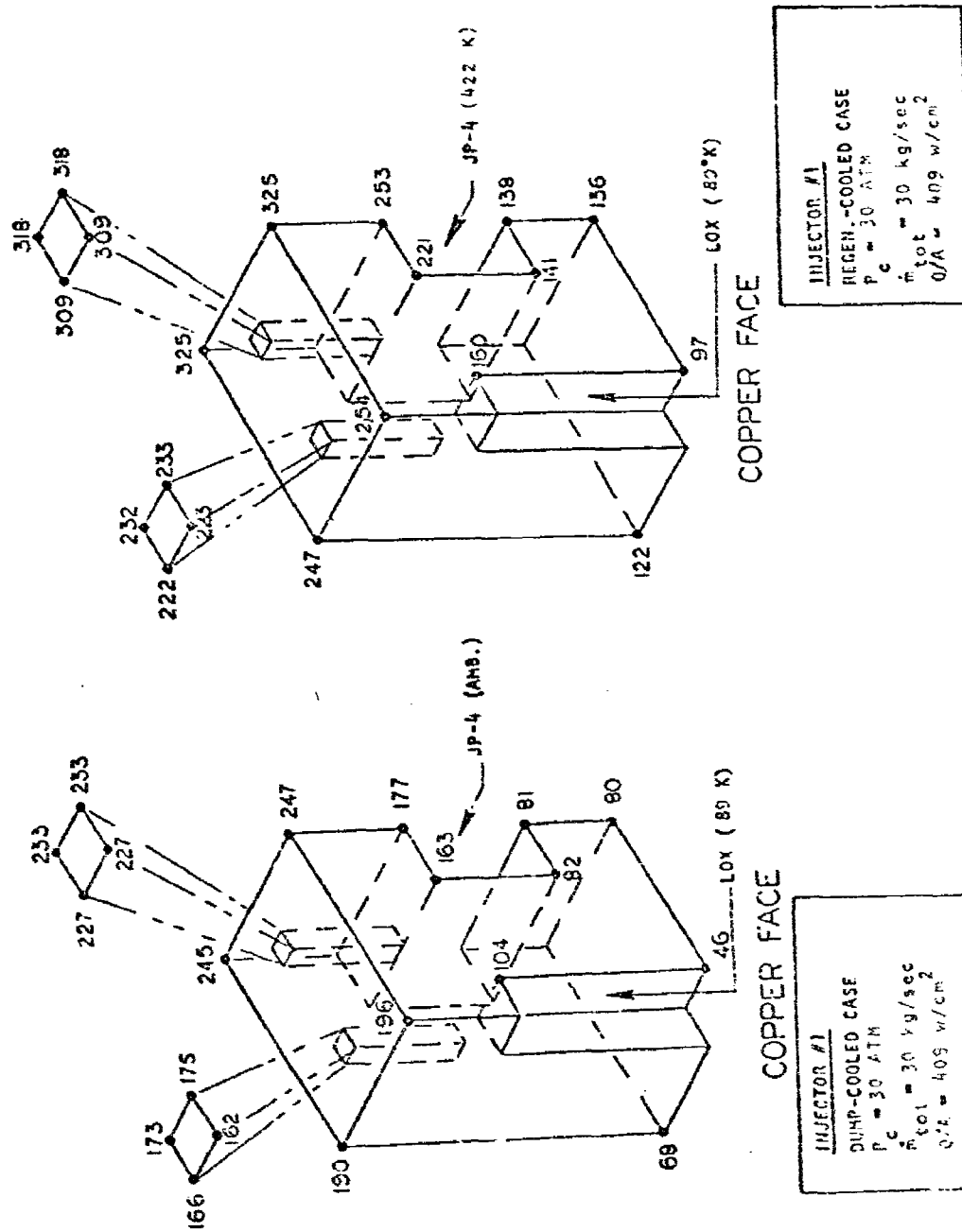
Figure 121. Injector Face Thermal Characteristics.

253

5. Structural Analysis

The ability of the injector body design to withstand the defined operating loads was verified through finite element analyses.[34] These analyses were conducted at maximum operating pressure for both steady and transient operating conditions. The pressure load safety factors were 8 or greater at all locations. The cyclic life of the injector was also analyzed under the combined pressure and thermal loads. The injector design was capable of over 700 full thermal cycles, including a safety factor of four. The minimum life location was at the rear of the LO_2 manifold.

The reactant manifolds were analyzed for pressure loading; safety factors on ultimate strength were greater than 4.5. Because of the axial growth of the combustor during operation, the manifolds could be subjected to large mechanical loads which would be difficult for the brazed connections to withstand if the control valves were rigidly mounted. The feed system was designed to avoid these loads. The fuel feed line and valve mount were designed to slide allowing axial movement which could be absorbed by the bends in the feed line. The LO_2 line from the rigidly mounted valve was designed with a double bend so that axial movement could be absorbed without inducing large injector load. With these design features manifold mechanical loads were within acceptable limits.

6. Design of 416 Element Injector

Following the initial design, the combustor was rotated 90 deg to accommodate a revised magnet. The 416 element injector design was not modified since the 160 element design had been selected. The 416 element injector assembly consisted of the injector body, mounting flange, LO_2 manifold and fuel manifold. The injector was designed to have a common interface with the 160 element injector.

a. Manifolds

The LO_2 and fuel manifolds were similar to those of the 160 element injector. The LO_2 manifold exited the injector on the centerline and made a right angle turn to connect to the double bend LO_2 feed line. The fuel manifolds entered at four places on the injector side and were brought to a common, on-centerline collector/flange.

b. Injector Body

The injector face plate and body are illustrated in Figure 122. The face plate was machined from Amzirc, a copper-zirconium alloy. The 416 injector element pairs were arranged in a rectangular pattern. This resulted in an injection element "density" of 1.75 elements/cm^2.

---

[34] SAAS 1, E. L. Wilson and R. M. Jones: "Finite Element Stress Analysis of Axisymmetric Solid with Orthotropic, Temperature Dependent Material Properties," TR-0158 (S3216-22)-1, The Aerospace Corporation, San Bernardino, California, (Sept., 1967).

285.6mm

43.2mm
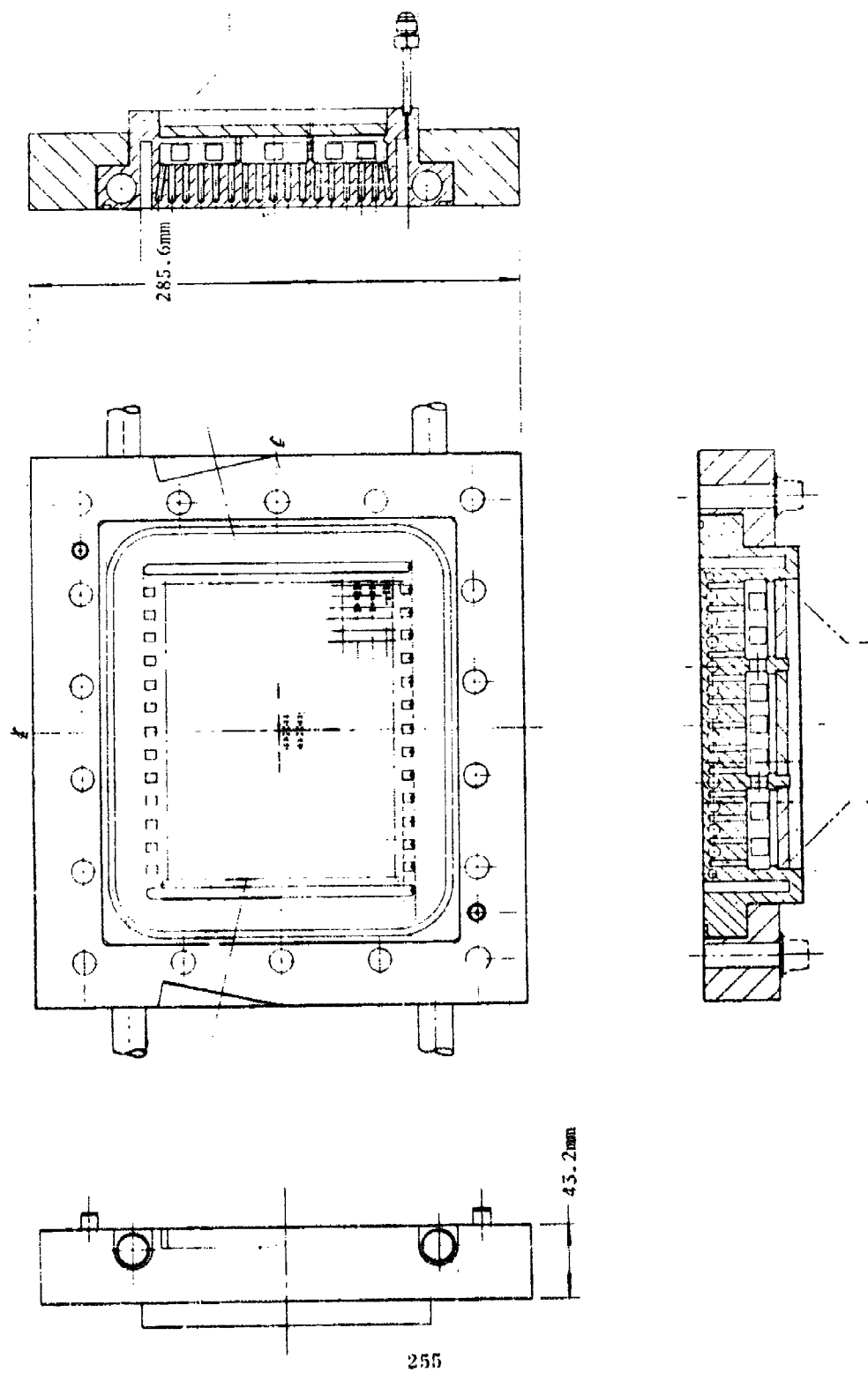
Figure 122. 416-Element Injector

255

The fuel entered the injector body at four locations on the side of the injector and was fed into fourteen vertical distribution passages which, in turn, fed a series of individual orifices. A typical fuel element is illustrated in Figure 123. The orifices were 0.058 cm diameter and are canted at an impingement angle of 30 deg. A total of 832 individual orifices were provided. The two outer distribution passages fed a series of single orifices. These orifices were canted inward to avoid wall impingement. The remaining passages fed orifice pairs. This is shown in Figure 124.

The liquid oxygen entered the rear of the injector and flowed to nine distribution manifolds through a series of rectangular passages. Restrictor plates in the distribution manifolds promoted uniform reactant distribution. Each distribution manifold fed approximately twenty-four axially-oriented orifice feeder passages. Each feeder passage delivered flow to two injector elements. A typical oxygen element is illustrated in Figure 123. The orifices were 0.086 cm diameter and were canted approximately 30 deg. The orifice length was 0.37 cm. A total of 832 individual orifices were provided. The outer row of individual orifices were directed axially to avoid impingement on the combustor wall.

A series of slots were machined into the copper to provide acoustic damping. Because of the fuel feed passages, the slots on the top and bottom were reduced to a series of individual holes. Each of the bottom slots was purged with gaseous nitrogen to avoid accumulation of reactants. An O-ring groove was machined into the copper to provide a gas seal.

c. Injector Flange

The injector body was brazed into a stainless steel flange. The flange contained the 18 bolt holes for mounting to the combustor. Sections on the flange edge were cut out to avoid interference with the ignitors. Locating pins were provided to assist in assembly of the injector to the combustor.

d. Material Analysis

The materials used in the injector were Amzirc and corrosion resistant stainless steel (CRES). The Amzirc, which is a copper zirconium alloy, was selected over OFHC copper because of its higher strength. The higher strength was necessary because of the large number of flow passages which reduced the amount of material cross section in the body. The CRES was selected on the basis of good strength and the ability to be brazed. The CRES also closely matched the thermal expansion characteristics of the Amzirc which contributed to long cyclic life.

0.50mm Cl. OXIDIZER

0.58mm DIA FUEL

11.0mm

30° TYP

12°30' TYP

15.7mm
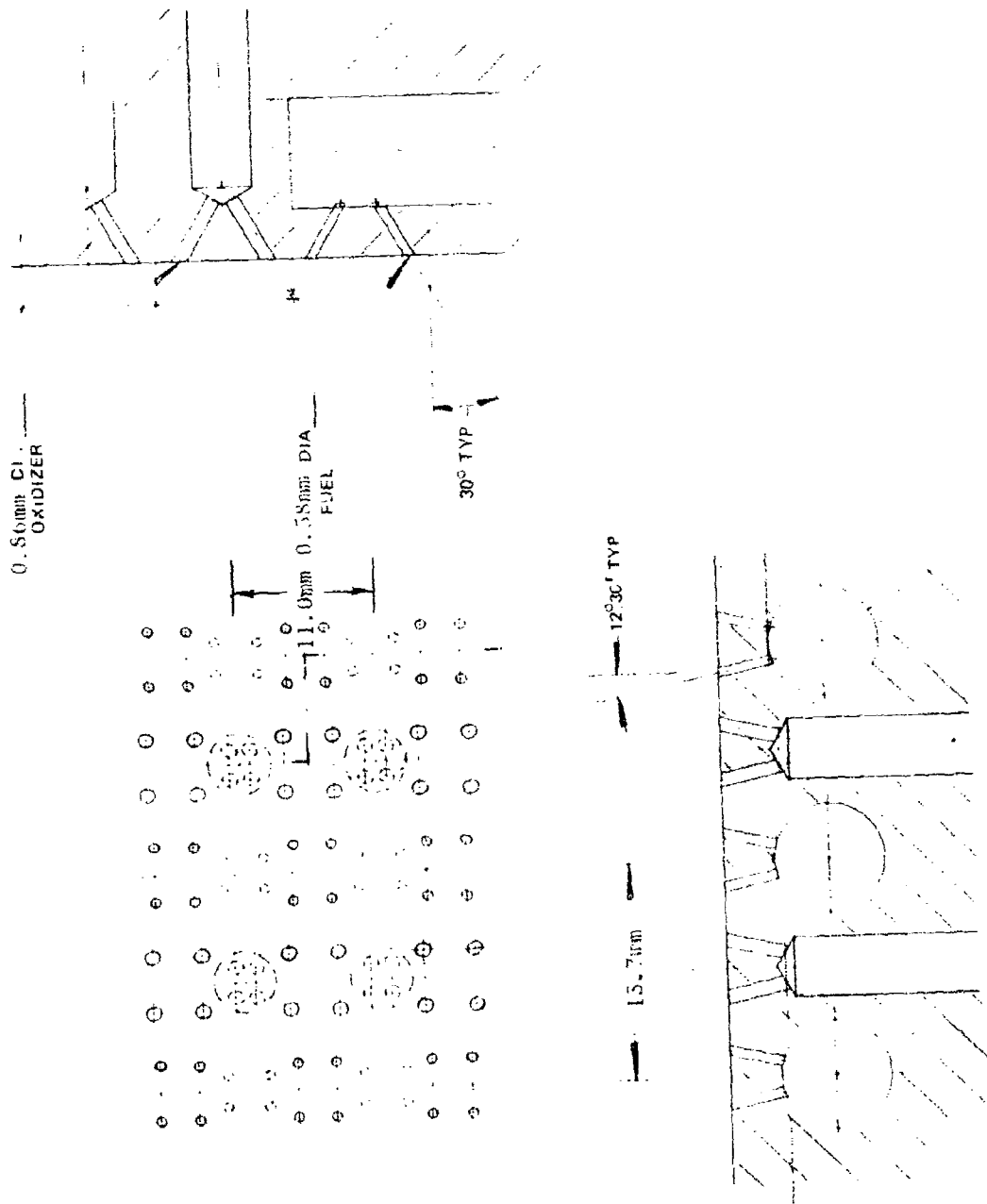
Figure 123. Fuel and Oxidizer Elements for 416-Element Injector
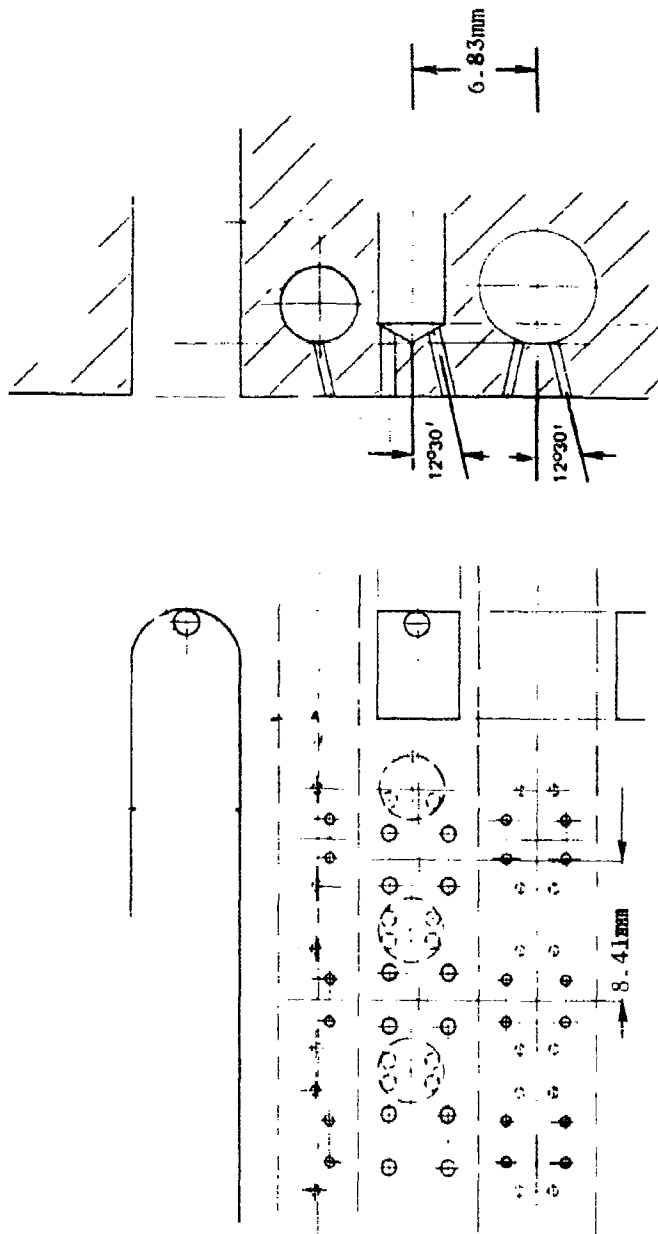
Figure 124. Wall Fuel Elements

7. Fabrication

Based on the evaluation of the relative fabrication difficulty, the 160 element injector was selected for fabrication. The 160 element injector was fabricated in four major components, which were brazed and welded into the injector assembly.

The injector body was machined from a solid piece of OFHC copper. The rear of the body, shown in Figure 125, was initially fabricated by machining out the three LO_2 manifolds, drilling the feeder passages for the fuel and oxidizer, and then electric discharge machining the square LO_2 manifold connector passages. Following this, the injection element orifices were drilled in the front of the body and the entire unit deburred.

The LO_2 and fuel external manifolds were fabricated from a variety of tubes which were cut and welded in place. The flange for the fuel manifold connection was welded directly to the manifold while an AN-type fitting was used on the LO_2 manifold to facilitate assembly. The manifolds were plugged and proof tested following fabrication.

Both the steel flange which housed the injector body and the acoustic cavity spacer were machined from solid pieces of material. Following acoustic cavity revision to provide added damping, the acoustic spacer was redesigned to include a water-cooled copper insert. This insert was machined from OFHC copper and fitted into the stainless steel spacer which had been modified to serve as a flange.

The injector body, flange, and internal elements were brazed together as illustrated in Figure 126. Following this, the LO_2 manifold was welded to the body. The fuel manifold was then torch brazed to the body to complete the injector assembly, which is shown in Figure 127.

In addition to the dimensional checks and internal inspections which were conducted during fabrication, the entire injector assembly was subjected to flow, proof and leak tests. The flow test illustrated in Figure 128 was used to verify that the reactant impingement pattern met the design goal. Although the flow rate in these tests was considerably lower than the nominal values ($\sim 30\%$), the impingement and spray fan formation of the fuel elements were found to be correct as shown in Figure 128. All of the orifices were clear, and the impingement points were consistent with the design. The impingement of the LO_2 elements was of similarly high quality.

259
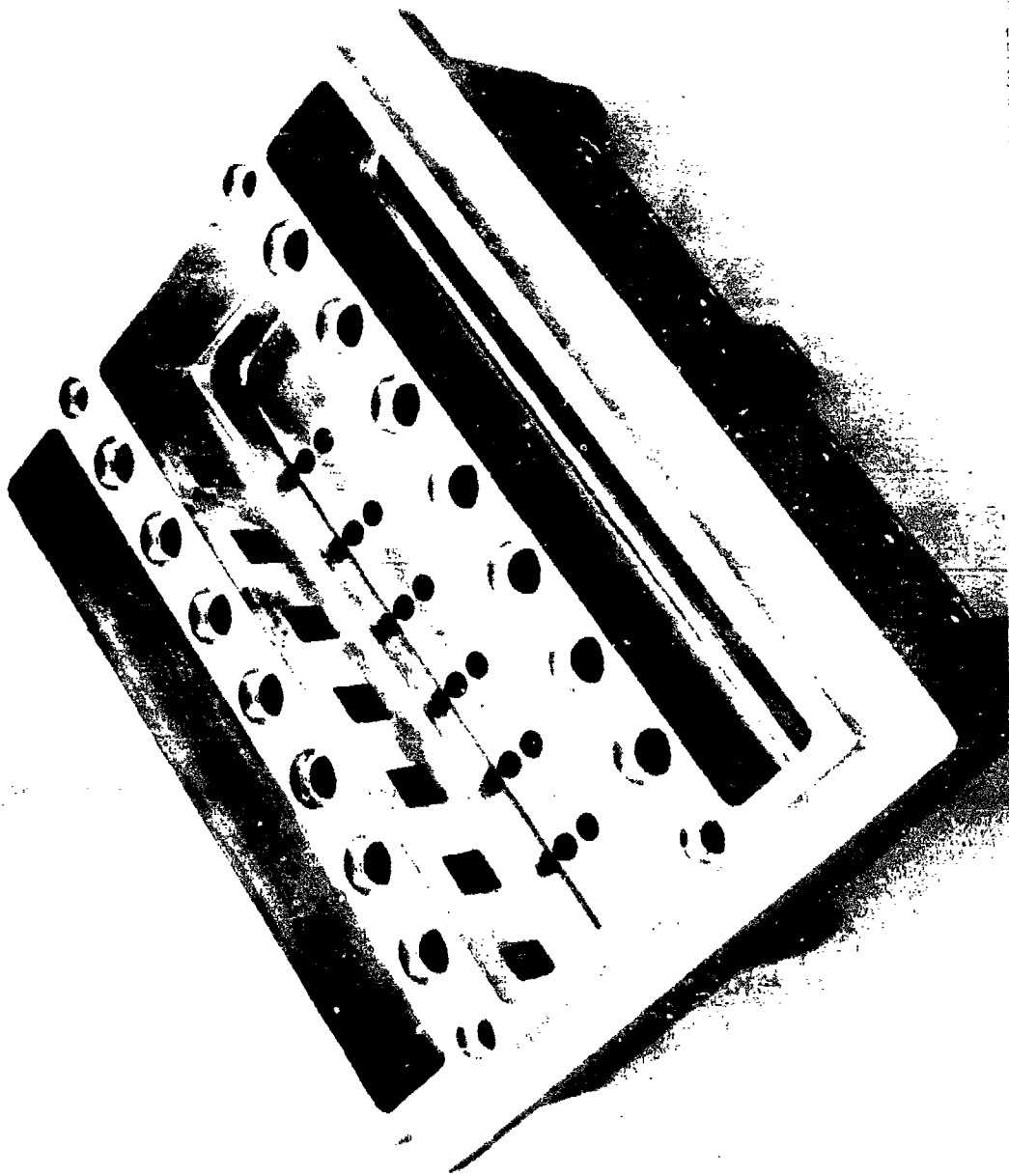
Figure 125 . Injector Body, Upstream Side
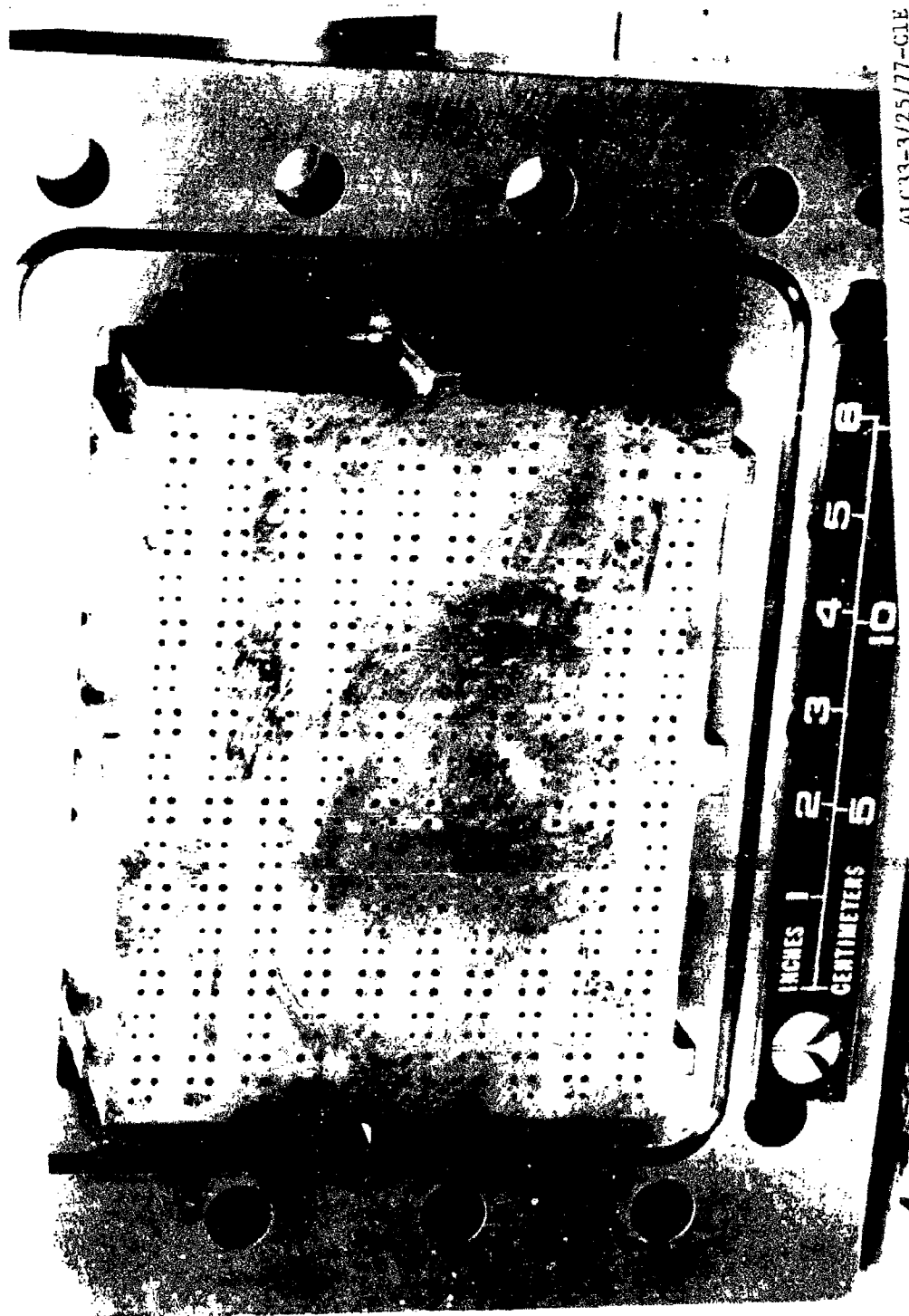
Figure 126. Assembled injector

INJECTOR

LOX MANIFOLD
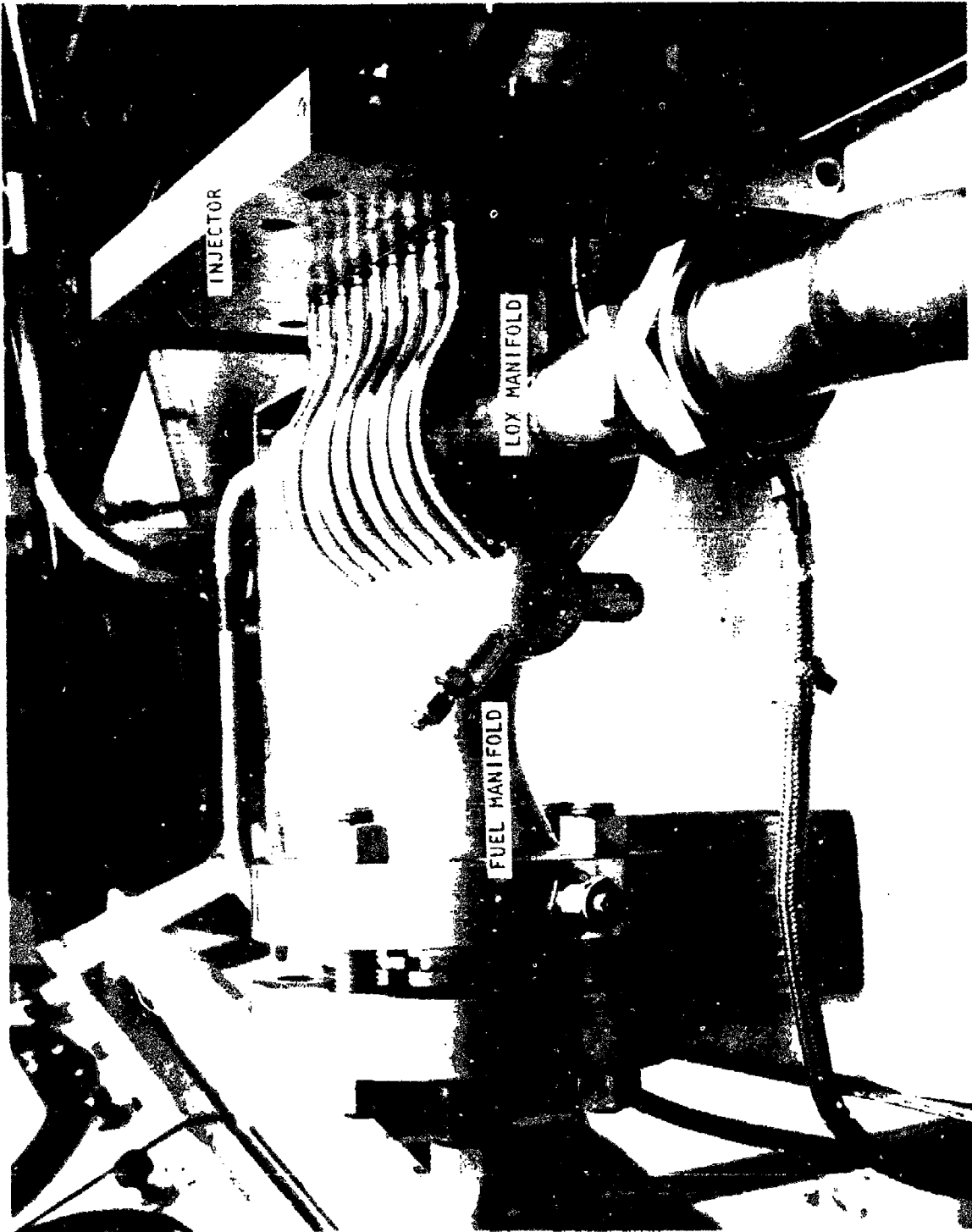
FUEL MANIFOLD

41E34-9/21/77-C1A

Figure 127. Assembled Manifold System
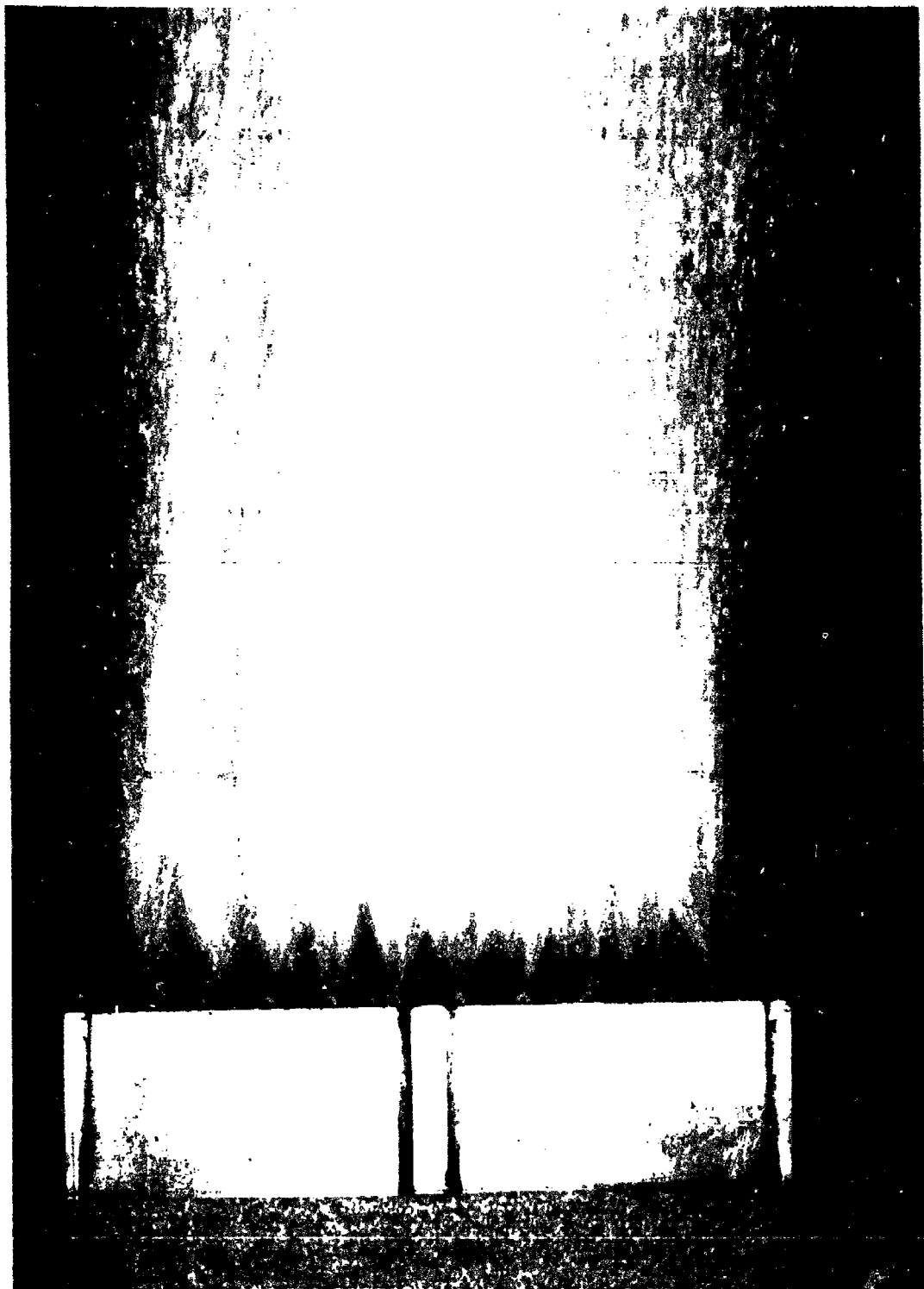
Figure 128. Injector Flow Test

41E34–9/21/77–C1E

263

The fuel and oxidizer sides of the injector were separately proof-tested at 109 atm and 116 atm, respectively, for a minimum of 30 sec. These proof pressures were 50% higher than the maximum anticipated pressure in the injector. The proof test used water under flowing conditions. A low pressure (6.8 atm) helium leak test, conducted following proof test, verified that no internal leakage paths were created. Following this, the injector was cleaned prior to installation on the combustor.

D. IGNITION SYSTEM

1. Component Requirement/Approach

The MHD gas generator combustor Augmented Spark Igniter (ASI) had several basic design requirements. These resulted in the hot core ignition device which supplied high temperature gases that ignited the reactants of the main combustor. The combustor ignition system design requirements were to (1) provide reliable and repeatable chamber reactants ignition; (2) permit unlimited restarts; (3) make maximum use of existing experience and J-2 hardware; (4) be capable of operating in an external environment of 273 to 373 K and an internal environment of 173 to 1273 K; (5) minimize system complexity; and (6) be compatible with a magnetic field.

Having established the component requirements, the combustor ignition system assessment approach was to make maximum use of past experience, to base the configuration on existing proven concepts, and to design for high reliability and redundancy. A review of the main combustor requirements dictated main chamber ignition within a second and a rapid restart capability. With these goals in mind the ASI was designed, fabricated and tested.

2. Performance Analysis

An analysis was conducted to compare the predicted 30 MW MHD gas generator ASI ignition thermal characteristics with those experienced on other test programs. A summary of the analytical results of the ASI are as follows:

Parameter	MHD ASI
Percent Flow: ASI to GG	0.5%
Stoichiometric	GO_2/CH_4
Temperature	3370 K
ASI Mean Temperature	1215 K
ASI Heat Release	0.429 MW
ASI Heat Release per Gas Generator Injector Mass Flux Density	21.6 kw-kg/cm^2-sec

Using these results, a comparison to other programs was made. The high power gas generator dual ASI ignition thermal output was concluded to be sufficient to ignite the main combustor LO_2/JP-4 reactants. The analysis conducted compared the ignition thermal characteristics predicted to those actually realized from the Atlas sustainer igniter. The percent of ASI to gas generator flow rate was higher for this ASI, the stoichiometric and mean temperature values were similar, the heat release was three times greater and the heat release per injector mass flux exceeded that used on the Atlas sustainer igniter.

3. Design

Previous Rocketdyne experience showed that when a close timing sequence was used to attain a rapid start and transition to main stage, the possibility existed for the formation of gelled JP-4 and LO_2 droplets in the combustion chamber at the time of ignition. These gelled droplets could be explosive and could spontaneously detonate, but they also retarded smooth ignition. Any detonation at ignition could result in hard starts and/or rough combustion. In order to preclude the possibility of gel formation/ignition delay/detonation, high heat energy for initiation of combustion uniformly throughout the combustor volume was required. The ignition device was located in a position to diffuse its hot gases over the entire combustor flow section. Since the analysis indicated that a single ASI would not be able to diffuse hot ignition gases throughout the combustor section, two ASI's, located opposite each other and firing at an angle down and across the combustor, were chosen as providing the best dispersion of ignition hot gases in order to achieve uniform ignition throughout the combustor.

a. Design Description/Illustration

The high power MHD gas generator combustor ASI was a hot core ignition device which supplied the high temperature gases that ignited the reactants of the main combustor. The high temperature gases were produced by combustion of gaseous oxygen and methane initiated by an electrical discharge spark. The ASI consisted of injector, combustion chamber, and discharge barrel. The device was designed to have a wide range in mixture ratios and, therefore, temperature across the chamber internal diameter. Mixture ratios and temperatures will range from oxidizer rich conditions at the center to extremely fuel rich at the walls. This was accomplished by using a doublet, oxidizer injector element to provide an oxidizer fan across the chamber diameter. Fuel was injected through eight tangential swirl orifices near the impingement point of the oxidizer jets. The fuel momentum caused some fuel to be mixed with the oxidizer in the center of the chamber to provide an oxidizer rich combustion and extremely high temperatures. The rest of the fuel formed a boundary layer

265

along the chamber wall and acted to film cool the wall from the hot core. Ignition of the oxidizer and fuel was accomplished by a capacitance discharge, surface gap spark ignition system. The oxidizer and fuel orifices, as well as the spark plug, have also been positioned such that a combustible mixture will be located in the high energy field of the spark discharge.

Figure 129 illustrates the fabricated and procured ASI components. During the ASI evaluation discussed in Section VIII, the concept was modified slightly, and a new chamber liner was used. This liner was an uncooled liner and had a one second maximum operational limit as shown in Figure 130. The ASI was fabricated from OFHC copper because this material was compatible with the reactants and combustion products, had a high conductivity for cooling, and possessed satisfactory structural properties. The ASI assembly is illustrated in Figure 131.

b. Supporting Analysis

Four basic ignition system designs were examined in an attempt to evaluate the outstanding characteristics of the system best suited for the gas generator requirements. The four basic systems and brief comments concerning each system are summarized in Table 31.

When the review of the four systems was completed, the augmented spark ignition system was chosen as having the most desirable characteristics for the application required. After selecting the ASI system concept, several other variables remained to be answered. The ASI concept was reviewed to determine the requirement for a hot core or uniform temperature device. Reactant candidates were reviewed, evaluating GO_2/GH_2 and GO_2/CH_4. A cooled liner versus an uncooled liner was investigated. The location of the ASI units, that is, axial or lateral or single versus multiple, was also evaluated. Finally, the spark system was analyzed to determine the spark system power output. The final configuration resulted in the following:

Reactants	GO_2/CH_4 (Ambient)
Liner	Cooled
Location	Lateral
Number	Two (Redundancy)
Spark	Cable Connected (90 mJ)
Concept	Hot Core (J-2)

HIGH VOLTAGE INTERCONNECT CABLE

SPARK PLUG

EXCITER ELECTRONICS

COOLED LINER

INJECTOR

U.S.
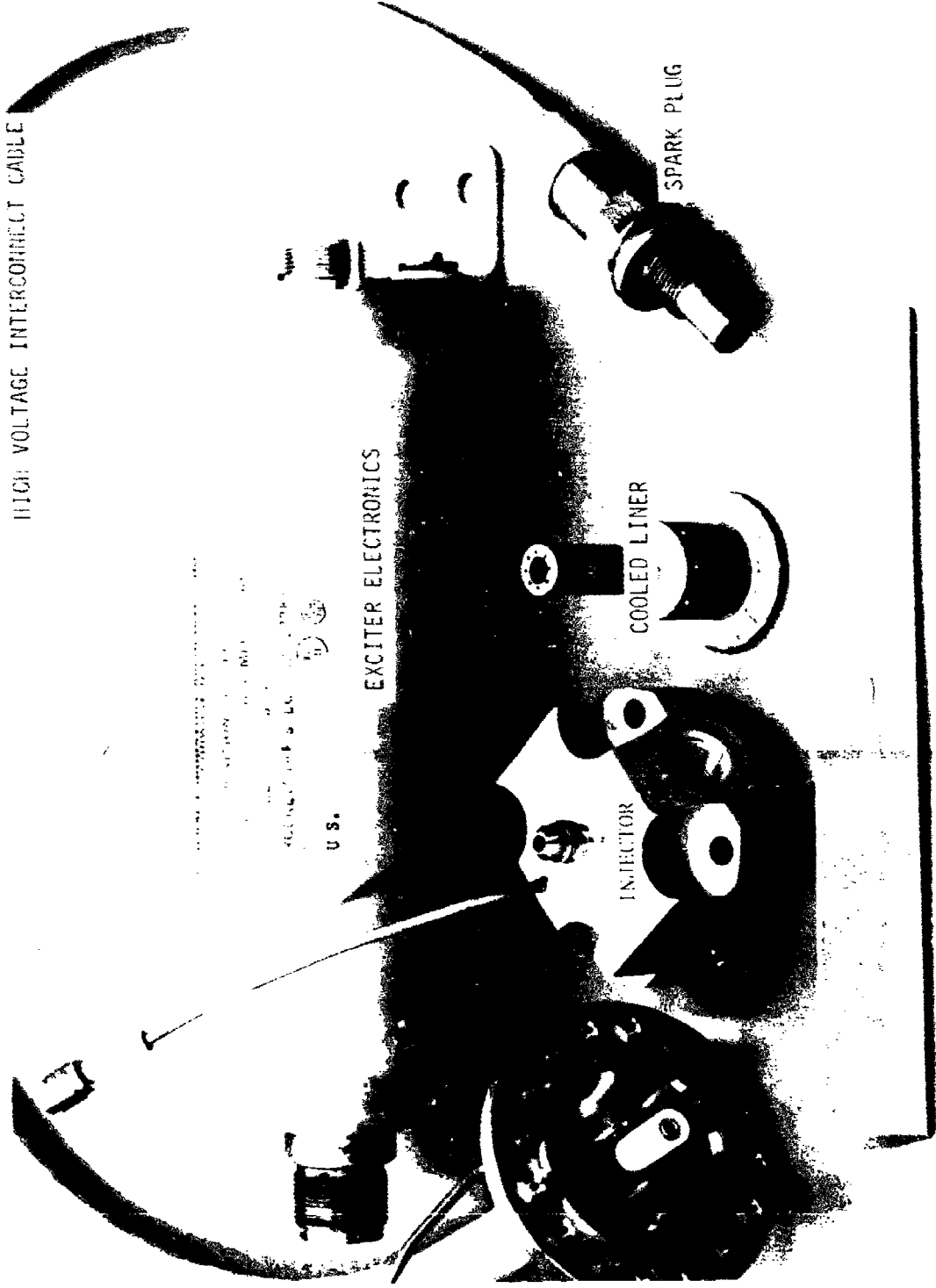
41C33-3/25/77-C1B

Figure 129. AS1 Hardware

267
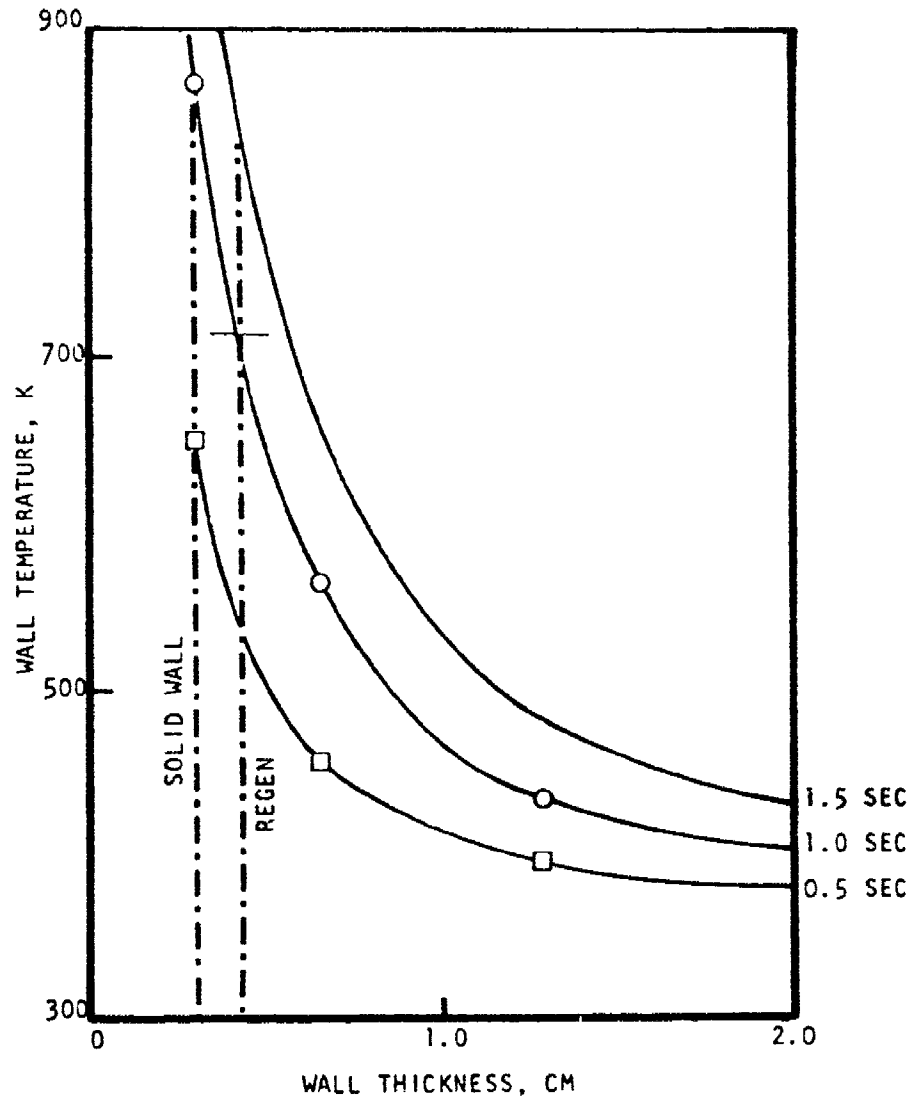
Figure 130. ASI Combustor Temperature Prediction.

FUEL INLET

OXIDIZER
INLET
FITTING

ASI COMBUSTOR

SPARK PLUG

HIGH VOLTAGE
INTERCONNECT
CABLE

EXCITER
ELECTRONICS
ASSEMBLY
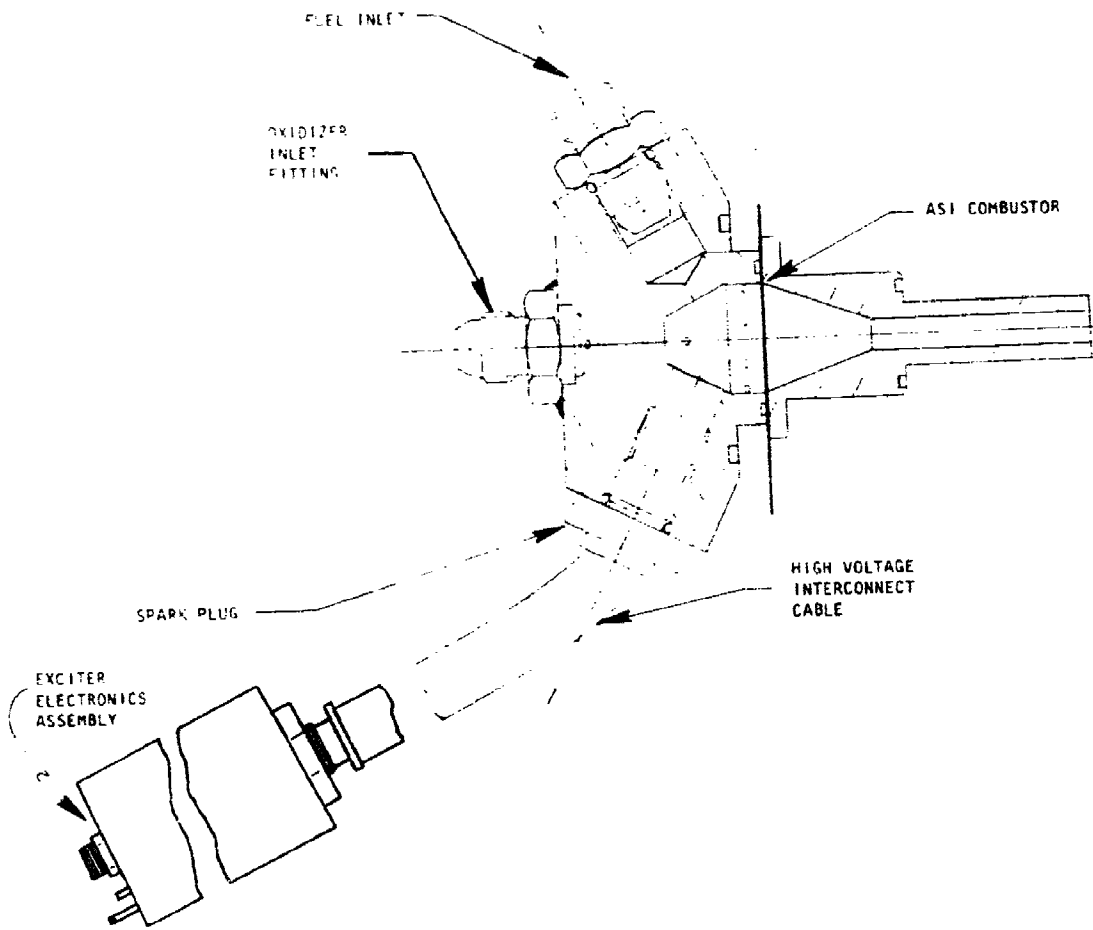
Figure 131.   ASI Assembly

TABLE 31. IGNITION SYSTEM ALTERNATIVES

PYROTECHNIC IGNITION

1.	Considerable experience in single start LO_2/RP-1 applications was available.

2.	A complex arrangement would be required for restart capability.

3.	The potential safety hazard because of electrical squibs in a magnetic field was considerable.

COMBUSTION WAVE IGNITION

1.	The ignition system would be external and outside of the magnetic field.

2.	Related experience applicable to multi-combustor LO_2/LH_2 and GO_2/NG systems was available.

3.	Because LO_2/JP-4 required a relatively large energy source for ignition, a continuous pilot would be required.

HYPERGOL IGNITION

1.	Considerable experience existed for LO_2/RP-1 applications.

2.	A complex feed system would be required to provide restart capability.

3.	A potential safety hazard because of the use of the hypergol fluid.

AUGMENTED SPARK IGNITION

1.	Considerable past experience existed.

2.	Unlimited restart capability was provided.

3.	Some concern pertaining to the routing of spark cables inside a magnetic field was needed.

4.	Two units could be used for increased reliability.

After evaluating the specified configuration, a change to the liner geometry was made. The cooled liner chosen after an extensive thermal analysis was replaced with an uncooled version and limited to one second operational time. A transient wall temperature analysis was conducted to support the change, a summary of this is presented in Figure 132.

Analyses conducted in support of the ASI design included performance, stability, thermal, materials and instrumentation. The performance analysis resulted in the following:

ASI Flow Rate	0.5% of main combustor ($\sim$150 g/sec)
Reactants	Ambient GO_2 and CH_4
Combustion M.R.	1.0
Combustion Temperature	1215 K
Combustion C*	1408 m/sec

An assessment of the instability potential of the ASI combustor was conducted and showed the calculated instability frequencies to be high. When the frequencies were high, they were not likely to have sufficient driving energy to excite an instability mode. Therefore, instabilities were not expected.

The material characteristics of the ASI were reviewed and the OFHC copper was shown to be compatible with the reactant and combustion products. The OFHC could also be brazed and possess high conductivity for cooling. The instrumentation analyses resulted in static pressure measurements for the chamber pressures and injection pressures. Spark on-off operation and ignition detection using chamber pressure were monitored.

4. Fabrication

a. ASI Body

The ASI body was fabricated from OFHC copper to the basic J-2 configuration as illustrated in Figure 131. The body contained the oxidizer manifold orifices and the tangential fuel orifices. Provisions were made to measure the combustion chamber pressure by a pickup located in the dome. The impinging oxidizer orifices were reworked during the hot fire test series to decrease the velocity. These orifice diameters were increased to 0.244 cm. The eight tangential fuel orifices remained at 0.118 cm diameter per the specified drawing.

271
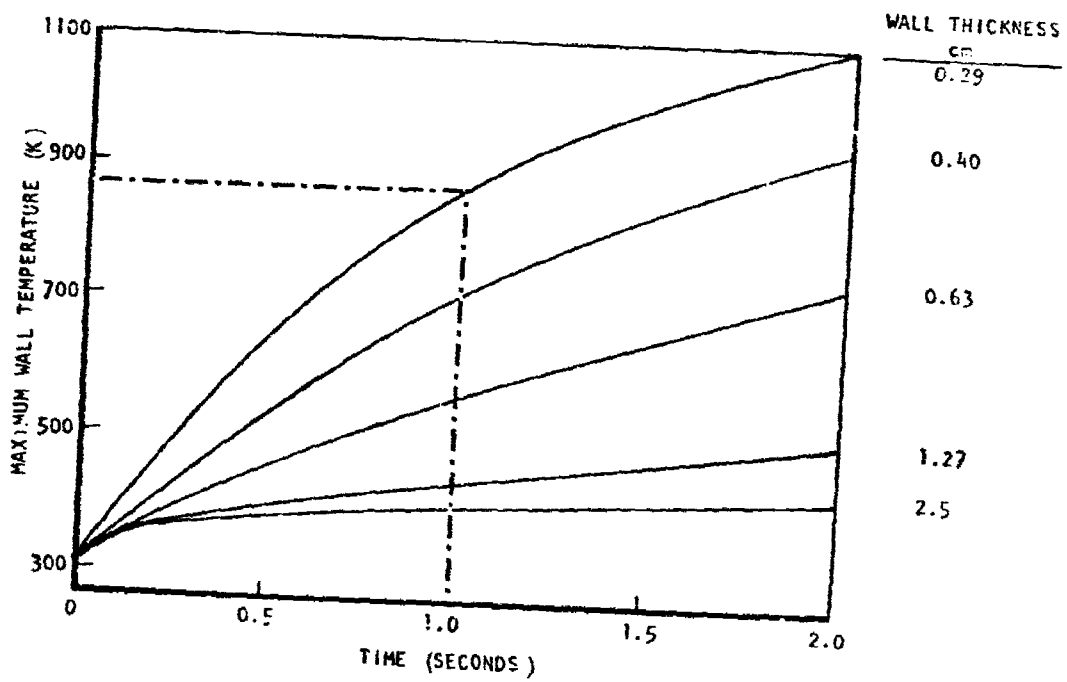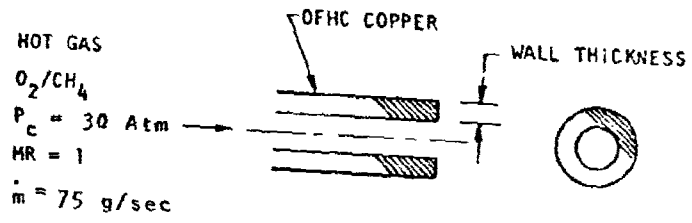
Figure 132. Transient Wall Temperature History for Uncooled MHD ASI.

272

b. Exciter and Cable Checkout

During the initial program evaluation exciters, spark plugs and cables were utilized from the J-2 program. These items were tested in the development laboratory in an attempt to find three exciters and four spark plug assemblies that would meet the specifications shown in Table 32.

The spark plug and cable assemblies were visually inspected for obvious damage or excessive plug wear. Initially the majority of the spark plug and cable assemblies failed the dielectric strength test. This was because of the accumulation of deposits inside the spark plug tip. To remove these deposits, the spark plug and cable assemblies were abrasively cleaned. After cleaning, the dielectric strength test was repeated. The performance of the spark plugs and cables improved to meet specification requirements.

The plug and cable assemblies that passed the dielectric strength test were then subjected to the insulation resistance test. A voltage of 500 V dc was applied between the cable conductor and the cable shield for one minute. The resistance was then measured with a megohm meter. Three plug and cable assemblies checked out per specification requirements. Two plug and cable assemblies checked out at one megohm, and these may be used as spares. Leak checks were performed on plug and cable assemblies after the above tests were completed and four assemblies passed this test.

The exciters were visually inspected for any obvious damage. An insulating resistance test was then performed on the exciters with a voltage of 500 V dc applied. The resistance measurement was made two minutes after the voltage was applied between all mutually connected ungrounded inputs and monitor pins and the enclosure. All units passed the test. For the monitor output test the exciter was mated with its proper igniter load and tested for its monitor output signal, +1 to +4 V dc. Again, all passed. The final test of the exciters was the spark rate test. The exciters were mated to their proper igniter loads and tested for a minimum spark discharge rate of 40 sparks/sec. All igniters passed the test.

In summary, five functional plug and cable sets and six functional exciters were identified. The tests performed on the exciters were: (1) visual inspection for any obvious damage; (2) insulation resistance; (3) monitor output; and (4) pulse rate.

273

TABLE 32. SPECIFICATION REQUIREMENT

PARAMETER	REQUIREMENTS
EXCITERS	
Spark Rate	40 Hz, min
Monitor Output	1 to 4 V dc
Insulation Resistance	$>$ 1000 mΩ @ 500 V dc
Dielectric Strength	None
Leakage	None
PLUG/CABLE ASSEMBLY	
Leakage	$\leq 6 \times 10^{-9}$ cm^3/sec
Insulation Resistance	$>$ 1000 mΩ @ 500 V dc
Dielectric Strength	30 μa, max @ 25 kVdc, 102 atm

The tests performed on the spark plugs and cables were: (1) visual inspection of spark plugs and cables for any obvious damage or excessive plug wear; (2) dielectric strength; (3) insulation resistance; and (4) leakage.

c. Igniter Assembly

The igniter assembly as illustrated in Figure 129 was fabricated primarily from OFHC copper. The body described previously was subsequently brazed to include the GO_2 inlet fitting and the chamber pressure measuring tube. This completed assembly formed the combustor dome.

The liner shown in Figure 129 was a cooled liner and was subsequently replaced by an uncooled liner during the hot fire test series. This substitution of ASI liners is described more completely in Section VIII. The liner was solid without the provisions for the dump coolant. The internal geometry was identical, with the liner forming the convergent combustor and a cylindrical throat. Figure 129 illustrates the igniter assembly as used in the first hot fire test series. The elimination of the liner dump coolant permitted stable operation with simple flow control devices.

SECTION VI

FEED AND SUPPORT SUBSYSTEM DESIGN AND FABRICATION

A. INTRODUCTION

The gas generator feed system for the 30 MW high power MHD system provided the fluid lines, flow control, and instrumentation for the gas generator. This feed system represented the test article and did not include the facility fluid supply system. The gas generator feed system was originally designed for testing at both Rocketdyne and AEDC. Therefore, simple line connections were used between the gas generator feed system and the facility fluid storage system. The feed system included: (1) liquid oxidizer feed system; (2) fuel (JP-4) feed system, (3) seed (cesium carbonate) feed system; (4) ignition oxidizer (GOX) feed system; (5) ignition fuel (methane) feed system; (6) gas generator combustor coolant (water) feed system; (7) MHD channel coolant (water) feed system; (8) purge gas (GN_2) feed system; (9) seed tank pressurizing gas (GN_2) feed system; (10) bleed, vent, drain, and relief discharges; and (11) associated components and pipings. The feed system was designed to interface with the AEDC facility feed system, liquid fuel gas generator assembly, and the Maxwell MHD channel. The system contained instrumentation components, i.e., flow control components, venturis, and pressure and temperature transducers. The system was integrated with the electrical control system and support structures.

B. SEED MIXER

The major design requirements considered for the design of the seed mixer were: (1) cesium carbonate (Cs_2CO_3) as the seed material; (2) variable seed injection rate ranging from zero to 10% by mass of the total reactant requirement including the seed material itself; (3) complete evaporation and ionization of the injected seed within the combustion chamber; (4) uniform flux seeding over the entire cross sectional area of the combustion chamber; and (5) minimum risk to the gas generator system (e.g. against oscillatory flow rate variation) and the injector (e.g. against plug-up of the orifices).

The physical conditions and operating characteristics of the combustor, which also constituted the baseline for the seeding system design are summarized in Table 33. The high temperature conditions prevailing in the combustor were favorable for effecting a chain of the necessary processes (evaporation/dis-association/ionization). The compact combustor design for a high power density

TABLE 33. CONDITIONS AT COMBUSTION CHAMBER

- OPERATING CONDITIONS

  Hydrocarbon Flame (Stoichiometric)

  Temperature, 3450 K (Target);   Pressure, 30 atm

Gas Density	2.9 kg/m^3
Velocity	335 m/sec
Thermal Conductivity	1.2×10^{-2} w/cm K
Viscosity	950×10^{-6} P

  Bulk Flow Residence Time (of Gas) 2×10^{-3} sec

- FLOW RATE

  Combustion Chamber

  $\dot{m}_{tot}$ -- Nominal 30 kg/sec;   Range $\pm 20\%$

  Seed Injection

  $\dot{m}_s$ -- Nominal 1.5 kg/sec

  Range   0, 1 to 10% of Total Flow

277

gas generator system, however, rendered extremely short flow residence times of the order of millisecond magnitude in the combustor chamber. The short residence time, therefore, limited the time available to complete the entire sequence of events required to ionize the seed. This limitation, in turn, limited the size of seed particles injected into the hot combustion gas.

A preliminary task for the seed system design was to establish an optimal seeding system concept configuration which had the capability of meeting all the system requirements. A number of candidate concepts were considered and evaluated in the preliminary phase. The results of this evaluation are summarized in Table 34. The proper selection of a seed transport medium constituted the key aspect of the system design.

1. Seed Transport Medium

The method of the seed transport was divided into three types by the phase of the transport medium: gas, liquid, and neat solid seed via mechanical means. A seeding system relying entirely on a mechanical feed system was ruled out because of the complexity needed for controlling the seed material transport and the injection. This complexity was particularly true for transient operation. Either liquid or gas phase fluid was viable as a transport medium because of the ease of handling. The use of a gaseous transport medium appeared attractive but required considerable development and, therefore, the concept was dropped.

For the selected liquid transport method both water and combustible liquids were evaluated as the cesium carbonate carrier. An assessment of cesium carbonate solubility was made:

Transport Liquid	Cs_2CO_3 solubility, % by Weight
Water	>70. %
Ethanol	~15. %
Assorted Combustible Liquids, (JP-4, etc)	< 1. %

Water provided exceptionally high solubility with cesium carbonate (a saturated water-seed solution was over 70% by mass Cs_2CO_3) and solution stability over a wide range of ambient temperatures. This characteristic was verified through laboratory tests. Alcohol (ethanol) was considered because of its combustible nature and somewhat significant solubility ($\leq$15% by weight). Other combustible liquids (including JP-4) were considered but discarded since the solubility was seldom over 1 wt %.

Both water and ethanol will reduce the temperature of the combustion products because of their lower heating values. However, for 1.5 kg/sec of seed some 9 kg/sec of ethanol is required while only 0.6 kg/sec of water is necessary. The ethanol would effectively replace the JP-4; because of its lower heating value (1460 cal/g vs. 2060 cal/g for JP-4). The temperature reduction would be severe and alcohol was rejected.

TABLE 34. MATRIX OF CANDIDATE APPROACHES

	MIXED-IN INJECTION		DIRECT INJECTION	
	Batch Mixing (Hybrid)	In-Situ Mixing Separate	Solid	Solution
TRANSPORT MATERIAL AND HANDLING	Pre-mixing emulsion (with partial JP-4) followed by simple one-pass mixing.	Transport of seed/water solution and JP-4, followed by one-pass mixing emulsion process.	As Pulverized Seed by Pneumatic Transport. Dense phase transport in GN_2 and gas feeding at storage. Dilute phase transport in GOX and mechanical feeding at storage.	As Dissolved Seed by Fluid Transport. Water Combustible Solvent (e.g. Ethanol).
INJECTION METHOD	Coflow Injection	Seed/JP-4 through JP-4 Injection Orifices	Coflow Injection Cross Flow Injection	Seeding Orifices at Main Injector Plate Seeding Orifices at Two Opposing Walls (e.g. Upper and Lower Walls)

279

Such unusually high solubility and stability definitely favored the seed injection in the form of an aqueous solution, although this method inevitably resulted in some decrease of the combustion gas temperature. According to the results of a series of equilibrium computations, the thermal loss effect was found to be only fractional. Seed injection as a concentrated aqueous solution was further pursued to develop a complete seeding system that was compatible with the overall system and its operation.

2. Configurat' n Selection

Two methods of seed injection were considered, direct injection and mixed-in injection. A description follows.

a. Direct Injection

Direct injection represented the methods and hardware which transported and injected the seed material separate from the main reactants (i.e., JP-1 and/or LOX). The concept involving gaseous transport medium was dropped early in the design selection phase because of the considerable need of development effort. An alternative concept which involved only the aqueous seed solution would facilitate the feed system control. However, the need for separate seed injection orifices and manifolding would have introduced added complexity to the already crowded main reactant injector. An alternate injector location in side walls near the main injector was considered, but after a preliminary analysis the concept was ruled out because of the prohibatively large momentum of the cross flow injectant streams needed to achieve full penetration and uniform distribution into the entire hot core region. Also, the secondary jet streams would be broken up prematurely soon after injection because of the high axial combustion gas velocity of nearly 300 m/sec, which will be attained within a few centimeters from the main injector face.

b. Mixed-In Injection

Mixed-in injection was an alternative configuration which was predicated on a mixing/transport/injection operation intimate with the main reactant flow streams. One candidate concept, wnich would have introduced the least alteration and complexity of the overall system hardware, was to inject the seed solution through the main reactant injector orifices,

The aqueous seed solution was found to be practically insoluble and inmisible in JP-4 and, because of greatly different physical properties of two fluids (e.g. density and surface tension), a homogeneous mixture formed by vigorous mechanical agitation was found to be unstable for an extended period of time (i.e. coalescing, separating and precipitating within a fraction of a second). A simple mixture of the two streams would not have likely provided a stable, homogeneous mixture prior to the point of final injection which was essential to achieve uniform seed flux at the combustor. For this reason a series of laboratory experiments were performed to find a means of affecting the mixing and emulsion with stable suspension of the seed solution in JP-4. The immiscibility of the two liquids was mainly because of the finite magnitude of the interfacial tension, and was reduced by the addition of a surfactant which has been generally determined in an empirical manner for each specific application. An extraordinary surfactant strength was needed for the present application because of the large difference of the surface tension ($\sigma_{JP-4} = 0.7$ cP and σ seed sol. = 7.4 cP as well as the density (S.G.$_{JP-4}$ = 0.78 and S.G. $_{seed\ sol.}$ = 2.33).

Three candidate surfactants were selected for laboratory test by screening each surfactant based on the magnitude of hydrophilic-lipophilic balance, HLB=4, or its neighboring value at which the water-in-oil (w/o) type emulsion was typically prepared in industrial practice. Only one surfactant of those investigated was found effective for the present application. This surfacant was SPAN-80 (sorbitan mono-oleate). A detailed account of the surfactant related test and the results is presented in the section on Surfactant Selection.

Two seeding system configurations which resulted from the mixed-in operation were that of batch mixing and two variations of the in-situ mixing mode. The batch mixing mode operation, despite simplicity of hardware, would have allowed only a single fixed seed input rate per preparation unless an auxiliary neat fuel supply/feed system was provided. Secondly, the batch mixing could have been incompatible with an advanced regeneratively cooled combustor as the additives, especially the seed present in fuel streams, could have unduly formed residue along the coolant passages. These two practical considerations rejected the batch mixing configuration in favor of the in-site mixing system.

The in-situ mixing configuration selected has the surfactant predissolved into the fuel supply rather than the fully subdivided configuration involving additional tankage and feed system for the surfactant. High solubility of the Span-80 in JP-4, in excess of twice the presently needed concentration, was verified experimentally. The JP-4/Span-80 mixture was expected to behave no differently than a pure JP-4 flowing through the regeneratively cooled combustor.

3. Performance Analysis

Seed performance analyses included evaluation of droplet ionization and droplet dispersion.

a. Ionization of Seed Droplets

The seed particles underwent heating, evaporation accompanied with dissocation, and finally ionization of the alkali metal atoms.

With cesium the theoretical characteristic time of the ionization under temperatures and pressures typical of present interest was in the order of 10^{-6} or 10^{-5} seconds. Hence, the ionization aspect of the seeding was excluded from the system design consideration. The maximum critical size of the seed particles vs a specified time or distance from the injector up to the evaporation process was important.

The energetics and mass transfer in the seed evaporation process have been modeled in a rigorous manner.[35] The time dependent variation of seed particle size was obtained by computations taking into account the particle acceleration and effect of drag, both of which vary continuously with time as well as to different extent with the particle sizes locally attained.

The evaporating seed particle size history is plotted in Figure 133 with distance as the abscissa. As expected, the seed particles accelerated to a varied extent depending on the size, the faster acceleration the smaller the particles, thus resulting in varied particle time coordinate as indicated on the curves.

In view of the conservatism practiced in the computation, the results further indicated that the seed particles in excess of 80 μm diam were handled in the 68.6 cm combustor with a comfortable margin. In addition, the upper limit of the particle size indicated above corresponded to over 90 μm diam of the aqueous seed droplet, which was greater than the mean droplet size, defined as the Sauter mean, D_{32}, 63 μm $\sim$ 81 μm attainable in the present mixer design.

Deviating somewhat from the actual reactant constituents, for the simplicity, the present evaporation analysis deleted the water constituent. The result, on the other hand, closely represented reality because of the fractional presence of water in the aqueous seed, and insignificant endothermicity of the solution (e.g., low boiling temperature) compared to the overall energetics leading to the evaporation of the seed particles.

---

[35]. "25 MW MHD Combustor Design Study Final Report", Report No. R-9967, Rocketdyne, 1976.
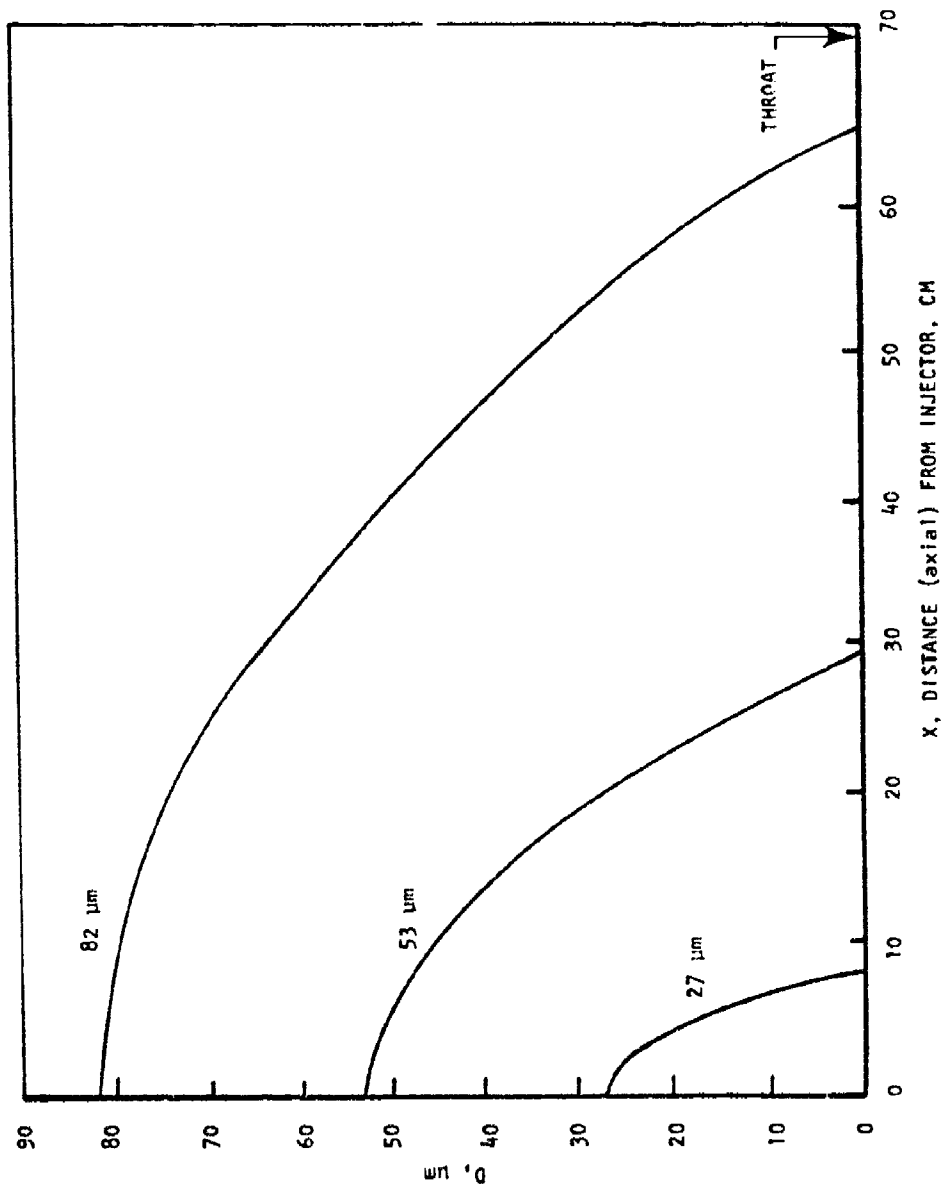
Figure 133. Seed Evaporation Characteristics.

b. Mixing/Dispersion

The static mixer had no moving parts, was relatively inexpensive and safe to operate, but was inherently less efficient than the ultrasonic device in reducing the globule sizes. The static mixer required increasingly greater pressure drops to produce finer globules; hence, selection of the static mixer was preceded by a lengthy trade off consideration between the attainable droplet size, D_{32}, and allowable net pressure loss at the mixer stage. The target values set for the mixer design were D_{32}, $\approx 60\,\mu m$ to $80\,\mu m$ and a pressure loss of less than 20 atm, respectively. The hardware design consisted of twelve modules of second stage, or main stage mixer, all in parallel, as shown in Figure 134. The first stage mixer served to mix the two streams with a uniform concentration.

Pressure loss characteristics were determined by following the procedure recommended by the manufacturer, Kenics Corp. of No. Hollywood, CA. On the other hand the transport properties relevant to the present mixture were not available from any reported literature sources and had to be estimated with some uncertainty. The viscosity of the mixture was approximated using the semi-theoretical correlations suggested in Reference 36. The interfacial tension between the aqueous seed droplet and the JP-4/SPAN-80 solution, which affected the prediction of the droplet size itself, was again estimated by Antonoff's rule, Reference 36.

Three additional references contained comprehensive information relevant to the method of performance prediction.[37,38,39] The design analysis extended the state-of-art of the static mixer by pushing the mixer up to the operational limit, which was supported by only a few experimental findings reported previously. However, the droplet size actually attainable was anticipated to be better than that predicted above on two accounts.

---

[36] Chemical Engineers'Handbook, 4th Edition, McGraw-Hill, 1959, Chapter 3, Prediction and Correlation of Physical Properties.

[37] Kenics Design Bulletin, Static Mixer Modules, Technology, Processing & Sizing, March 1976.

[38] S.J.Chen, "Drop Formation of Low Viscosity Fluids in the Static Mixer Units," KTEK-5, Kenics Corporation, 1972.

[39] Middleman, S., "Drop Size Distributions Produced by Turbulent Pipe Flow of Immiscible Fluids Through a Static Mixer," Ind. Eng. Chem., Process Research & Development, Vol. 13, No. 1, 1974.
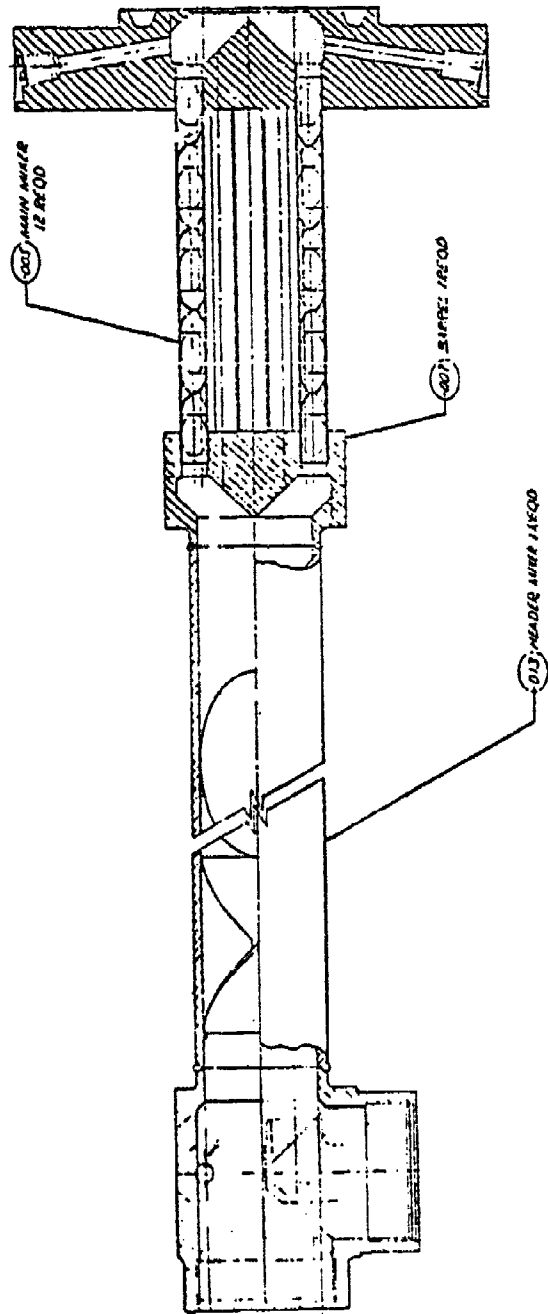
Figure 134. Seed/Fuel Mixer Assembly.

First, for the Weber number (We), a relative measure of available deformation energy to the resisting surface energy typical of the main mixer operation, We ~ 1.2×10^5, the break-up of the dispersed phase (i.e., the aqueous seed droplets) should have taken place at a rate exceeding the coalescence rate, resulting in droplet sizes more comparable to the "dissipation scale" of the turbulence. The dissipation scale under the conditions of present mixer design and operation was estimated to be 10^{-3} of the tube diameter, or of the magnitude of 10 μm.

Secondly, a review of the experimental findings reported, which is summarized in Figure 135.[40,41,42] indicated that in the case of turbulent pipe flow, the maximum stable droplet size, d_{max}, corresponding to a critical Weber number, $W^* \sim 10^5$, was below 100 μm. This result correlated with either the predicted Sauter mean diameter, D_{32}, and the dissipation scale, within an order of magnitude.

The foregoing results also ensured that the preatomized seed droplets maintained the size distribution and stable homogeneous dispersion through process of flowing from the mixer to the injector.

4. Surfactant Selection

A surfactant or wetting agent was used to promote mixing of the seed solution with the JP-4. Surfactant investigation was carried out within the frame of practical importance as summarized in the following selection criteria: (1) water-into-oil (W/O) type dispersion with extraordinary density of the aqueous seed (S.G. = 2.33); (2) effective by small concentration and preferably combustible; and (3) compatible with the combustor's inner liner material.

Water-into-oil emulsification was a relatively rare practice and the existence of an emulsifier for the present application had not been previously reported. A survey of potential candidates was, therefore, conducted. The selection criteria imposed served to narrow down the prospective candidate materials. For instance, all the emulsifiers containing sulfur were eliminated for fear of corrosive attack on the combustor material.

[40] C.A. Sleicher, "Maximum Stable Drop Size in Turbulent Flow," AIChE Journal, Vol. 8, No. 4, pp 471-477, 1962.

[41] C.A. Sleicher, H.I. Paul, "The Maximum Stable Drop Size in Turbulent Flow: Effect of Pipe Diameter," Chem. Engr. Sci., Vol. 20, pp 57-59, 1965.

[42] S.B. Collins, J.G. Knudsen, "Drop Size Distributions Produced by Turbulent Pipe Flow of Immiscible Liquids," AIChE Journal, Vol. 16, No. 6, pp 1072-1080, 1970.
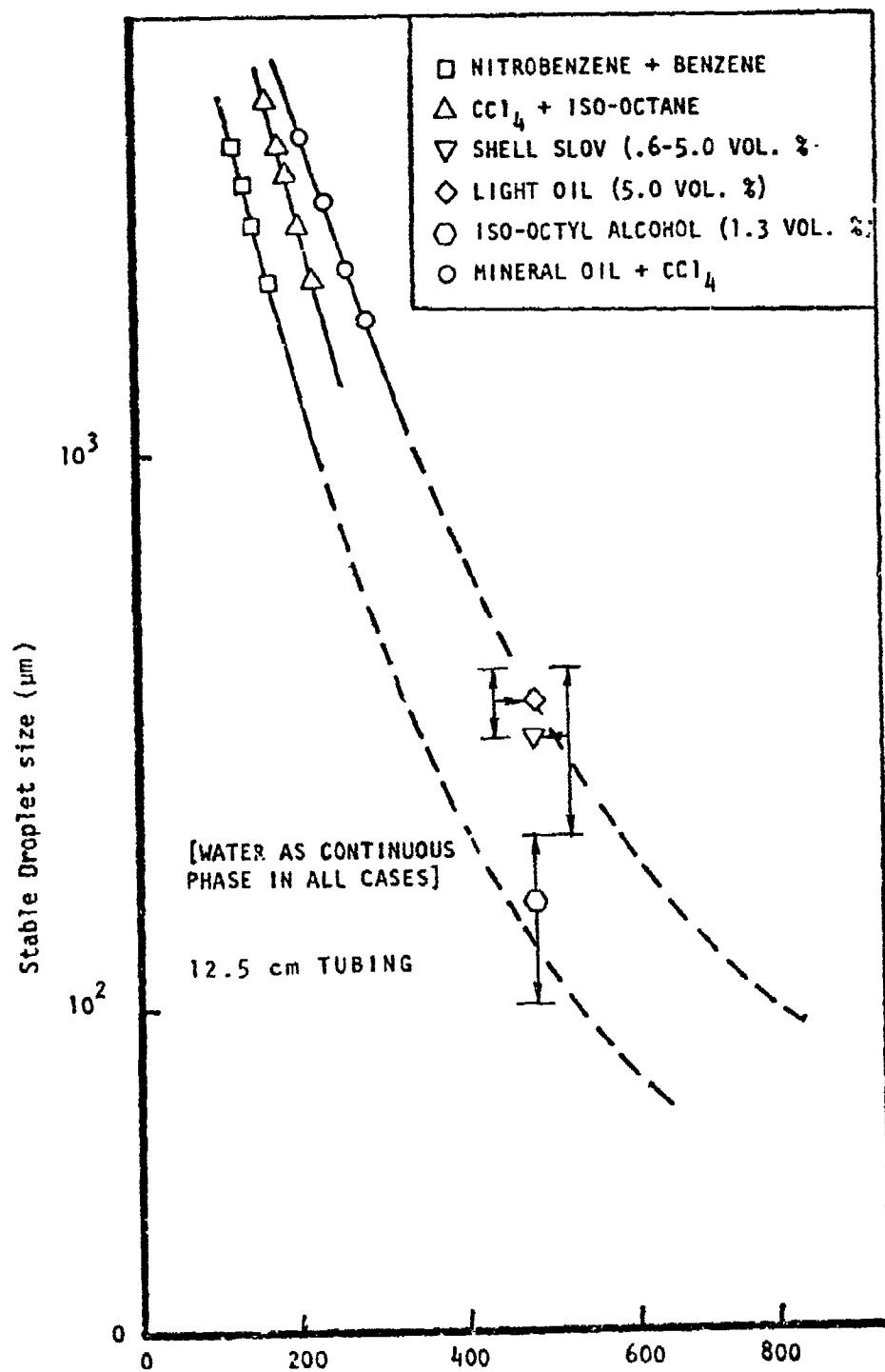
Figure 135. Maximum Stable Globule Sizes.
[$(d_{max}$ or $d_{95\%})$ of dispersed phase]

Primary selection of the potential emulsifiers was made on the basis of the classification already in existence. Namely, a usual classification of the emulsifiers was by their hydrophilic-lipophilic balance (HLB) value. The reduction of interfacial tension was responsible for the formation of emulsion and was accomplished by the size and balanced strength of hydrophilic (affinity with the aqueous phase) and/or lipophilic (affinity with the fat or oil phase) character of the emulsifying agents. The HLB number varied from one to forty, and those strongly lipophilic in character were assigned low HLB numbers whereas large HLB values were assigned for those strongly hydrophilic. Table 35 lists the representative characteristics and applications of the emulsifiers classified according to the HLB numbers.

The search effort was directed to the emulsifiers with HLB $\approx$ 4. The three candidate emulsifiers initially selected were: (1) BRIJ92 (Polyoxyethylene (2) Oleyl Ether); (2) SPAN-80 (Sorbitan Mono-oleate); and (3) TRITON (Alkylphenoxy polyethoxl ethanel).

To be consistent, the JP-4/seed solution was prepared uniformly. Seed solution was prepared as a stock, fully saturated at ambient conditions. The mixture of JP-4 and seed solution corresponded to the nominal operating condition of 1.5 kg Cs_2CO_3, 0.6 kg H_2O, and 6.3 kg JP-4. Nine specimens were prepared and grouped into three sets. Each set contained varied emulsifier concentration. The matrix of the preliminary test specimens is listed below.

Emulsifier	.2%	.5%	1.2%
Water	6.9%	7.0%	7.0%
Cs_2CO_3	17.8%	18.0%	18.0%
JP-4	75.1%	74.5%	73.8%

The laboratory investigations proceeded in the following order.

(1)   Preparation of the total mixture (including the emulsifier) without significant stirring action. Any signs of spontaneous dispersion were observed.

(2)   In all cases no spontaneous dispersion was obtained, and subsequently, the specimens were stirred one by one by a short rod which spun in an alternating magnetic field. No satisfactory result was obtained. However, a relatively conspicuous sign of globule formation appeared with the specimens containing SPAN-80. The results were, however, far from being acceptable.

(3)   The nine samples were then treated in an ultrasonic bath to increase the intensity of the stirring action. The specimens containing either BRIJ92 or TRITON displayed quick separation of the ageous seed from the JP-4.

TABLE 35.   INFLUENCE OF HLB ON PERFORMANCE

HLB Range	Dispersibility in Water	Suitable Application
1-4	Nil	
3-6	Poor	W/O emulsifier
6-8	Milky dispersion on agitation	Wetting Agent
8-10	Stable milky dispersion	Wetting Agent: O/W emulsifier
10-13	Translucent to clear dispersion	O/W emulsifier
13	Clear solution	O/W emulsifier; solubilizing agent

The three specimens containing SPAN-80 showed a positive sign of dispersion (yellowish white in appearance). However, dispersion in the two specimens with low SPAN-80 concentrations was considerably poor as evidenced by the fact that separation took place within 15 to 30 seconds. The critical concentration of SPAN-80 appeared to be near 5 wt % of the seed solution.

A separate specimen was prepared with 10 wt % of SPAN-80. An increased duration of dispersion for 10 to 15 minutes was obtained along with milky white appearance which was indicative of microscopic globule size, $1 \sim 10 \, \mu m$. The presence of SPAN-80 in 10 wt % of the seed solution represented less than 3 wt % of the JP-4/seed solution mixture and much less than 1 wt % of the total reactant flow rate. Further, little coalescence of the globules, as indicated by ready dispersion by small disturbances such as shaking, turbulence, etc., favored the solution of SPAN-80 for the present application.

5. Design

The seed mixing system that was adopted is shown schematically in Figure 132. The aqueous seed solution was stored in a pressure vessel, and the flow rate was controlled by the pressure of the gaseous pressurant. The complete seed system included part of the main fuel feed system although the feed system carrying a neat seed solution physically ended where the seed system merged with the main fuel feed system near the injector.

The two major operating characteristics of the seeding system were: (1) steady state flow of the aqueous seed at predetermined flow rates was not influenced by fuel flow rate or by combustion pressure variations; and (2) pre-atomization of the aqueous seed into fine droplets with 100 micron as a typical mean diameter.

The in-situ mixing operation tolerated modest mismatch and/or fluctuations of the feed system, by incorporating cavitating venturis in each transport line. This allowed accurate control of the flow rate by controlling the pressure level at the supply tanks.

Both preatomization and homogeneous dispersion of the fuel/seed mixture were effected simultaneously by a two-stage static mixer assembly which was positioned along the main fuel line immediately downstream of the mixing point.

The first stage mixer, or header mixer, was a single module with 5 cm i.d. and 50 cm long containing six blade elements and simply served to

produce a uniform mixture of fuel/seed. The resultant mixture containing large size globules of aqueous seed was then evenly divided and fed into twelve parallel modules with 1.11 cm i.d. and 18 cm length of the main mixer stage.

Because of the large turbulent energy dissipation associated with the pre-atomization, which yielded $D_{32} = 60 \sim 80 \, \mu m$, the main mixer stage accounted for nearly 80% of the pressure drop suffered in both stages. The following comparison compares the two types of mixers which were evaluated in the early design phase.

Comparison of Mixer Performance Characteristics

Type	Typical size of the dispersed droplet	Typical pressure loss	Atomizing elements
Static Mixer	$\leq 100 \, \mu m$	13.5 atm	Static blades
Ultrasonic Mixer	$< 10 \, \mu m$	13.5 atm	Vibrating blade

Both devices were operated entirely in the passive energy mode; break-up and dispersion were carried out by the fluid flow motion itself. The small size of the dispersed droplets or globules was produced at the expense of large, localized pressure at the mixer. The static mixer was preferred because of the low procurement cost, the operational safety present without any moving parts, and the capability of producing fine aqueous seed droplets with a reasonable pressure drop.

a. Material Preparation

The aqueous seed was prepared in a batch mode by gradually introducing the cesium carbonate granules into a mixing vessel containing a predetermined quantity of water. The purity of the cesium carbonate (Cs_2CO_3) used was greater than 99%. The water for the aqueous seed preparation was deionized and filtered before the solution was transferred to the seed tank.

The results of a laboratory investigation indicated that an increase in seed solution concentration required proportionally larger Span-80 concentration. For simplicity of operation, the surfactant concentration level was fixed at a point value which corresponded to that required for maximum seeding operation:

	Wt %	Vol. %
Span-80	7.4	5
JP-4	92.6	95

The surfactant, Span-80, had a specific gravity equal to 1.0, and a viscosity of 1000 cP at standard temperature, but was readily transferred by diluting it with JP-4 by one-to-one mass ratic. An appreciable viscosity reduction to less than one tenth of the original pure state was experienced during this dilution.

b. Flow Control

A cavitating venturi was used to provide a steady flow rate seeding operation independent of the disturbance likely to occur when two feed lines merge in the in-line mixing design. To cover the range of flow rates and operating pressures, four different venturis were required.

c. Pressure Balance

A pressure balance was carried out in a conservative manner by consistently using the larger value of the pressure drop estimate. The frictional pressure loss was relatively insignificant, but was included for the sake of accuracy in estimating the maximum tank pressure corresponding to the maximum seeding level. The values of the pressure loss were accumulated, reversing the flow direction, starting from the combustor chamber pressure, injector face ΔP and so forth.

6. Fabrication

The seed/fuel mixer assembly shown in Figure 136 was fabricated and assembled. The single header mixer was welded to the barrel and a "tee" connector to form the initial segment of the mixer. This section was subsequently brazed to twelve mixer assemblies and the end flange which formed the second mixer stage. The mixer units were procured from the Kenics Corporation as a commercial product and subsequently tack welded internally for positive retention. The individual components were fabricated from 304 stainless steel.

On completion of the mixer, a proof pressure test was conducted. The mixer assembly, injector assembly, and test fixtures are shown in Figure 137. The proof pressure test consisted of bleeding all the air from the sealed assembly and pressurizing the assembly at room temperature with water to 185 atm. The pressure was maintained for a minimum of 90 seconds, reduced to zero pressure and cycled for five complete cycles. The calculated burst pressure at room temperature was 514 atm.

SECOND STAGE
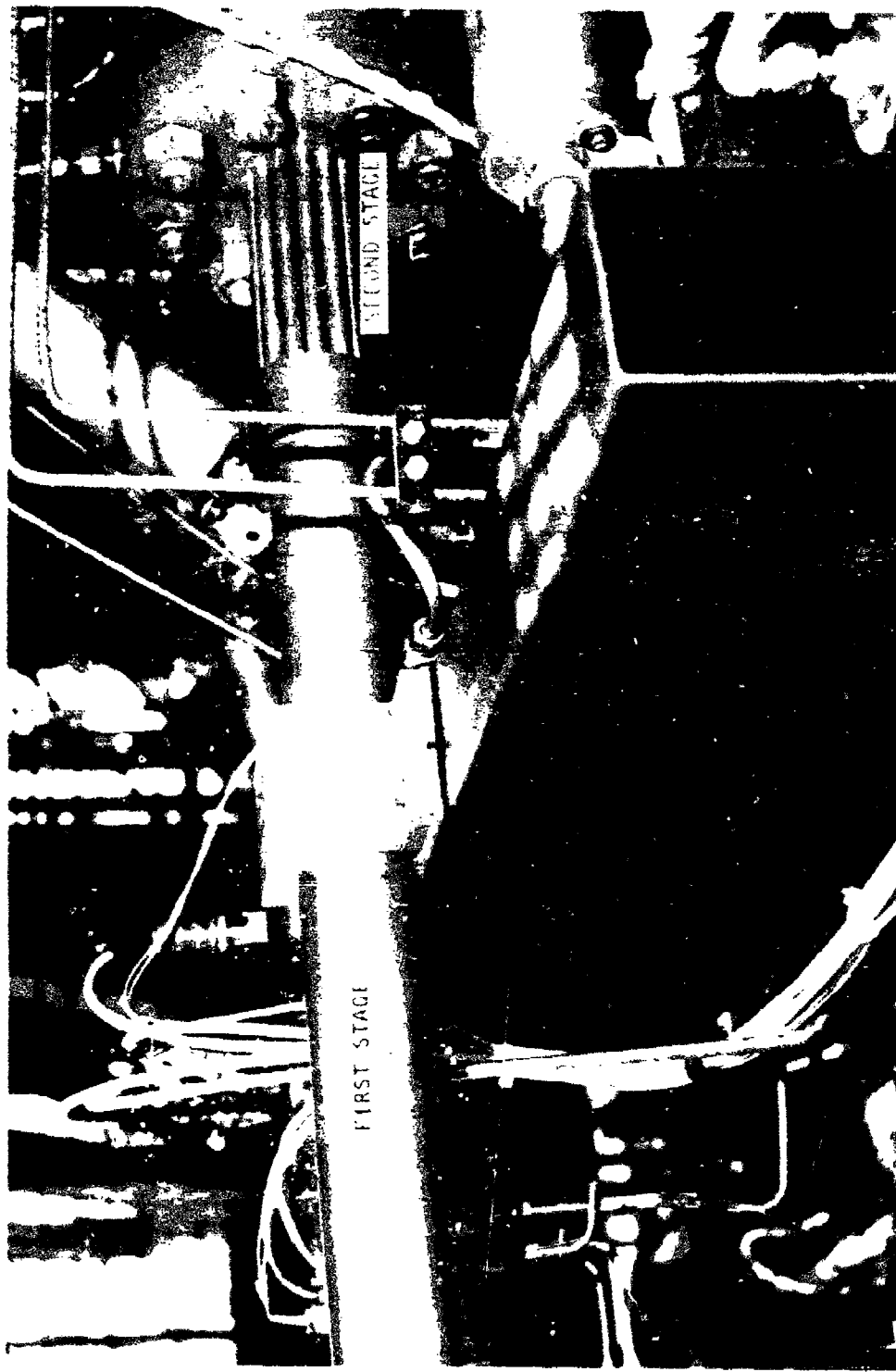
FIRST STAGE

Figure 136. Seed/Fuel Mixer Assembly
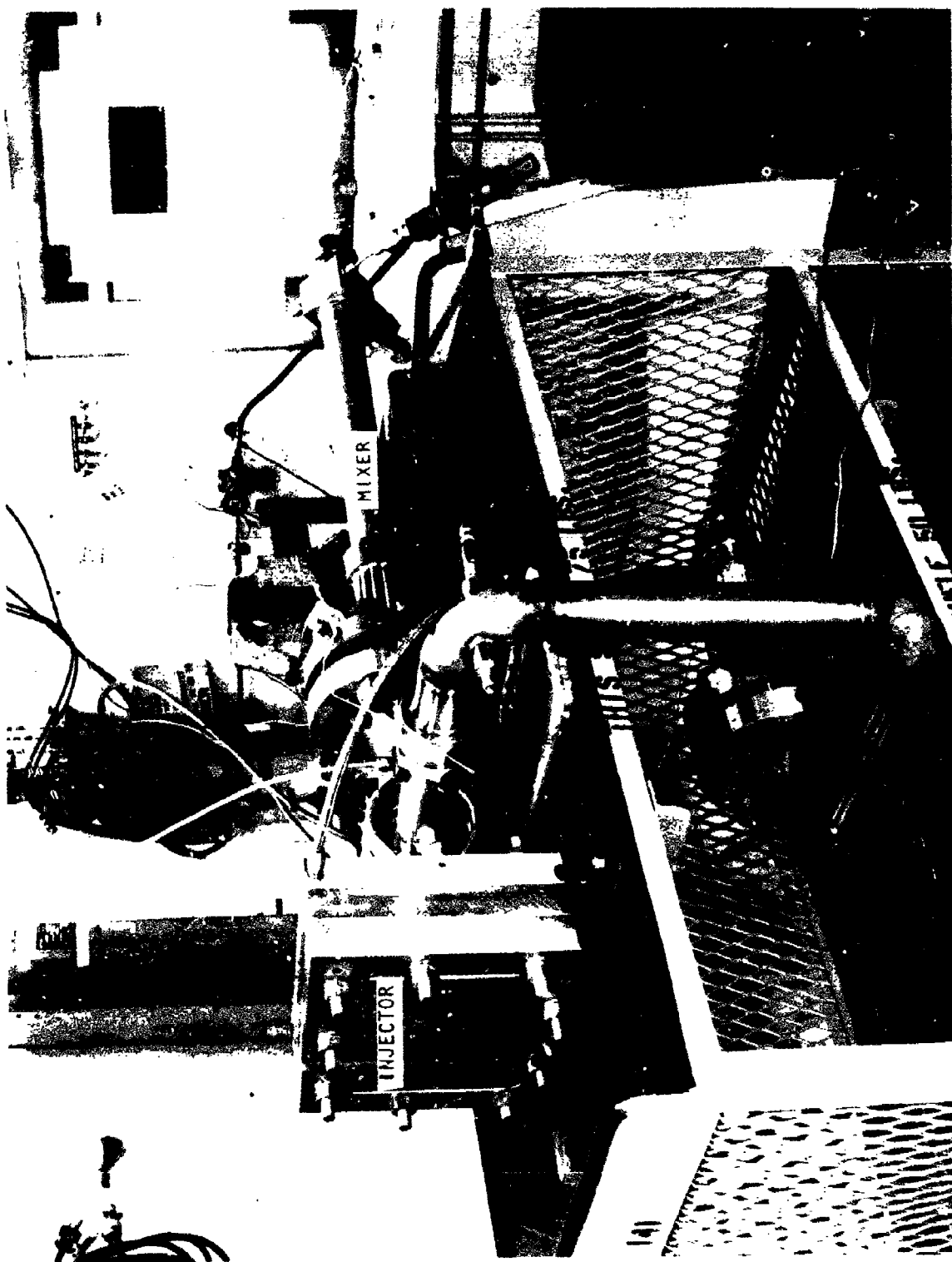
Figure 137. Proof Test of Injector and Mixer Assembly

4LC49-4/27/77-C1

C. FEED SUBSYSTEM

The high power MHD gas generator feed system provided the fluid lines, the flow control devices, and the instrumentation for operation of the gas generator at Santa Susana and AEDC. The deliverable feed system represented the test article and did not include the facility fluid supply system. The gas generator feed system was originally designed for testing at both Rocketdyne and AEDC. Simple line connections were designed for connecting the gas generator feed system to the facility fluid storage systems.

1. Subsystem Requirements/Approach

The purpose of the Rocketdyne supplied MHD feed system was to provide and control the reactants, seed solution, and other necessary fluids from the Rocketdyne test facility and the AEDC test facility system to the MLI channel system. The MHD feed system handled various fluids and consisted of the following subsystems:

LO$_2$ Feed	Channel Coolant Water Feed
JP-4 Feed	Purge Gas Feed
Seed Solution Feed	Valve Pneumatic Control Feed
GOX Feed	Valve Hydraulic Control Feed
Methane Feed	Seed Tank Pressurizing Gas Feed
Gas Generator Combustor Coolant Water Feed	

The gas generator fluid feed system requirements were developed through discussions between Rocketdyne, Maxwell Laboratories, and AEDC. The fluid feed system, illustrated in Table 36, was designed to be consistent with these requirements.

The nominal design fluid requirements for the feed system were:

Reactants	Liquid oxygen (LO$_2$) and JP-4/SPAN-80
Total Flow Rate (including Cs$_2$CO$_3$ seed)	30 kg/sec
Flow Rate Variation	$\pm$ 20% from nominal
Chamber Pressure (Nozzle stagnation)	30 atm
Mixture Ratio	3.34

The MHD feed system was designed to meet these requirements, and in addition, provided seed solution flow rates up to 10% of total flow rate.

295

TABLE 36. FLUID FEED SYSTEM REQUIREMENTS

FLUIDS

- JP-4/SPAN-80
- LO_2 (Liquid Oxygen)
- GN_2 - Purge for Feed Lines (Gaseous Nitrogen)
- Cooling Water
- GCH_4 (Methane)
- GO_2 (Gaseous Oxygen)
- Cs_2CO_3 (Cesium Carbonate)

OPERATIONAL

- Start/Shutdown Time - 1 sec
- Run Time - 3 sec
- External Leakage - No bubble leakage within 1 minute at 1.7 atm GN_2 pressures
- Cooling water is provided to the channel and combustor prior to start, continuously during operation, and subsequent to cutoff.

OPERATIONAL GOALS

- The feed system was designed for limited pressure surges occurring in the Start/Shutdown sequence.
- Channel Limitations (MHD-GRAM 9Q)
  - General - fuel rich or raw JP-4 environment to be avoided.
  - Start
    - Maximum channel pressure is 4.5 atm.
    - Gaseous oxygen and oxidizer-rich conditions to be tolerated for ~ 0.5 sec.
    - Maximum pressure rise rate ≤ 204 atm/sec.
  - Shutdown
    - Gaseous oxygen and oxidizer-rich conditions to be tolerated for ~1 sec.

TABLE 36. FLUID FEED SYSTEM REQUIREMENTS (Cont'd)

THERMAL

- Ambient Temperature - 21 C

STRUCTURAL DESIGN

- Meets or exceeds safety factor criteria
- Minimal Loads on Combustor/Injecter Assembly

INTERFACE

- Compatible with SSFL Facility Fluid Supply System

    - JP-4   - facility supply line
    - LO_2 - facility supply line
    - GN_2 - facility supply line
    - GCH_4 - K-bottle
    - GO_2 - K-bottle
    - Combustor Cooling Water   - facility cooling system
    - Diagnostic Channel Cooling Water - facility cooling system

- Compatible with AEDC Fluid Supply System

    - JP-4   - facility supply line
    - LO_2 - facility supply line
    - GN_2 - facility supply line
    - GCH_4 - facility supply line
    - GO_2 - facility supply line
    - Combustor Cooling Water - closed circuit facility cooling system
    - Power Channel Cooling Water - facility cooling system

MAXIMUM OPERATION PRESSURE* (Based on supply tank or facility supply limitations)

- JP-4   136 atm
- LO_2 136 atm
- GN_2 Purge   142.8 atm
- GCH_4 170 atm
- GO_2 170 atm
- Seed Solution   136 atm
- Deionized Water   272 atm
- Hydraulics   170 atm

INSTRUMENTATION

- Flow rate, pressure, and thermal measurements sufficient to control and characterize the gas generator operation were provided.

* Limits based on Rocketdyne Santa Susana Test Facility.

297

The flow rate and chamber pressure values that met the design requirements are shown in a subsequent section. To meet the $\pm 20\%$ flow rate variation, chamber pressure ranges from 24 to 36 atm, fuel flow rate ranges from 5 to 7.9 kg/sec, and LO_2 flow rate ranges from 16.9 to 27.5 kg/sec were required. The fuel flow rate value were the sum of the JP-4 and SPAN-80. The mixture ratio was the ratio of the LO_2 flow rate to the fuel flow rate. The Cs_2CO_3 flow rate was a percentage of the total flow rate. Five cm diam tubing was selected for the line size of the LO_2 and fuel feed systems and 2.5 cm diam tubing was selected for the Cs_2CO_3 feed system.

The ignition system GO_2 and methane flow rate requirements were established by using 0.5% of total nominal chamber flow rate. Therefore, the GO_2 and methane system flow rates were each 0.074 kg/sec at the design mixture ratio of 1.0. The ignition system chamber pressure requirements was 30 atm, which was the value at nominal gas generator chamber pressure.

The nominal gas generator combustor coolant water requirements for the solid wall chamber design were 17.3 kg/sec at 53.7 atm inlet pressure of demineralized water. The high power MHD channel/diffuser coolant water feed system requirements were 164 kg/sec of filtered industrial water at 28.2 atm inlet pressure.

The required purge gas feed system inlet pressure was 137 atm GN_2. The flow requirements varied at the different test conditions which occurred during the test program. Previous experience indicated that the purge GN_2 flow requirements were not excessively high. Therefore, no problem was anticipated for the AEDC facility to meet the requirement. The valve pneumatic control feed system requirement was regulated GN_2 at 11.2 atm, and the hydraulic control feed system requirement was regulated hydraulic fluid at 137 atm. The seed tank pressurizing gas feed system requirement was to provide a maximum regulated GN_2 flow rate of $3.6 \times 10^{-5} m^3$/sec at 123.4 atm.

2. Subsystem Schematic Description

The feed system arrangement and components are illustrated in Figure 138. Major control components are listed along with their approximate size in Table 37.

3. Seed System

The high power MHD system utilized cesium carbonate (Cs_2CO_3) seed to provide the high conductivity necessary for power generation. The Cs_2CO_3 seed was supplied in a fine powder form, dissolved into water, injected into the combustion zone of the liquid fueled gas generator, and ionized under the high

298

AEDC RKDN

INTERFACE

PANEL ASSY
IGNITER-PURGE

VENTURI SEED SOLUTION

MIXER

SEED SOLUTION
FEED ASSY.

VENTURI LOX

INJECTOR

COMBUSTOR

GG ASSY

CHA

99R0020539

COMBUSTOR
COOLANT WATER VENTURI

INTERFACE

CHANNEL COOLANT
WATER SUPPLY
BY AEDC

RKDN
MLI

RKDN   AEDC

CHANNEL   INTERFACE MLI

RKDN

LEGEND

	HYDRAULIC VALVE
	HAND VALVE
	PNEUMATIC VALVE
	SOLENOID VALVE
	RELIEF VALVE
	REGULATOR HAND
	CHECK VALVE
	FILTER
	PRESSURE REG. VALVE
	VENTURI
	GAUGE
	ORIFICE

O - ORIFICE
V - VALVE

R - REGULATOR
G - GAUGE
P - PUMP
F - FILTER
VE - VENTURI
M - MIXING SOLUTION SYSTEM
J - JPA SYSTEM
W - WATER COOLANT SYSTEM
LO - LIQUID OXYGEN SYSTEM
GO - GAS OXYGEN SYSTEM
RG - FUEL GAS (CH4) SYSTEM
S - SEEDING SYSTEM
SP - SPAN BO SYSTEM

Figure 138. Fluid Flow Schematic.

SCHEMATIC, FLUID
FLOW MHD.

J 02602 R0020539

TABLE 37. COMPONENT LIST

No.	Nomenclature	Line Size, cm
VM1	Seed Mixing Water Supply Valve	1.27
VS1	Seed Solution Tank Inlet Valve	1.27
VS2	Seed Solution Tank Drain Valve	1.27
VS3	Seed Solution Tank Sight Gauge Valve	0.64
VS4	Seed Solution Tank Shutoff Valve w/Solenoid Valve	2.54
VS5	Seed Solution Check Valve	2.54
VS6	Seed Solution Relief Valve	2.54
VS7	Seed Solution Main Valve w/Solenoid Valve	2.54
VS8	Seed Solution Bleed Valve	1.27
VGO 1	GOX Purge Valve	0.64
VGO 2	GOX Purge Check Valve	0.64
VGO 3	GOX Main Valve	0.95
VGO 4	GOX Bleed Valve	0.64
VFG 1	Methane Purge Valve	0.64
VFG 2	Methane Purge Check Valve	0.64
VFG 3	Methane Main Valve	0.95
VFG 4	Methane Bleed Valve	0.64
VLO 1	LOX Purge Valve	1.27
VLO 2	LOX Purge Check Valve	1.27
VLO 3	LOX Main Valve	5.08
VLO 4	LOX Bleed Valve	2.54
VCP 1	Acoustic Cavity Purge Valve	0.95
VCP 2	Acoustic Cavity Purge Check Valve	0.64
VW1	Combustor Coolant Water w/Solenoid Valve	5.08
VJ1	JP-4 Purge Valve	2.54
VJ2	JP-4 Purge Check Valve	2.54

TABLE 37 - COMPONENT LIST (Cont'd)

No.	Nomenclature	Line Size, cm
VJS	JP-4 Main Valve w/Solenoid Valve	5.08
VJ4	JP-4 Bleed Valve	1.27
OGO1	GOX Orifice	0.64
OGO2	GOX Orifice	0.64
OFG1	Methane Orifice	0.64
OFG2	Methane Orifice	0.64
FMW2	Channel Coolant Water Flow Rate	5.08
OW 1	Combustor Coolant Outlet Orifice	5.08
VGL 1	Oxidizer Purge Panel Check Valve	2.54
FSP 1	SPAN-80 Filter	1.27
PSP1	SPAN-80 Transfer Pump	
FM1	Seed Mixing Water Supply Filter	1.27
PM1	Seed Solution Transfer Pump	1.27
FS1	Seed Solution Tank Inlet Filter	1.27
GS1	Seed Solution Tank Sight Gauge	0.64
VEJ1	JP-4 Venturi	5.08
VES1	Seed Solution Venturi	2.54
VELO1	LOX Venturi	5.08
RGO1	GOX Purge Pressure Regulator	0.64
RGO2	GOX Pressure Regulator	0.64
RFG1	Methane Purge Pressure Regulator	0.64
RFG2	Methane Pressure Regulator	0.64
RLO1	LOX Purge Pressure Regulator	0.64
RLO2	LOX Dome Loader	1.27
RJ1	JP-4 Dome Loader	0.64
RJ2	JP-4 Purge Pressure Regulator	2.54
RCP1	Cavity Purge Pressure Regulator	0.64

TABLE 37.   COMPONENT LIST (Cont'd)

No.	Nomenclature	Line Size, cm
GGO1	GOX Supply Pressure Gauge	0.64
GGO2	GOX Regulator Pressure Gauge	0.64
GGO3	GOX Purge Pressure Gauge	0.64
GFG1	Methane Supple Pressure Gauge	0.64
GFG2	Methane Regulator Pressure Gauge	0.64
GFG3	Methane Purge Pressure Gauge	0.64
GJ1	JP-4 Purge Pressure Gauge	0.64
GCP1	Cavity Purge Pressure Gauge	0.64
GLO1	LOX Purge Pressure Gauge	0.64

combustion gas temperature prior to flow into the MHD channel. To obtain maximum operational efficiency, the seeding system was required to provide: (1) complete ionization; (2) uniform distribution; (3) a range of flow rates of 1-10%; (4) adjustment for the desired flow rate; (5) a constant flow rate; and (6) quick on-off response.

After an extensive analysis and comparative evaluation study, the liquid mixed-in method employing in-situ mixing of JP-4 fuel and aqueous solution of Cs_2CO_3 was selected as the most suitable approach for this application. With this method, Cs_2CO_3 was homogeneously mixed with JP-4 and injected into the combustion zone through JP-4 injector orifices which were uniformly distributed over the injector face.

Since Cs_2CO_3 was not readily mixable with or soluble with JP-4, Cs_2CO_3 powder was first dissolved into water. The aqueous solution of Cs_2CO_3 was still not miscible with JP-4. Therefore, the solution was emulsified with JP-4 using SPAN-80 emulsifying agent which was added to the JP-4 in advance. The emulsifying operation took place in the fuel and seed solution mixer.

During operation the seed solution tank was pressurized with GN_2 to a specified pressure. The solution was discharged from the tank assembly through the flow control cavitating venturi, which maintained a specific flow rate for the test and measured the actual flow rate. The Cs_2CO_3 aqueous solution was then fed into the fuel and seed solution mixer where the solution was mixed and emulsified with JP-4.

The seed solution venturi assembly consisted of a commercial cavitating venturi made of stainless steel. Various throat sizes were utilized to cover a wide range of Cs_2CO_3 flow - 1 to 10% of total flow rate which varied as much as $\pm$ 20% of the nominal value. The number of venturis and the actual throat size were to be established upon finalization of the AEDC installation details. The initial procurement consisted of four throat sizes for the development test program at SSFL. The seed solution flow control assembly consisted of a commercial cavitating venturi, a section of tubing for upstream flow control, and instrumentation taps for fluid pressure and temperature measurement. The flow venturi line size was 2.54 cm.

The seed solution mixing tank assembly consisted of a 0.21 m^3 stainless-steel mixing tank, Cs_2CO_3 feed funnel, water supply filter assembly, water supply valve, and a recirculation/transfer pump assembly. All elements were located at the top of the mixing tank and were removable for operation and service. The

seed solution tank assembly shown in Figure 139 consisted of a 0.57 m^2, stainless-steel, high pressure coded tank with 136 atm rating, Cs_2CO_3 solution supply filter assembly solution supply valve, fluid level sight gauge assembly, pneumatic-controlled tank shutoff valve, tank drain valve, and associated plumbing.

The seed solution feed assembly, consisted of a commercial 2.54 cm check valve, liquid pressure relief valve, hand-controlled seed bleed valve, pneumatic-controlled 2.54 cm seed solution main valve, hydraulic-controlled 5.08 cm JP-4 main vlave, fuel and seed solution mixer, and a hand controlled 1.27 cm fuel bleed valve which is shown in Figure 140. The check valve was to prevent JP-4 reverse flow into the Cs_2CO_3 line during transient flow periods, and bleed valves were to ensure complete priming of feedlines with the respective fluid prior to initiation of a test. The main valves controlled the starting and stopping of the respective flow. The fuel and seed solution mixer was made up of a two-stage Kenics static mixing device to produce a homogenized mixture of Cs_2CO_3 aqueous solution with JP-4/SPAN-80. The first stage, header mixer, was a single, 5.08 cm unit and the second stage, main mixer, was a cluster of twelve, 1.27 cm units to produce Cs_2CO_3 globules of 60 to 80 μm size emulsified in JP-4. The pressure drop across the mixer was approximately 8.5 atm with JP-4 only, and 10.5 atm with 5% and 11.9 atm with 10% Cs_2CO_3 solution mixed with JP-4, respectively, at nominal flow rates.

4. LO2 System

The purpose of the Rocketdyne supplied gas generator LO_2 system was to provide and control liquid oxygen from the AEDC test facility system to the combustor at conditions desirable for safe operation. The gas generator LO_2 feed system, illustrated in Figure 141, was designed to meet all the requirements of the high power MHD gas generator assembly, and to interface with the AEDC facility feed system. The system contained instrumentation components, i.e., flow control component (venturis, etc.), and operational and data instrumentation.

The LO_2 feed system was a 5.08 cm system rated for 136 atm and consisted of a LO2 venturi, hydraulically controlled 5.08 cm main LO2 valve, a 2.54 cm pneumatically controlled LO2 seed valve, and a LO2 bleed check valve. The LO2 bleed line was provided to bleed off gaseous oxygen until the system had been chilled and primed to ensure liquid oxygen upstream of the main oxidizer valve, a requirement for satisfactory combustor start. The bleed line also functioned as a safety device, permitting the liquid oxygen/high pressure gaseous oxygen to be bled from the lines posttest after the main LO_2 valve had been closed.
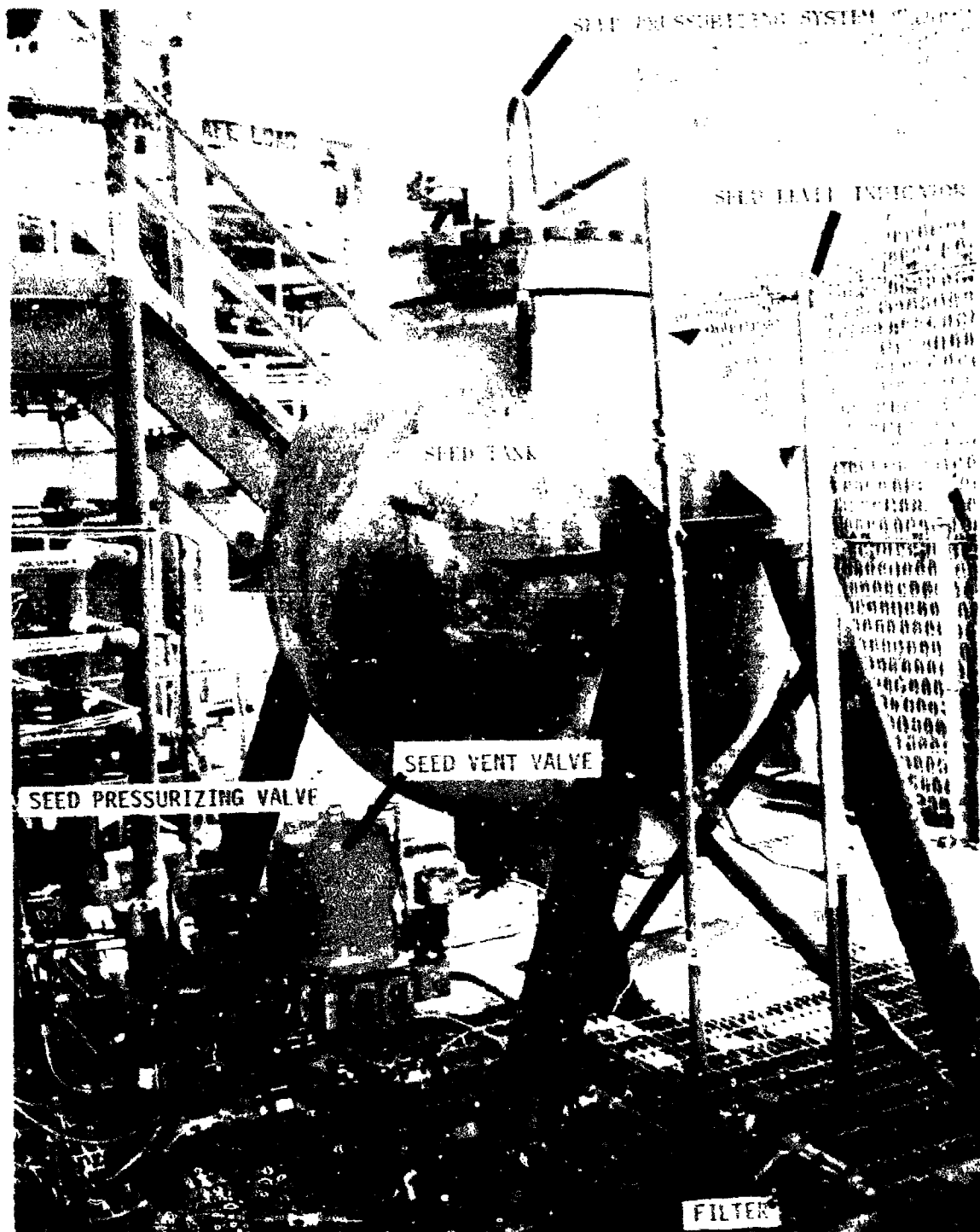
Figure 139. Seed Solution Tank Assembly

Figure 140. Seed/Plant Shaker System.

GOX SUPPLY

METHANE SUPPLY

4LC31-6/21/77-S1H

LOX MAIN VALVE

OUTLET H₂O LINE

LOX BLEED VALVE

LOX INLET
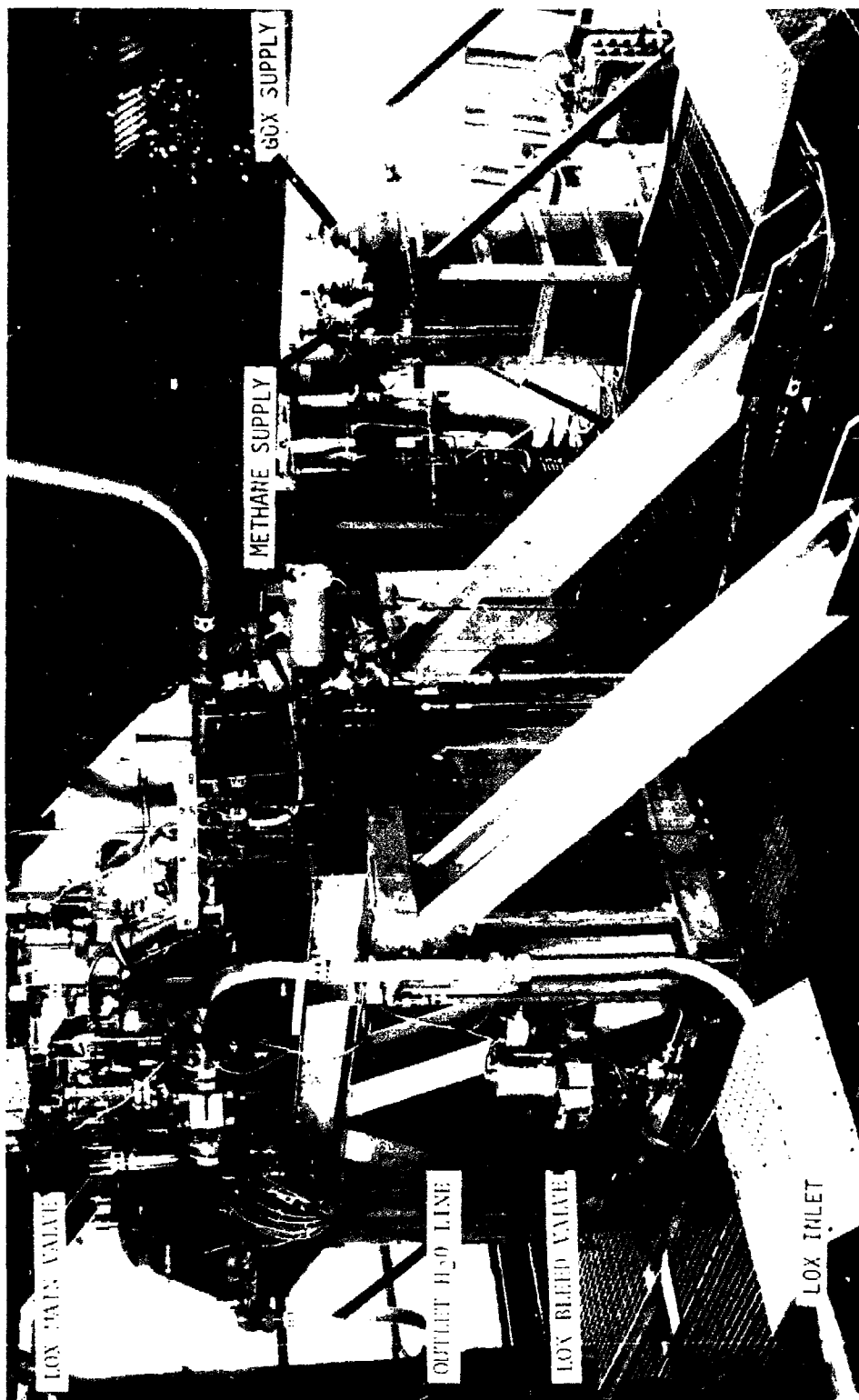
Figure 141. LO_2 Feed System

The oxidizer valve was a 5.08 cm, hydraulically controlled Annin valve, rigidly mounted in the vertical position to a gusset plate permanently attached to the combustor mounting plate. To accommodate the axial thermal excursions and deflections realized during operating conditions, the oxidizer inlet line (≈ 102 cm in length) was formed in a "U" shape and designed to prevent overloading of the injector LO_2 cavity braze joints.

5. Fuel System

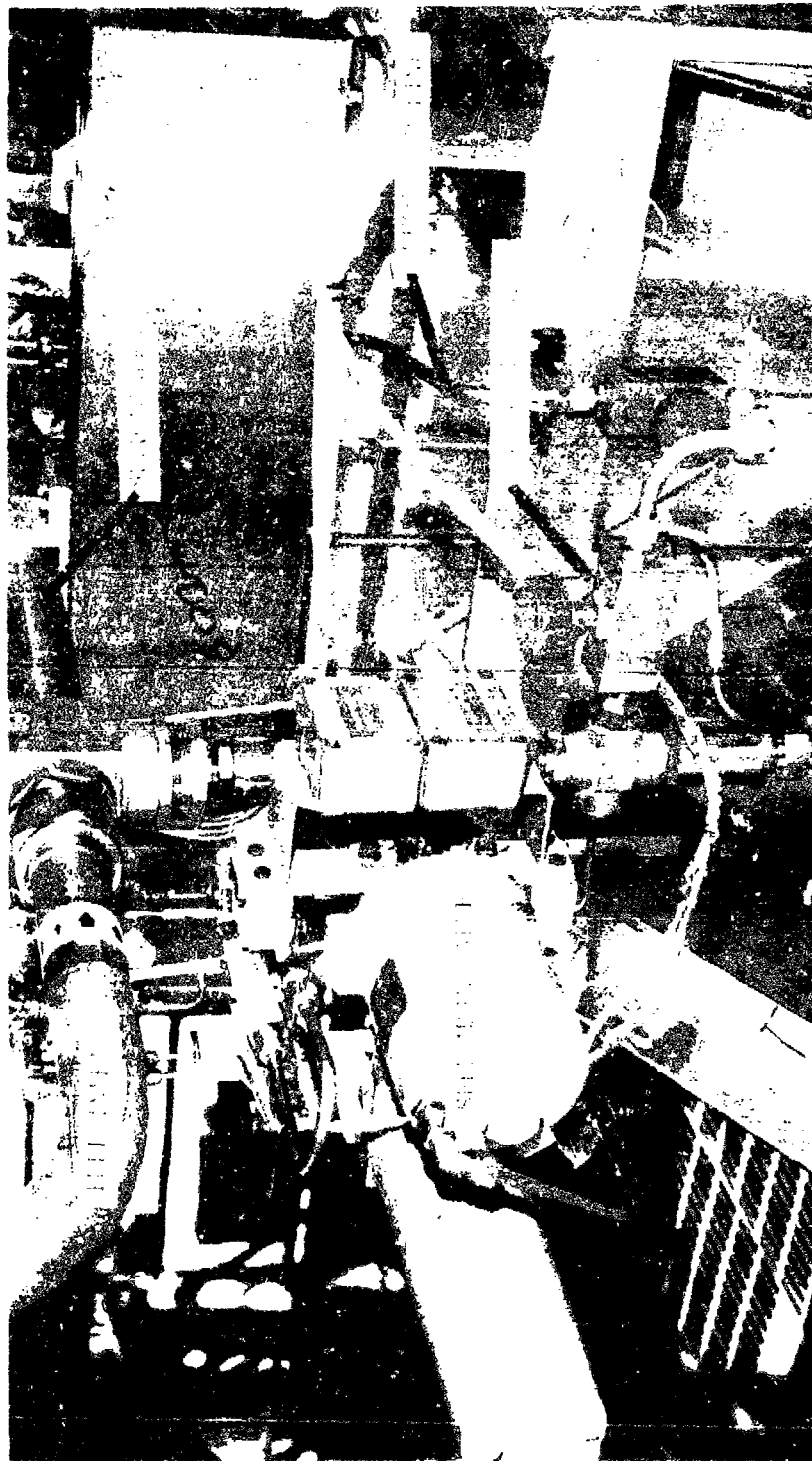The purpose of the Rocketdyne supplied MHD fuel system was to provide and control JP-4/SPAN-80 from the AEDC test facility system to the combustor at conditions which were desirable for safe operation. The gas generator fuel system, illustrated in Figure142, was designed to meet all of the requirements of the high power MHD gas generator assembly and to interface with the AEDC facility feed system. The system contained instrumentation components, i.e., flow control component (venturis, etc.), and operational and data instrumentation. Unlike the LO_2 system, the fuel system included a Kenics mixer just upstream of the fuel main valve that permitted a mixing operation to take place when the JP-4/SPAN-80 and aqueous solution of Cs_2CO_3 enter the mixer.

The JP-4 feed system was also a 5.08 cm system rated for 136 atm and consisted of a flow control and measuring cavitating venturi, fuel and seed solution mixer, 1.27 cm manual fuel bleed valve, and hydraulically controlled 5.08 cm main fuel valve. The JP-4 line contained a cavitating venturi, as did the seed line, for the purpose of controlling fuel flow at the same level regardless of whether seed was flowing or not. Upstream of the main fuel valve and downstream of the mixer, a JP-4 manual bleed line was provided to ensure complete priming of the line upstream of the main fuel valve prior to test initiation.

The fuel valve was also a 5.08 cm hydraulically controlled Annin flanged and ring groove sealed valve mounted in a vertical position. The valve was mounted to the combustor mounting plate in such a way as to restrain movement in a plane perpendicular to the combustor centerline, but allowed movement axially by means of a tongue and groove mounting during thermal excursions of the combustor hardware.

The seed mixer was mounted to the fuel valve at one end and was held in a bracket at the other end. The bracket restrained motion in a plane perpendicular to the combustor centerline but allowed movement axially. The seed system has been previously described.
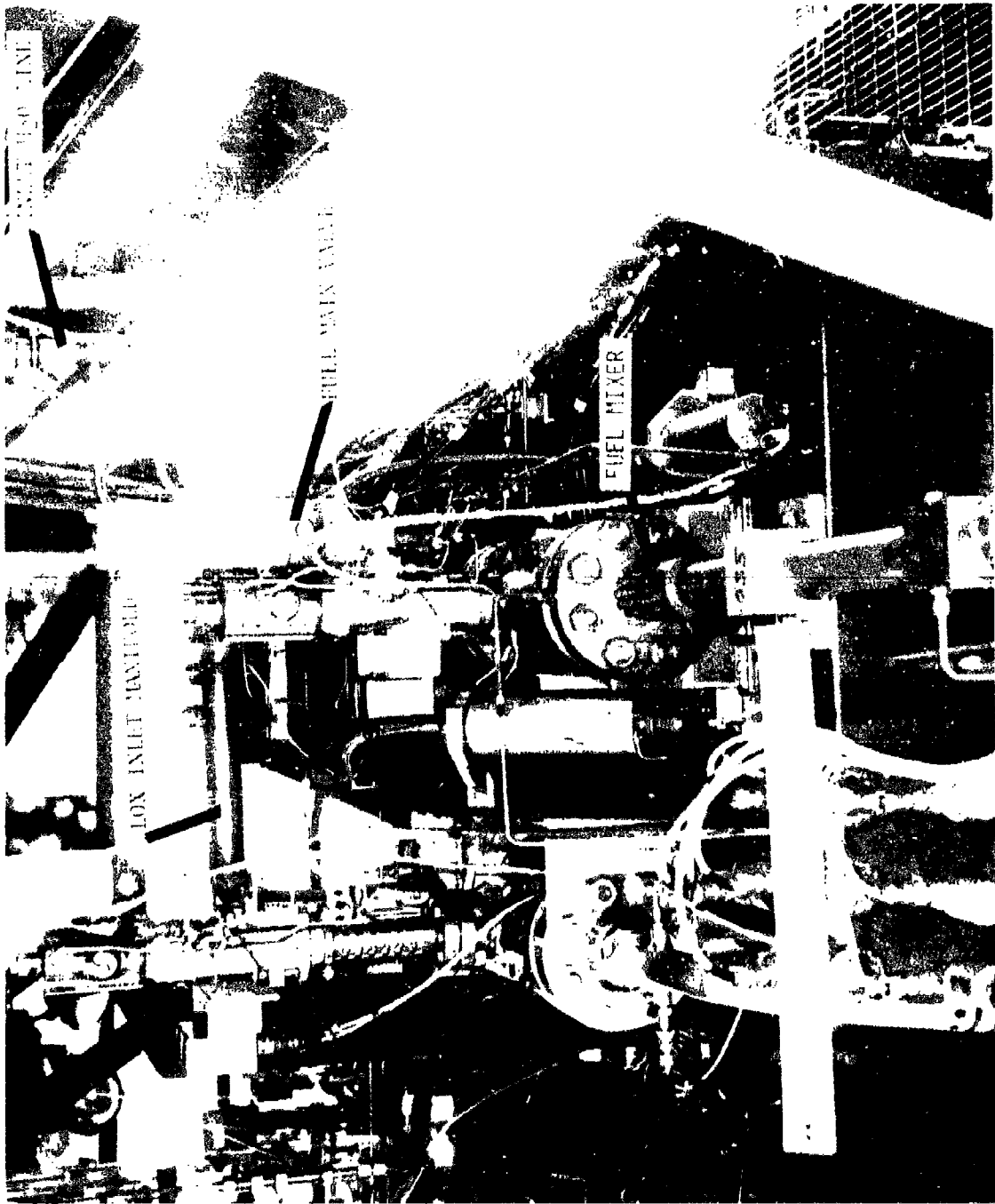
Figure 142. Fuel Feed System

6. Ignition System

The ignition system GO_2 feed and methane feed system were identical 0.64 cm systems rated for 137 atm. The systems consisted of a pressure regulator, inlet and regulated pressure gauges, flow control orifices, solenoid operated shut-off valve, and a hand bleed valve. Each system supplied ignition gas to two augmented spark igniter assemblies.

Facility support systems at SSFL were used for the storage tanks and shut off valves. The igniter reactant regulation system was mounted on regulator panel along with the purges as illustrated in Figure 143. As shown in the system schematic, a single regulation system was used for each of the reactants and supplied both igniter units.

The spark igniters were turned off when the ASI chamber pressure was confirmed to exceed a minimum preset value, determined during the ASI ignition test series. The ASI was then allowed to burn for one second, the time required to ensure main chamber ignition. When main chamber ignition was detected, the ASI main valves were turned off, and the ASI purge valves were turned on. To ensure a high degree of safety, a fuel lead and lag was used in the sequencing of the ASI oxidizer and fuel valves, respectively.

7. Purge System

The purge gas feed system was a GN_2 system rated for 136 atm. The panel assembly, shown in Figure 143, defined a panel and the associated gauges and valves. This panel was built as a subassembly and was mounted on the structure as part of the deliverable system.

The system consisted of an inlet manifold including a 2.54 cm isolator check valve and five purge branches, e.g., LO_2 injector manifold purge, fuel injector manifold purge, acoustic cavity purge, igniter GO_2 purge, and igniter methane purge. Each purge branch included a pressure regulator, regulated pressure gauge, shutoff solenoid valve, and a check valve for preventing contaminant reverse flow into the purge system.

The purge system was separated into two parts isolated by a check valve. The down stream system purged the methane and JP-4 systems and the acoustic cavity, while the upstream system purged the gaseous oxygen and liquid oxygen systems. The check valve was used to prevent any passage of fuel back up the purge lines into the oxidizer system. Each purge line had an individual regulator to adjust the pressure; a gauge was also provided in each purge line for pressure setting and a Marotta solenoid valve for on-off control. All purges were provided with check valves, just downstream of the shutoff valves to prevent reverse flow and to provide automatic purge flow control as the downstream pressure varies during transient operation.
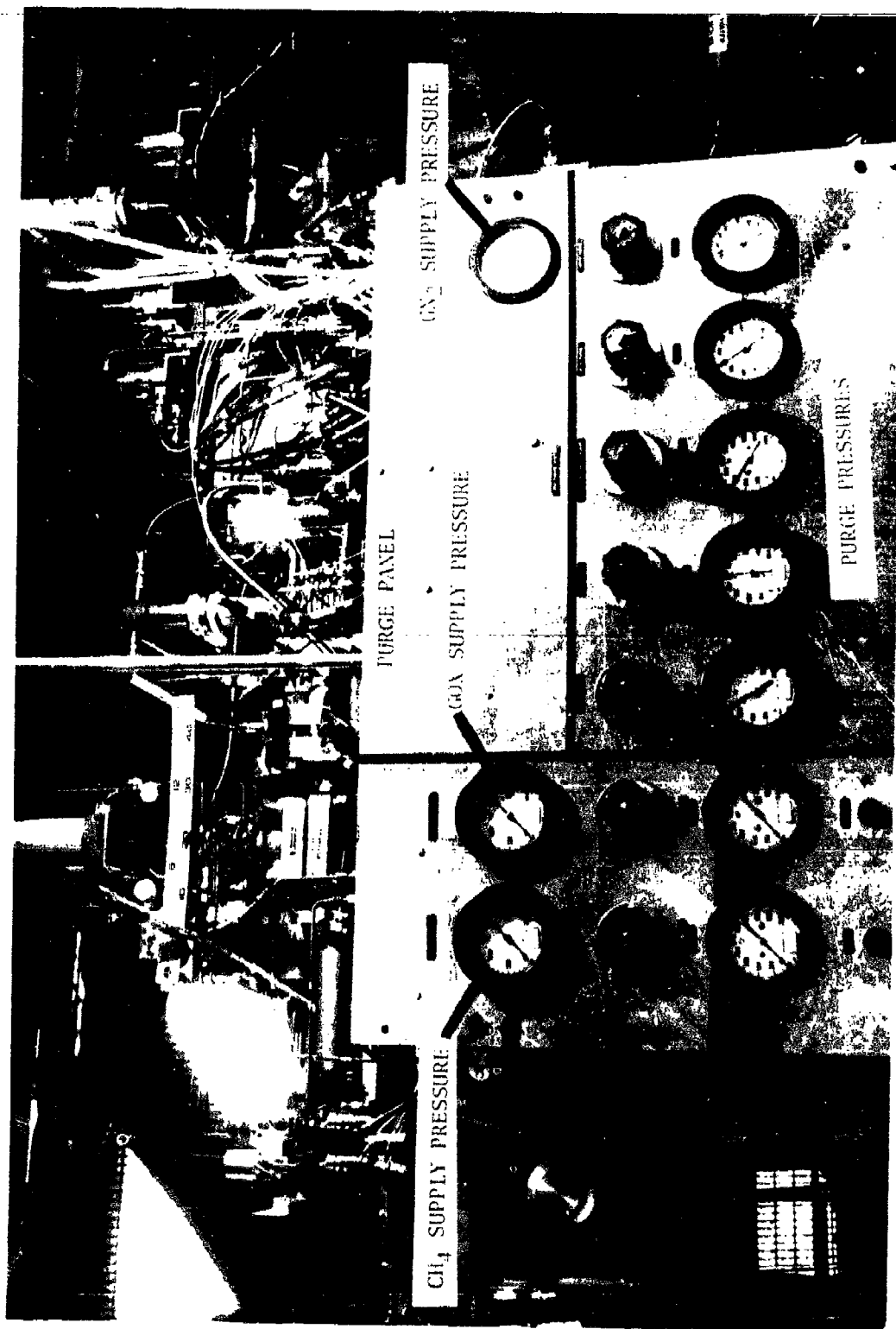
Figure 143. Regulator Purge Panel

4LC31-6/21/77-S10

8. System Operation

Operation of the fluid feed system is described in terms of flow rates, pressure drops, transient operation and control sequence.

a. Reactant Flow Requirements

The purpose of the high power gas generator feed system was to provide and control the reactants, seed solution, and other necessary fluids from the test facility system to the MHD and diagnostics channel system. To size the feed system and determine the required pressure drops, fluid flow requirements were determined for the basic reactants, igniter reactants, and component coolant. The reactant flow rates targeted during the SSFL testing are presented in Table 38. The GN_2 flows required for purging were determined empirically and were substantiated/modified during the SSFL test effort. The requirements varied for different test conditions.

Prior to testing, a decision was made to use a mixture of 7% SPAN-80 and 93% JP-4 as the fuel for all tests. This mixture was required for the 10% or maximum seed condition to ensure emulsification of the aqueous seed solution in the SPAN-80/JP-4 mixture.

If the concentration of the SPAN-80 was varied in proportion to the amount of seed used, there would have been a significant impact on schedule and cost. There would also have been an increase in the amount of SPAN-80 and JP-4 used and in addition, a disposal problem.

Accordingly, the theoretical performance with shifting equilibrium was determined for liquid oxygen with JP-4 and 7% SPAN-80: 93% JP-4, using the Rocketdyne thermochemical program for combustors. The difference in the nozzle exit static temperature, shown in Figure 144, was negligible, being a decrease of less than 4 K and a minimal change in fuel flow at maximum temperature. The mixture ratio change was also minimal; therefore, the 7% SPAN-80: 93% JP-4 mixture was used for all testing.

The performance at the remaining operating points of $\pm 20\%$ of nominal flow and at 0, 1, 5, and 10% seed (percent of cesium carbonate to total flow) was then determined and is shown in Figure 145.

The data compiled in Table 38 show the nominal chamber pressure maintained and the total flow rate corrected by using the expression for c^*:

TABLE 38. REQUIRED REACTANT FLOW RATES

COMBUSTOR SEED CONCENTRATION, %

	0			5			10		
Characteristic Velocity, m/s	1698	1702	1707	1644	1649	1652	1591	1594	1597
Chamber Pressure, atm	24	30	36	24	30	36	23	30	36
Mixture Ratio	3.35	3.35	3.35	3.35	3.35	3.35	3.35	3.35	3.35
Weight Flow, kg/sec									
Total	23.91	29.81	35.67	24.68	30.77	36.86	25.51	31.83	38.12
Fuel	5.50	6.85	8.20	5.28	6.58	7.89	5.05	6.31	7.55
LOX	18.41	22.95	27.47	17.70	22.06	26.42	16.93	21.12	25.30
Seed	--	--	--	1.23	1.54	1.84	2.55	3.18	3.81
H_2O	--	--	--	0.47	0.59	0.70	0.98	1.22	1.46
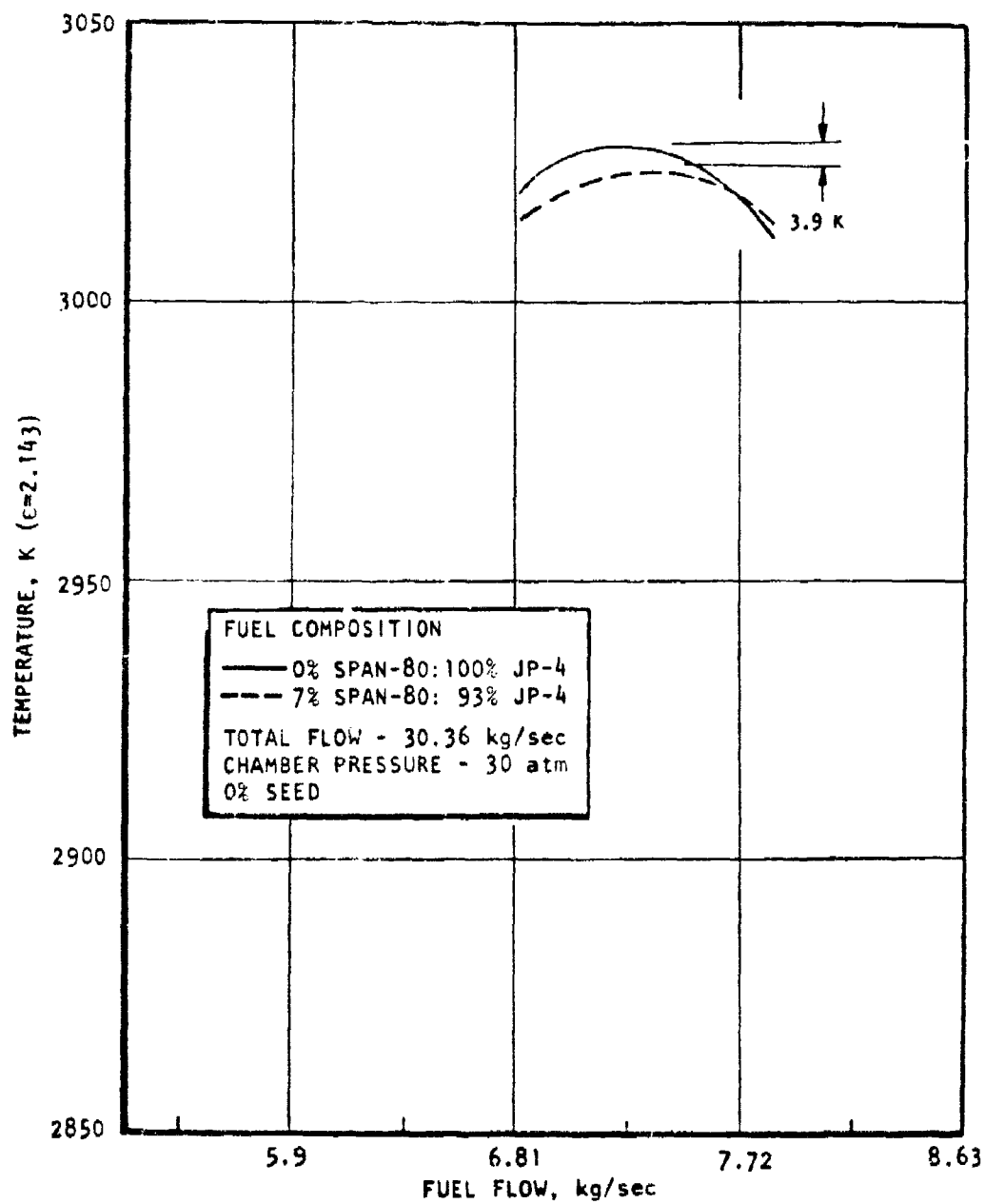
Figure 144. Effect of 7% SPAN-80 on MHD Combustor Temperature
at $\epsilon = 2.143$ vs Fuel Flow.
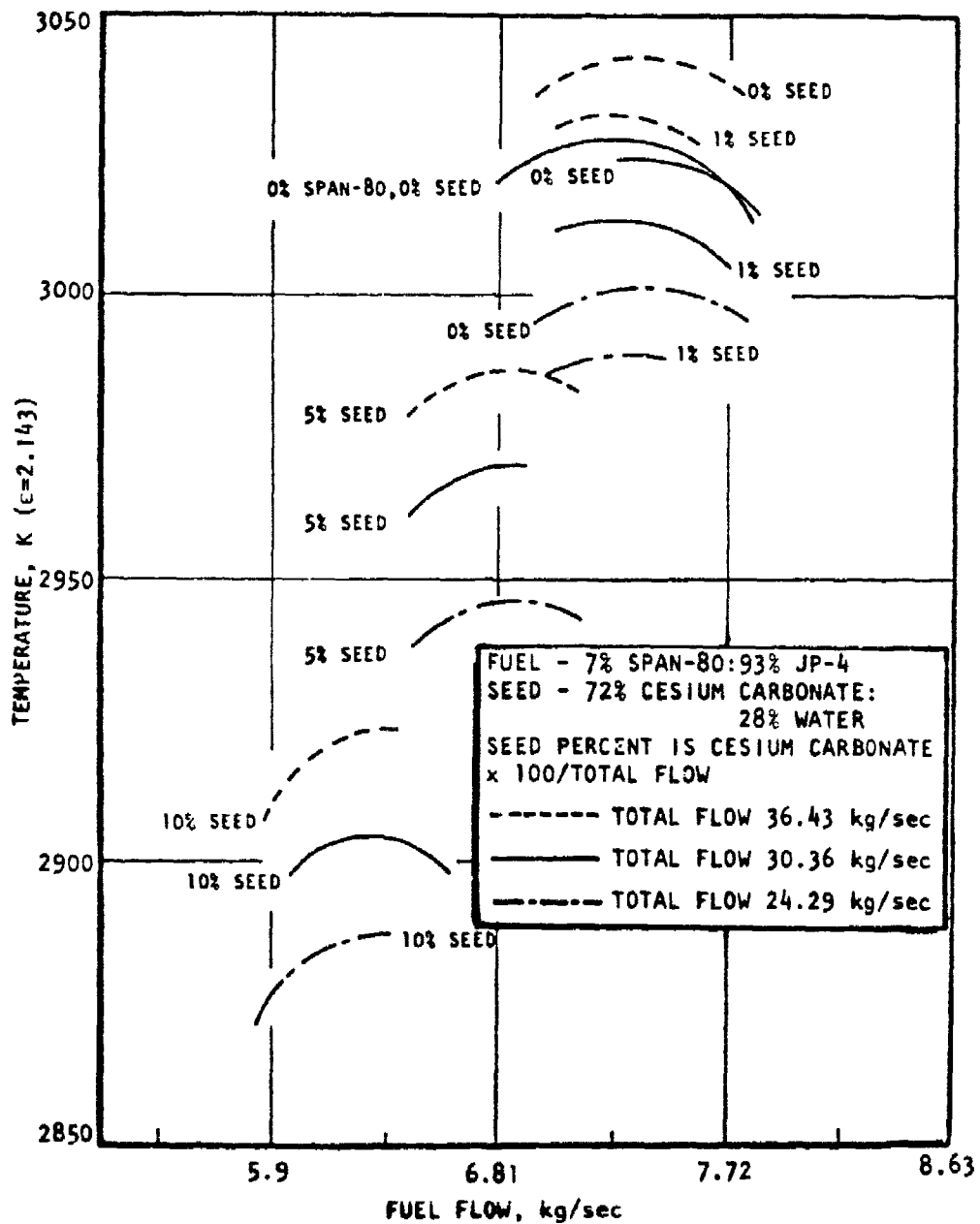
Figure 145. Effect of Varying Percentages of Seed on MHD Combustor
Temperature at $\epsilon = 2.143$ vs Fuel Flow.

$$c^* = \frac{P_c A_t}{\dot{m}}$$

where

c^* = characteristic velocity
P_c = chamber pressure
A_t = throat area
$\dot{m}$ = total flow

b. System Pressure/Flow Calibration

The system pressure drops from the interface to the ends of the manifolds were originally calculated using a C_v of 35 for the valves where:

$$C_v = Q/\sqrt{\Delta P}$$

and Q = water flow rate and ΔP = pressure drop. The JP-4/seed mixer pressure drop was based on the seed system design information pressure drop in the mixer tubes with an allowance for the manifold pressure drops.

The injector pressure drops were calculated using the assumption that friction could be ignored because of the short lengths of passages; hence, the pressure drop resulted from the loss of velocity head at the right angle turns and sudden expansions and contractions which made up the injector passages. The orifice pressure drops were also included. The pressure drops were taken from the inlet manifold just before entering the injector passages to the combustion chamber.

Using this approach and the following densities; JP-4/SPAN-80 density = 0.796 g/cm^3 for a 7% SPAN-80/93% JP-4 mix; 2.299 g/cm^3 density for a seed solution of 72% cesium carbonate/28% water; and densities of fuel and seed mixed of 0.940 g/cm^3 and 1.076 g/cm^3, respectively, for seed mixtures of 5 and 10%, the injector pressure drops for the referenced operating conditions were calculated as shown in Table 39. The injector pressure drops, as established during the test effort at SSFL, are presented in the same table for a direct comparison. Differences realized were caused primarily by erroneous assumptions of the reactant temperatures, and discharge coefficients selected for the analysis.

The original analysis assumed flow meters were used in the fluid reactant analysis. Since this time, the flow meters have been replaced with cavitating venturis. A cavitating venturi was used in the JP-4 line in conjunction with the seed solution cavitating venturi to avoid the effect of a small pressure mismatch at the junction of the two flows in the seed solution mixer. Four venturis each,

TABLE 39.   INJECTOR PRESSURE DROPS

Fluid	$\dot{m}$ kg/sec	Calculated Atmospheres	Actual Atmospheres	P_c, atm
0% Seed				30
LOX	22.95	22.5	20.0	
Fuel	6.85	12.9	12.2	
5% Seed				30
LOX	22.06	20.8	18.6	
Fuel	6.58	17.3	15.4	
10% Seed				30
LOX	21.12	19.2	17.1	
Fuel	6.31	22.5	20.7	

318

fuel and seed, with different throat sizes were used to provide the required flow pressure coverage. Two venturis were used for LO_2 flow control and measurement. A wider operational range was available with these two venturis as they were dependent only on the facility and injector limitations. Some flow overlap was available through variations in the tank pressure.

The pressure drop through facility feed lines was established for SSFL testing, but was not applicable to the AEDC facility. The system interface for fluid feed lines was just upstream of the cavitating venturis. Line lengths at the AEDC facility were not completely defined so that pressure drops could only be estimated. Facility characterization, when conducted at AEDC, will adequately define these pressure drops.

Tests conducted indicate that the venturis operated with a pressure recovery > 90% of the upstream pressure. Setup procedures during the system pressure balance included an allowance of 15% for an adequate operating margin.

The igniter flow rates and system pressure drops have been adequately defined during the SSFL test program. Figure 146 illustrates the reactant orifice calibration for the GO_2 and methane. These drilled orifices were sonic during all operational conditions; again, the throat diameters are indicated for references only. The conditions realized during the test are presented in Table 40.

The cooling water was used to partially cool the heat sink combustor and was intended to cool the cooled-wall combustor. The flow rates used for the heat sink combustor were determined during the heat sink combustor design analyses. The coolant water was provided by the facility water systems, and the requirements for the heat sink combustor are summarized in Table 41. Water requirements for cooling the diagnostic channel and high power MHD channel were provided by Maxwell Laboratories and are presented in Table 42.

The system surge pressures determined in the dynamics analyses are presented in Appendix D. Surge pressures realized during hot fire testing at SSFL varied with the individual venturi inlet pressures and desired flow rates. The values realized have been established by the test configurations and represented many modifications to valve timing in an attempt to eliminate/minimize cutoff problems.

c. Start/Shutdown Analysis

To evaluate the dynamic performance of the system, a mathematical model was formulated and programmed for solution on an analog computer. The entire deliverable system was simulated. The model was used to evaluate the system

319
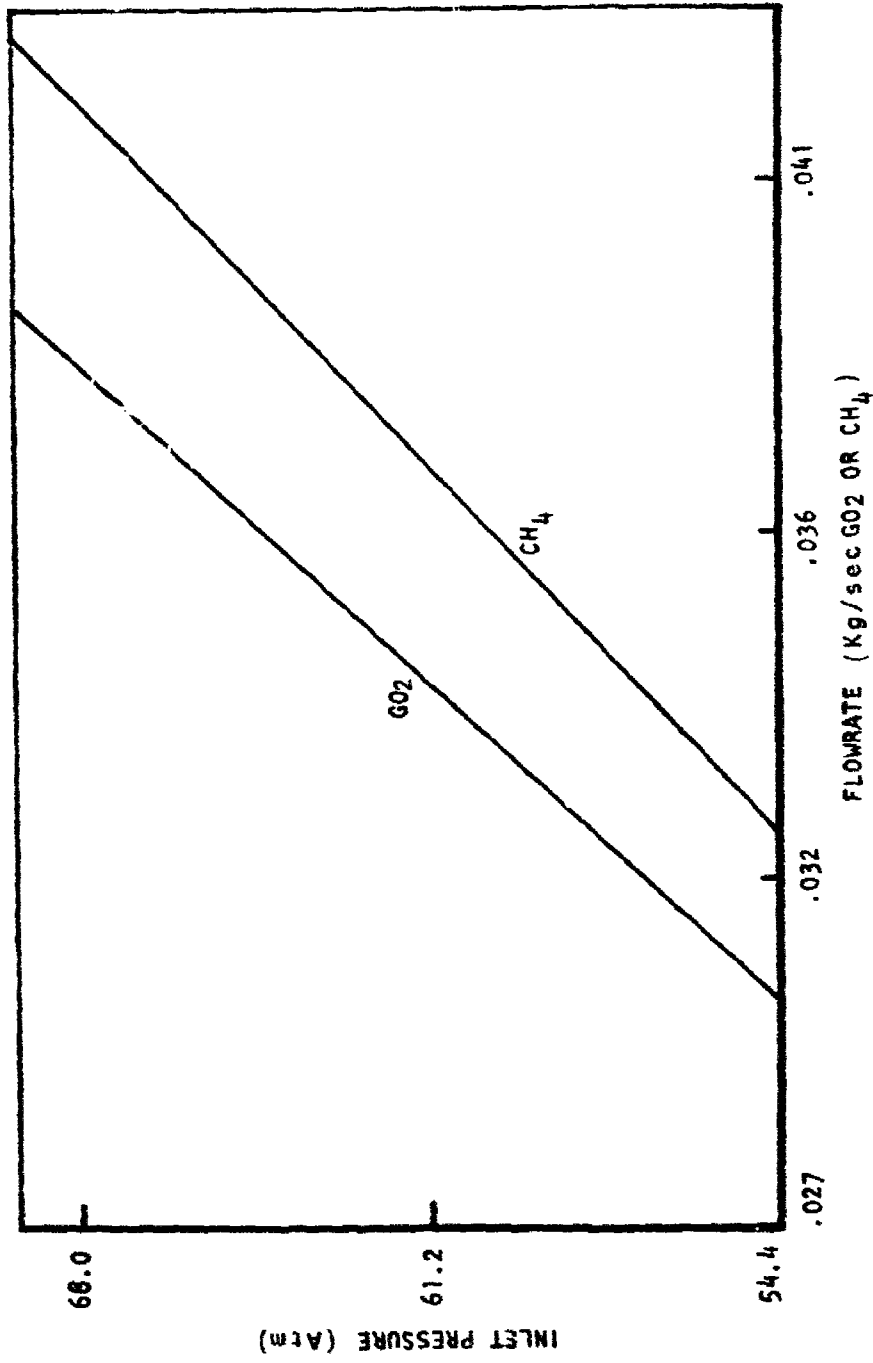
Figure 146   ASI Orifice Calibration.

320

TABLE 40. IGNITER FLOW REQUIREMENTS AT DESIGN CHAMBER

PRESSURE = 30 ATM

Reactant	Flow Rate kg/sec	Injector Δ Pressure, atm	Orifice Inlet Pressure, atm
GOX	0.0375	5.2	66.7
GCH$_4$	0.0375	5.6	61.6

TABLE 41. HEAT SINK COMBUSTOR COOLANT REQUIREMENTS

P_c, atm	Flow Rate, kg/sec			Outlet Pressure, atm	Inlet Pressure, atm
	Throat	Middle	Exit		
24	7.3	4.5	5.4	10.2	36.2
30	7.3	4.5	5.4	10.2	36.2
36	14.5	6.4	9.0	10.2	88.8

TABLE 42. DIAGNOSTIC CHANNEL COOLANT REQUIREMENTS

P_c, atm	Flow Rate, kg/sec	Outlet Pressure (min), atm	Inlet Pressure (min), atm
24	41.65	16.99	31.95
30	41.65	16.99	31.95
36	50.48	12.56	32.97

start and cutoff performance. The start studies included a determination of the effect of valve sequencing and system geometry on pressure surges, volume priming, and overall start time. The cutoff studies consisted of determining the effect of valve area contour and closing time on surge pressures.

Three standard throttle plug contours were available for the Annin valves: (1) semi-throttle; (2) linear; and (3) percentage. The contours referred to the shape of the C_v curve versus valve position, as shown in Figure 147. The LO_2 and fuel valves used the percentage plug and the seed valve used the semi-throttle plug.

In selecting the best plug for the fuel and oxidizer valves, a start and cut-off transient was predicted for each contour using 0.6 sec linear position versus time opening and 0.5 sec linear position versus time closure. The operating conditions used were those resulting in the maximum LO_2 system pressure, and the maximum fuel system pressure, with 10% seed flow. The results of the analysis showed that the transient pressure surges to which the system was subjected were minimized when percentage plugs were installed in the LO_2 and fuel valves.

The seed system was relatively short, and the semi-throttle plug, with a valve closing time of 0.250 sec, resulted in a valve inlet pressure surge of only 7.8 atm above its tank pressure.

The start and cutoff required accurate control of the three reactant valves to provide the short transient and to avoid introducing JP-4 into the combustor prior to the LO_2. A hydraulic system was essentially a positive displacement system and resulted in predictable, repeatable sequencing. For this reason, a hydraulic actuation system was used on the LO_2 and JP-4 valves. A pneumatic actuation system was used on the seed valve because repeatable valve character-istics were not as critical.

Start Analysis. The criteria for the evaluation of the start sequence were: (1) the time from the signal to open the ASI methane valve to reaching 90% of operating chamber pressure must be less than or equal to 1.0 sec; and (2) chamber fuel flow must not be initiated prior to oxidizer flow.

Both of these criteria were dependent on the volumes downstream of the valves, which have to be primed, and the priming characteristics. The maximum priming times resulted from the operating conditions which had the lowest LO_2 and fuel tank pressures. The recommended time from the initial methane valve opening to achieving 90% of operating chamber pressure as a function of LO_2 and fuel valve opening times dictated that a LO_2 and fuel valve opening time of 0.600 sec be used. This time minimized any transient pressures and remained within the one second criteria time.
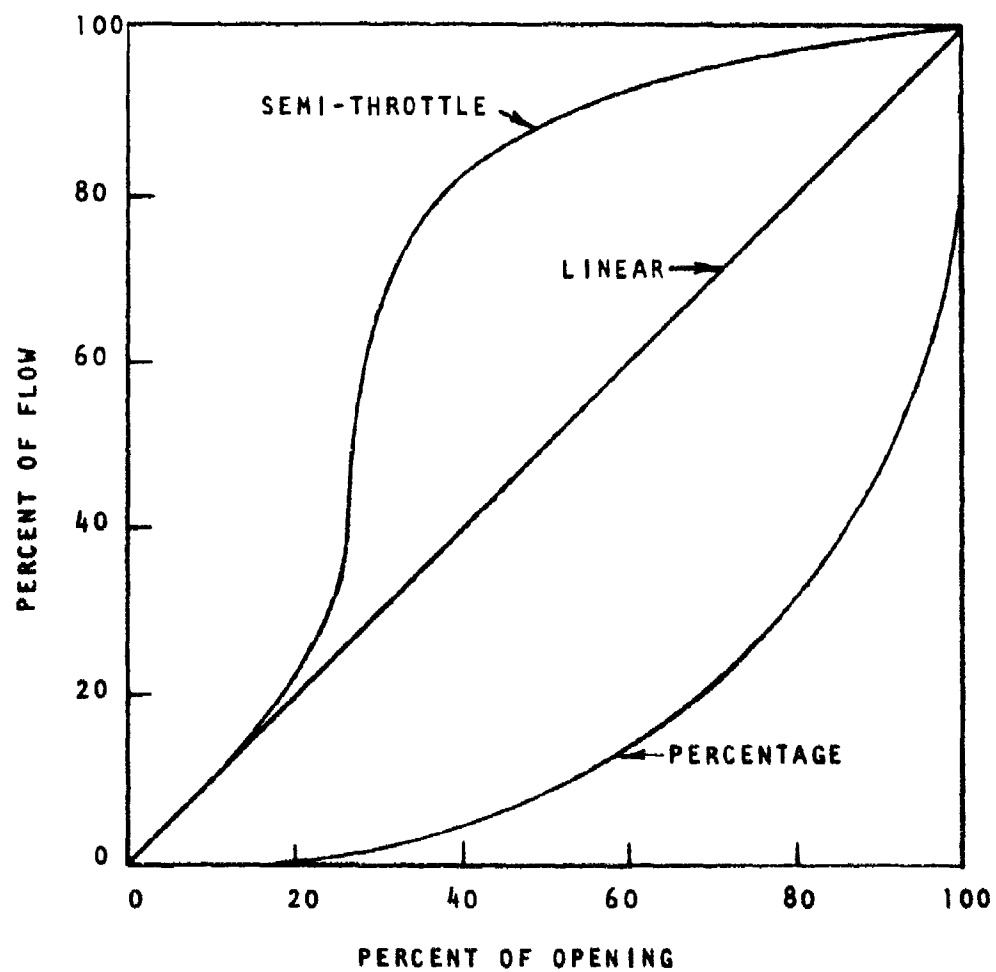
Figure 147. Annin Valve Throttle Plug Contours.

During the start sequence the maximum surge pressures occurred down-stream of the main valve. These pressures were approximately 25% overshoot for the fuel and insignificant for the LO_2 of the steady-state values. At nominal operating conditions the pressure overshoot was well within the channel limits. A pressure rise rate of < 205 atm/sec was observed during the analysis.

Shutdown Analysis. The criteria for cutoff was that the combustor be capable of initiating a restart approximately two seconds after a cutoff signal and that the chamber fuel flow rate was terminated prior to termination of the LO_2 flow rate. The latter criterion was ensured by delaying the start of closing of the LO_2 valve and using injector purges. The first criterion was met by the valve closure times. In addition, predicted valve inlet pressure surge values were considered in arriving at valve closure times. Shown in Table 43 are the maximum predicted LO_2 and fuel valve inlet pressures as a function of valve closing time.

For initial testing, closing times of 0.75 sec were recommended for the LO_2 and fuel valves. The seed valve closing time was not critical; hence, 0.25 sec was used for this study. The predicted cutoff pressures and flow rates were established for nominal, maximum fuel and LO_2 tank pressures and mini-mum fuel and LO_2 tank pressures. In addition to nominal LO_2 and fuel line lengths, the effect on cutoff surge pressures was predicted for 10 and 20% increase in line lengths.

During the shutdown sequence, the maximum surge pressures occurred upstream of the main valve. These pressures were experienced by the shutoff valves and adjacent line but not downstream of the valve or in the supply tank.

d. Redline/Blueline Interlock Description

The redline/blueline system used at Rocketdyne maintained all the opera-tional critical parameters within safe operating limits. A blueline was a value that, if the parameter value was exceeded, the test conductor was notified and appropriate action was taken. A redline was a value that, if the parameter value was exceeded, a cutoff signal was initiated immediately or at some predetermined time delay. These items are verified prior to each test run and any modification or deviation to the redline/blueline values immediately prior to or during a test required the project office concurrence. These values were defined prior to each test and could be modified as necessary based on test data prior to each test.

The interlock system realized in the sequence was used to prevent events from occurring in an unplanned sequence. Timers/instrumentation parameters

TABLE 43. VALVE CLOSURE RATE

MAXIMUM VALVE INLET PRESSURE, ATM

Valve Closing Time, Sec	0.25	0.50	0.75	1.0
Reactant				
LOX	187	122	112	107
JP-4	125	101	98	45

were monitored to ensure that a series of events had occurred prior to permitting the combustor to continue in a predescribed sequence of operation. Each interlock must be satisfied in a predetermined way; otherwise, a cutoff signal was initiated terminating the test. Interlocks were established during the initial system characterization and were continually modified if experimental data substantiated the requirement. These interlocks also were supplied prior to each test initiation.

e. Start/Shutdown Sequence

The system time constants established during the combustor test effort resulted in the following:

LO_2 Valve	– Signal to open	820 msec	
	Signal to close	820 msec	
Fuel Valve	– Signal to open	840 msec	
	Signal to close	410 msec	
Seed Valve	– Signal to open	500 msec	
	Signal to close	170 msec	

All the other valves were solenoid valves and realized operational times of approximately 25 to 35 msec.

The sequence time lines established during the combustor hot fire test effort are illustrated in Figures 148 and 149. The start and cutoff transition sequence shows the events as they occur; actual times varied slightly because the pneumatic and hydraulic valve position signals were actuated by mechanical means and priming times varied slightly with changing flow rate requirements.

The test operational sequence and gas generator operating logic are described in Table 44. Typical start and shutdown times (from command) were 1400 and 850 msec, respectively. Typical parameter values for the operational sequence are listed below:

Timing	Continue Signals	Redlines
T_1 = 1100 msec	P_1 = 11.2 atm	24.8 atm $\leq$ P (ASI) $\leq$ 41.14 atm
T_2 = 750 msec	P_2 = 24.8 atm	24.8 atm $\leq$ P (combustor) $\leq$ 41.14 atm
T_4 = 500 msec	P_3 = 14.6 atm	
T_6 = 2900 msec	P_4 = 24.8 atm	
T_m = 3800 msec	V = 100 g (p-p)	
	for 50 msec	

These values were specifically defined in each test request.
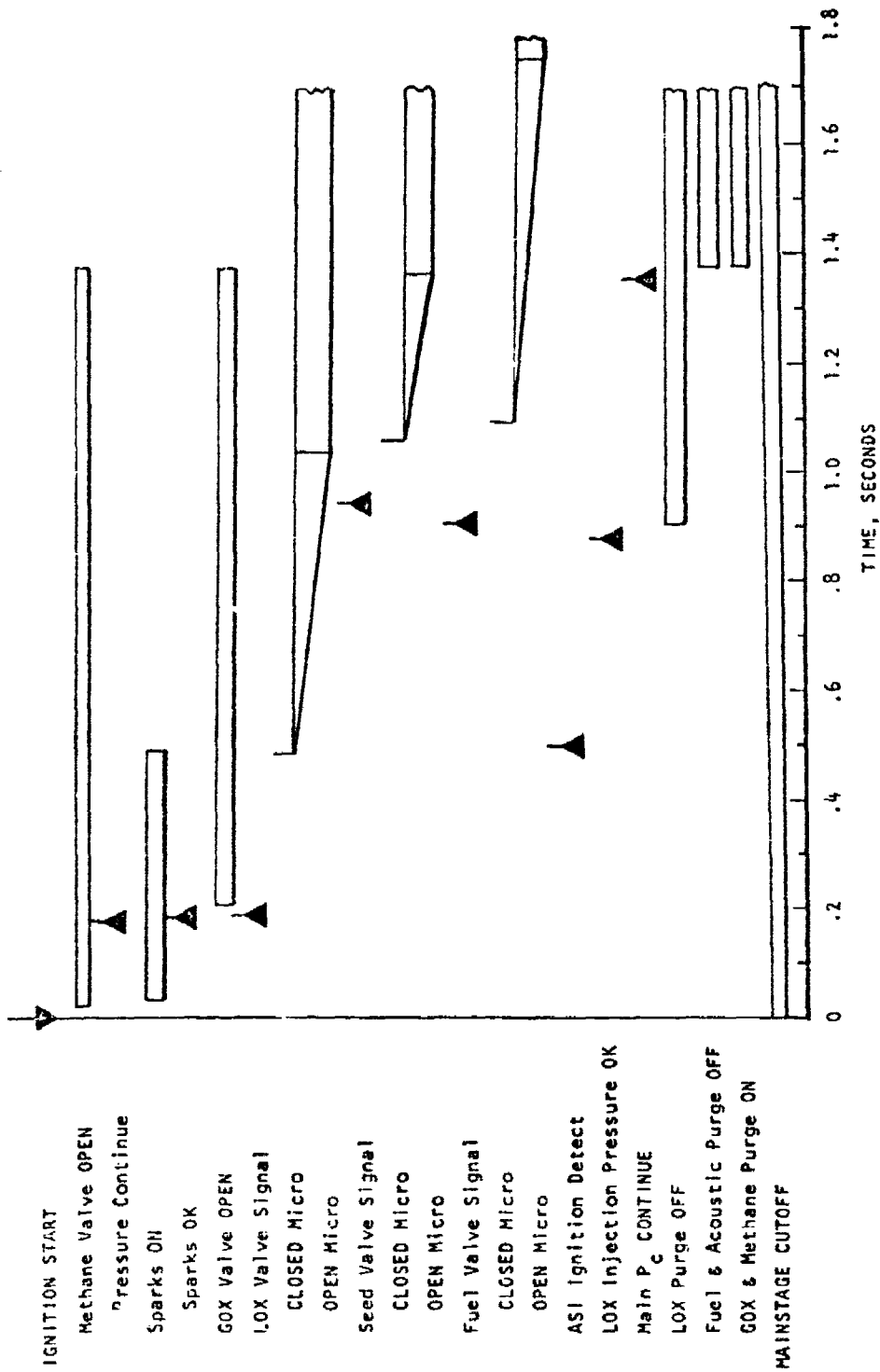
Figure 148. MHD Combustor Start Transition.

IGNITION START

Methane Valve OPEN
Pressure Continue

Sparks ON

Sparks OK

GOX Valve OPEN

LOX Valve Signal
CLOSED Micro
OPEN Micro

Seed Valve Signal
CLOSED Micro
OPEN Micro

Fuel Valve Signal
CLOSED Micro
OPEN Micro

ASI Ignition Detect

LOX Injection Pressure OK

Main P_c CONTINUE

LOX Purge OFF

Fuel & Acoustic Purge OFF

GOX & Methane Purge ON

MAINSTAGE CUTOFF

TIME, SECONDS

328

CUTOFF

Fuel Purge

Acoustic Cavity Purge

LOX Purge

GOX Purge

Methane Purge

LOX Valve Signal
   OPEN Micro
   CLOSED Micro

Fuel Valve Signal
   OPEN Micro
   CLOSED Micro

Seed Valve Signal
   OPEN Micro
   CLOSED Micro

BOMB INITIATED

TIME, SECONDS

Figure 149.   MHD Combustor Shutdown Transition.

TABLE 44. GAS GENERATOR SEQUENCE/INTERLOCK LOGIC – SYSTEM OPERATIONAL SEQUENCE

1. Conduct Facility Pretest Preparation (Table 45)
2. Verify Facility Pretest Preparation Completion
3. Initiate Countdown
4. Open Cooling Water System Valve – Channel
5. Open Cooling Water System Valve – Combustor
6. Open LO_2 Tank Valve
7. Open LO_2 Bleed Valve
8. Verify LO_2 System Priming
9. Close LO_2 Bleed Valve
10. Pressurize Seed, Fuel, and LO_2 Tanks
11. Prime Combustor Cooling Water Circuits
12. Prime Channel Cooling Water Circuit
13. Energize Magnet
14. Open GO_2 System Purge Valve
15. Open Methane System Purge Valve
16. Open LO_2 System Purge Valve
17. Open JP-4 System Purge Valve
18. Open Acoustic Cavity Purge Valve
19. Start Channel Water Pump
20. Start Combustor Water Pump
21. Open Combustor Cooling Water Main Valve
22. Open Channel Cooling Water Main Valve
23. Verify Cooling Water Main Valve – Open Microswitch
24. Open Seed Solution Main Valve
25. Verify System Preparation Complete
26. Verify Cooling Water Flow – Combustor
27. Verify Cooling Water Flow – Channel

TABLE 44.   GAS GENERATOR SEQUENCE/INTERLOCK LOGIC –

SYSTEM OPERATIONAL SEQUENCE (Cont'd)

28.   Verify System Blueline Parameter

29.   Arm Redline Cutoff Circuits   (Figure 150)

30.   Verify Redline Circuits

31.   Redline/Blueline Activation Complete

32.   Verify LO_2 System Priming (Bleed as necessary)

33.   Start Instrumentation Data Recording

34.   Start Cameras

35.   Start Firing Sequencer   (Figure 151)

36.   Stop Data Recording

37.   Stop Cameras

38.   Close Seed Solution Tank Valve

39.   Close JP-4 Tank Valve

40.   Open LO_2 Bleed Valve

41.   Close LO_2 Tank Valve

42.   Vent LO_2, JP-4, and Seed Solution Tanks

43.   De-energize Magnet

44.   Close Combustor Cooling Water Main Valve

45.   Close Channel Cooling Water Main Valve

46.   Stop Cooling Water Pumps

47.   Close GO_2 System Purge Valve

48.   Close Methane System Purge Valve

49.   Close JP-4 System Purge Valve

50.   Close Acoustic Cavity Purge Valve

51.   Open Continuous LO_2 Purge Valve (Manual)

52.   Close LO_2 System Purge Valve

53.   Begin Post-Operation Evaluation

54.   Lift Personnel Access Restriction
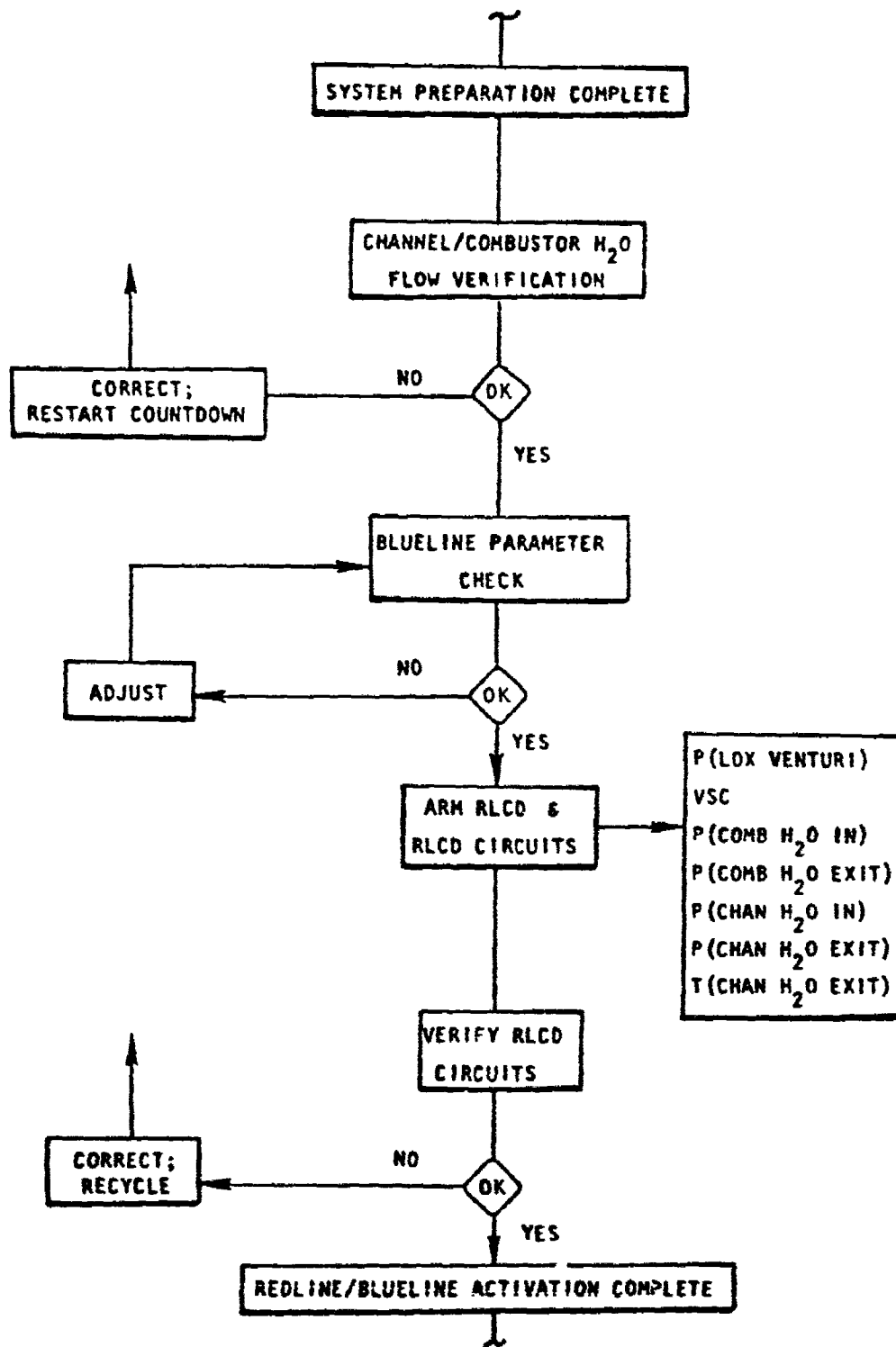
Figure 150. Redline/Blueline Activation.

Figure 151. Gas Generator Start Sequence.

333
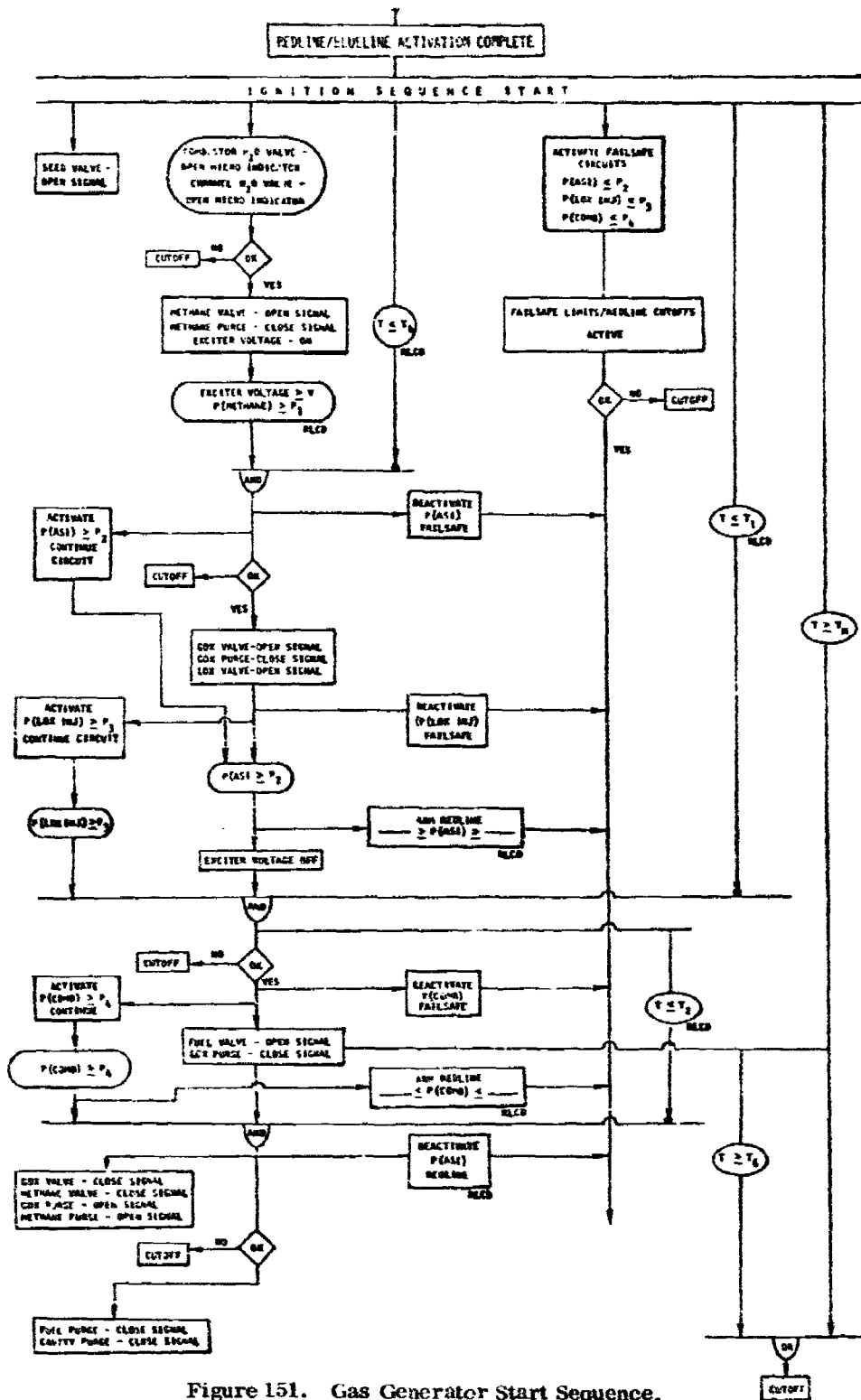
TABLE 45.   FACILITY PRETEST PREPARATION

The following operations should be performed prior to test.   The sequence and procedures should be determined by the AEDC test engineer:

1.   Test Request Reviewed and Approved

2.   Instrumentation Calibration Completed

3.   Safety Circuit Checks Completed

4.   Flow Control Venturis Installed   (Test Request)

5.   Leak Checks Completed

6.   Sequence Checks Completed

7.   Hardware Inspections Completed

8.   Fuel Tank Level Check

9.   Fuel Recirculation Pump Started

10.   Gaseous Nitrogen Supply Check

11.   Seed Solution Supply Check

12.   Methane/GO_2 Supply Check

13.   LO   Transfer to Run Tank Completed

14.   Set System Purge Pressure Levels   (Test Request)

15.   Set Redline Cutoff Parameter Values   (Test Request)

16.   Set Operating Parameter Values   (Test Request)

17.   Test Request Parameter Setting Check

18.   Open Seed Solution Tank Valve

19.   Open Seed Solution Bleed Valve

20.   Verify Seed Solution Line Priming

21.   Close Seed Solution Bleed Valve

22.   Open Fuel Tank Valve

23.   Open Fuel Bleed Valve

24.   Verify Fuel Line Priming

25.   Close Fuel Bleed Valve

26.   Open Methane Tank Valve

27.   Open GO_2 Tank Valve

334

D. SUPPORT STRUCTURE

A structure was designed and fabricated to support the combustor, channel and feed system control components. In the course of the system assembly, many supporting components were mounted to the structure to result in a relatively self-contained assembly.

1. Design Requirements

Requirements for the support structure were developed in the course of the program through discussions of the high power MHD channel/diffuser, gas generator, magnet and facility requirements. These requirements are listed in Table 46.

There were two general categories of requirements: (1) Performance Test Requirements - high power MHD channel/diffuser, cooled wall combustor, HPMS magnet at AEDC, and AEDC facility; and (2) Development Test Requirements - diagnostics channel, heat sink combustor, and SSFL facility. An attempt was made to provide commonality between the support structures for the two requirement categories; however, the requirements and combustor size differences forced some structural differences.

In the development testing the heat sink combustor and diagnostics channel must be supported along with the feed system and control valves, and be installed at the SSFL test facility. The diagnostics channel and heat sink combustor interface were defined to be identical to the high power MHD channel/cooled wall combustor interface; this led to an exit support for the combustor and established much of the support structure configuration. There were no envelope or location restrictions; however, the combustor instrumentation and components must be readily accessible because of the frequent problems which could be associated with development testing.

In the performance test program, the cooled wall combustor, high power MHD channel/diffuser, and feed system control valves must be supported within the limitations imposed by the HPMS magnet and the AEDC test facility. The support structure around the combustor was restricted to a 61 cm x 61 cm envelope and the structure mounting to the facility floor was required to be more than 91.4 cm from the combustor/channel interface. The axial location of the combustor/channel interface was not fixed and provisions were made for approximately 41 cm extension of this interface from the nominal position. These requirements imposed severe design limitations on the performance test support design.

335

TABLE 46.   SUPPORT STRUCTURE DESIGN REQUIREMENTS

SUPPORT

1.   Combustor/Nozzle Assembly (Heat Sink and Cooled Wall)

2.   Channel (Diagnostics/MHD)

3.   Feed System

SSFL FACILITY INTERFACE

1.   Mount to Test Stand Structural Members

2.   Support Diagnostics Channel Water Manifold

3.   Diagnostics Channel Cantilevered from Combustor Exit

4.   Envelope Restriction - Not Constraining

5.   Location Restriction - Not Constraining

6.   Alignment Accuracy - None

7.   Installation Restriction - Not Constraining

8.   Instrumentation/Handling Access Required

AEDC FACILITY INTERFACE: COMBUSTOR END

1.   Concrete Floor*

2.   Support MHD Channel*

3.   Envelope Restriction - 61 cm x 61 cm

4.   Location Restriction

a. Support Foot 91 cm Away From Reference Location
b. Combustor/Channel Located on Magnet Axis - 152 cm from floor
c. Nozzle Exit 19.8 cm to 59.9 cm from Reference Location

5.   Alignment Accuracy - None Defined

6.   Installation Restriction - Split Magnet; No Constraint

* Requirements not yet defined

336

TABLE 46.   SUPPORT STRUCTURE DESIGN REQUIREMENTS (Cont'd)

LOADS

		Power Test (AEDC)	Development Test (SSFL)
1.	Thrust Load		
	a. Axial	119,260 N	85,880 N
	b. Off-Axis	2,670 N	890 N
2.	4 g Load (All Axes)	4,450 N	33,550 N

STRUCTURAL DESIGN CRITERIA

1.   Safety Factor of 4 or greater on Ultimate Strength

2.   Avoid Loads on Diagnostics or MHD Channel

The structure must be designed to withstand the loads imposed by the system operation with very low movement of the combustor/channel interface. This avoided imposing loads on the channel.

2. Design Description

Based on the design requirements, a two piece structure was designed. The initial piece, the base structure, was a truss type structure which formed the basic mounting platform. This structure was common to both the development test and power test assembly. The second piece, the gas generator mount, rested upon the base structure and contained the actual gas generator components. Two versions of the gas generator mount were designed: (1) development test mount; and (2) performance test mount. The performance test mount was a structurally efficient, partially enclosed box-type of configuration necessary to provide high rigidity within the limits of the performance test envelope restrictions. The development test mount was an open-type mount to provide the ready access necessary for system development.

a. Base Structure

The base structure, illustrated in Figure 152, was a truss-type structure consisting of four vertical H-beam sections joined at the top and bottom to rectangles of H-beam sections. The vertical H-beams were crossed-braced with beams and plates on the ends for rigidity. These beams were made of aluminum 6061-T6 and were welded in place. The 6061-T6 material selected for its strength and resistance to chemical and stress corrosion. The top and bottom surfaces were machined to be parallel to assure proper position of the gas generator mount. The large axial thrust loads were reseated by a pair of inclined, pin-connected beams which connected the upper portion of the base structure to the test facility.

At the SSFL facility the base structure was bolted to structural members of the test stand. In the AEDC facility the structure could be bolted into the concrete floor through the use of anchor bolts.

b. Performance Test Mount

The performance test mount, illustrated in Figure 153, consisted of an aluminum box 58.4 cm x 58.4 cm on cross section; 1.27 cm were allowed on each side for clearance. The combustor nozzle exit was attached to the structure around the entire periphery. This mount absorbed the axial loads. Adjustable supports from the side and bottom of the box were used to restrain the lateral motion of the combustor and assist with alignment. The MHD channel was bolted to the combustor.
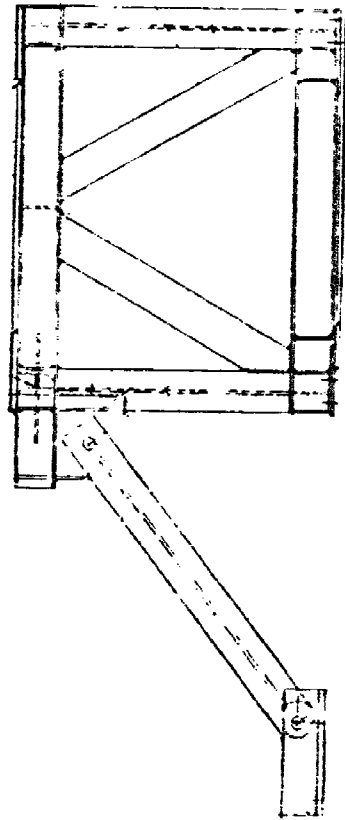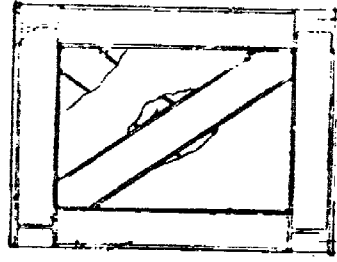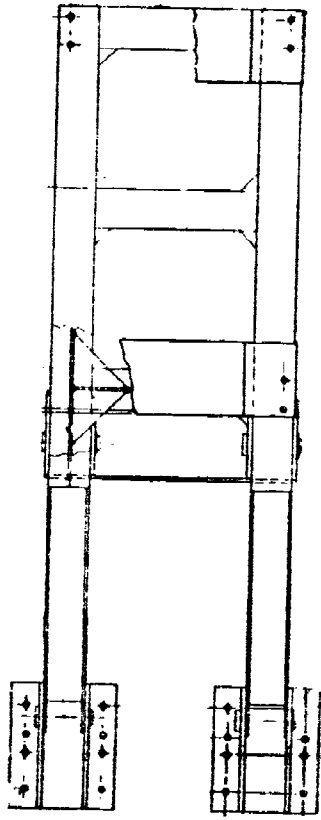
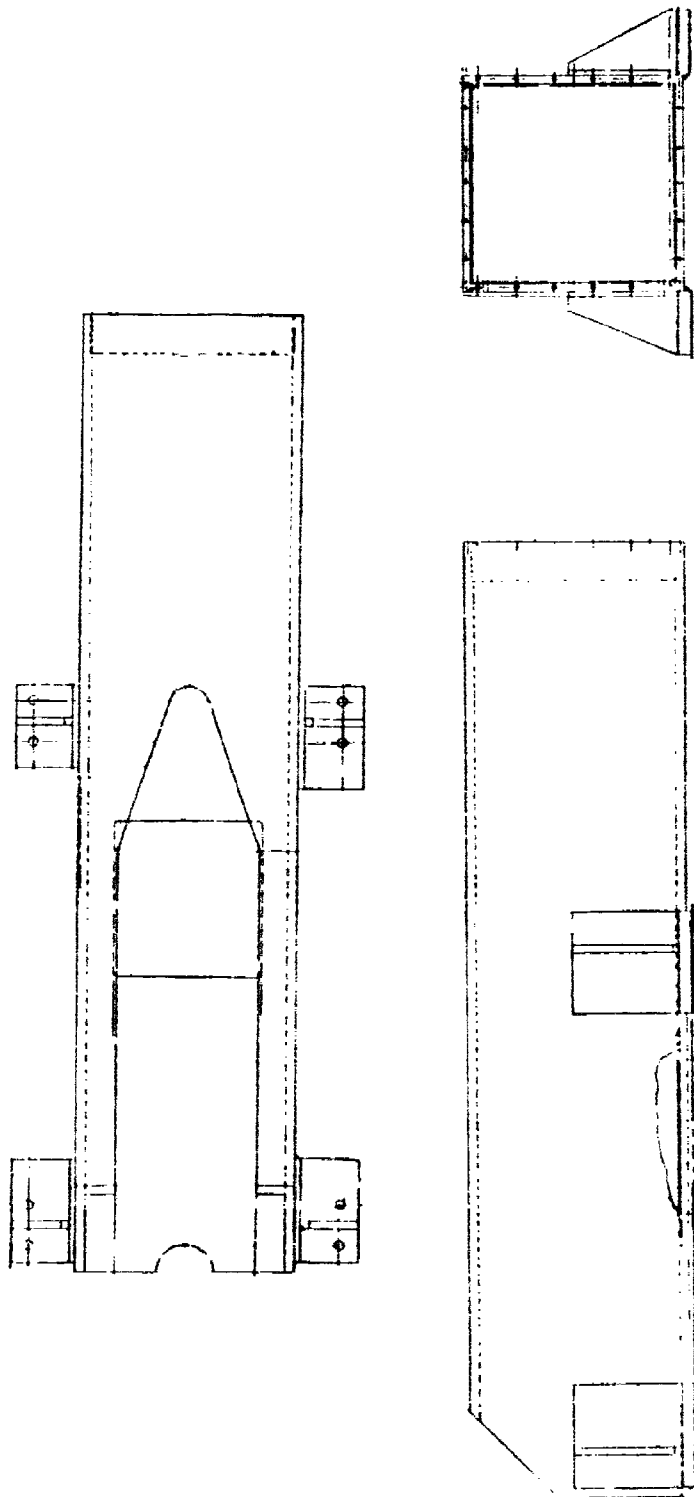338

Figure 152. Support Structure Base

339

Figure 153. Performance Test Support Structure

340

The top of the box was cut away to allow mounting of the fuel control valves. The valve was supported by a mount which rested on a machined surface provided on the interior bottom of the structure. The mount will slide to allow slight axial motion of the valve and avoid placing loads on the injector. The seed mixer was placed directly behind the fuel valve and was mounted to allow slight axial motion. The total axial motion was absorbed by bends in the supply lines. The oxidizer valve was mounted to the side of the structure. Combustor motion was absorbed by the double bend in the oxidizer manifold line.

The entire mount was attached to the base support using bolts. When the axial position of the channel in the magnet was finalized, specific attached points could be defined.

Provisions for inspection and instrumentation access were made in the side panels. These were limited to maintain a rigid structure. Small auxiliary components can be internally mounted on the sides of the support and externally mounted at axial locations outside the restricted envelope section.

c. Development Test Mount

The development test support was used at SSFL. This support was basically a flat plate reinforced in specific areas. Components were mounted to the plate in a manner similar to the mounting for the performance test support. Since a high degree of rigidity was not needed, the structure was open to allow ready access.

The combustor was constrained from axial motion at the nozzle exit using a slot and key method. Axial motion was not restrained at any other point. Lateral loads were absorbed by the exit mount and a constraint midway along the combustor. Control valves and seed mixer were mounted in a manner identical to the method used in the performance test mount.

The mount was made of carbon steel which was selected to reduce fabrication cost. The mount was bolted to the base structure allowing an approximately 45 cm overhang. The diagnostics channel was mounted to the combustor exit.

d. Structural Analysis

A static load space frame beam analysis on the support structure was conducted. This is shown in Figure 154. The structure consisted of the base support with the performance test mount. Axial and off-axis loads applied at the combustor exit were:
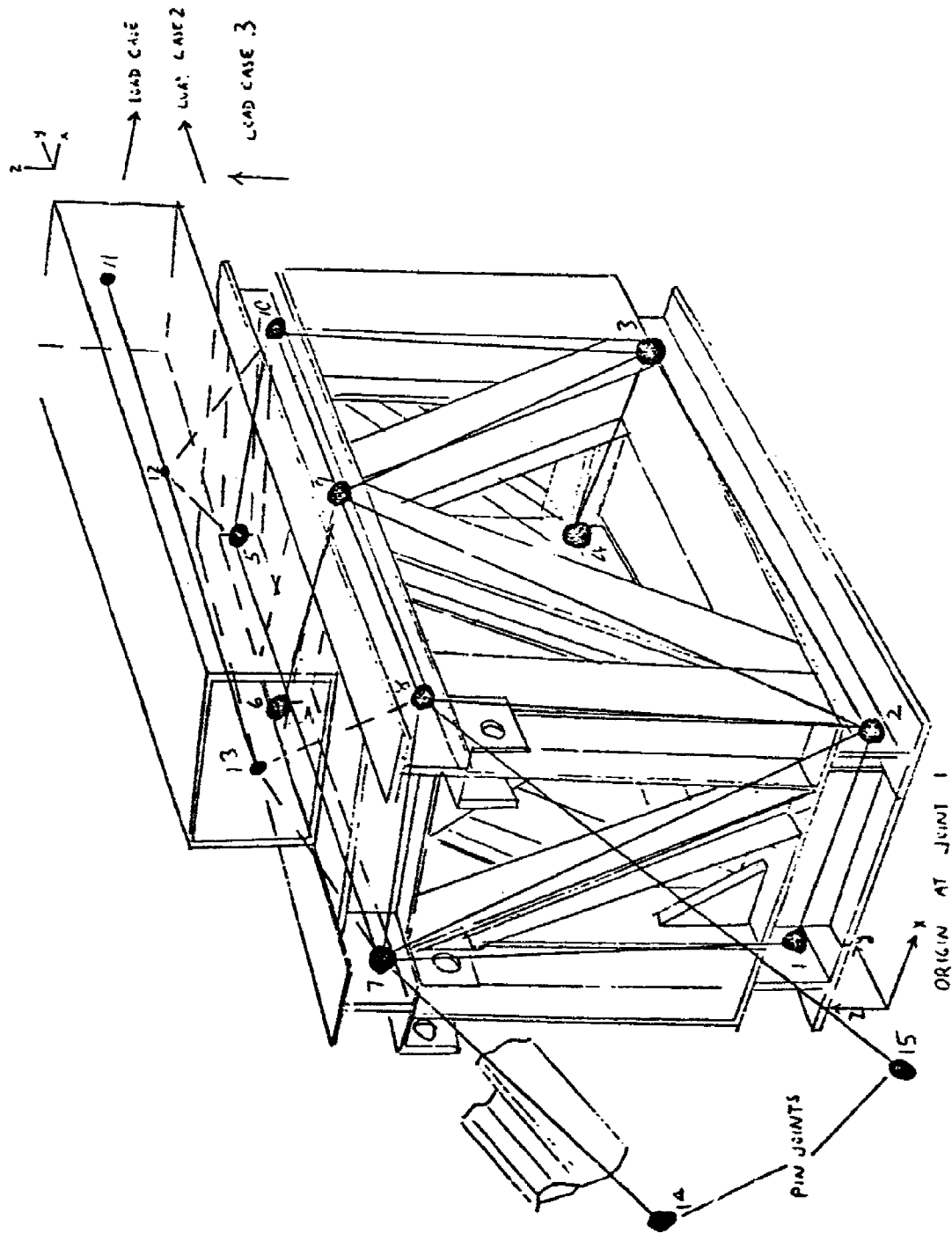
341

Figure 154. Static Load Space Frame Beam Analysis of Support Structure.

(1) Cooled Combustor/MHD Channel

      119,260 N axial
        7,120 N off-axis

(2) Heat Sink Combustor/Diagnostics Channel

      85,890 N axial
      34,440 N off-axis

The support was found to be structurally adequate, having low member stresses, small deflections, and small rotations. In addition to the beam structure analyzed in the space frame model, there were flat plates at the ends acting as a shear panel which should have made the calculated deflections and rotations conservative.

Reaction forces at the support structure base were small under combined conditions. Maximum reactions range up to 151,300 N with a maximum applied moment of 4,930 N-m. Since all members had more than 30 sq. cm of cross sectional area, the stresses were low.

Deflections and resulting rotations were small. For the Case (2) combined loads, the maximum deflection was 0.168 cm. For the Case (1) combined loads, the maximum deflection was 0.064 cm. Rotation was minimal in all cases, with a maximum of 0.048 deg at the combustor channel interface.

A more detailed picture of reaction loads and deflections is outlined in Table 46. Except in the heat sink combustor Δx deflection, all deflections were in the range of 0.03-0.05 cm. This larger Δx deflection was caused by the twisting of the structure from side loads.

3. Fabrication

The base support and the development test mount were fabricated as illustrated in Figure 155. The two pieces were fabricated separately, cutting and welding the larger pieces and machining the more precise components. The two pieces were assembled and parallel surfaces machined on the development test mount. Gas generator component installation and final structure assembly was performed at the SSFL test facility.
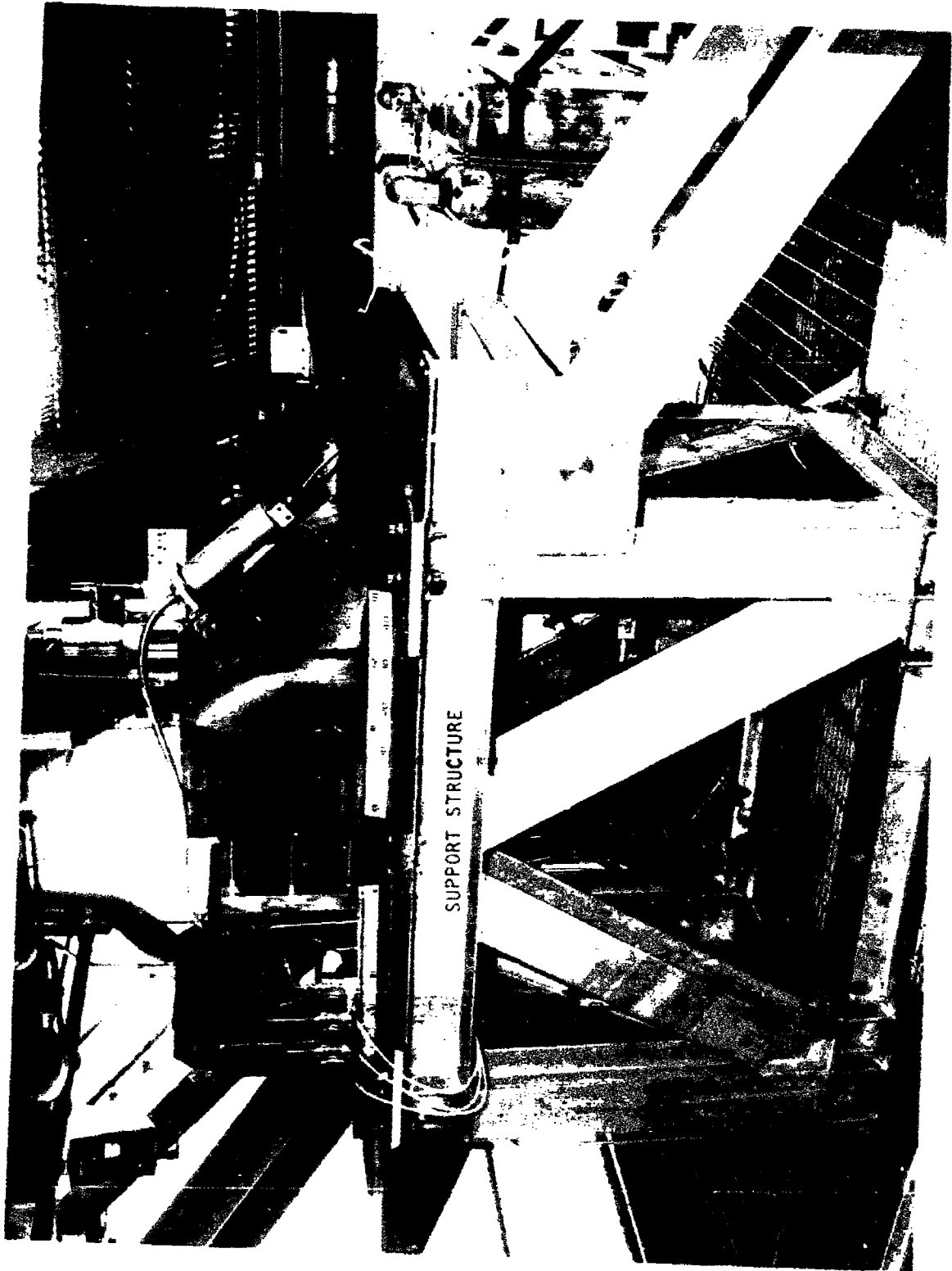
SUPPORT STRUCTURE

4LZ34-4/14/77-S1C

Figure 155. Development Test Support Structure

344

THIS REPORT IS CONTINUED IN VOLUME II

(See Statement in the Foreword)

- Volume I, Section VI, Stops at Page 354

- Volume II, Section VII, Resumes at Page 355

- The Tables of Contents, Lists of Illustrations, and Lists of Tables are tailored to each Volume.

- The Lists of References and Abbreviations are common to the two Volumes and are included at the end of each Volume.

REFERENCES

1. O. K. Sonju and J. Teno, "Study of High Power, High Performance Portable MHD Generator Power Supply Systems," AFAPL-TR-76-87, AD#AO40381, August 1976.

2. "Combustion Stability Specifications and Verification Procedures for Liquid Propellant Rocket Engines," CPIA Publication 247, October 1973.

3. O. K. Sonju, J. Teno, R. Kessler, L. Lontai, and D. E. Meader, "Status Report on the Design Study Analysis and the Design of a 10 MW Compact MHD Generator System," AFAPL-TR-74-47, Part II, June 1974.

4. D. W. Swallom, O. K. Sonju, D. E. Meader, and G. T. Heskey, "MHD Lightweight Channel Development," AFAPL-TR-78-41, June 1978.

5. O. K. Sonju, J. Teno, J. W. Lothrop, and S. W. Petty, "Experimental Research on a 400 kW High Power Density MHD Generator," AFAPL-TR-71-5, May 1971.

6. O. K. Sonju, D. W. Swallom, D. E. Meader, H. Becker, R. V. Burry, A. W. Huebner, and R. F. Cooper, "Development of a Compact, Lightweight High Performance 30 MW MHD Generator System," 17th Symposium on Engineering Aspects of Magnetohydrodynamics, Stanford University, March 1978.

7. G. W. Sutton and A. Sherman, "Engineering Magnetohydrodynamics," McGraw Hill, 1967.

8. O. K. Sonju, "Viscous Magnetohydrodynamic Flows," Stanford University Institute for Plasma Research, SUIPR Report No. 245, 1968.

9. H. C. Garner, "The Development of Turbulent Boundary Layers," ARC of Britain R&M 2133, 1944.

10. J. Teno, T. R. Brogan, S. W. Petty, J. W. Lothrop, and O. K. Sonju, "Research Studies and the Development of MHD Generators and Accelerators," AEDC-TR-70-14, January 1970.

11. Kreith, F., _Principles of Heat Transfer_, International Textbook Co., 1961.

12. User Information Manual for MITAS (Martin Marietta Thermal Analyzer System); Publication No. 86615000, Rev. A; Cybernet Service Control Data Network; September 1972.

347

13. Anon., "Flow of Fluids Through Valves, Fittings, and Pipes," Crane Company Technical Paper No. 410, 1976.

14. Coffin, L. F., "Internal Stresses and Fatigue in Metals," G. Rossweiter and W. Grube, Elsevier Publishing Co., 1959.

15. Majors, H., "Comparison of Thermal Fatigue with Mechanical Fatigue Cycling," ASTM STP 165, 1954.

16. Manson, S. S., "The Challenge to Unify Treatment of High Temperature Fatigue," ASTM STP 520, 1973.

17. Dietz, A. G. H., "Composite Engineering Laminates," MIT Press, 1969.

18. Broutman, L. J. (Ed.), "Composite Materials, Vol. 5, " Academic Press, 1974.

19. Timishenko, S., "Strength of Materials - Part I," D. Van Nostrand, 1968.

20. "Chamber Technology for Space Storable Propellants," Fourth Interim Report No. R7985, Rocketdyne, Division of Rockwell International, September 1969.

21. M. D. Schuman and D. C. Behosse, "Standardization Distribution Energy Release (SDER) Computer Program", 13th JANNAF Combustion Meeting, CPIA Publication 281, Volume III, December 1976, pp 79-91 (Also AFRPL-TR-77-1, AFRPL).

22. W. S. Hines, "Turbulant Force Convection Heat Transfer to Liquids at Very High Heat Fluxes and Flow Rates", RR61-14, Rocketdyne, a Division of Rockwell International, 30 November 1961.

23. "Investigation of Thermal Fatique in Non-Tubular Regeneratively Cold Thrust Chambers (FO4611-70-C-0014) Isothermal Fatigue Tests, Task III," No. SR-2112-7001, February 1972.

24. "High Temperature Low Cycle Fatique of Copper Base Alloys in Argon, Part II - Zirconium Copper at 482C, 538C, and 590C, " No. NASA CR-121-260, August 1973.

25. "Correlation of Injector Spray Drop Size Distribution and Injector Variables," Final Report No. R8455, Rocketdyne, Division of Rockwell International, December 1971.

26. J. H. Rupe, "A Correlation Between the Dynamic Properties of a Pair of Impinging Streams and the Uniformity of Mixture Ratio Distribution in the Resulting Spray". Progress Report No. 20-209, JPL, Pasadena, California, 28 March 1956.

27. Oberg, C.L., R.C. Kesselring, C. Warner III, and M.D. Schuman, "Analysis of Combustor Instability in Liquid Propellant Engines With or Without Acoustic Cavities," NAS9-12077, June 1974.

28. 14th NASA F-1 Program Review, May 1964.

29. Dykema, O.W., "An Engineering Approach to Combustion Instability," Second JANNAF Combustion Conference, CPIA No. 105, pp 205-223, May 1966.

30. Oberg, C.L., et al, "Evaluation of Acoustic Cavities for Combustion Stabilization," Seventh JANNAF Combustion Meeting, CPIA No. 204, pp 743-756, February 1971.

31. Oberg, C.L., and T.L. Wong, "Combustion Instability Suppression Devices," Eighth JANNAF Combustion Meeting, CPIA No. 220, pp 781-794, November 1971.

32. Kuluva, N.M., and C.L. Oberg, "Acoustic Liners for Large Engines," Final Report Contract NAS8-21345, (R7792), Rocketdyne, Division of Rockwell International, March 1969.

33. Hines, W.S., "Turbulent Forced Convective Heat Transfer to Liquids at Very High Heat Fluxes and Flow Rates," RR61-14, Rocketdyne, Division of North American Aviation, November 1961.

34. Saas I, E.L. Wilson and R.M. Jones, "Finite Element Stress Analysis of Axisymmetric Solids with Orthotropic, Temperature Dependent Material Properties", TR-0158, (S3316-22)-1, The Aerospace Corporation, San Bernardino, California (September 1967).

35. "25 MW MHD Combustor Design Study Final Report", Report No. R-9967, Rocketdyne, 1976.

36. Chemical Engineers' Handbook, 4th Edition, McGraw-Hill, 1959, Chapter 3, Prediction and Correlation of Physical Properties.

37. Kenics Design Bulletin, Static Mixer Modules, Techno'ogy, Processing & Sizing, March 1976.

38. S.J. Chen, "Drop Formation of Low Viscosity Fluids in the Static Mixer Units," KTEK-5, Kenics Corporation, 1972.

39. Middleman, S., "Drop Size Distributions Produced by Turbulent Pipe Flow of Immiscible Fluids through a Static Mixer," Ind. Eng. Chem, Process Research & Development, V 13, No. 1, 1974.

40. C. A. Sleicher, "Maximum Stable Drop Size in Turbulent Flow," AIChE Journal, Vol. 8, No. 4, pp 471-477, 1962.

41. C. A. Sleicher, H. I. Paul, "The Maximum Stable Drop Size in Turbulent Flow: Effect of Pipe Diameter," Chem. Engr. Sci., Vol. 20, pp 57-59, 1965.

42. S. B. Collins, J. G. Knudsen, "Drop Size Distributions Produced by Turbulent Pipe Flow of Immiscible Liquids," AIChE Journal, Vol. 16, No. 6, pp 1072-1080, 1970.

43. J. M. Coulson and J. F. Richardson, Chemical Engineering, Vol. 1, 2nd Ed., Pergamon Press, 1970.

44. "AEDC Test Plan", MLI No. MHD 218-10-1, January 1978.

45. "Interface Control Document", MLI No. MHD 218-9-1, April 1978.

46. Earles, D. R. and M. F. Eddins, Reliability Engineering Data Series Failure Rates, Avco Corporation, April 1962.

47. Nonelectric Reliability Notebook, Hughes Aircraft Company, January 1975.

48. A. H. Shapiro, "The Dynamics and Thermodynamics of Compressible Fluid Flow", Book, Volume I, 1953 Ronald Press.

49. "Thermophysical Properties of Oxygen from the Freezing Liquid Line to 600 R for Pressures to 5000 psia," NBS Technical Note 384, issued July 1971.

50. "ICRPG ODE Equilibrium Reference Program, A Computer Program for the Calculation of Chemical Equilibrium Compositions with Applications". ICRPG Performance Standardization Working Group, July 1968.

LIST OF ABBREVIATIONS, ACRONYMS, AND SYMBOLS

A	Amperes
A_t	Aerodynamic Throat Area
AEDC	Arnold Engineering Development Center
AFAPL	Air Force Aero Propulsion Laboratory
AMS	Amplitude Mean Square
APL	Aero Propulsion Laboratory
ASI	Auxiliary Spark Ignitors
atm	Atmosphere
B	Magnetic Field Strength
C	Velocity of Sound in Combustor
C_s	Velocity of Sound in Acoustic Slots
c^*	Characteristic Velocity
cal	Calorie
CDA	Copper Development Association
cm	Centimeter
cP	Centipoise
CPIA	Chemical Propulsion Information Agency
CRES	Corrosion Resistant Stainless Steel
csc	Copper to Superconductor Ratio
d	Diameter
D	Diameter
$\bar{D}$	Mass-mean Droplet Diameter
D_{30}	Mean Droplet Diameter Based on a Mean Volume Calculated by Dividing Total Volume of Sample by Number of Droplets
D_{32}	Sauter Mean Diameter
D_H	Hydraulic Diameter
dc	Direct Current
deg	Degree
diam	Diameter
E	Modulus of Elasticity
E	Electric Field
EB	Electronbeam
ED	Electrodeposited
ELF	Electroforming
f	Frequency
F	Force
g	Gravitational Constant
g	Grams
G	Mass Flux per Area

LIST OF ABBREVIATIONS, ACRONYMS, AND SYMBOLS (Continued)

GN_2	Gaseous Nitrogen
GO_2	Gaseous Oxygen
GTA	Gas Tungsten Arc
h	Hour
h	Case Thickness
h	Enthalpy
h_c	Convective Heat Transfer Coefficient
h_w	Wall Enthalpy
$h(\ell)$	Local Enthalpy
H	Force
HGFT	Hot Gas Flow Train
HLB	Hydrophilic-lipophilic Balance
HPMS	High Power MHD System
hr	Hour
Hz	Hertz
I	Moment of Inertia
I_{xx}	Moment of Inertia about Principal Central Axis
ICD	Interface Control Document
ICWG	Interface Control Working Group
Jy	Transverse Current Density
JP-4	A Liquid Hydrocarbon Fuel
K	Average Coolant Wall Thickness
K	Kelvin
kg	Kilogram
kV	Kilovolt
kW	Kilowatt
ℓ	Distance from Wall Surface
L	Length
L	Transverse Combustor Length
L^*	Combustion Chamber Characteristic Length
L/D	Length to Diameter Ratio
LO_2	Liquid Oxygen
m	Meters
$\dot{m}$	Mass Flow Rate
M	Bending Moment
$\overline{M}$	Edge Moment
Me	Exit Mach Number
M_o	Moment of Inertia
MCA	Magnetic Corporation of America
MHD	Magnetohydrodynamic

MIL-STD	Military Standard
min	Minute
MJ	Megajoules
MLI	Maxwell Laboratories, Inc.
mm	Millimeters
MOV	Main Oxygen Valve
msec	Millisecond
MW_e	Megawatt Electrical
N	Newton
N	Number of Cycles
N_{Nu}	Nusselt Number
N_{Pr}	Prandtl Number
N_{Re}	Reynolds Number
OFHC	Oxygen Free, High Conductivity
p	Pressure
P	Poise
Pc	Main Chamber Pressure
Pns	Nozzle Stagnation Pressure
PcF	Correction Factor for Reactant Viscosity, Surface Tension and Density
pk-pk	Peak to Peak
PSD	Power Spectral Density
PWT	Propulsion Wind Tunnel
q	Heat Flux
Q	Heat Flow
R	Radius
R_T	Radius of the Throat
rad	Radian
RMA	Reliability and Maintainability Analysis
rpm	Revolutions per Minute
RTV	Room Temperature Vulcanizing
SCM	Superconducting Magnet
sec	Second
SF_{tu}	Safety Factor on Ultimate Strength
SF_{ty}	Safety Factor on Yield Strength
SHA	Safety and Hazards Analysis
SSFL	Santa Susana Field Laboratory
t	Wall Thickness
T	Temperature
T	Tesla

LIST OF ABBREVIATIONS, ACRONYMS, AND SYMBOLS (Continued)

U	Velocity
$U(\ell)$	Local Velocity
v	Water Velocity
VSC	Vibration Safety Cutoff
w	Width
W^*	Critical Weber Number
We	Weber Number
WG/W	Waterglass/Water Volume Ratio
Z	Section Modulus
α	Coefficient of Thermal Expansion
δ	Bending Deflection
ϵ	Strain
ϵ_1	Circumferential Membrane Strain
η_c^*	Characteristic Velocity Efficienty
ρ	Density
σ	Bending Stress
σ_1	Circumferential Membrane Stress
σ_2	Axial Stress
θ_w	Nozzle Exit Angle
μ	Micron
ν	Poisson's Ratio